

Synthetic and Mechanistic Studies on the Cross-Coupling Reactions Catalyzed by Ruthenium Complexes

Ruili Gao
Marquette University

Recommended Citation

Gao, Ruili, "Synthetic and Mechanistic Studies on the Cross-Coupling Reactions Catalyzed by Ruthenium Complexes" (2011).
Dissertations (2009 -). Paper 105.
http://epublications.marquette.edu/dissertations_mu/105

SYNTHETIC AND MECHANISTIC STUDIES ON THE
CROSS-COUPLING REACTIONS CATALYZED BY
RUTHENIUM COMPLEXES

by

Ruili Gao, B.S.

A Dissertation submitted to the Faculty of the Graduate School,
Marquette University,
in Partial Fulfillment of the Requirements for
the Degree of Doctor of Philosophy

Milwaukee, Wisconsin

May, 2011

ABSTRACT
SYNTHETIC AND MECHANISTIC STUDIES ON THE
CROSS-COUPLING REACTIONS CATALYZED BY
RUTHENIUM COMPLEXES

Ruili Gao, B.A.
Marquette University, 2011

Transition metal catalyzed C-H bond activation reaction is a powerful synthetic method for forming functionalized products directly from unreactive hydrocarbons, and has enormous synthetic potentials for developing chemical processes ranging from petroleum products to pharmaceutical agents. In an attempt to mimic the high stereo selectivity and region selectivity of catalytic reactions by transition metal catalysts, recent research has focused on design and synthesis of transition metal complex and the application on the coupling reactions involving C-H bond activation.

Herein, we wish to report the highly effective coupling reactions involving C-H bond activation by using well-defined ruthenium catalysts. Ruthenium hydride complex was found to have high activity and selectivity for hydrosilylation, silyl enol ethers formation and enol esters formation reactions. Throughout the course of the mechanistic investigation of the reactions, we found compelling evidence for mechanism of reactions by spectroscopic, structural techniques and computational (DFT) analysis.

ACKNOWLEDGMENTS

Ruili Gao, B.A.

Herein, I would like to thank the people who have contributed to this thesis. I would like to first thank my advisor, Dr. Yi for his guidance. Through these four years in the lab, you have taught me how to think and act like a chemist and to demand more from myself. I would like to thank my committee members, Dr. Donaldson, and Dr. Steinmetz, for their time, patience and suggestions. I would like to thank Dr. Timerghazin for the helps on the computational studies. I would like to thank Dr. Cai, who was always willing to share his expertise in NMR with me. Thank you for the help with the advanced NMR experiments. I would like to thank Dr. Sergey for the X-ray crystal structures of the organometallic complexes. Moreover, I would thank Chemistry Department of Marquette University for financial support. I would like to thank the Graduate School and all of the Marquette University administration.

I would like to thank my friends and family for understanding and help me. I would like to dedicate this thesis to my husband. Thank you for standing behind me and fully understanding me all the time. Without you, I would not have gotten this far.

Table of Contents

ACKNOWLEDGMENTS	i
List of Figure	ix
List of Table.....	xiv
Chapter 1. Introduction	1
1.1 ARENE C-H BOND ACTIVATION REACTIONS.....	2
1.1.1 Photo-initiated C-H Bond Activation Reactions.....	2
1.1.2 Non-Chelation-Assisted Arene C-H Bond Activation.....	4
1.1.3 Chelation-Assisted Arene C-H Bond Activation.....	5
1.2 C-H BOND ACTIVATION OF NITROGEN-CONTAINING COMPOUNDS	8
1.2.1 C-H Bond Activation of Pyrroles	8
1.2.2 C-H Bond Activation of pyridine and other Nitrogen Containing Compounds	23
1.3 THE FORMATION OF SILYL ENOL ETHER INVOLVING C-H BOND ACTIVATION	30
1.4 ALKYNE C-H BOND ACTIVATION	34
1.4.1 The Formation of Enol Esters from the Coupling Reactions of Alkynes and Carboxylic Acids	34
1.4.2 The Hydrosilylation of Alkynes.....	44

Chapter 2. Regioselective Formation of α-Vinylpyrroles from the Ruthenium-Catalyzed Cross Coupling Reaction of Pyrroles and Terminal Alkynes Involving C-H Bond Activation	57
2.1 RESULTS AND DISCUSSION.....	57
2.2 SCOPE OF THE COUPLING REACTIONS OF PYRROLES WITH TERMINAL ALKYNES	59
2.2.1 Catalyst Survey	59
2.2.2 Solvent Effects	62
2.2.3 Reaction Scope.....	63
2.3 MECHANISM STUDIES	65
2.3.1 Hammett Study	65
2.3.2 Isotope Effect Study.....	69
2.3.3 Deuterium Labeling Studies	72
2.3.4 Carbon Isotope Effect Study.....	75
2.3.5 Proposed Mechanism of the Coupling Reactions of Pyrroles and Alkynes	78
2.4 CONCLUSIONS	80
Chapter 3. Scope and Mechanistic Investigations on the Solvent-Controlled Regio- and Stereoselective Formation of Enol Esters from the Ruthenium-Catalyzed Coupling Reaction of Terminal Alkynes and Carboxylic Acids.....	81

3.1 RESULTS AND DISCUSSION.....	82
3.2 OPTIMIZATION STUDIES FOR THE COUPLING OF CARBOXYLIC ACID WITH TERMINAL ALKYNES	83
3.2.1 Catalyst Activity Survey.....	83
3.2.2 Solvent Effects.....	85
3.3 REACTION SCOPE	87
3.4 MECHANISTIC STUDY.....	93
3.4.1 Phosphine Inhibition Study.....	93
3.4.2 Deuterium Labeling Study.....	95
3.4.3 Hammett Study	97
3.4.4 Synthesis of Catalytically Relevant Ruthenium-Carboxylate.....	101
3.4.5 Synthesis of Catalytically Relevant Ruthenium–Vinylidene-Carboxylate Complexes	102
3.4.6 Kinetic Experiments on the Conversion of Complex 64 to Complex 62 and Complex 63	104
3.4.7 Derivation of the Kinetic Equation of the Conversion of 64 to 63	106
3.4.8 Proposed Mechanism.....	109
3.5 CONCLUSIONS	112

**Chapter 4. Catalytic Formation of Silyl Enol Ethers from the Reaction of Ketones
with Vinylsilanes and Their Use in Aldol-Type Condensation and Fluorination**

Reactions.....	113
4.1 RESULTS AND DISCUSSION	114
4.2 OPTIMIZATION STUDIES FOR THE COUPLING OF KETONES WITH VINYLSILANE	115
4.2.1 Catalyst Activity Survey	115
4.3 THE SCOPE FOR THE REACTIONS OF KETONES WITH VINYLSILANE AND THE REACTION OF ENOL ETHER WITH ALDEHYDE UNDER THE TITANIUM (IV) CHLORIDE	117
4.3.1 The Use of Enol Silyl Ether in Fluorination Reactions and Diketone Reactions.....	122
4.4 MECHANISTIC STUDY ON THE REACTION OF KETONES AND VINYLSILANES ..	125
4.4.1 Deuterium Labeling Study.....	125
4.4.2 Deuterium Isotope Effect Study.....	127
4.4.3 Phosphine Inhibition Study.....	128
4.4.4 Hammett Study	130
4.5 PROPOSED MECHANISM OF THE REACTION OF KETONE AND VINYLSILANES .	132
4.6 CONCLUSIONS	135

Chapter 5. Highly Stereoselective and Regioselective Hydrosilylation of Alkynes and Alkenes Catalyzed by $(PCy_3)_2(CO)RuHCl$.....	136
5.1 RESULTS AND DISCUSSION.....	136
5.2 SCOPE OF THE HYDROSILYLATION OF ALKYNES	137
5.2.1 Catalyst Survey	137
5.2.2 Scope of the Hydrosilylation of Alkynes.....	139
5.2.3 The Scope of the Hydrosilylation of Alkenes.....	143
5.3 MECHANISTIC STUDY ON THE HYDROSILYLATION OF ALKYNES.....	146
5.3.1 Deuterium Labeling Study on the Hydrosilylation of Alkynes	147
5.3.2 Phosphine Inhibition Study on the Hydrosilylation of Alkynes....	148
5.3.3 Rate Dependence on the Substrate Concentration.....	152
5.3.4 Rate Dependence on the Catalyst Concentration.....	155
5.4 MECHANISTIC STUDY ON THE HYDROSILYLATION OF ALKENES	156
5.4.1 Deuterium Labeling Study on the Hydrosilylation of Alkenes	156
5.4.2 Isotope Effect Study on the Hydrosilylation of Alkenes	158
5.4.3 Carbon Isotope Effect Study.....	160
5.4.4 Hammett Study on the Hydrosilylation of Alkenes.....	163
5.4.5 Phosphine Inhibition Study on the Hydrosilylation of Alkenes	166
5.4.6 Rate Dependence on the Substrate Concentration.....	173
5.4.7 Rate Dependence on the Catalyst Concentration.....	175

5.5 THE REACTION OF TRIETHYLSILANE WITH RUTHENIUM VINYL COMPLEX.....	176
5.6 COMPUTATION STUDIES ON THE HYDROSILYLATION OF ALKYNES	181
5.7 PROPOSED MECHANISM OF THE HYDROSILYLATION OF ALKENES	196
5.8 CONCLUSIONS	199
Chapter 6. Experimental Sections.....	200
6.1 GENERAL INFORMATION	200
6.2 FOR CHAPTER 2.....	200
6.2.1 Typical Procedure of the Catalytic Reaction	200
6.2.2 Hammett Study of the Catalytic Reaction	201
6.2.3 Isotope Effect Study.....	202
6.2.4 Preparation of the Phenylpyrrole-d ₄	202
6.3 CHARACTERIZATION DATA OF SELECTED ORGANIC PRODUCTS	205
6.4 FOR CHAPTER 3.....	211
6.4.1 General Procedure of the Catalytic Reaction.....	212
6.5 CHARACTERIZATION DATA OF SELECTED ORGANIC PRODUCTS	218
6.6 FOR CHAPTER 4.....	225
6.6.1 Typical Procedure of the Catalytic Reaction	225
6.6.2 Typical Procedure of the Aldol-Type Condensation Reaction	226
6.6.3 Typical Procedure of the Fluorination Reaction.....	227
6.6.4 Typical Procedure of the Diketone Reactions	227

6.6.5 Typical Procedure of Aminomethylation Reaction	228
6.6.6 Hammett Study	228
6.7 CHARACTERIZATION DATA OF ORGANIC PRODUCTS.....	229
6.8 FOR CHAPTER 5.....	235
6.8.1 General Procedure of the Hydrosilylation of Alkynes.....	235
6.8.2 General Procedure of the Hydrosilylation of Alkenes	236
6.8.3 Hammett Study on the Hydrosilylation of Alkenes	236
6.8.4 Isotope Labeling Study on the Hydrosilylation of Alkynes.....	237
6.8.5 Phosphine Inhibition Study on the Hydrosilylation of Alkynes	237
6.8.6 Kinetic Studies on the Hydrosilylation of Alkenes.....	238
6.8.7 Isotope Effect Study on the Hydrosilylation of Alkenes	238
6.8.8 Carbon Isotope Effect Study on the Hydrosilylation of Alkenes ..	239
6.8.9 Synthesis of Carbonylchlorohydridotris(triphenyl-phosphine) Ruthenium (II)	241
6.8.10 Computational Study on Hydrosilylation of Alkynes.....	241
6.8.11 Characterization Data of Selected Organic Products of Hydrosilylation of Alkynes.....	242
6.8.12 Characterization Data of Selected Organic Products of Hydrosilylation of Alkenes	243
References	246

List of Figure

- Figure 1.** ^1H NMR Spectroscopy for complex **53c** 58
- Figure 2.** X-ray Crystal Structure of **53c**..... 59
- Figure 3.** Hammett Plot of the Coupling Reaction of *para*-Substituted $p\text{-X-C}_6\text{H}_4\text{N}$
(X = OMe, CH₃, H, Cl, F) with 4-ethynylanisole Catalyzed by
 $\text{Ru}_3(\text{CO})_{12}/\text{NH}_4\text{PF}_6$ (1:3 molar ratio)..... 67
- Figure 4.** Hammett Plot of the Coupling Reaction of *para*-Substituted
 $p\text{-X-C}_6\text{H}_4\text{CCH}$ (X = OMe, CH₃, H, Br, F) with Pyrrole Catalyzed by $\text{Ru}_3(\text{CO})_{12}$
 $/\text{NH}_4\text{PF}_6$ (1:3) at 95 °C 69
- Figure 5.** ^1H and ^2H NMR Spectra for the Deuterated N-phenyl Pyrrole 70
- Figure 6.** First Order Plot of $-\ln[\text{product}]$ vs Reaction Time for the Coupling
Reaction; \blacklozenge -Phenyl pyrrole- d_4 ; \blacksquare -Phenyl pyrrol 72
- Figure 7.** (a) ^1H NMR Spectrum of the Undeuterated Compound; (b) ^1H NMR
Spectrum of the Compound **54a**; (c) ^2H NMR Spectrum of the Compound **54a**.
..... 74
- Figure 8.** Plot of the Initial Rate (v_i) vs. $[\text{PCy}_3]$ for the Coupling Reaction of
Benzoic Acid and Phenylacetylene. Reaction conditions: benzoic acid (0.20
mmol), phenylacetylene (0.40 mmol), **1** (3 mg, 2 mol %), CDCl_3 (0.5 mL).... 94

Figure 9. Hammett Plot of the Coupling Reaction of <i>para</i> -Substituted <i>p</i> -X-C ₆ H ₄ CO ₂ H (X = OMe, CH ₃ , H, CF ₃ , CN) with Phenylacetylene in CDCl ₃ (●) and in THF (■).....	98
Figure 10. Hammett Plot of the Coupling Reaction of <i>para</i> -Substituted <i>p</i> -X-C ₆ H ₄ C≡CH (X = OMe, CH ₃ , H, CF ₃ , F) with Benzoic Acid in CDCl ₃ (●) and in THF (■)	99
Figure 11. Molecular Structure of 62	102
Figure 12. Molecular Structure of 63	104
Figure 13. High-temperature VT-NMR of the Conversion of Complex 62 and 63 from Complex 64	105
Figure 14. Kinetic Profile of the Conversion of 64 to 63 . Notations: 64 (▲), 62 (●) , 63 (■).....	107
Figure 15. ¹ H NMR Spectroscopy of Product 67g	118
Figure 16. ¹ H NMR Spectroscopy for complex 67s	124
Figure 17. A- ¹ H NMR Spectroscopy of the Reaction Mixtures; B- ² H NMR Spectroscopy of the Reaction Mixtures.	126
Figure 18. Plot of the Initial Rate (v _i) vs. [PCy ₃] for the Coupling Reaction of Acetophenone and Vinyltrimethylsilane	130
Figure 19. Hammett Plot of the Reaction of <i>para</i> -Substituted <i>p</i> -X-C ₆ H ₄ COCH ₃ (X = OMe, CH ₃ , H, Cl, Br) with Vinyltrimethylsilane	132

Figure 20. ^1H and ^2H NMR for the Deuterated Complex 69a . A- ^1H NMR Spectroscopy of <i>cis</i> -vinylsilane 69a ; B- ^1H NMR Spectroscopy of Deuterium Vinylsilane; C- Deuterium NMR Spectroscopy of Deuterium Product and Acetone- d_6 is the Reference.....	148
Figure 21. The Phosphine Inhibition for the Coupling Reaction of Phenylacetylene and Triethylsilane; ^a Reaction conditions: phenylacetylene (0.20 mmol), triethylsilane (0.40 mmol), 1 (1 mol %), PCy_3 (0.0-0.014 mM).....	149
Figure 22. Plot of the Initial Rate vs. $[\text{PhC}\equiv\text{CH}]$ at different PCy_3 Concentrations	150
Figure 23. Lineweaver-Burke Plot of $1/v_i$ vs. $1/[\text{PhCCH}]$	151
Figure 24. Plot of the Initial Rate vs. $[\text{PhC}\equiv\text{CH}]$	153
Figure 25. Plot of the initial rate vs. $[\text{HSiEt}_3]$	154
Figure 26. Plot of the initial rate vs. $[\text{RuH}]$	156
Figure 27. ^1H and ^2H NMR for the complex 70a	158
Figure 28. Kinetics Plot of the Reaction of Styrene and HSiMe_3	159
Figure 29. Hammett Plot of the Coupling Reaction of <i>para</i> -Substituted $p\text{-X-C}_6\text{H}_4\text{CH}=\text{CH}_2$ (X = OMe, CH ₃ , H, Cl, F) with Triethylsilane	165
Figure 30. Possible Transition State for the Intermediate of the Hydrosilylation of Alkenes	166

Figure 31. The Phosphine Inhibition for the Reaction of Styrene and Triethylsilane	167
Figure 32. Plot of the Initial Rate vs. [styrene] at Different PCy ₃ Concentrations. Without PCy ₃ (■); 0.21 mM (0.4 equiv) PCy ₃ (▲); 0.42 mM (0.8 equiv) PCy ₃ (◆); 1.01 mM (1.8 equiv) PCy ₃ (○);	168
Figure 33. Lineweaver-Burke Plot of 1/v _i vs. 1/[styrene]. No PCy ₃ (■); 0.21 mM (0.4 equiv.) PCy ₃ (▲); 0.42 mM (0.8 equiv.) PCy ₃ (◆); 1.01 mM (1.8 equiv.) PCy ₃ (○);	170
Figure 34. Dixon plot of 1/v versus [PCy ₃]	171
Figure 35. The replot of slope vs. 1/[S]	172
Figure 36. Plot of the initial rate vs. [styrene]	174
Figure 37. Plot of the initial rate vs. [HSiEt ₃]	175
Figure 38. Plot of the initial rate vs. [RuH]	176
Figure 39. ³¹ P NMR of the Formation of Ruthenium Hydride Complex 1 from Rutheniumvinyl Complex 2.....	178
Figure 40. The Plot of the Reaction Rate vs the Concentration of PCy ₃	179
Figure 41. The Plot of Reaction Rate vs the Concentration of Styrene	180
Figure 42. The Energy of intermediate 71i , 71j and Transition State 1 and Transition State 2	192

Figure 43. The Energy of *cis* and *trans* Intermediate and Transition State 1 and
Transition State 2 for 3,3-Dimethylbutyne 195

List of Table

Table 1. Catalyst Activity Survey for Coupling Reaction of Pyrroles with Alkynes ^a	61
Table 2. Solvent Effect Survey on Coupling Reaction of Pyrroles with Alkynes ...	62
Table 3. Coupling Reactions of Pyrroles with Terminal Alkynes	64
Table 4. Average ¹³ C Integration of the Recovered and Virgin Samples of N-phenylpyrrole.....	77
Table 5. Catalyst Survey on the Coupling Reaction of Benzoic Acid and 4-Ethynylanisole. ^a	84
Table 6. Solvent Effect on the Coupling Reaction of Benzoic Acid and 4-Ethynylanisole ^a	86
Table 7. Alkyne-to-Carboxylic Acid Coupling Reaction Catalyzed by Complex 1 . ^a	89
Table 8. Coupling Reaction of Carboxylic Acids with Propargyl Alcohols and Diyne. ^a	92
Table 9. Catalyst Activity Survey for the Coupling Reaction of Vinyltrimethylsilane and Acetophenone. ^a	116
Table 10. Coupling Reaction of ketones with Vinyltrimethylsilane ^a and the Reaction of Enol Ether with Aldehyde under the Titanium (IV) Chloride. ^b ..	120

Table 11. Catalyst Activity Survey for the Coupling Reaction of Phenylacetylene and Triethylsilane.....	139
Table 12. The Coupling Reaction of Alkynes and Triethylsilane ^a	142
Table 13. The Coupling Reaction of Alkenes and Hydrosilane. ^a	145
Table 14. Average ¹³ C Integration of the Samples of trans-vinylsilane 70a	162
Table 15. Crystal Data and Structure Refinement for 63	217

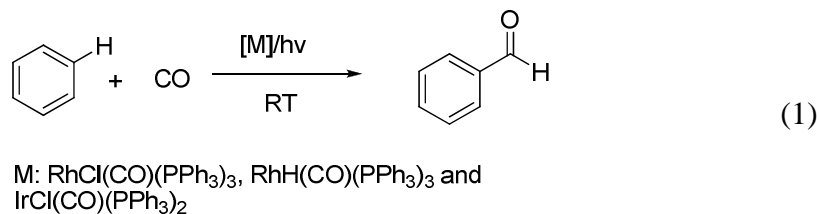
Chapter 1. Introduction

Over the past decades, the quest for the most economic ways to form C-C bonds has become a matter of increasing importance among both industrial and academic research units. Catalytically efficient activation of unreactive C-H bonds leading to synthetically useful C-C bond formation is of considerable interest for the chemical and pharmaceutical industries and remains a long term challenge for chemists. It would provide a simple, clean and economic method for making functionalized molecules. Although there are many studies on the reaction of arenes C-H bonds with the transition metal compounds, transition metal mediated catalytic C-H bond activation reactions have emerged as an attractive method for forming carbon-carbon bonds. In particular, transition metal-catalyzed C-H bond activation and functionalization reactions of nitrogen heterocyclic compounds have attracted considerable attention, in part due to their prominent role in the synthesis of natural products and pharmaceutical agents. Highly regioselective catalytic C-H bond insertion reactions of nitrogen-containing aromatic compounds, such as pyridines, pyrroles, and indoles, have been reported in recent years. In this chapter, the literature survey of transition metal catalyzed C-H bond activation, the formation of enol ester and the silylation reactions will be discussed.

1.1 Arene C-H Bond Activation Reactions

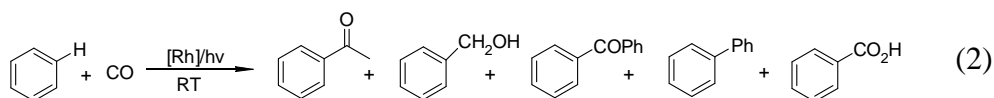
1.1.1 Photo-initiated C-H Bond Activation Reactions

In 1983, Eisenberg reported the preparation of the complex $\text{IrH}_3(\text{CO})(\text{dppe})$ ($\text{dppe} = 1,2\text{-bis(diphenylphosphino)ethane}$),¹ and its photochemical behavior. Irradiation of a benzene solution of $\text{IrH}_3(\text{CO})(\text{dppe})$ under CO produced a small amount of benzaldehyde. Despite the fact that the reaction was not catalytic, the authors had stumbled on a system that not only activated arene C-H bonds but also inserted CO to give a functionalized product. These results were followed by studies among which only complexes of Rh(I) and Ir(I) containing the ligand PPh_3 can promote catalytic arene carbonylation photochemistry (Eq 1).



However, the use of a loosely related rhodium complex bearing a stronger electron donating ligand, such as the PMe_3 , gave better yields.² In addition to the expected benzaldehyde, small amounts of biphenyl, benzyl alcohol and benzophenone also formed. These compounds are presumably secondary products formed from

benzaldehyde. Only biphenyl seems to be a primary product because it is formed catalytically even under nitrogen (Eq 2).

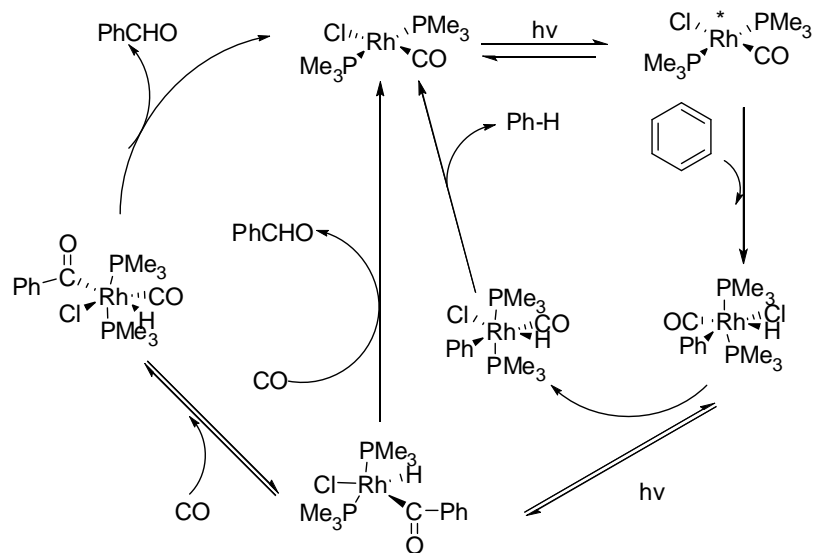


According to Tanaka et al., the restricted yield of benzaldehyde is not due simply to thermodynamic limitations,³ but to two other factors. The first arises from secondary photoreactions of benzaldehyde and the second arises from the decomposition of the catalyst.

Other transition-metal complexes, including some ruthenium complexes are less efficient than Rh complexes.⁴ The application of $\text{RhCl}(\text{CO})(\text{PR}_3)_3/h\nu$ system to substituted benzene such as toluene, anisole or chlorobenzene gave meta- and para-substituted products in a 2/1 statistical ratio.⁵

The mechanism for the full catalytic cycle of the Rh-catalyzed photochemical carbonylation of benzene is shown in Scheme 1.

The most unusual aspect of this cycle is that the primary photo process does not involve ligand loss. Therefore, the C-H addition step proceeds predominantly via an associative process. Another striking aspect of the proposed mechanism is that a secondary photo process, favored by short wavelengths. In addition to the primary photoprocess which lead to a reactive state of the starting complex.

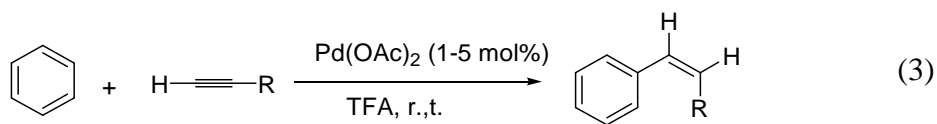


Scheme 1. Mechanism for Arene Carbonylation

1.1.2 Non-Chelation-Assisted Arene C-H Bond Activation

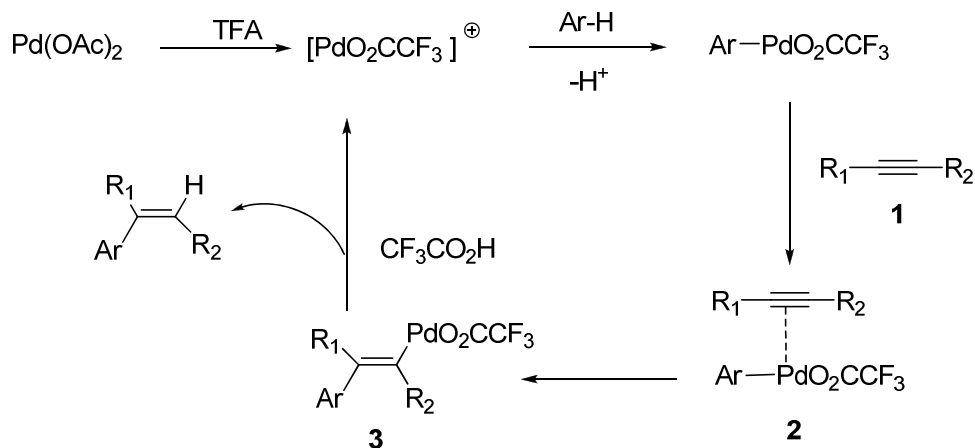
Examples of the non-chelation-assisted C-H bond activation are relatively rare.

Fujiwara reported the efficient metalation of aromatic C-H bonds at room temperature using a highly electrophilic in situ generated Pd(II) and Pt(II) cationic species in trifluoroacetic to C-C multiple bonds (Eq 3).⁶



In most cases, the addition of alkynes exclusively afforded the thermodynamically less stable *cis*-aryl alkene. The intramolecular hydroarylation of C-C triplet bonds is facile and regioselective because of the electrophilic metalation of

aromatic C-H bonds by the Pd(II) cationic species which is assisted by the ethyl coordination. In fact, this intramolecular reaction combines both chelation assisted and electrophilic metalation. A possible mechanism has been outline in Scheme 2.

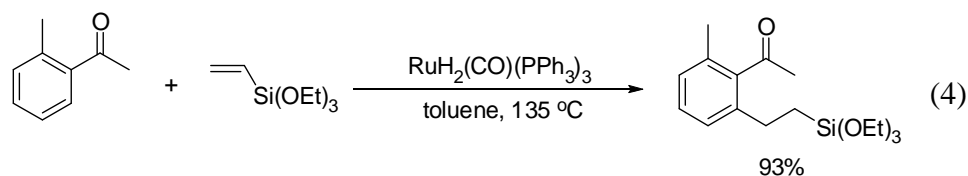


Scheme 2. Mechanism for the Addition of Alkynes to Alkenes

The proposed mechanism indicates the electrophilic attack of the aromatic C-H bond by the cationic Pd (II) species to form complex **1** followed by coordination of alkyne to give complex **2**. A *trans* insertion of the C-C triple bond to the σ -aryl Pd bond results in complex **3**, and the 1 to 1 coupling product would be released from Pd (II) upon protonation of complex **3**.

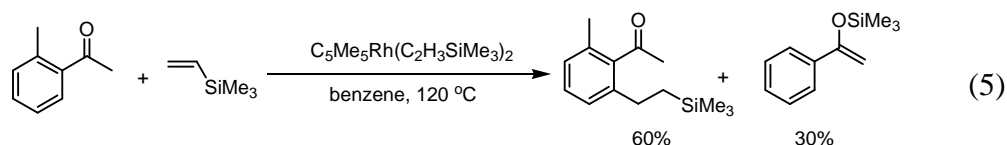
1.1.3 Chelation-Assisted Arene C-H Bond Activation

Murai discovered the first example of a chelation-assisted, regioselective, catalytic C-H bond activation of arene and olefin coupling reactions.⁷ For example, acetophenone is added to vinyl silane to yield a regioselective alkylated product at the *ortho* position (Eq 4).



The ruthenium $\text{RuH}_2(\text{CO})(\text{PPh}_3)_3$ was found to be an effective catalyst for this reaction. This coupling reaction is easy to carry out, and in many cases, the reaction gives a nearly quantitative yield.

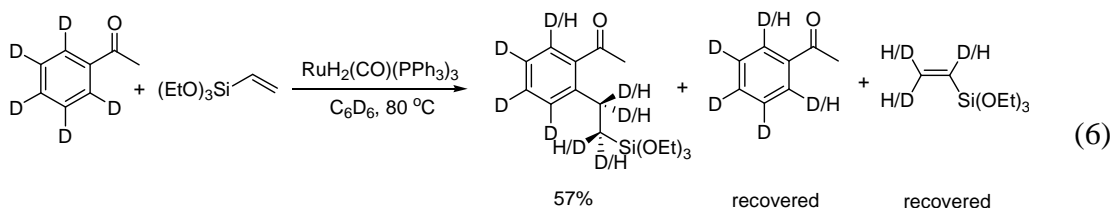
The reaction was extended to various arenes and olefins coupling reactions. Mechanism studies indicate that the C-H bond cleavage step is not rate-determining. Instead a rapid equilibrium exists prior to the reductive elimination step that leads to the C-C bond formation. Murai established that reductive elimination of alkylated products is the turnover-limiting step (Eq 5).



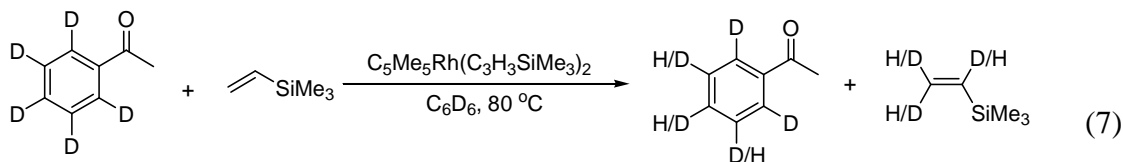
The rhodium bis-olefin complexes $[\text{C}_5\text{Me}_5\text{Rh}(\text{C}_2\text{H}_3\text{SiMe}_3)_2]$ have been shown to be effective catalysts for the selective addition of olefin to the *ortho* position of aromatic ketone.⁸ The reactions of ketones and vinylsilane take place in benzene at 120 °C to

generate the addition of the olefin and the silyl enol ether, and the ratio of these products is around 2 to 1. For these catalytic reactions, a key difference in the mechanism from the ruthenium-catalyzed processes is that the carbonyl coordination is presumed to be the first step which directs the C-H bond activation to the *ortho* position of the aromatic substrate.

From the isotope effects studies, the H/D exchange experiments establish that the *para* and *meta* C-H bonds are not activated in the ruthenium system (Eq 6).



These rhodium complexes, on the other hand, are not discriminating in the C-H bond activation step and activation of all sites (*ortho*, *meta*, *para*) of the substrate is observed (Eq 7).



Murai has established that the C-H bond activation is fast and reversible in the ruthenium system and the reductive elimination of the alkylated products is the turnover-limiting step. It is believed that the same feature applies to the rhodium system as well, but no conclusive evidence is available concerning this point. In both system,

chelation of the carbonyl group to the metal center lower in the energy barrier for reductive elimination leads to form the products.

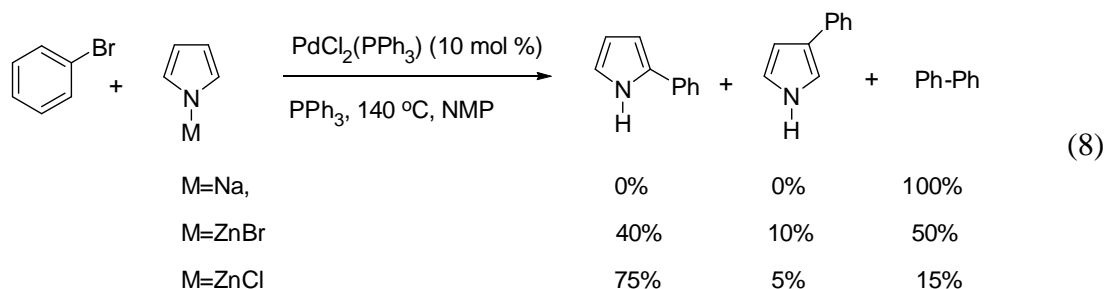
1.2 C-H Bond Activation of Nitrogen-Containing Compounds

Transition metal-catalyzed C-H bond activation and functionalization reactions of nitrogen heterocyclic compounds have attracted considerable attention, in part due to their prominent role in the synthesis of natural products and pharmaceutical agents. Highly regioselective catalytic C-H bond insertion reactions of nitrogen-containing aromatic compounds, such as pyridines, pyrroles, and indoles, have been reported in recent years.

1.2.1 C-H Bond Activation of Pyrroles

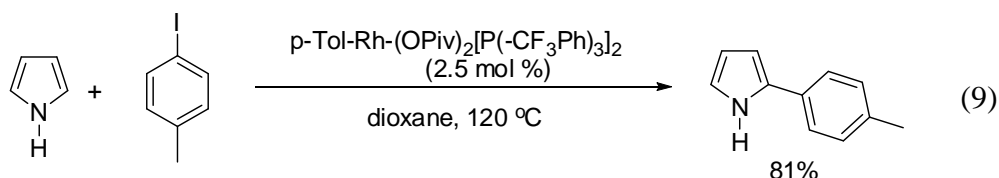
Pyrrole moieties are important structural elements of many natural compounds of biological interest and they are important building blocks for forming biologically active family of porphyrins and related nitrogen macrocycles as well as for serving as precursors for electroactive polymeric materials. Therefore, the development of an efficient pathway for the functionalization of these compounds will be important to

pharmaceutical science, and the development of direct C-H bond functionalization strategies for the facile generation of compounds with useful molecular architecture remains high interest to academic and industrial chemists. People are particularly interested in the development of new methods for direct metal catalyzed oxidative C-H transformation of organic molecular under mild and operationally simple conditions.⁹ Filippini reported an interesting palladium-catalyzed direct arylation of N-metalated pyrrole with bromobenzene in which the nature of the cation had varying effects on product distribution (Eq 8).¹⁰

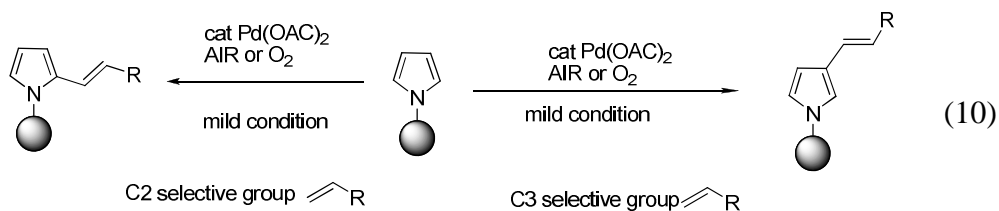


While the use of sodium pyrrole gave the aryl bromide-homocoupled product in quantitative yield, trans-metalation to a harder pyrrole-1-yl zinc bromide gave the desired 2-substituted pyrrole in 40% yield along with some of the 3-substituted pyrrole and dimerized bromobenzene product.¹¹ Further improvement in reaction selectivity was possible using ZnCl₂, which afforded the desired 2-substituted pyrrole product in 75% yield with very little of the 3-substituted pyrrole and Ullman coupling byproduct.¹²

Sames reported several alternative procedures for the intermolecular C-2 arylation of pyrrole. The first approach uses $\text{ArRh}(\text{OPiv})_2[\text{P}(p\text{-CF}_3\text{Ph})_3]_2$ as the catalyst system for the C-2 arylation of *NH*-containing pyrrole (Eq 9).¹³



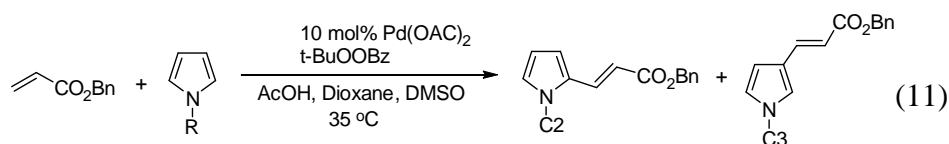
C-vinylated pyrroles are important building blocks for forming porphyrins and related nitrogen macrocycles as well as for serving as precursors for photoactive polymeric materials. Recently Pd catalysts have been found to be particularly versatile in mediation C-H oxidative coupling reactions of substituted pyrroles, pyridines and indoles,¹⁴ where the regioselectivity has often found to be dictated by both the steric and electronic nature of the arene substituents. Elizabeth reported an efficient aerobic palladium oxidation system for C-H bond functionalization of sensitive molecular under ambient conditions (Eq 10).¹⁵



This method can be used to directly generate a range of functionalized and annulated pyrrole architectures and it is possible to control the position of C-H bond

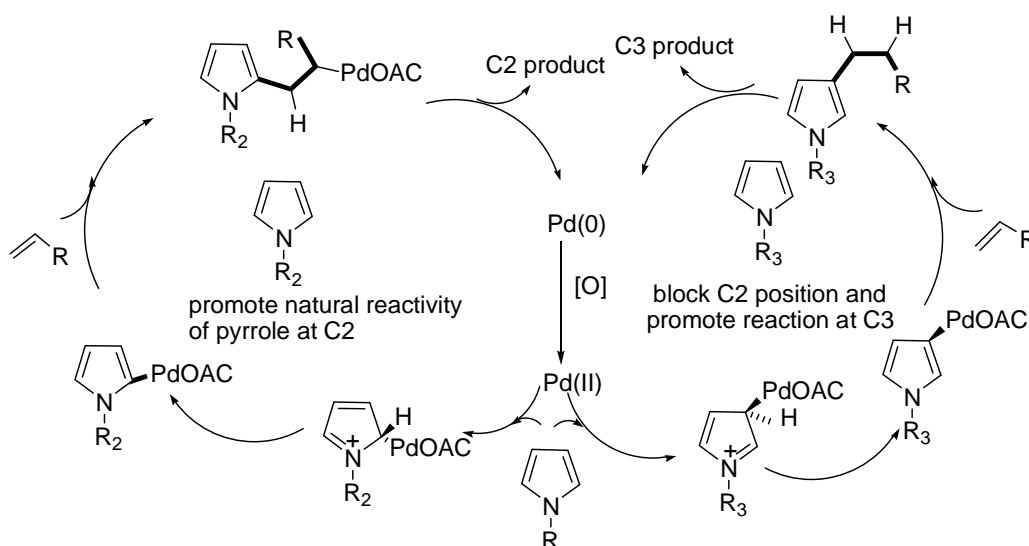
functionalization via simple steric and electronically tuned N-pyrrole protecting groups to form products with either C2 or C3 elaboration.

For the reaction conditions, they identified that 10 mol % Pd(OAc)₂ in a dioxane–AcOH–DMSO solvent system and tBuOOBz as oxidant provided an effective system for pyrrole functionalization. They found that N-Bn pyrrole reacted smoothly with benzyl acrylate at only 35 °C to form the alkenylated products. Although it was expected that the natural reactivity of pyrrole would direct reaction to the C2 position, they observed a mixture of C2 and C3 isomers with the ratio of 2 to 1. They tried different N-group, and found that an electron withdrawing N-protecting group would reduce the reactivity of the pyrrole and yield a more selective process (Eq 11).



In this reaction, N-Ac, N-Ts(tosyl) and N-Boc pyrrole afforded only the C2 products in good yield under mild conditions. In contrast N-TIPS pyrrole gave only C3 product. The switch in selectivity is attributed to the sterically demanding nature of the TIPS group shields the C2 position from reaction with the palladium catalyst, forcing the reactive pyrrole to palladate at C3. So this is a new method for controlling catalytic activation and functionalization of pyrroles under mild conditions.

They surveyed the catalyst loading and found that the catalyst loading can be reduced to 1 mol %, but the complete conversion takes longer to achieve. The turnover number (TON) at 60% (96 h) conversion is 55 %, suggesting that the process displays a high efficiency for palladium (II) processes.

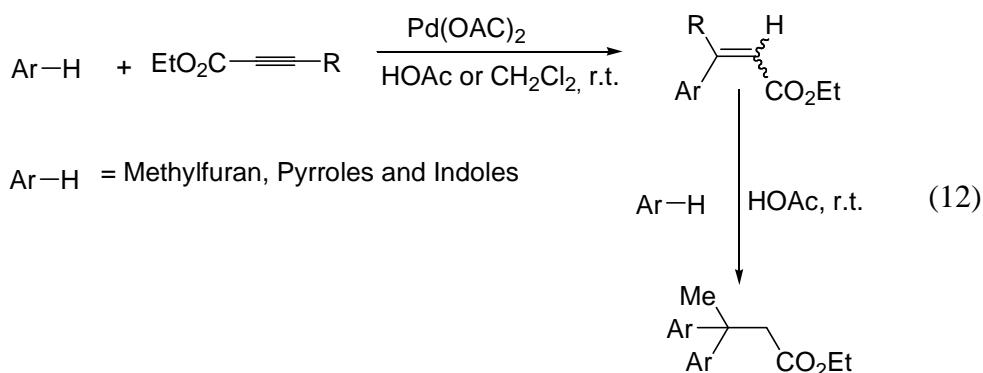


Scheme 3. Stereoelectronic Control Concept: Proposed Mechanism

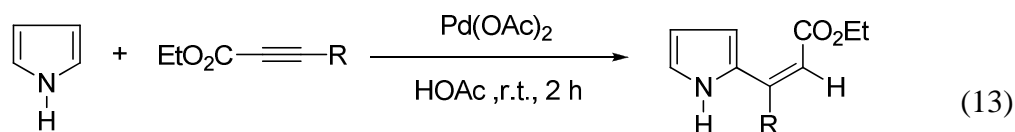
The catalytic cycle started at the oxidation of Pd (0) complex to generate reactive species Pd (II). In this catalytic cycle, the key step was the pyrrole insertion to the metal center and this step is the selectivity-determined step. For the bulky R group, the C2 position was blocked and there was strong steric hindrance between the metal complex and pyrrole. So the pyrrole coordinates to the metal center at C3 position. On the other hand, with less steric hindrance R group, the C2 position was more reactive than C3

position. Then with the hydrogen elimination and the insertion of alkene, the product was generated.

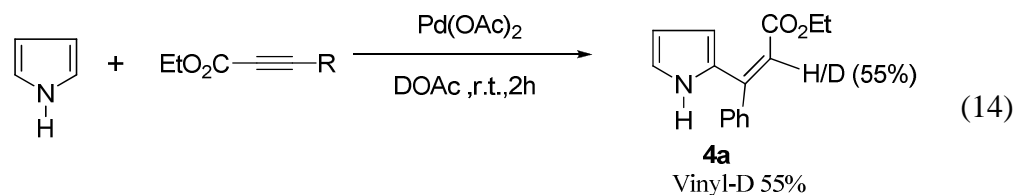
Fujiwara reported the pyrroles undergo the addition reaction to C-C triple bond in the presence of a catalytic amount of Pd(OAc)₂ under very mild conditions, affording cis-heteroarylalkenes in most cases (Eq 12).¹⁶



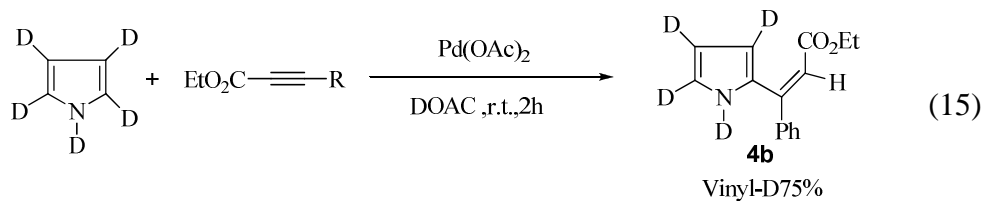
For pyrrole, 1-methylpyrrole and 2-methylfuran, the substitution of aromatic C-H bonds occurred at the 2- or 5-position of the arenes, characteristic of electrophilic substitution (Eq 13).



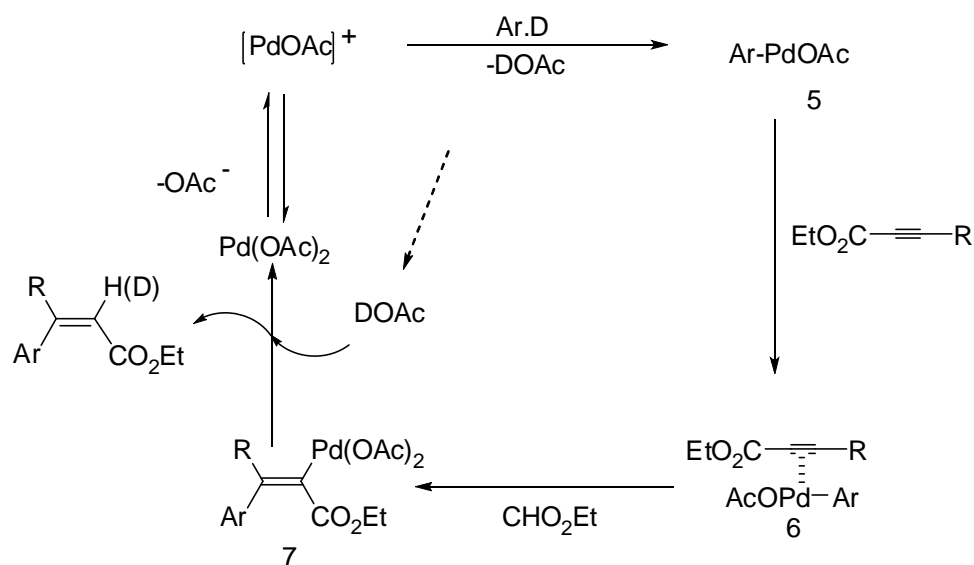
To investigate the possible mechanism of this reaction, they carried out several isotope experiments using either DOAc as a solvent or d₅-pyrrole as an arene. When the reaction of pyrrole with ethyl phenylpropiolate was run in the DoAc, D atoms incorporated into the product **4a** at a rate of 55% at the 2-vinyl position (Eq 14).



On the other hand, D atoms incorporated into the product **4b** at the rate of 75% at the 2-vinyl position when the reaction of d_5 -pyrrole with ethyl phenylpropiolate was run in dichloromethane. This suggested that the Vinyl-D atoms of the product may result from the protonation of C by DOAc and DOAc itself may be formed from metalation of pyrrole C-H by Pd (II) species (Eq 15).



They also noticed that in these two separate reactions the initial rate of the reaction of pyrrole with ethyl phenylpropiolate in dichloromethane was three times faster than that of d_5 -pyrrole with ethyl phenylpropiolate in dichloromethane, $k_H/k_D = 3$, which indicated that the cleavage of the pyrrole C-H bonds is the possible rate-determining step in the present reaction.

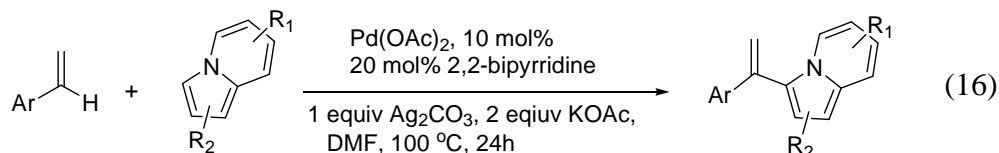


Scheme 4 . Possible Mechanism for the Addition of Heteroarenes to Alkynoates

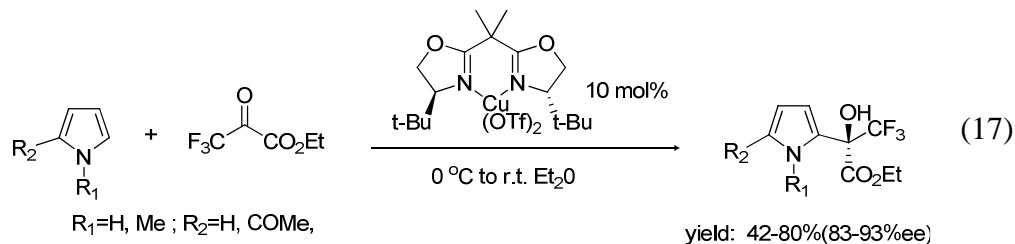
Based on this information, they showed a possible mechanism in Scheme 4. The electrophilic substitution of the aromatic C-H bond by cationic Pd (II) species would result in the formation of an σ -arylpalladium complex **5** which is followed by coordination of alkyne to give complex **6**. Trans-Insertion of C-C trip bonds to the σ -aryl-Pd bond would afford vinyl-Pd complexes **7**, and upon protonation of complex **7**. The 1:1 coupling product would be released from the Pd (II) species.

Recently Zhang reported that the highly regioselective Palladium-catalyzed oxidative coupling reaction of indolizines and vinylarenes via C-H bond cleavage.¹⁷ In this report, they used the 10 mol % Pd(OAc)₂ with one equiv. Ag₂CO₃ as oxidant and 20 mol % ligand to catalyze the coupling reactions of styrene with indolizines. They found that the ligands added showed the relationship with the selectivity of the product, they got

only the geminal isomer as the product by using 2, 2'-bipyridine, by using PPh₃, pyridine or phenanthroline as ligands, they got the geminal and the (Z)-isomers mixtures (Eq 16) and the ratio of these two isomers is around 1 to 1.

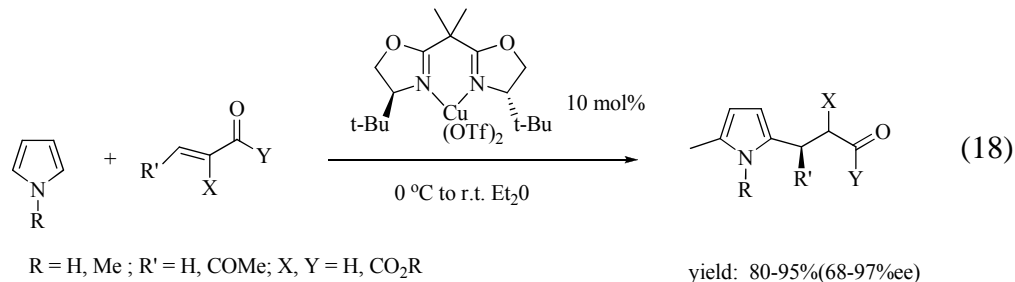


The Friedel-Crafts reaction has gained substantial synthetic and industrial significance as an immensely powerful tool to effect C-C bond formation. Recently Jorgensen has reported highly enantioselective Friedel-Crafts reactions of aromatic and heteroaromatic compounds to trifluoropyruvate. He showed that the reactions of pyrroles with ethyl trifluoropyruvate in the presence of (s)-*t*-Bu-BOX-Cu(OTf)₂ as the catalyst show the highly enantioselectivity on the introduction of a chiral hydroxyl-trifluoromethyl ethyl ester group. Substitution occurred into the 2-position on the pyrrole ring, and the reaction proceeded good yield and high enantioselectivity (Eq 17).¹⁸

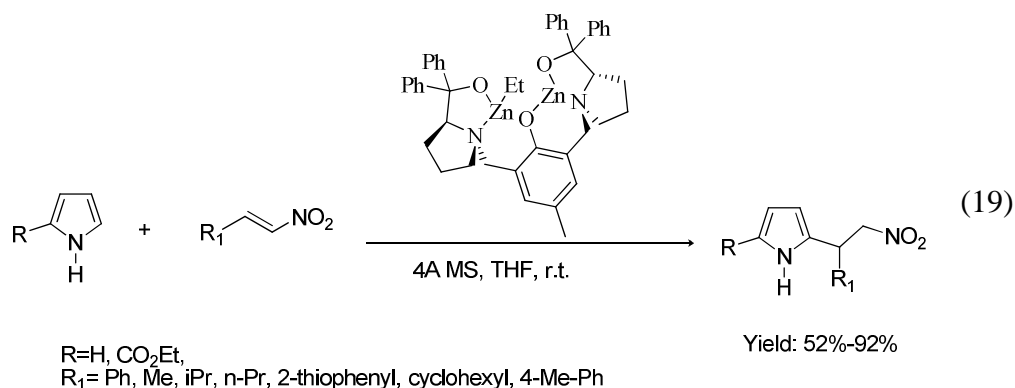


Four years later, Linden reported these highly enantioselective Friedel-Crafts alkylations of pyrroles and indoles with the enones by using the same catalyst

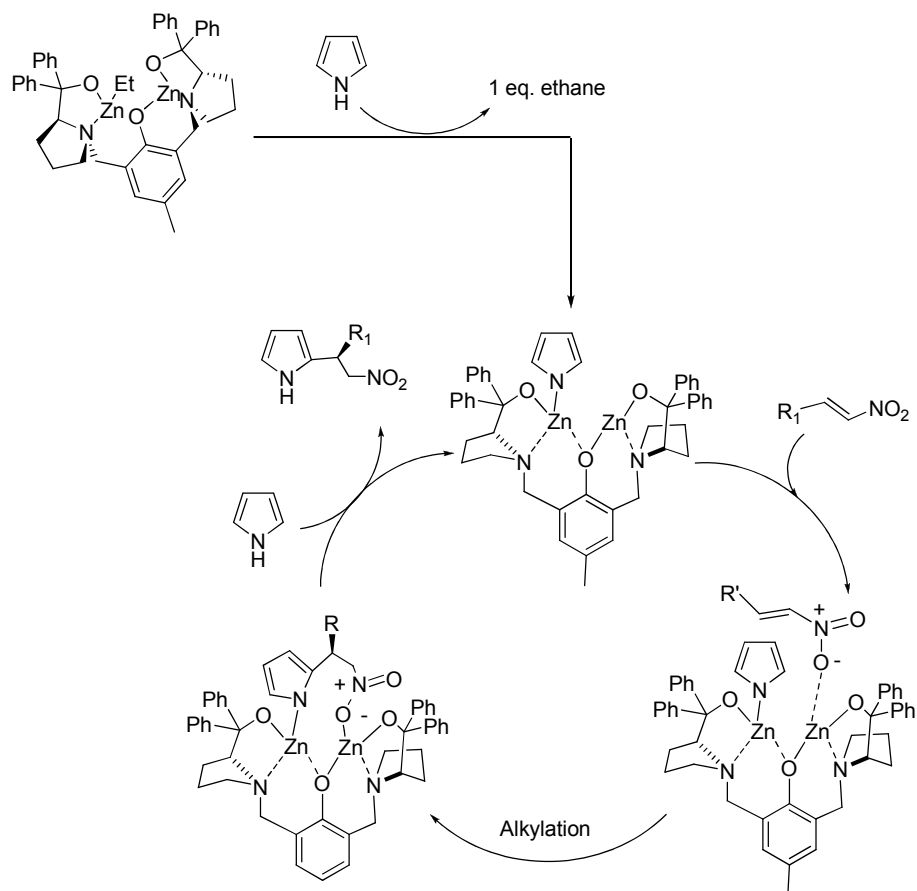
(s)-*t*-Bu-BOX-Cu(OTf)₂ (Eq 18).¹⁹ Compared with Jorgensen's results, Linden's report shows higher yield and ee value.



Muller also reported the asymmetric Friedel-Crafts alkylation of pyrroles with nitroalkenes by using a binuclear zinc catalyst (Eq 19).²⁰



For this reaction, various nitroalkenes were reacted with the pyrrole. When aromatic substitutes were used, in all these cases, excellent enantioselectivities were obtained, which ranged from 87% for the *o*-methoxy substrate to 97% for the tolyl substituent compound. The position of the methoxy-substituent of compounds did not affect either the reactivity or the selectivity of the reaction. An improvement of the yield was observed by using a furanyl substituent.



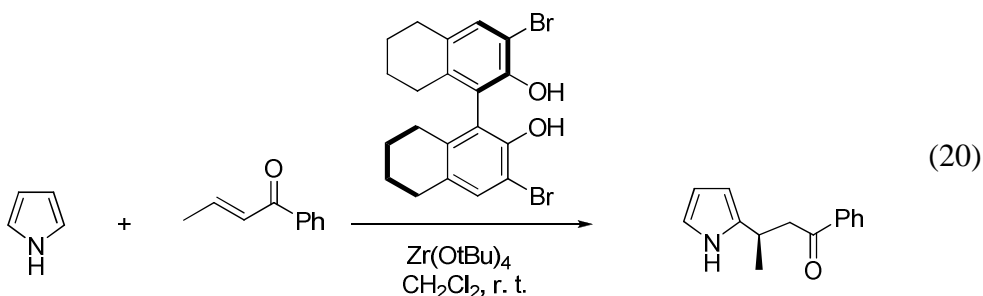
Scheme 5. Proposed the Mechanism for the Reaction of Nitroalkenes and Pyrroles

He proposed a mechanism for this type reaction that involves the deprotonating of pyrrole by Zinc complex accompanied by the formation of one equiv of ethane (Scheme 5). The nitroalkene coordinates to zinc catalyst and undergoes the alkylation reaction. The catalytic cycle closed by a proton exchange with an incoming pyrrole to release the product and reform the active catalyst.

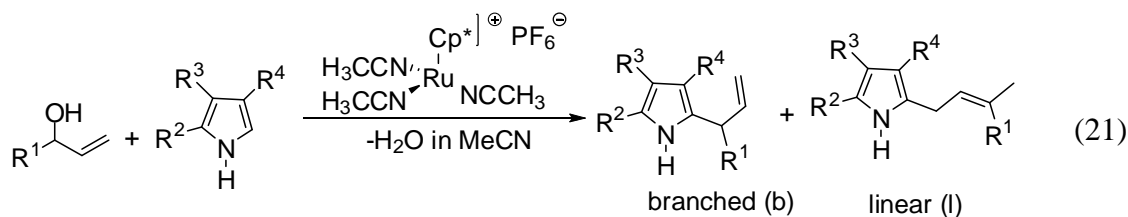
Muller demonstrated the use of the binuclear zinc bis-ProPhenol complex in an atom economic Friedel-Crafts reaction of unprotected pyrroles with a variety of

substituted nitroalkenes to give both mono- and disubstituted pyrroles. The reactions gave excellent stereoselectivities in most cases.

Pedro has reported that the complexes of BINOL-based ligands with $Zr(O^tBu)_4$ catalyze the Friedel-Crafts alkylation reaction of indoles and pyrroles with nonchelating β -substituted α, β -enones at room temperature affording the expected products with good yield and above 95% ee in most case (Eq 20).²¹

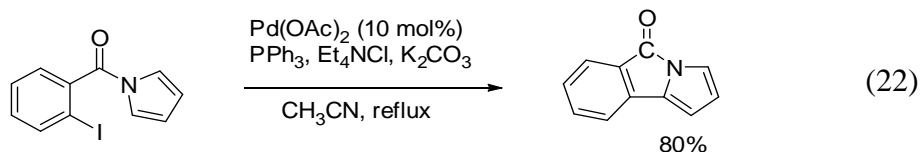


Due to the usefulness on the synthesis, transition- metal catalyzed allylation chemistry continues to draw attention. The allylation reactions can be carried out by using allyl carbonate or acetates together with palladium, molybdenum or iridium. Cationic Ru-allyl and vinylidene complexes have been successfully utilized as catalysts for allylation and alkenylation of indoles and pyridine derivatives, respectively.²² Recently Pregosin reported that several Ru(IV) rather than Ru(II)-allyl catalysts readily tolerate alcohols as substrates in acetonitrile solution.²⁴ They found that the reactions are fast and highly regioselective allylation of pyrrole compounds by allyl alcohols using Ru-Sulfonate as the catalyst (Eq 21).²³

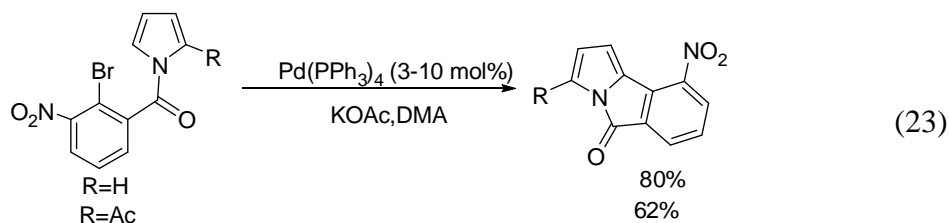


In this reaction, R^1 can be Ph, 1-naphthyl, mesityl, *o*-MeO-C₆H₄-, *o*-Me-C₆H₄-, *o*-Cl-C₆H₄-, R^2 can be Et and Me, R^3 and R^4 can be H, Me and Et. All the reaction can be done in almost 5-7 min with high conversions. In most case, the others only got the branched product, when R^1 = Ph, R^2 = Me, R^3 = H, R^4 = Me, the ratio of l/b= 1/12, R^1 = Ph, R^2 = Me, R^3 = Et, R^4 = Me, the ratio is 1 to 22.

Grigg reported the first example of the direct arylation of pyrroles using a tethered aryl iodide under palladium-catalyzed conditions (Eq 22).²⁴

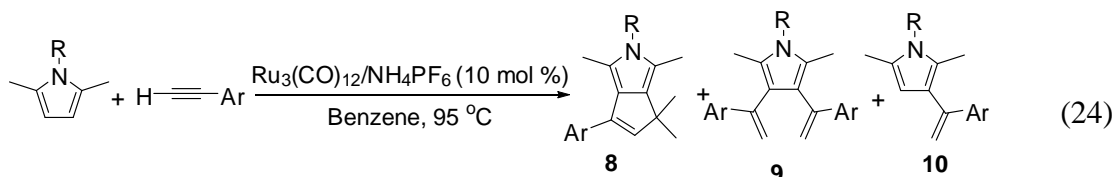


The utility of this type of cyclization has been applied to the synthesis of the core structure of lamellarin as well as a library of potent cyclin-dependent kinase inhibitors (Eq 23).²⁵



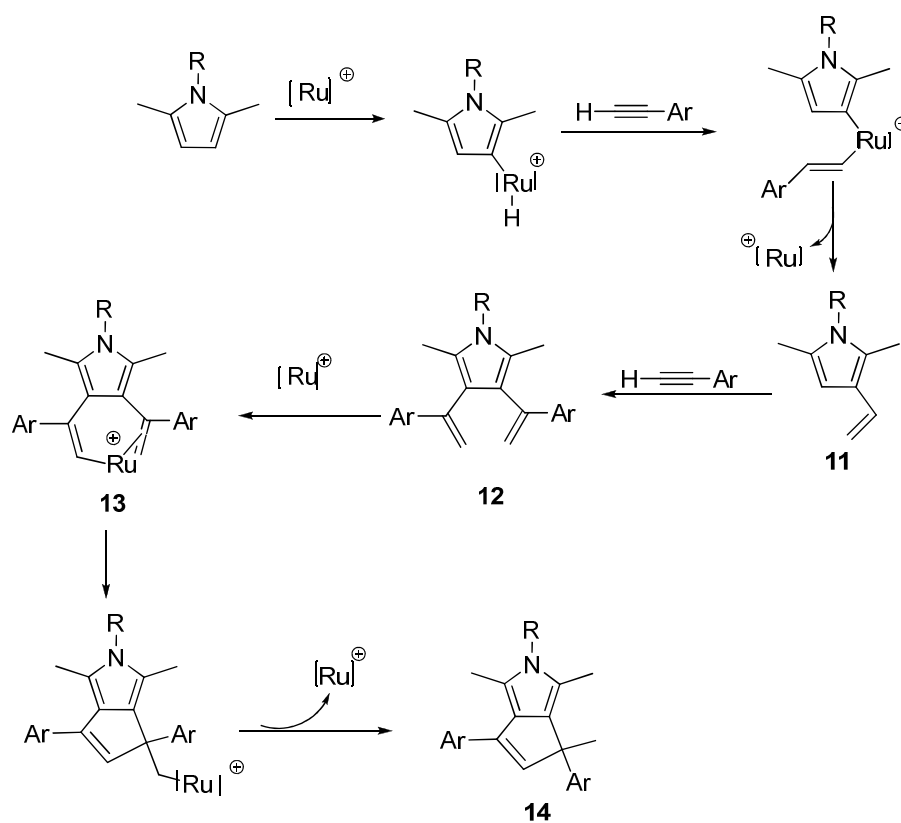
An additional example of the power of this methodology was demonstrated by Trauner during the total synthesis of rhazinilam.²⁶ Cyclization of aryl iodide onto the pyrrole was carried out using catalytic palladium and Buchwald's Davephos ligand to give the desired rhazinilam precursor. They reported that the introduction of a MOM protecting group proved necessary to avoid deiodination of the starting material, presumably via protonation of a stable palladacycle intermediate.

Recently, our group developed a new catalytic coupling reaction between 2,5-disubstituted pyrroles and terminal alkynes which involves multiple C-H bond activation and cyclization steps (Eq 24).²⁷



The formation of both 1:1 and 1:2 products suggested that product 1 is resulted from the cyclization of 1:2 coupling product 2. Through the kinetic studies, we got the $k_{\text{obs}} = 2.1 \times 10^{-2} \text{ h}^{-1}$. The coupling reaction of 1,2,5-trimethylpyrrole with deuterated 4-ethynylanisole- d_1 (2.0 equiv.) in the presence of $\text{Ru}_3(\text{CO})_{12}/\text{NH}_4\text{PF}_6$ in C_6D_6 shows that nearly 15% of the deuterium from 4-ethynylanisole- d_1 had exchanged with 35% of the β -vinyl hydrogen of the unreacted 1,2,5-trimethylpyrrole, prior to the formation of the coupling products. The product from this reaction contained deuterium at both the α -methyl (33%) and vinyl (37%) positions. Also in supported of the rapid H/D exchange

between the two substrates, a relatively small deuterium isotope effect was observed from a separate reaction of 1, 2, 5-trimethylpyrrole with phenylacetylene/phenylacetylene- d_1 when forming 1:1 coupling products. The pseudo first-order plots for the reaction gave $k_{\text{obs}} = 1.65 \times 10^{-2} \text{ h}^{-1}$ and $1.38 \times 10^{-2} \text{ h}^{-1}$, which translated into $k_{\text{H}}/k_{\text{D}} = 1.2$.



Scheme 6. Proposed Mechanism for the Coupling Reaction of Pyrroles and Alkynes

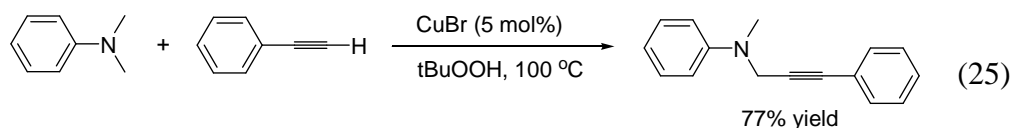
We proposed the mechanism which involving sequential alkyne insertion and cyclisation steps (Scheme 6).

The sequential C-H activation and regioselective insertion of alkynes would be mediated by an electrophilic ruthenium catalyst to form 1:2 coupling product **12**. The subsequent ruthenium-mediated vinyl C-H bond activation and cyclization steps should be facilitated by coordination of the adjacent olefin to ruthenium via the formation of alkene-hydride species **13**. Cyclization and reductive elimination would give the product **14**.

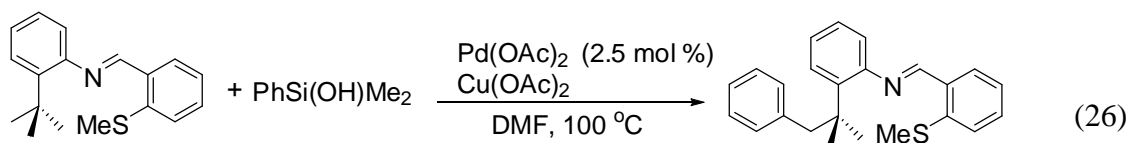
1.2.2 C-H Bond Activation of pyridine and other Nitrogen Containing Compounds

Direct oxidative functionalization of tertiary amines is important both enzymatically and synthetically. Propargylic amines are of great pharmaceutical interest and are synthetic intermediates for the synthesis of various nitrogen compound as well as carbohydrates. Li has reported an effective CuBr-catalyzed oxidative cross coupling of amines and alkynes via a direct C-H bond alkylation.²⁸

The reaction of N,N-dimethylaniline with phenylacetylene in the presence of a CuBr Catalyst and tert-butyl hydroperoxide to give the product in 77% isolate yield (Eq 25).

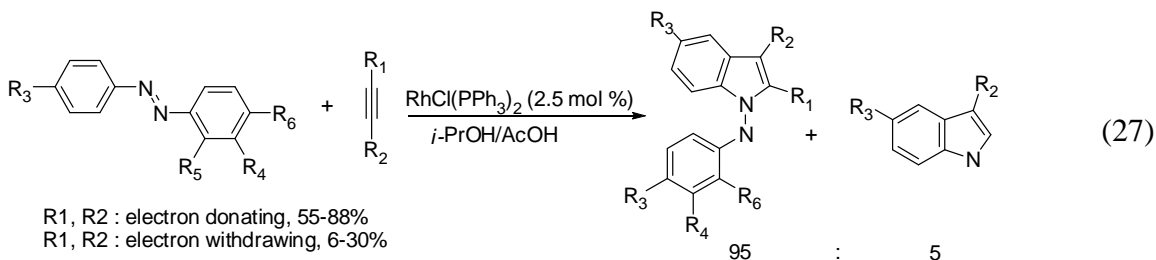


Sames has developed a new system for catalytic arylation and alkenylation of alkane segments (Eq 26).

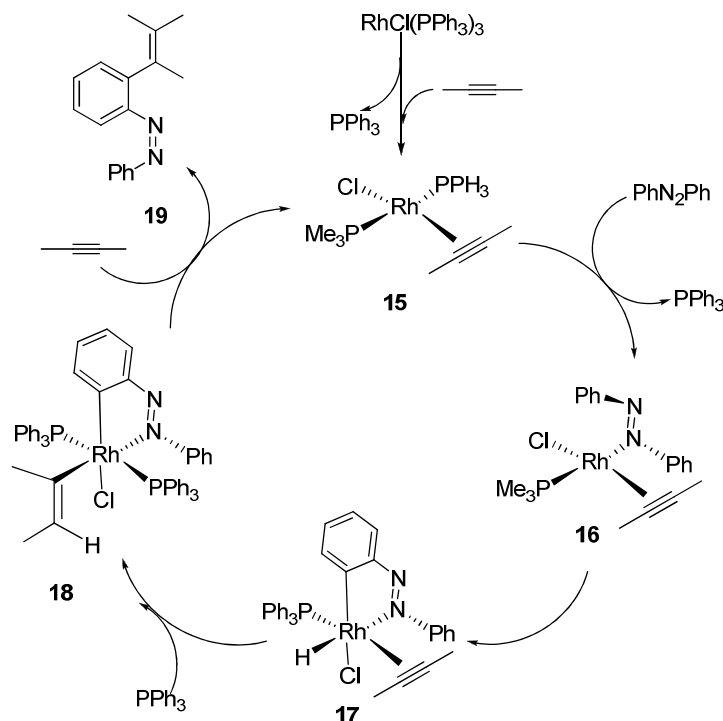


The *ortho-tert*-butylaniline substrates and 2-pivaloylpyridine may be arylated and alkenylated at the *tert*-butyl group, while no functionalization occurred at more reactive C-H and other bonds.²⁹ Arylation and alkenylation of these substrates are achieved in the presence of Ph₂Si(OH)Me and PHCHCHSi(OH)Me₂, with a catalytic amount of Pd(OAc)₂ and stoichiometric oxidant Cu(OAc)₂ in DMF. He hypothesize that the high selectivity of this system stems from the confluence of directing effect of the Schiff base and unique reactivity properties of phenyl-palladium acetate species.

The addition of 1, 2-diarylazenes to aliphatic or aromatic internal alkynes in the presence of catalytic amount of Wilkinson's catalyst afforded N-(arylamino) indole derivatives (Eq 27).



Isolated yields were in the range of 55-85% for symmetrically substituted alkynes with electron-donating substituent. Asymmetrically substituted alkynes and all alkynes with electron-withdrawing substituent gave yields in the range of 6-30%.³⁰

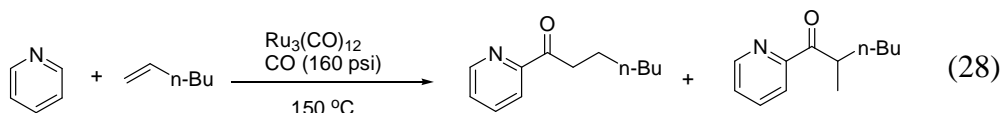


Scheme 7. Proposed Mechanism for the Formation of N-(arylamino) Indole

The mechanism is believed to be essentially the same as that for the olefin hydroarylation. Thus, the key steps are *ortho*-metalation of the diazene followed by insertion of the alkyne into Rh-H bond and reductive elimination to afford the intermediated **19**. This mechanism is substantiated by H NMR experiments. In this particular case, the kinetic measurements tended to show the rate-determining step is the

formation of the cyclometalated complex **17** instead of the usual reductive elimination step.

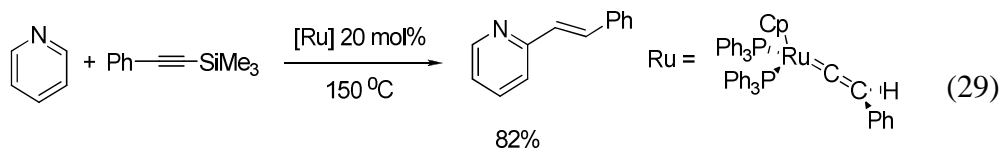
$\text{Ru}_3(\text{CO})_{12}$ has been reported to selectively activate the *ortho* positions in pyridine. In a typical reaction, pyridine is employed as a solvent and the reaction is conducted at 150 °C under 150 psi of CO_2 . Conversion of 1-hexene to pyridyl ketone mixture results in the high regioselectivity of the reaction (Eq 28). In addition, no other pyridine-containing products are observed.³¹



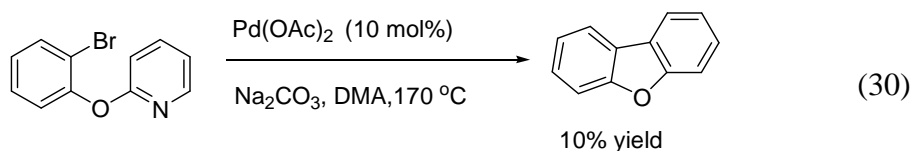
Murakami has reported the alkenylation reaction of pyridine.³² Heating a cationic ruthenium vinylidene complex $[\text{CpRu}(\text{=C}=\text{CHR})(\text{PPh}_3)_2] \text{PF}_6$ in pyridine at 100-125 °C for 24 h affords (E)-2-alkenyl pyridine. Initially, pyridine coordinates to ruthenium by displacement of one of the phosphine ligands. Then, [2+2] heterocycloaddition occurs to form a four-membered ruthenacyclic complex. Deprotonating of the β -hydrogen affords a neutral π -allyl complex. Protonolysis furnishes the product. As a result, a vinylidene group is inserted into the α -C-H bond of pyridine. The alkenylation reaction is made catalytic in ruthenium by using (alkyn-1-yl) silane as the vinylidene source.

Treatment of (alkyn-1-yl) trimethylsilane with pyridine in the presence of a cationic ruthenium complex $[\text{CpRu}(\text{=C}=\text{CHR})(\text{PPh}_3)_2] \text{PF}_6$ affords the corresponding (E)-2-alkenylpyridine not only in a good yield but also in a region and stereoselective

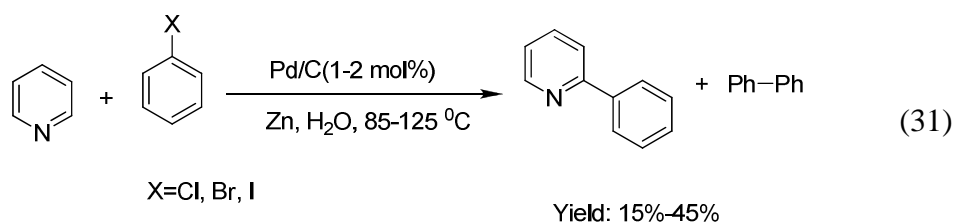
manner (Eq 29).



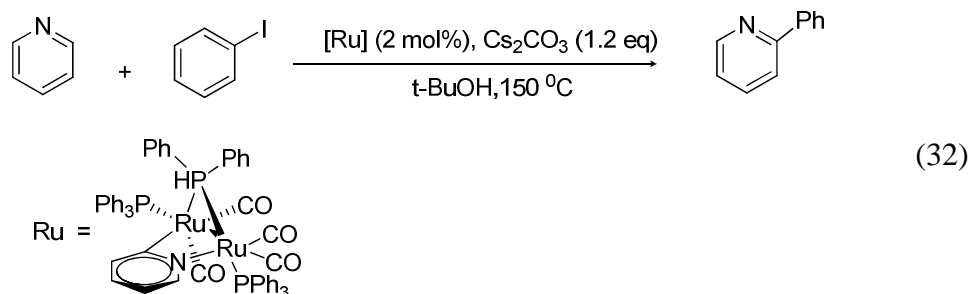
Ames reported the first intramolecular direct arylation reaction involving pyridine in the early 1980s. In this example, treatment of 2-(2-bromophenoxy)pyridine with $\text{Pd}(\text{OAc})_2$ and Na_2CO_3 afforded the tricyclic compounds in a low 10% yield (Eq 30).³³



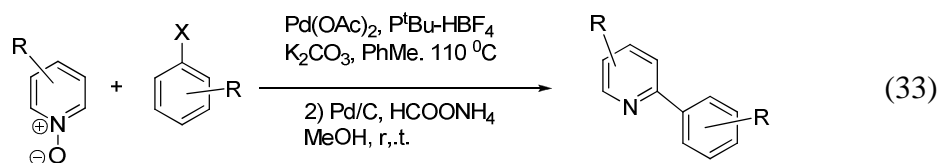
Due to the pyridine moiety is a key component of pharmacophores, natural products and synthetic building block. Many groups work on pyridine reactions. Sasson has reported that the access to 2-arylpyridines via an intermolecular coupling has been achieved using palladium on charcoal in the presence of zinc metal in water (Eq 31).³⁴



Later, Sames reported that direct and selective catalytic arylation of α -C-H bond in pyridine with iodobenzene was achieved in up to 70% yield (Eq 32).⁸⁹

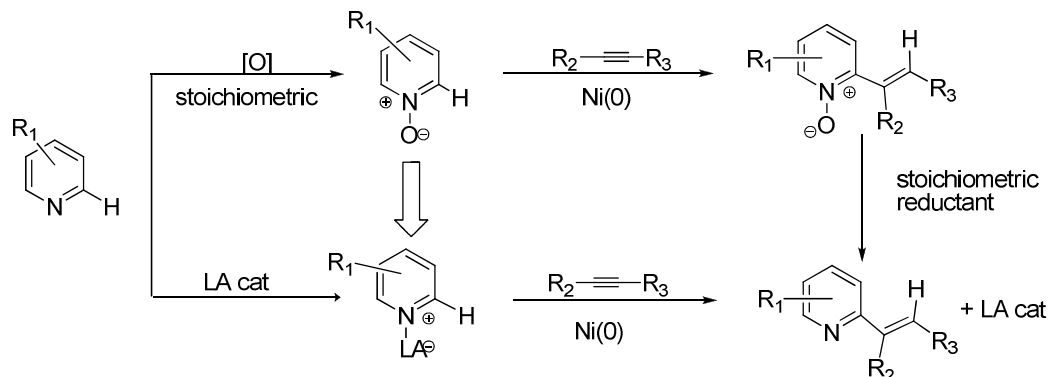


Recently, Fagnou reported that the direct arylation reactions of pyridine N-oxides occur in excellent yield with complete selectivity for the 2-position with wide range of aryl bromides (Eq 33).³⁵ In these reactions, palladium acetate in combination with tri-tert-butylphosphine emerged as the optimal metal-ligand combination.



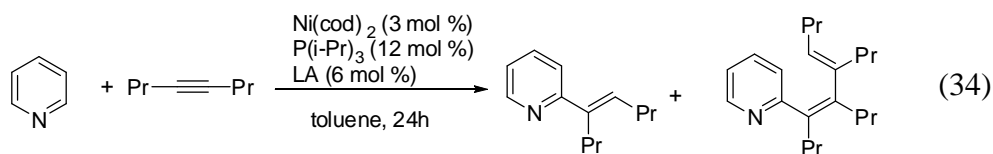
In contrast to reactions performed with many types of organometallics, these reactions are completely insensitive to the presence of water since 5.0 equiv. of water added at the reaction outset has no deleterious impact on the reaction outcome. From these example, they found that these reaction involving pyridine need harsh conditions of over 150 °C, and limited to the scope of substrates, and also require the presence of a direction group or employs N-oxide. Recently, Hiyama reported the C-2 alkenylation of pyridine by mild nickel catalysis.³⁶ Since the enhance reactivity of pyridine-N-oxides compared with that of parent pyridine, is apparently attributed to an electron-deficient nitrogen that increase the acidity of the C-2 bond, they also reported a similarly activated pyridine species be generated catalytically in situ by the coordination of the nitrogen to a

Lewis acid(LA) catalyst (Scheme 9). They have reported a combination of nickel and LA catalyst allows the direct C-2 alkenylation of pyridine under mild conditions. Moreover, the single or double insertion of alkynes into the C-2-H bond of pyridine is successfully controlled by simply changing the LA catalyst.



Scheme 8. Mechanism for Alkenylation of Pyridine by Mild Nickel Catalysis

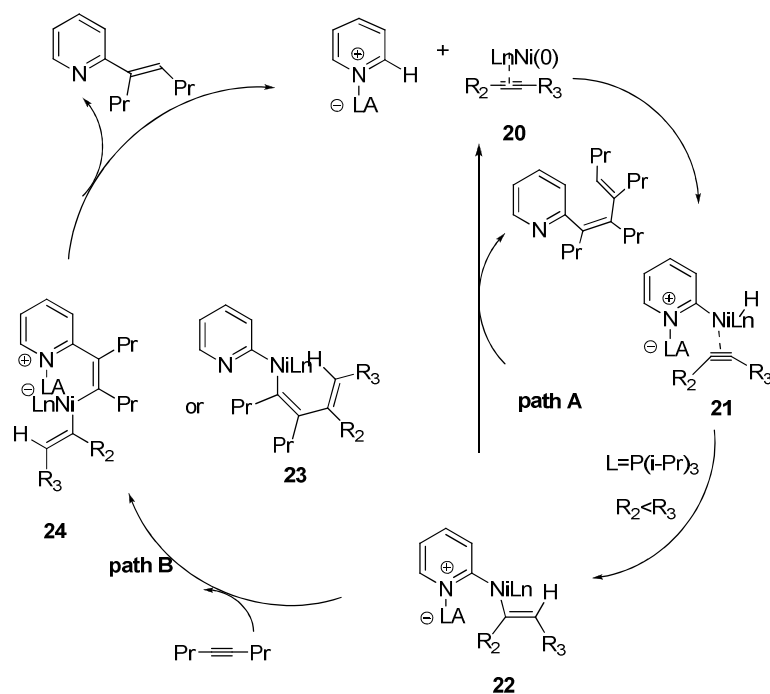
In this report, he found that the zinc and aluminum catalysts with mild Lewis acidity were highly effective for the alkenylation of pyridine (Eq 34).



He also gave the plausible Mechanism for this reaction. The pyridine activated by coordination to a LA would be responsible for the oxidative addition of the C(2)-H bond to nickel(0) species **20**, a plausible initiation step of the present catalysis.

Hydroniclation across the alkyne coordination to the nickel center in the direction avoiding a steric repulsion between the bulkier R3 and the pyridyl group in B takes place

to give **22**, which upon reductive elimination affords the product in the presence of zinc LA catalyst (**path A**). The use of AlMe_3 , a strong Lewis acid than dioranzincs, or lower reaction temperature retards the reductive elimination and /or promotes the second insertion of an additional alkyne into either of the C-Ni bonds in **22** to give **23** or **24**, resulting in the formation of the product in the **path B**.

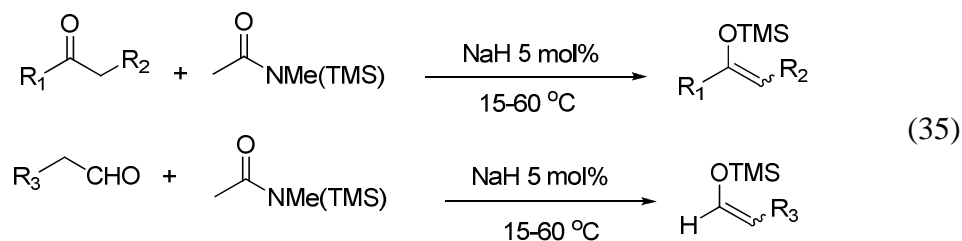


Scheme 9. Mechanism for Alkenylation of Pyridine by Mild Catalysis

1.3 The Formation of Silyl Enol Ether Involving C-H Bond Activation

Due to silyl enol ethers are widely employed in the organic synthesis as the

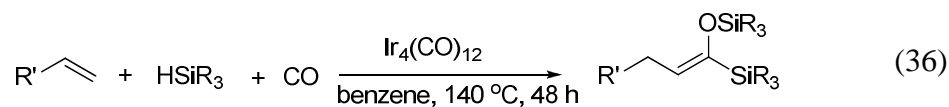
reactive precursors for carbonyl compounds, they are useful in various synthetic transformations in a variety of regio-, chemo- and stereo- selective reactions.³⁷ Over the past decades, many methods to generate the enol silyl ethers were reported, one of the early and still one of the mostly frequently used route to (E) or (Z)-silyl enol ethers is the trapping of ketone or aldehyde enolates generated under the kinetics or equilibrium-control conditions.³⁸ And another mostly used methods are using chlorosilans with amine as triethyl-amine and amide (as LDA) agent. Although these methods work well, there still remains a need to look the alternative method with improved efficiency and can work for an elaborate and practical scale synthesis by generating less waste. Recently, Tanabe and co-workers reported a new method to generate enol silyl ethers from ketone and aldehydes (Eq 35).³⁹



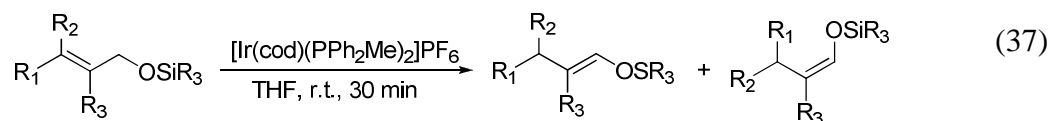
Tanabe and the co-workers used NaH to catalyze the reactions under mild conditions, comparing with the silyl halide method which requires a slightly tedious work-up procedure to remove HX, their neutral reaction conditions have a practical advantage of easy isolation of enol silyl ethers.

Due to the convenience and straightforward of the transition-metal catalyzed isomerization of the allyl ether, which can generate the silyl enol ether,⁴⁰ many metal

complexes have been reported to synthesize the silyl enol ethers.⁴¹ Recently, Murai reported the conversion of alkenes to the enol silyl ether by using the iridium carbonyl complex,⁴² which involves the reactions of the alkenes with a hydrosilane and carbon monoxide to yield the enol silyl ether of acylsilans. These reactions generate the (*E*) and (*Z*)-products, in the most case, the (*E*) isomers are the major (Eq 36).



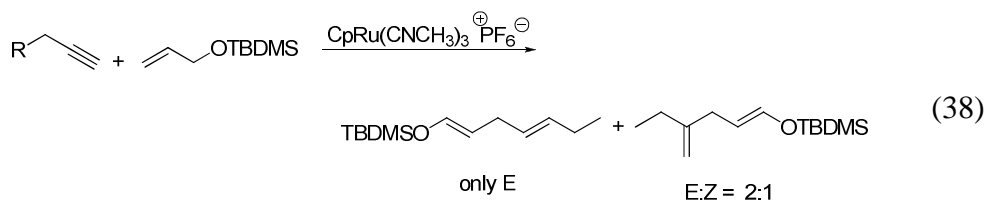
Due to the high temperature and the high pressure of carbon monoxide (50 atm at 25 °C), the reactions require the high pressure tube and some content, it is unsafe for the people working with the experiments. Later on Milyaura reported the stereoselective synthesis of the silyl ethers catalyzed by iridium COD complex under the mild conditions (Eq 37).⁴³



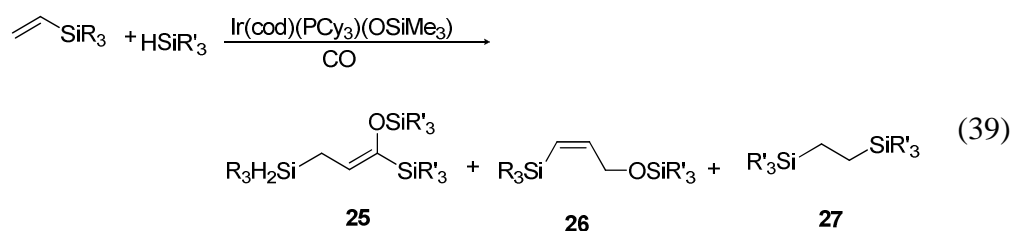
For the less bulky substitutes, the reactions all were carried out the room temperature and showed the high conversion and the selectivity, but when using more bulky groups as phenyl ether, the reaction was very slow. These results may due to the steric hindrance to the coordination to the iridium center. In the report, they also gave the proposed mechanism for the isomerization reaction. This mechanism involves the oxidative addition of an allylic C-H bond to the iridium complex to give the ally iridium

intermediates, and next go through the reductive elimination to afford enol ether. In the mechanism, they also mentioned that the isomerization involves two processes: the first and selective formation of the *E* isomer is the kinetically control process, and then following is the equilibration to give a mixture of the (*E*) and (*Z*) isomers. This process can be retarded in a solvent that strongly coordinates to the metal center, but they are fast in the solvent which have the medium donor strength such as CH₂Cl₂ and acetone can favor the formation of the mixture. So they motioned that the formation of the product was highly dependent on the catalyst, the solvent, reaction time and also the substitutes.

As the important synthetic intermediates, the enol silyl ether can be used in the carbon extension reactions. Three carbon chain extensions of the alkynes to geometrically define enol silyl ethers requires stoichiometric conversion to a vinyl halide followed by a heck reaction or to a vinyl organometallic followed by conjugate addition. Recently, Trost reported a simplified protocol to affect a direct catalytic three-carbon chain extension of alkynes to *E*-enol silane (Eq 38) by using ally silly ether.⁴⁴



Marciniec reported the silylcarbonylation of vinylsilanes catalyzed by iridium siloxide complexes (Eq 39).⁴⁵



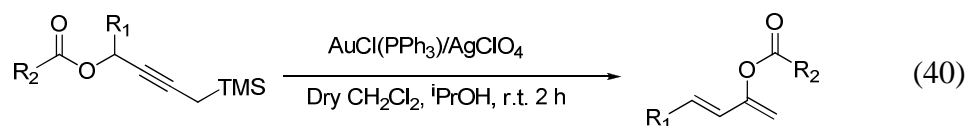
In this reported, the yields of the silylcarbonylation products depends strongly on the reaction conditions such as the ratio of substrates and pressure of the carbon monoxide, as well as the loading of the catalyst.

1.4 Alkyne C-H Bond Activation

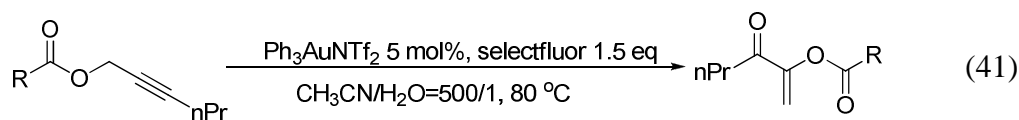
1.4.1 The Formation of Enol Esters from the Coupling Reactions of Alkynes and Carboxylic Acids

Enol esters are a versatile class of precursors for a variety of synthetically important organic transformations such as cycloaddition,⁴⁶ asymmetric hydrogenation,⁴⁷ C-C bond coupling,⁴⁸ and Aldol- and Mannich-type of condensation reactions.⁴⁹ Since enol esters can also serve as a synthon for aldehydes and ketones, much research efforts has been devoted to develop efficient catalytic methods to control both regio- and stereoselectivity in forming substituted enol esters. From an industrial perspective of increasing synthetic efficiency and tolerating functional groups as well as for reducing

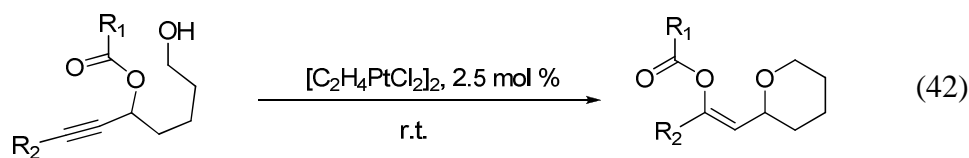
waste byproducts, catalytic methods for producing enol esters are highly desired compared to the classical methods that utilize stoichiometric amounts of strong base or toxic Hg salts.⁵⁰ Recently Zhang reported the synthesis of enol esters by using gold complexes as catalyst (Eq 40).⁵¹



Later on the same author reported the homogeneous oxidative C-O bond formation by using the different gold catalyst (Eq 41).⁵²

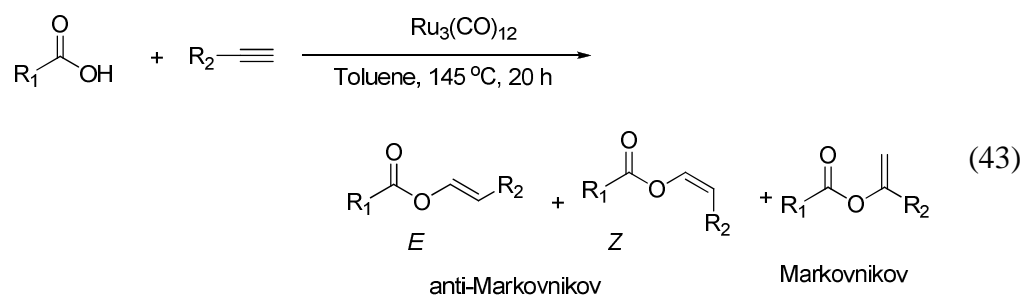


Qian recently reported that the cycloetherification of hydroxyl propargylic esters by using the Au(I) and Pt (II) complexes (Eq 42).^{24d}



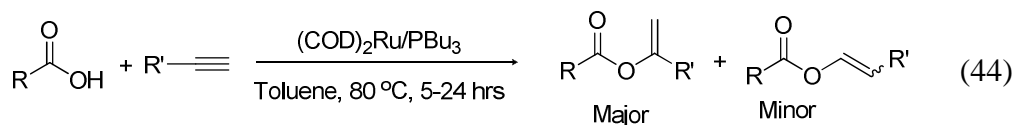
There are also some other examples on the catalytic synthesis of enol esters such as Zr-catalyzed methyl alumination of alkynes,⁵³ Au-catalyzed intramolecular rearrangements of propargylic esters and alcohols⁵⁴ Cu-catalyzed oxidative esterification of aldehydes with β -dicarbonyl compounds,⁵⁵ and asymmetric couplings of ketenes with aldehydes by chiral Fe catalysts.⁵⁶

Transition metal-catalyzed alkyne-to-carboxylic acid coupling reaction offers an attractive route to enol esters, there has also been a large amount of work on the additions of carboxylic acids to alkynes to form enolesters. the first report describing this reaction dates back to 1983 by Youval Shvo,⁵⁷ in this report, $\text{Ru}_3(\text{CO})_{12}$ was used to catalyze the coupling reaction of aliphatic and aromatic carboxylic acid to di- and mono-substituted acetylene and they got the anti-markovnikov (*E* and *Z*) and Markovnikov product by 10 examples with 40% - 95% conversion (Eq 43).

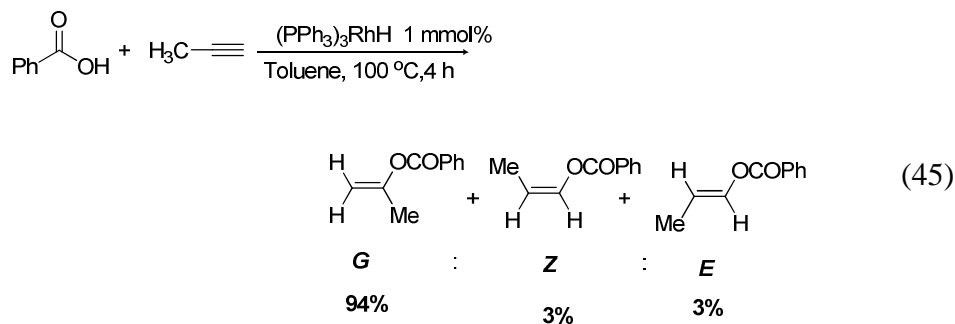


Later on the process has been developed by Mistsudo,⁵⁸ Dixneuf,⁵⁹ and Verpoort,⁶⁰ although other groups have been and still involved in this field. But its synthetic potential has not been fully realized in part because the catalytic method typically produces a mixture of *gem*- and (*E*)/(*Z*)-enol ester products. Considerable research has been devoted to control both regio- and stereoselectivity in forming the enol ester products by modulating steric and electronic nature of the metal catalysts. Generally, late transition metal catalysts have been found to be effective for the coupling reaction to produce a mixture of (*E*) - and (*Z*)-enol esters from *anti*-Markovnikov

addition of carboxylic acids to terminal alkynes over *gem*-enol ester products.⁶¹ The regioselectivity of the Markovnikov addition has been significantly increased by using a variety of ruthenium precursors such as $(C_5H_5)_2Ru$, $(arene)RuCl_2(PR_3)$.⁶² Mitsudo used bis (C_5H_5) ruthenium (PBu_3) as the catalyst, and they found that for the linear alkynes such as 1-hexyne and 1-pentyne the reactions showed high selectivity for Markovnikov addition to give the *gem*-enol esters. For other substituted alkynes such as phenylacetylene addition of acetic acid gave Markovnikov and anti-Markovnikov products and yields were around 55 % (Eq 44).⁶³

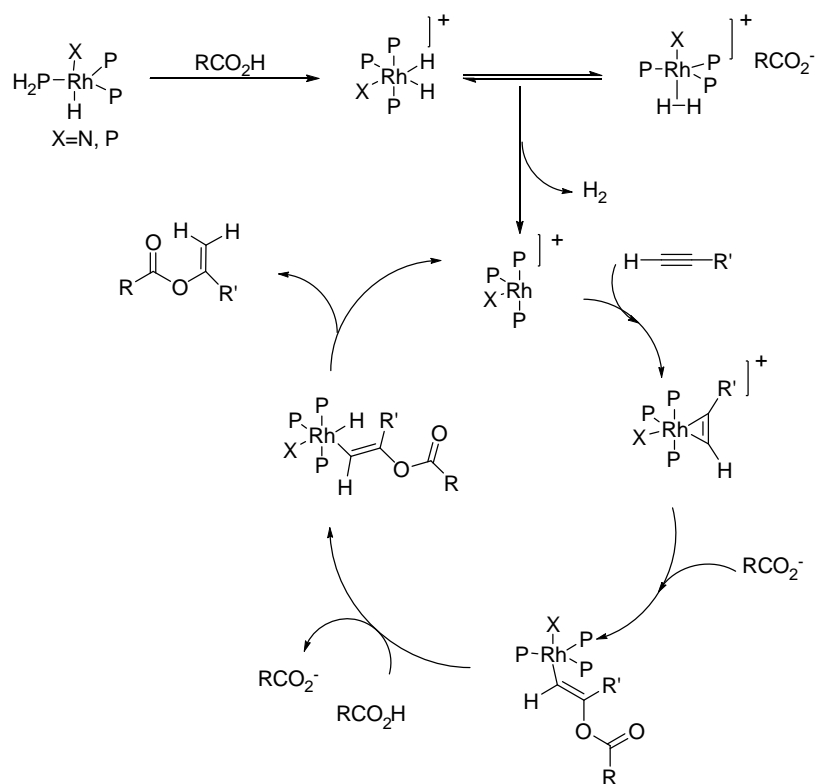


Mitsudo used the bis (C_5H_5) ruthenium-P $(n-Bu_3)$ to generate the geminal product as the major. Other groups are still working on this type of reaction to get the regioselective formation of *gem*-enol esters by using a variety of metal complexes such as mercury (II), silver (I), rhodium (I) and palladium (II). And the regioselective formation of *gem*-enol esters has recently been achieved by using cationic Rh catalysts.⁶⁴ Bianchini and Dixneuf got the regioselective formation of 2-(benzyloxy) propene from the addition of benzoic acid to propyne in the presence of the trigonal-bipyramidal Rh(I) monohydrides $(PPh_3)_3RhH$ and $(NP_3)_3RhH$ and they were the first group to show the mechanism study on this reaction (Eq 45).



The proposed catalysis cycle for the coupling reaction of carboxylic acid and alkynes was given by Dixneuf (Scheme 10). Firstly, the rhodium (III) dihydride complex was detected by NMR by the reaction of rhodium phosphine complex with the carboxylic acid at the room temperatures. Dixneuf assumed this was the starting point of the catalysis cycle, and the 16- electron systems $[(\text{L})\text{Rh}]^+$ was the real catalyst. And then by using rhodium (III) dihydride compound to react with alkyne they detected the H_2 by the GC and get the Rh(I) alkenyl complex that may form upon nucleophilic attack by carboxylate at alkyne. This Rh(I) alkenyl complex is ready to be protonated at the metal by a second molecule of carboxylic acid. Then with the elimination this cycle generates the geminal product and the 16-electron fragment $[(\text{L})\text{Rh}]^+$ are regenerated and the catalysis cycle can continue.

Among these methods all showed high regioselectivity for the Markovnikov addition to form the *gem*-enol esters, but no general preparation of alk-1-en-1-yl esters corresponding to an *anti*-Markovnikov addition of the carboxylic acid to the triple bond was discovered.

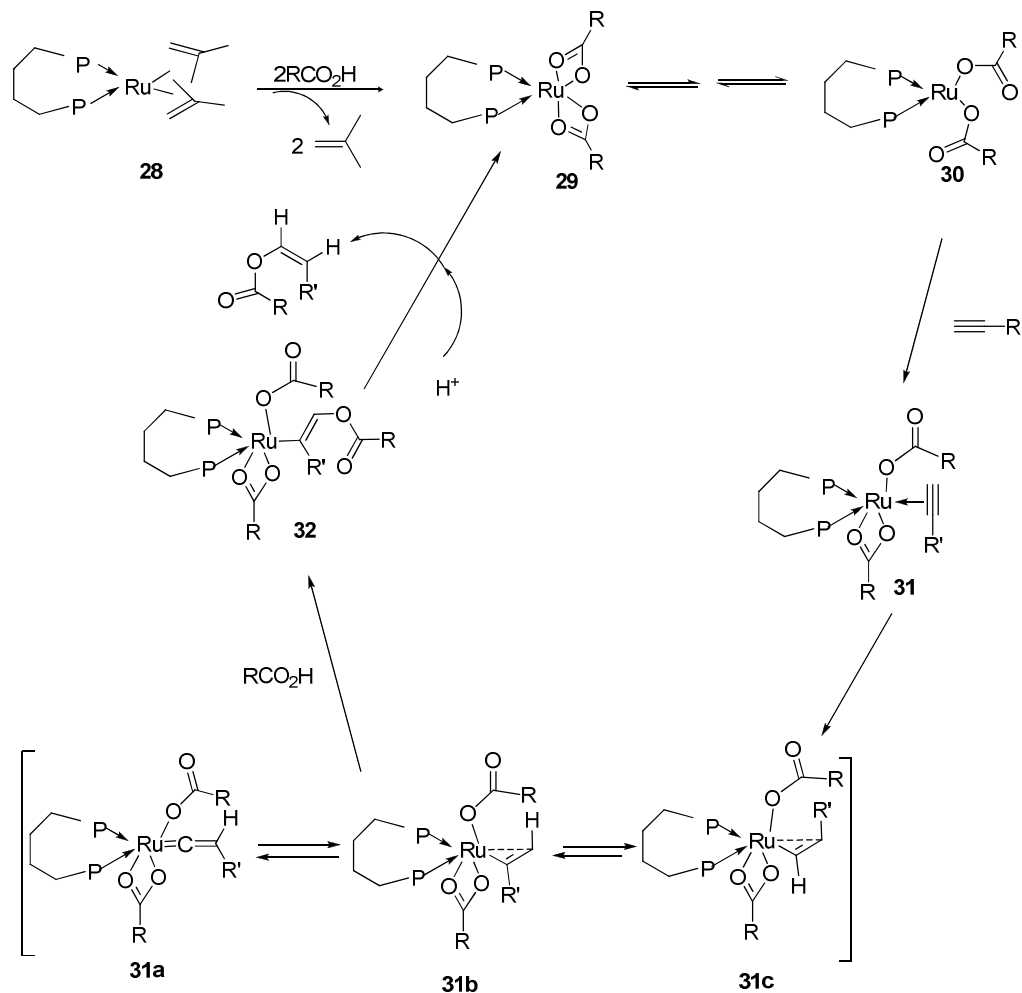


Scheme 10. Proposed Mechanism for the Reaction of Carboxylic Acid and Alkynes

Doherty tried to control the selectivity for the formation of the anti-Markovnikov addition product by changing the ligands of the ruthenium complexes, although they could get the (*Z*)-isomers as the major, they still got mixtures of three products. Dixneuf and co-workers work on the formation of enol ester reaction since 1995,²⁴ they got three mixtures at their first report on this type reaction, and later on they focused on the study on the regioselectivity of the this type reaction in presence of ruthenium complexes by changing the ligands. Recently they showed the relationship between steric environment of the ruthenium-phosphine catalysts and the stereoselective formation of the (*Z*)-enol

esters.⁶⁵ They reported that modification of the active ruthenium (II) center by coordination of a chelating diphosphine and labile allylic ligands in complexes $(\text{Ph}_2\text{P}(\text{CH}_2)_2\text{PPh}_2)\text{Ru}(\text{methallyl})_2$ provides suitable catalyst precursors for the *anti*-Markovnikov addition of carboxylic acid to terminal alkynes to stereoselectivity afford (Z)-alk-1-en-yl esters.

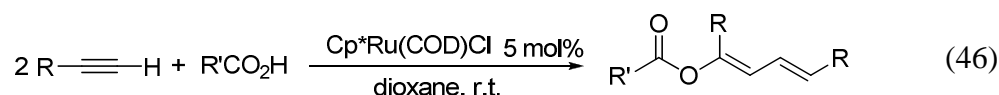
This ruthenium compound **28** was used to demonstrate the mechanism of this reaction (Scheme 11). In presence of carboxylic acid at the reaction temperature, a ligand exchange took place from the ruthenium complex **28** and gave the new ruthenium complex **29**. The addition of benzoic acid to hexyne, carried out at 65 °C for 3 hours in the presence of 1 mol % of compound **29** as catalyst precursor, led to a complete conversion of the starting materials and formation of (Z)-hex-1-en-1-yl benzoate in 97% selectivity. Moreover this complex **29** was recovered at the end of the reaction and thus appeared to be the actual catalyst precursor or the catalyst itself. Based on these observations, they proposed that the first step is the ligand substitution of the allylic group by the carboxylates with elimination of isobutene to produce complexes **29**, a rearrangement of the carboxylate to get complex **30** would make possible the coordination of the alkyne to give intermediate **31**.



Scheme 11. Proposed Mechanism for the Coupling Reaction of Carboxylic Acid and Alkynes by Ruthenium Complex

From this intermediate, several resonance forms (**31b** and **31c**) and the vinylidene tautomer **31a** can be postulated, depending on the ancillary bidentate ligands. The external addition of the carboxylate to the electrophilically activated C (1) of the alkyne might then take place to form the intermediate **32**. On subsequent protonolysis of the Ru-C bond, or protonation of the ruthenium center followed by reductive elimination, the

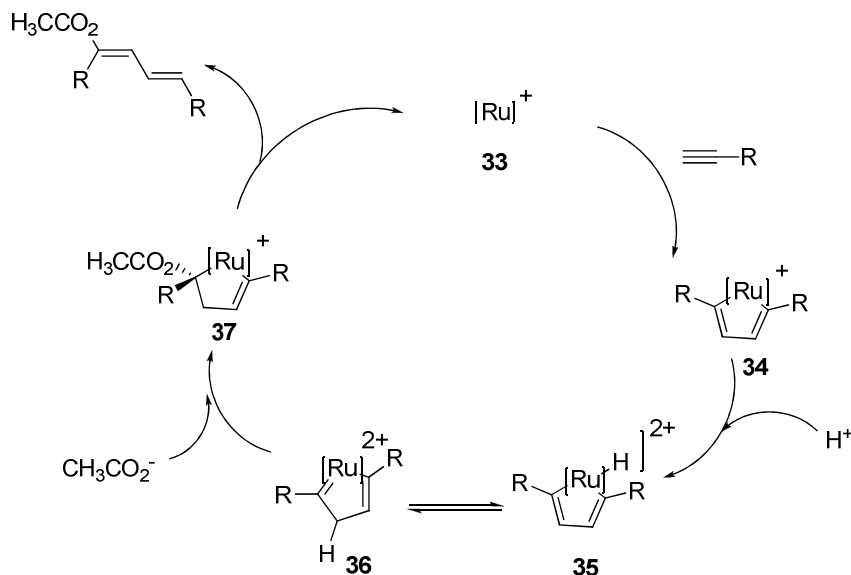
alkyl ester is liberated. The regioselectivity of the reaction may depend on the electron deficiency of the coordinated triple bond. Its polarization according to **31b** with a positive charge at the unsubstituted carbon atom of the alkyne due to electronic effects of the diphosphine ligand, or the formation of the tautomeric ruthenium –vinylidene complex **32**, easily formed from a terminal alkyne and ruthenium complex, would favor the addition of the carboxylate at the electrophilic of C (1) of the terminal alkyne. Due to the steric interactions between the diphosphine ligands and the substituted the formation of (Z)-isomers suggested a ruthenium intermediated of type **32**, which on protonation would lead to a formal *trans*- addition of carboxylic acid to the terminal alkyne is low with catalyst **28** (Eq 46).⁶⁶



This reaction is proposed to proceed via metallacyclopentadiene intermediate **34**. Protonation of ruthenium complex **33** followed by addition of the carboxylate produces ruthenacyclopentene **37**.

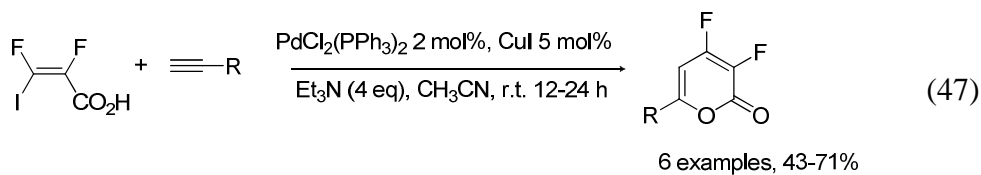
A $\hat{\alpha}$ -hydrogen elimination of Ha followed by a reductive elimination releases the 1,3-diene product and regenerates the active ruthenium catalyst (**33**). For example, aryl alkyne and acetic acid combine to form 1,3-dienyl ester in 85% yield. Another potential mechanism for this reaction involves the *trans* addition of a carboxylic acid catalyzed by ruthenium to generate a vinyl ruthenium which generates *cis* carbometalation of another

alkyne.



Scheme 12. Proposed Mechanism for the Formation of Dienyl Esters

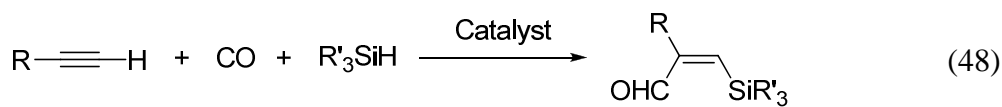
Both intra- and intermolecular versions of the catalytic alkyne-to-carboxylic coupling methods have been successfully applied to the synthesis of complex organic molecules.⁶⁷ Burton and the co-workers reported that the reaction of difluoro-3-iodoacrylic acid with a variety of the terminal acetylenes under cocatalysis of $\text{PdCl}_2(\text{PPh}_3)_2$ and CuI gave difluorinated 2-pyrones as the sole product in good yields (Eq 47).⁶⁸



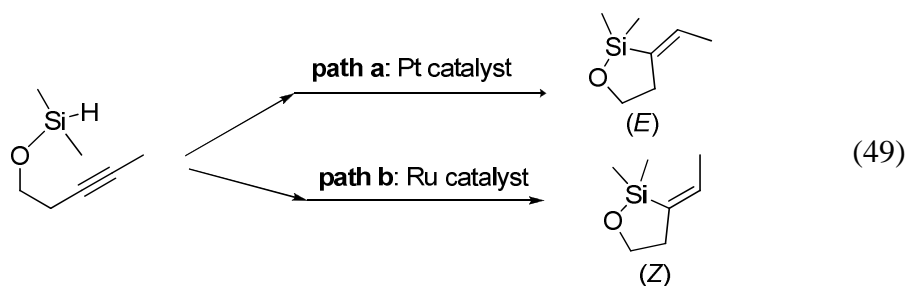
Despite considerable synthetic and mechanistic progress, however, neither the nature of reactive intermediate species nor controlling factors for the formation of *gem*- vs (*E*)/(*Z*)-enol esters has been clearly established.

1.4.2 The Hydrosilylation of Alkynes

Vinylsilanes are very useful intermediates in organic synthesis,⁶⁹ they have emerged as versatile building blocks. Because of their low toxicity, low cost, high stability, and innocuous byproduct vinylsilanes play a growing role in the synthesis and particularly in metal-catalyzed cross-coupling reactions.⁷⁰ Vinylsilanes are very useful as acceptors in conjugate addition reactions,⁷¹ as masked ketones through Tamao-Fleming oxidation,⁷² and as terminators for cation cyclizations.⁷³ They can be readily carried through many synthetic operations. Over the past decades, many groups are working on the routes to syntheses vinylsilanes, and among the most straightforward and atom-economical method to assemble vinylsilanes is transition metal catalyzed hydrosilylation of alkynes. This method started at the addition to the alkynes by both carbon monoxide and trialkylsilanes in the manner depicted in Eq 48.

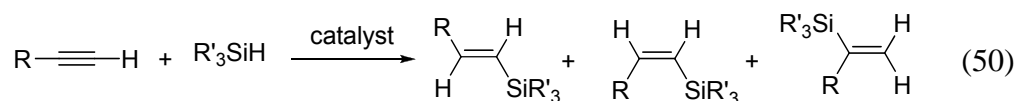


The original discovery of “silylcarbonylation” by Murai⁷⁴ using $\text{Co}_2(\text{CO})_8$ found olefin conversion to silyl enol ethers of the homologous aldehydes as the sole carbonylation products. The same outcome has been reported for enamines catalyzed by $[\text{RhCl}(\text{CO})_2]_2$ and for the terminal alkenes catalyzed by $\text{Ru}_3(\text{CO})_{12}$ and $(\text{Ph}_3\text{P})_3\text{RhCl}$.⁷⁵ And later on Matsuda and Ojima⁷⁶ independently reported the silylcarbonylation of alkynes catalyzed by $\text{Rh}_4(\text{CO})_{12}$ or Rh-Co mixed metal carbonyl clusters. In contrast silylcarbonylation reactions catalyzed by $\text{Rh}_4(\text{CO})_{12}$ or Rh-Co mixed metal carbonyl clusters yield the carbon-centered silane exclusively, and with terminal alkynes these transformations generally occur under mild conditions with a high degree of regiocontrol. There are many reports on the intramolecular version and intermolecular silylcarbonylation reactions. Recently Trost reported the intramolecular endo-dig hydrosilylation catalyzed by ruthenium.⁷⁷ For the intramolecular hydrosilylation, there are two major pathways (Eq 49), one is catalyzed by the platinum compounds to generate the (E)-vinylsilanes, the other one is catalyzed by the ruthenium complexes to generate the (Z)-vinylsilanes.

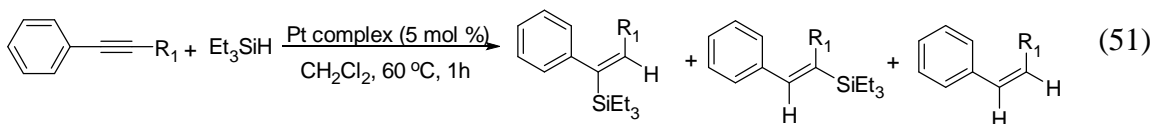


Trost and the co-workers show some details on the pathway in this report, they

extend the scope of the reactions by using function substitutes such as the alcohol, ester and ether. Moreover, all these reactions show the high selectivity on the formation of (*Z*) isomer and good yields. For the intermolecular silylcarbonylation reactions, the hydrosilylation of alkynes is still the simplest and most straightforward method for their preparation. The main difficulty with this transformation is control of the stereo- and regiochemistry of the alkenesilane. Generally, these type reactions always generate the mixture (Eq 50).

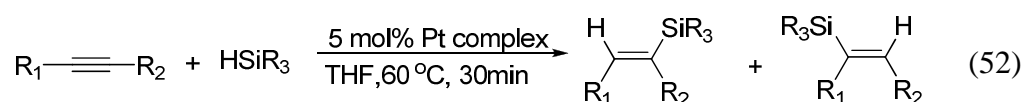


Although radical and Lewis acid⁷⁸ induced procedures have been reported, the transition-metal-catalyzed reaction continues to play a dominant role since it proceeds in a stereoselective manner. Recently Alami reported platinum oxide catalyzed hydrosilylation of unsymmetrical internal aryl alkynes under *ortho*-substituent regiocontrol (Eq 51).⁷⁹

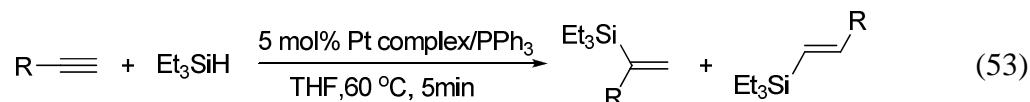


Alami and co-workers compared the reactivity of the catalyst PtO₂ with Speier's catalyst (H₂PtCl₆) in hydrosilanes of terminal alkynes, and they found that these two platinum complexes show the good reactivity for hydrosilylation of terminal alkynes, and in most case PtO₂ shows better reactivity and higher selectivity on the α -isomer and

β -isomer than Speier's catalyst (H_2PtCl_6). They tried to control the selectivity on one isomer by modifying the reactions conditions, but they still get the mixtures, and they did not give the explanation on the factor of the formation of the mixtures. Later on Marko⁸⁰ and Folch⁸¹ improved the selectivity on β -hydrosilylation isomers by using platinum complexes as catalyst. Marko used platinum complex with bulky ligand to get the high selectivity on the β -(*Z*) isomers (Eq 52).



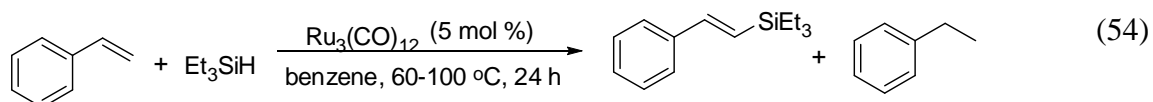
Floch focused on improving the selectivity on the β -(*E*) isomers by using platinum (0) phosphine complex as the catalyst (Eq 53).



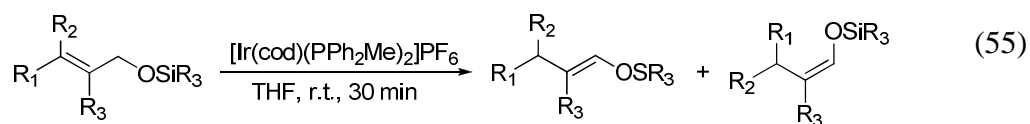
The reactions of terminal alkynes and triethylsilane generate the vinylsilanes in mild conditions in about 5 min. These reactions generate β -(*E*) isomers and α -isomer. Floch found the ratio of these two isomers shows the dependence on the alkynes. When using less bulky substitutes as linear alkynes the reactions show the high selectivity on the β -(*E*) isomers, and the ratio of β -(*E*) isomer to α -isomer is about 99/1. The ratio of these compounds decreased by using the bulky substituents, for example the reaction the phenyl acetylene with triethylsilane generates the mixture of β -(*E*) isomer and α -isomer,

the ratio of them is around 80/20, but they did not mention the details on the mechanism of these reactions.

Ruthenium complexes are also good catalysts for the hydrosilylation of alkynes and alkenes. In 1986 Muri reported the single-operation synthesis of vinylsilanes from alkenes and hydrosilanes with the aid of ruthenium carbonyl complex (Eq 54).⁸²



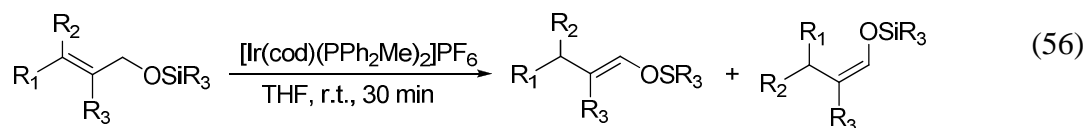
The reaction of excess amount of styrene with triethylsilane gives the *trans*-vinylsilane and one equiv. ethylbenzene as by product. At high temperature, this reaction also generates some amount of alkylsilanes. These reactions show the high limitation on the alkenes, Muri found that, only the terminal alkenes can show the reactivity and generate the products but some substituents need high temperature. Later on, many groups had been working on the synthesis of vinylsilane by hydrosilylation of alkynes and alkenes, but most of them focused on the selectivity for the reactions of alkynes and hydrosilanes. Recently, Chang reported the highly stereoselective and efficient hydrosilylation of terminal alkynes catalyzed by $[\text{RuCl}_2(\text{p-cymene})]_2$ (Eq 55).⁸³



Under mild conditions, the reactions of terminal alkynes with hydrosilane favor to generate the (*Z*)-vinylsilanes and give high yields. However, when Chang uses some

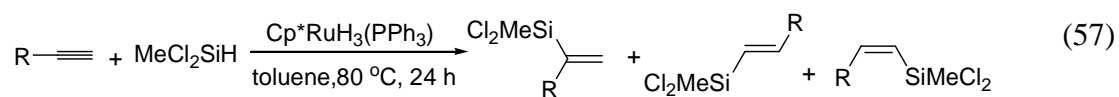
function substitutes such as the hydroxyl groups, the reactions lose the selectivity, they get α -isomer and β -(Z) isomer as the mixture and the ratio of them changes with the different substitutes, in this report, they did not mention the factor of these results, and no mechanistic details were given by them.

Later on Ball reported the Markovnikov alkyne hydrosilylation catalyzed by the ruthenium cationic complexes,⁸⁴ they reported that the reactions of alkynes with hydrosilanes were smoothly converted in 30 min at ambient temperature to the branch the (1,1-disubstituted) vinylsilane in good yields without detectable formation of (1,2-disubstituted) products with only 1 mol % of $\text{CpRu}(\text{MeCN})_3^+\text{PF}_6^-$. A variety of terminal alkynes proved amenable to the reaction, including those with substantial steric bulky groups. The reaction is tolerant to a wide range of functional groups, including sp^2 halides, alkenes, esters, free alcohol, protected amines and even free carboxylic acid. Overall good yield and good regioselectivity are maintained through a wide range of substrates in this report. The details on the mechanism for this reaction have not been discussed (Eq 56).

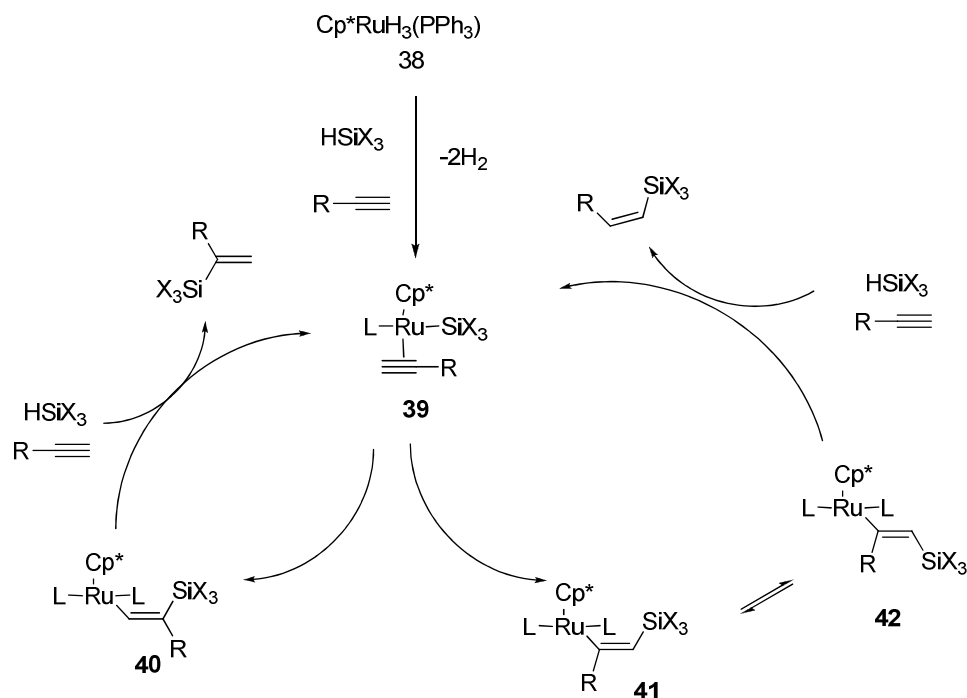


Yamamoto also reported hydrosilylation of the terminal alkynes by using the $\text{Cp}^*\text{RuH}_3(\text{PPh}_3)$, they observed the similar results as Ball's: the reactions of terminal alkynes with hydrosilane generate the germinal vinylsilane as the major product with

some amount of (*Z+E*) isomers. The ratio of these products can be 99/1-89/11 (Eq 57).⁸⁵



On the basis of these the NMR observation of the stoichiometric mixture of complex **38** and HSiMeCl_2 for liberation of hydrogen, a plausible catalytic loop of the present hydrosilylation of terminal alkyne is depicted as Scheme 13, where the key intermediate **39** would originate from the precursor **1**, the hydrosilane, and the substrate alkyne. Thus they assume that a key step may involve the silylruthenation, probably in a manner syn to the coordinated alkyne to form either β -silylated alkenylruthenium **40** or **41**. And the intermediate **40** would be sterically less demanding and constitutes the major loop, while **41** may be more congested due to an additional steric repulsion between the ruthenium center and the substituent R, becoming the minor one.

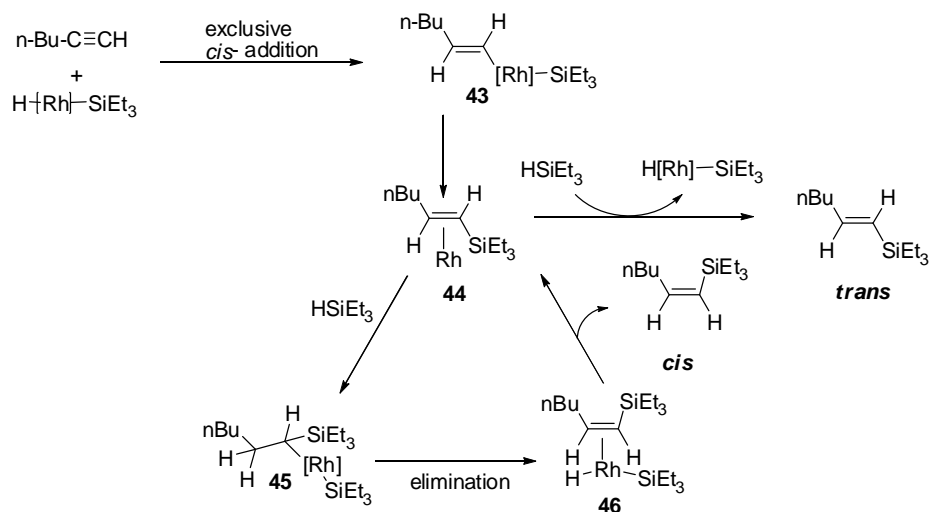


Scheme 13. Proposed Mechanism of the Hydrosilylation of Alkynes

They also did the study on the ligands of the ruthenium, and found that the presence of a bulk Cp^* ligand and PCy_3 on the ruthenium center in complex **39** would help silyruthenation proceed highly regioselectivity in favor of **40** rather than **41**. Moreover, this can give the explanation the ratio of the germinal and *cis* vinylsilane products.

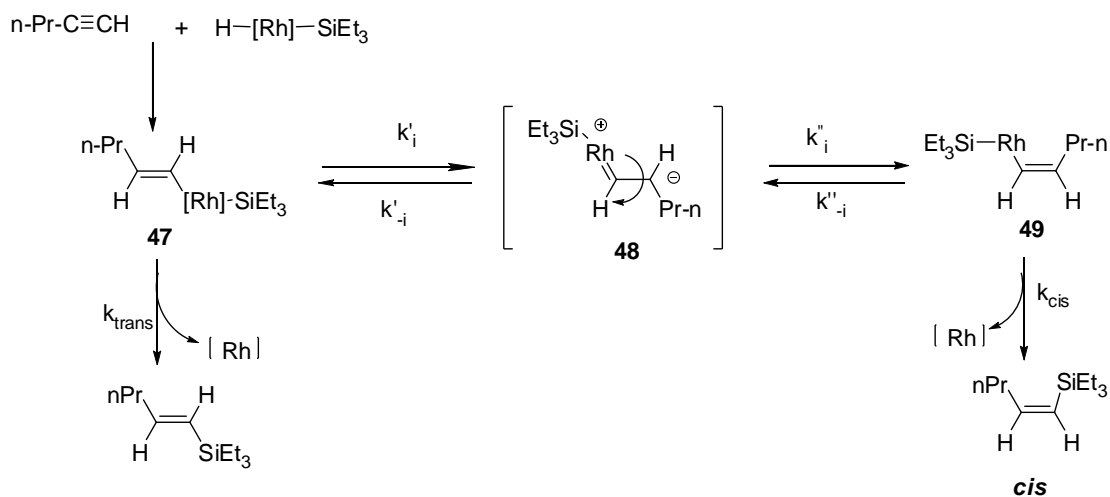
Although Yamamoto and the co-workers give some details on the mechanism for the hydrosilylation of alkynes, there are still something unclear for this reaction. Up to now, the better catalyst for mechanistic study on the hydrosilylation of alkynes is the

rhenium complexes. There are four types proposed mechanism for the hydrosilylation reactions catalyzed by rhenium complexes in Scheme 14 was proposed by Haszeldine,⁸⁶ the catalytic cycle starts at the addition of terminal alkynes to the Rh-Si complex to give the complex **43**, and with another equiv. HSiEt₃ coming, there are two path ways, one is going through the elimination to generate the *trans* product, due to the steric conflict between the silyl group and alkynes this way should favor if there is some bulky substitutes. The other one is the formation of the *cis* product through β -hydride elimination of the 1- Et₃Si-hexyl-Rh(SiEt₃) species **45**, but there are some problems on this scheme. This step should not favorable since there is a steric conflict between the silyl and the butyl groups in the transition state, and it is unreasonable to assume that the sterically more demanding *trans* product selectively substitutes the *cis* product from the intermediate **46**. Overall, it is against thermodynamics to assume isomerization of the more stable *trans* product to the less stable *cis* product.



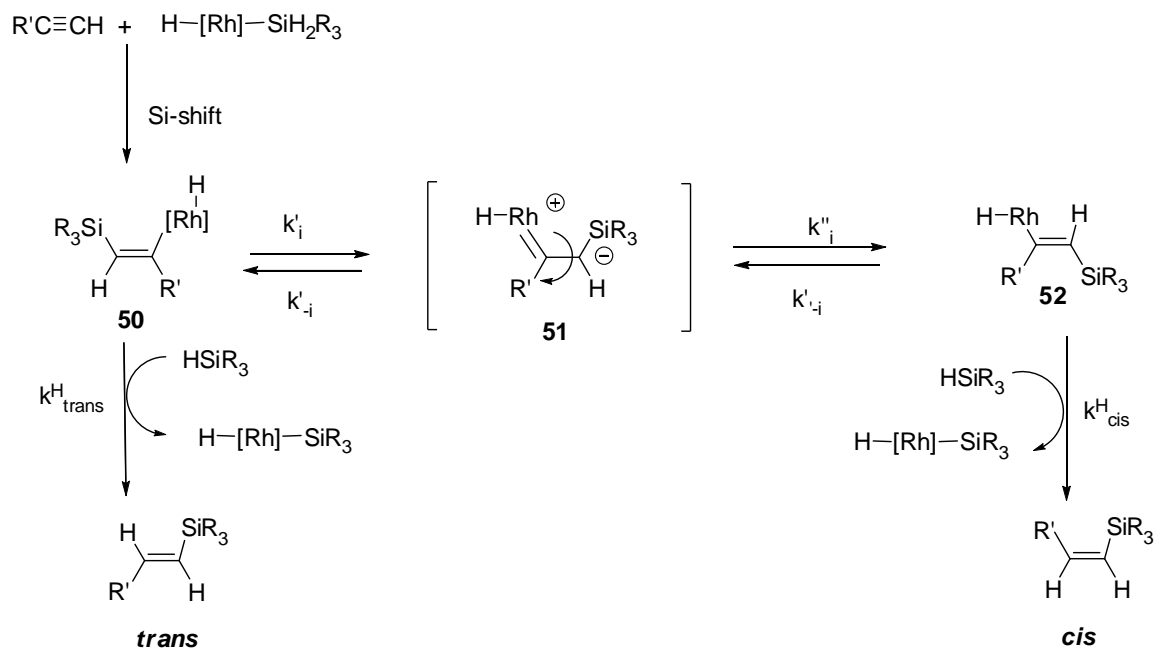
Scheme 14. Proposed Mechanism of the Hydrosilylation of Alkynes by Rhodium Complexes

Nile improved this mechanism (Scheme 15)⁸⁷, the first step of the catalytic cycle is the addition of rhenium silane complex to generate the *trans* intermediated **47**, and then the same way to get the *trans* product. For the formation of the *cis* product, he proposed the rotation of the single bond in the zwitterionic carbene intermediated VI to give the *cis*-1-pente-nyl-Rh-(SiR₃) complex **48** and then go through the elimination to generate the *cis* product, but the intermediated complex **49** is sterically much more hindered, so it is unflavored, and the n-propyl group would destabilize the negative charge developing on C-2 of VII, so we can see clearly, this mechanism can't explain the formation of the *cis* product.



Scheme 15. Nile's Proposed Mechanism of the Hydrosilylation of Alkynes

Later on, Ojima proposed a different mechanistic cycle,⁸⁸ which can explain the formation of the *cis* product.



Scheme 16. Ojima's Proposed Mechanism of the Hydrosilylation of Alkynes

The proposed mechanism starts at the insertion of an alkyne into the silicon-rhodium bond in the first place to form the (Z) -1-silyl-1-alken-2-yl-Rh intermediate **50**, instead of the previously proposed insertion into the hydrogen-rhodium, this is one of the most important steps in the whole mechanism. The intermediate **50** thus formed suffers from serious steric hindrance between the silyl group and the rhodium moiety, which are both bulky. Thus, **50** undergoes isomerization to the sterically more favorable (E) -1-silyl-1-alken-2-yl-Rh complex (**X**) via the zwitterionic carbene complex **51**, which is somewhat similar to the one proposed by Nile, but the silyl group is at C-1, to the rhodium. By the oxidative addition of another molecule of another molecule of the hydrosilane and reductive elimination, the reaction generates the *cis* product. The

formation of *trans* and *cis* product depends on the k'_i and k^H_{trans} . If the oxidative addition of another molecular of the hydrosilane to **50** is much faster than the isomerization, the *trans* product should be formed selectively. So this mechanism can explain the factor of the formation of the *cis* and *trans* isomers and furthermore, the reaction with the hydrosilanes bearing electron-withdrawing substituents should be not give any *cis* products arising from the isomerization of **50** to **52**.

Chapter 2. Regioselective Formation of α -Vinylpyrroles from the Ruthenium-Catalyzed Cross Coupling Reaction of Pyrroles and Terminal Alkynes Involving C-H Bond Activation

C-vinylated pyrroles and indoles are not only important building blocks in formation of biologically active porphyrins and related nitrogen macrocycles but also serve as precursors of electroactive polymeric materials.⁸⁹ Allylation and alkenylation of such indoles and pyridine derivatives have been achieved by using cationic Ru-allyl and -vinylidene catalysts, respectively.⁹⁰ Pd-catalyzed direct oxidative arylation of indoles and quinoline-*N*-oxides have also been achieved by using Pd catalysts.⁹¹ Despite such remarkable progress, regio- and stereo-controlled vinylation still remains as a major problem in the catalytic C-H alkenylation methods. Lack of *cis*- and *gem*-selective vinylation method, *trans*-selective product is formed in most cases. While exploring the scope of the catalytic coupling reactions involving C-H bond activation, here we report a method promoting highly regioselective formation of α -vinylpyrroles from ruthenium-catalyzed cross coupling reaction of pyrroles and terminal alkynes.⁹²

2.1 Results and Discussion

The initial activity studies showed the cationic ruthenium catalyst

In the ^1H NMR (Acetone- d_6 , 400 MHz), the singlet peak at δ 3.71 ppm is assigned to the 3H of OCH_3 . The peaks at δ 5.34 ppm and 5.03 ppm respond the two vinyl proton, they are showed as doublets, and their coupling constant are the same ($J = 1.6$ Hz). The peaks at δ 6.26 ppm are from the two β -hydrogens, and the peak at δ 6.98 ppm belongs to the other α -position, the other peaks are from the aromatic H.

Needle-like crystals of Compound **53c** formed after slow evaporation of a sample dissolved in $\text{CH}_2\text{Cl}_2/n$ -hexane mixture. X-ray crystallography shows that it is α -vinylpyrroles (Figure 2) and its C(2A)-C(3A) bond length is 1.4815 Å.

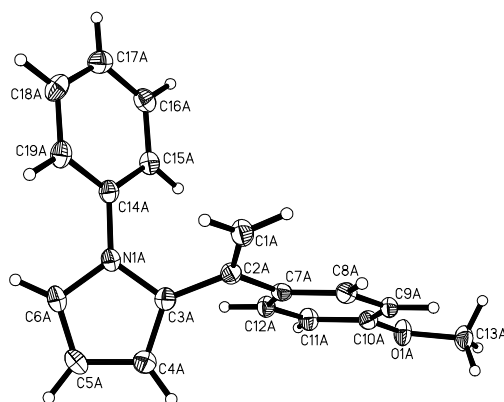


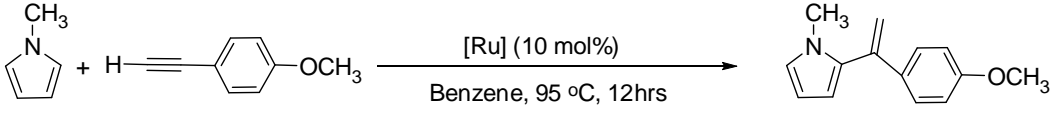
Figure 2. X-ray Crystal Structure of **53c**

2.2 Scope of the Coupling Reactions of Pyrroles with Terminal Alkynes

2.2.1 Catalyst Survey

In order to find the best condition for this coupling reaction, we used the reaction of N-methyl pyrrole (143 mg, 1 mmol) with 4-ethynylanisole (2 mmol) to test the activity of ruthenium complexes (10 mol %). The amount of the coupling product was determined by GC/MS. This catalyst activity survey showed that $\text{Ru}_3(\text{CO})_{12}/\text{NH}_4\text{PF}_6$ (1:3 molar ratio) has the highest activity in this coupling reaction among selected ruthenium complexes (Table 1).

$\text{Ru}_3(\text{CO})_{12}/\text{NH}_4\text{PF}_6$ and $\text{Ru}_3(\text{CO})_{12}/\text{HBF}_4\text{OEt}_2$ showed high yield while $\text{Ru}_3(\text{CO})_{12}$ alone produced only 30% coupling product. Other common ruthenium complexes such as $\text{RuH}_2(\text{PPh}_3)_4$, $\text{RuHCl}(\text{CO})(\text{PCy}_3)_2$ and $\text{RuCl}_3 \cdot 3\text{H}_2\text{O}$ showed no activity to the coupling reaction under similar reaction conditions. Although $\text{Ru}_3(\text{CO})_{12}/\text{HBF}_4\text{OEt}_2$ shows similar yield of coupling products as the $\text{Ru}_3(\text{CO})_{12}/\text{NH}_4\text{PF}_6$, we chose $\text{Ru}_3(\text{CO})_{12}/\text{NH}_4\text{PF}_6$ as the catalyst for this coupling reactions, since HBF_4OEt_2 is liquid and not easy to handle.

Table 1. Catalyst Activity Survey for Coupling Reaction of Pyrroles with Alkynes^a


Entry	Catalyst	Additive	yield(%) ^b
1	None	None	0
2	Ru ₃ (CO) ₁₂	None	30
3	Ru ₃ (CO) ₁₂	NH ₄ PF ₆	>99
4	Ru ₃ (CO) ₁₂	HBf ₄ OEt ₂	96
5	RuCl ₃ ·3H ₂ O	None	0
6	(PCy ₃) ₂ (CO)RuHCl	None	0
7	(PCy ₃) ₂ (CO)RuHCl	HBf ₄ OEt ₂	0
8	(PCy ₃) ₂ (CO)RuHCl	NH ₄ PF ₆	0
9	(PPh ₃) ₃ (CO)RuH ₂	None	0
10	(PPh ₃) ₃ RuCl ₂	None	0
11	(PPh ₃) ₃ RuHCl	None	0
12	[RuCl ₂ (COD)] _x	None	0
13	(PCy ₃) ₂ (CH ₃ CN) ₂ (CO)Ru [⊕] H [⊖] BF ₄	None	0

^a Reaction condition: 0.1 mmol of methyl pyrrole, 0.2 mmol 4-ethynylanisole, [Ru] 10 mol %, benzene 2 mL, 95 °C, 12 h. ^b GC yields based on N-methylpyrrole.

2.2.2 Solvent Effects

A variety of solvents was tested to optimize the reaction condition. Methyl pyrrole (0.1 mmol) was reacted with 4-ethynylanisole (0.2 mmol) in the presence of 3.3 mol % $\text{Ru}_3(\text{CO})_{12}/\text{NH}_4\text{PF}_6$ (1:3 molar ratio) and the yield of the product was determined by GC-MS. It was found that the nature of the solvent affects reaction efficiency significantly. Benzene was found to be the best among the tested solvents. Toluene and dichloromethane also showed respectable yield, but with some byproducts. Coordinating solvents such as THF, MeCN showed low conversion in this reaction.

Table 2. Solvent Effect Survey on Coupling Reaction of Pyrroles with Alkynes

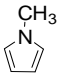
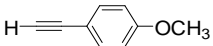
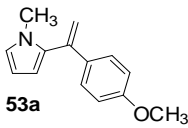
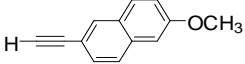
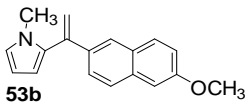
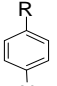
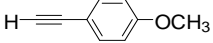
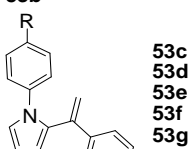
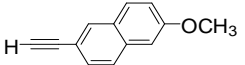
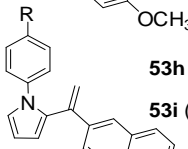
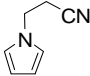
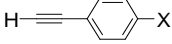
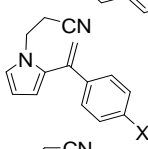
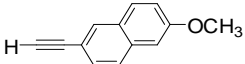
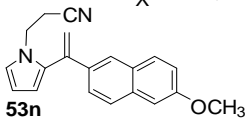
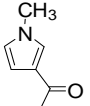
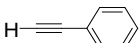
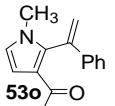
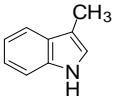
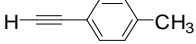
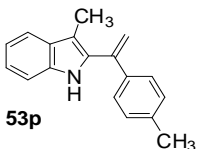
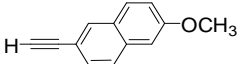
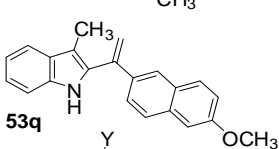
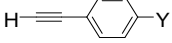
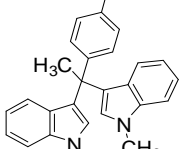
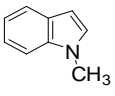
entry	solvent	yield(%) ^b
1	benzene	>99
2	CH_2Cl_2	95
3	Toluene	90
4	THF	20
5	MeOH	20
6	MeCN	5

^a Reaction condition: 0.1 mmol of methyl pyrrole, 0.2 mmol 4-ethynylanisole, 10 mol %, $\text{Ru}_3(\text{CO})_{12}/\text{NH}_4\text{PF}_6$ (3.3 mol %) (1:3 molar ratio); 2 mL solvent; 95 °C; 12 h. ^b GC yields based on N-methyl pyrrole.

2.2.3 Reaction Scope

To demonstrate the synthetic utility of the catalyst $\text{Ru}_3(\text{CO})_{12}/\text{NH}_4\text{PF}_6$ (1:3 molar ratio), we explored the scope of this coupling reaction (Table 3). All of the tested reactions yielded only one to one coupling product and alkyne-trimer as byproduct. We also performed the survey on coupling reactions of different N-pyrrole substrates (0.1 mmol) with 4-Ethynylanisole (0.2 mmol) in the presence of 3.3 mol % $\text{Ru}_3(\text{CO})_{12}/\text{NH}_4\text{PF}_6$ (1:3 molar ratio). Results showed that existence of an electron donating group (EDG) in an N-pyrrole would promote the reaction. For those with electron withdrawing group (EWG) at N-pyrroles, the conversion was low, which was usually less than 10% and isolation of products was thus impractical. So, here we show only the results from the coupling reaction of the N-pyrroles with electron donating substrates with the alkynes. For terminal alkynes, we scanned reactions of methyl-N-pyrrole with triethyl(ethynyl)silane, phenylacetylene, 1,2-diphenylethyne, pent-2-yne, pent-1-yne under the same condition and checked the reaction by GC-MS. The reaction involving phenylacetylene produced 1:1 coupling product in good yields. For 1-pentyne, only trace amount of product was observed.

Table 3. Coupling Reactions of Pyrroles with Terminal Alkynes^a

Entry	Pyrrole	Alkyne	Product	Yield (%) ^b
1			 53a	99
2			 53b	95
3			 53c (R=H) 53d (R=CH ₃) 53e (R=OCH ₃) 53f (R=Cl) 53g (R=F)	83 80 78 73 70
4				
5				
6				
7				
8			 53h (R=H) 53i (R=OCH ₃)	75 75
9				
10			 53j (X=H) 53k (X=CH ₃) 53l (X=OCH ₃) 53m (X=NMe ₂)	80 83 85 75
11				
12				
13				
14			 53n	78
15			 53o	81
16			 53p	78
17			 53q	80
18			 53r (Y=H) 53s (Y=CH ₃)	85 87
19				

^a Reaction condition: 1.0 mmol pyrrole; 2.0 mmol alkyne; 3 mL benzene; Ru₃(CO)₁₂/NH₄PF₆ (3.3 mol %) (1:3 molar ratio); ^b isolated yield.

For triethyl(ethynyl)silane and 1,2-diphenylethyne pent-2-yne, there were no coupling products formation was observed, the GC-MS showed only peaks of starting materials and trimerized byproducts, even after prolonged reaction time. Therefore, we focused our effort on the phenyl acetylene and different substrates on the *para*-X-phenyl acetylene, such as 1-ethynyl-4-methylbenzene, 4-ethynylanisole, 1-bromo-4-ethynylbenzene, 1-chloro-4-ethynylbenzene and 1-ethynyl-4-fluorobenzene. All these reactions generated products at 1:1 ratio. We performed kinetic analysis on these reactions, and it was found that electron donating groups such as OMe and Me group can promote this reaction, while the electron withdrawing groups (such as Br, Cl, and F,) showed low conversion. There were no reactions observed for furan, thiophene with the phenylacetylene, and N-methyl pyrrole with the alkynes.

2.3 Mechanism Studies

2.3.1 Hammett Study

Hammett studies were performed on *para*-substituted N-phenylpyrroles and alkynes to determine the electronic effects on the pyrrole substrates in the coupling reaction. It was found that the substituents at *para*-position of the aromatic ring could

transfer their electronic information through bonds. During the reaction, the substituents create a dipole interaction at the α -carbon, influencing the energy associated with the development of possible charge at the reaction center. Charge development occurs during formation of the most stable transition state of the reaction through bond formation or rupturing. The effect that electron-donating and electron-withdrawing substituents have on the reactions rates is correlated to the nature of the transition state.⁹³

Encouraged by the differences in the appearance of the reaction mixtures for the coupling reactions, we performed a Hammett study using a series of *para*-substituted phenyl pyrroles (X = OMe, CH₃, H, Cl, F). We monitored the coupling reactions using the initial rate method. In the study, Ru₃(CO)₁₂ (0.003 mmol), NH₄PF₆ (0.01 mmol), pyrrole (0.1 mmol), alkyne (0.25 mmol) and hexamethylbenzene (26 mg as the internal standard) were dissolved in 0.5 mL benzene-*d*₆ solution and transferred into Wilmad J-Young NMR tubes with a Teflon screw cap. The tubes were cooled in liquid nitrogen twice, and were degassed three times. The tubes were gradually warmed to room temperature and then heated in oil bath at 95 °C. The reactions were monitored every hour by ¹H NMR spectroscopy. The rates were measured by integration of the product ¹H peak (OCH₃ δ 3.71 ppm), and the results were normalized against the internal standard. The k_{obs} was estimated from a first-order log-linear plot of ln[product] vs. reaction time. Through these reactions, we found that an electron-donating group on the phenyl pyrroles could accelerate the rate of the reaction. A Hammett plot was constructed by plotting the

$\log(k_x/k_H)$ vs σ_p and a Hammett value of $\rho = -0.9$ was obtained from the correlation of *para*-substituted *p*-X-C₆H₄N (X=OMe, CH₃, H, Cl, F) with 4-ethynylanisole (Figure 3).

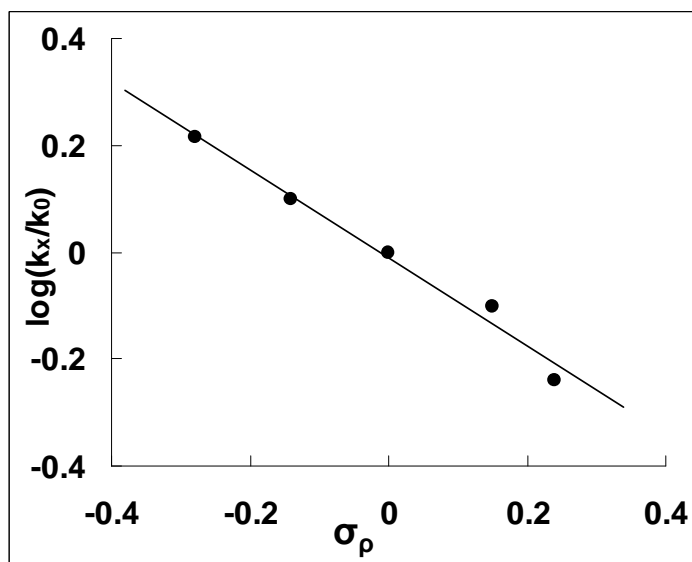
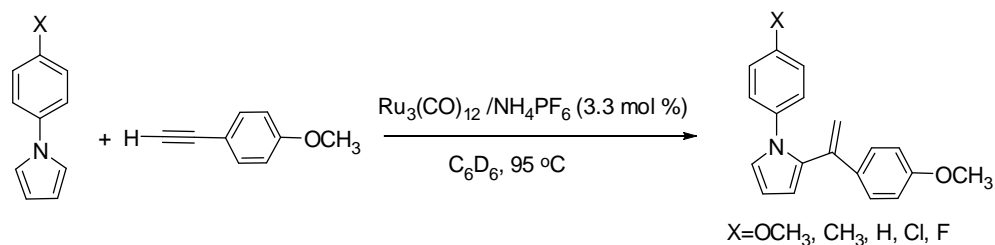


Figure 3. Hammett Plot of the Coupling Reaction of *para*-Substituted *p*-X-C₆H₄N (X = OMe, CH₃, H, Cl, F) with 4-ethynylanisole Catalyzed by Ru₃(CO)₁₂/NH₄PF₆ (1:3 molar ratio).

Generally, Hammett plot having a sharp change in the direction of the slope is an indication of a change in the rate-determining step of the mechanism, or alludes to the possible existence of a different mechanism together. The negative ρ value for pyrroles

suggests considerable cationic character of the transition state. Because of the developing positive charge on the transition state, electron-donating groups stabilizing the transition state enhanced the overall rate of the reaction and the promotional effect by electron-releasing group is indicative of a nucleophilic nature of the pyrrole group.

In order to learn the electronic effects on the alkyne substrates for the coupling reactions we also performed analysis the Hammett studies of *para*-substituted phenyl acetylene. Analogous correlation from the reaction of *N*-phenylpyrrole with aryl-substituted alkynes $p\text{-X-C}_6\text{H}_4\text{C}\equiv\text{CH}$ ($X = \text{OMe}, \text{CH}_3, \text{H}, \text{Br}, \text{F}$) resulted in a considerably less negative Hammett ρ value of -0.42 (Figure 4). In this case, the negative ρ value suggests a considerable cationic characteristic on the transition state of the C-C bond formation step, which is stabilized by electron-releasing group of the alkyne substituent. These results are consistent with the notion that the C-C bond formation step is promoted by both a nucleophilic pyrrole and electrophilic alkyne substrate via a cationic transition state.

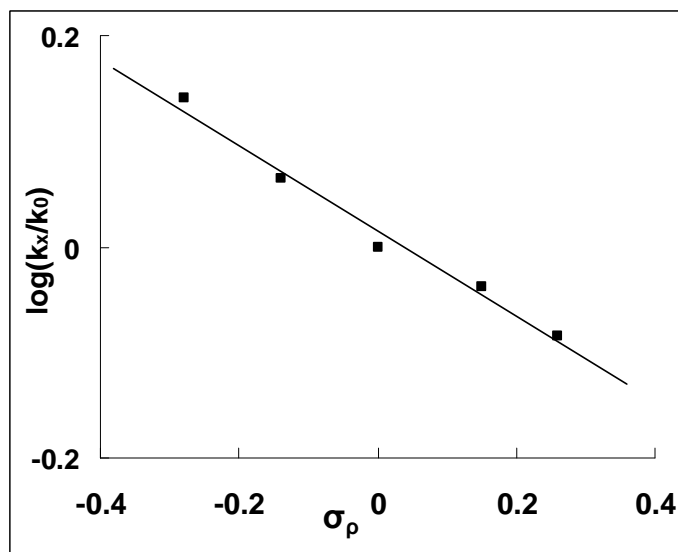
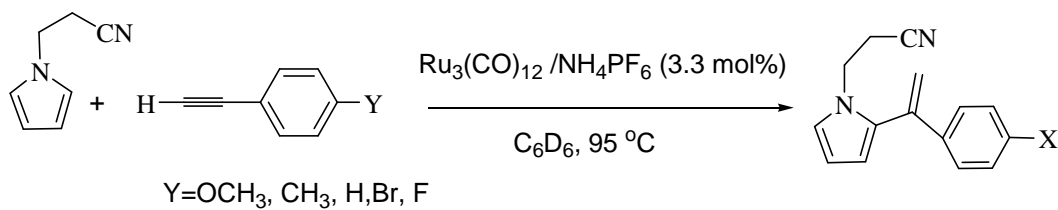


Figure 4. Hammett Plot of the Coupling Reaction of *para*-Substituted *p*-X-C₆H₄CCH (X = OMe, CH₃, H, Br, F) with Pyrrole Catalyzed by Ru₃(CO)₁₂/NH₄PF₆ (1:3) at 95 °C

2.3.2 Isotope Effect Study

To determine the possibility of a rate-limiting C-H bond cleavage step in the coupling reaction of alkynes and pyrroles, a series of experiments based on kinetic isotope effect on were performed. Again, the initial rate method was used to calculate the rate for each reaction. In this investigation, the N-phenyl 2,4-dideutopyrrole was made using *n*-Buli and D₂O (for the procedure, see the experiment section). The crude deuterium product was purified though the silica gel column, and the product was

characterized by ^1H and ^2H NMR spectroscopy (Figure 5). In this figure, the 2 α -position hydrogen and the ^2H from aromatic rings were deuterated.

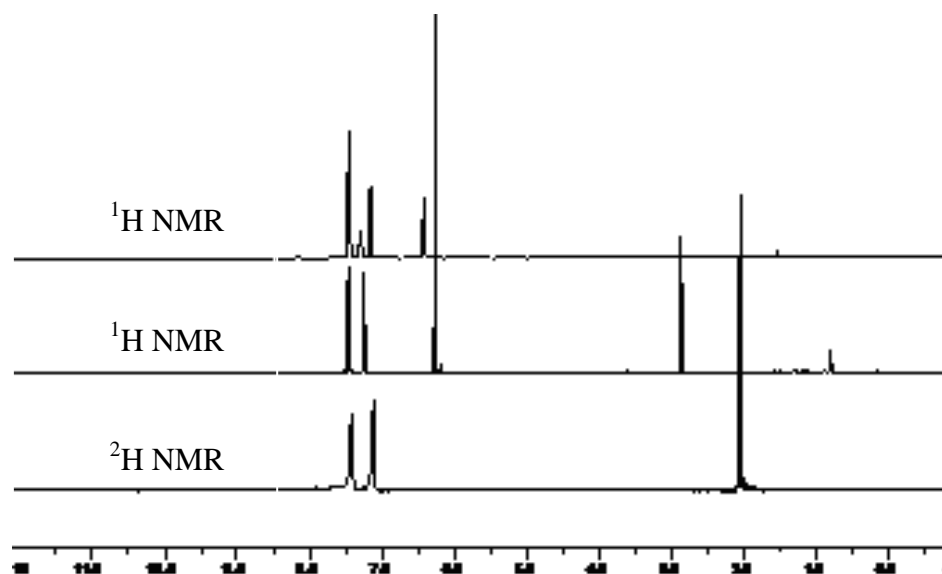


Figure 5. ^1H and ^2H NMR Spectra for the Deuterated N-phenyl Pyrrole

The top one is the ^1H NMR for the N-phenyl pyrrole, spectrum in the middle show the ^1H NMR of the deuterium product, and the bottom one is the ^2H NMR spectrum of the deuterium product. The peaks at 7.6 ppm was signed for the α -position H of the phenyl pyrrole.

The coupling reactions of $\text{C}_6\text{H}_5\text{NC}_4\text{H}_4$ with the 4-ethynylanisole and $\text{C}_6\text{H}_3\text{D}_2\text{NC}_4\text{H}_2\text{D}_2$ with 4-ethynylanisole were performed separately, and the reaction was monitored by NMR spectroscopy. These type reactions were set up in the same condition.

$\text{Ru}_3(\text{CO})_{12}$ (0.003 mmol), NH_4PF_6 (0.01 mmol), pyrrole (0.1 mmol) and alkyne (0.25 mmol) and hexamethylbenzene (26 mg as the internal standard) were dissolved in 0.5 mL benzene- d_6 solution in a Wilmad J-Young NMR tube with a Teflon screw cap. The tube was cooled in the liquid nitrogen, and degassed for three times. The tube was gradually warmed to room temperature and was heated in 95 °C oil bath. We monitored the reaction every hour by NMR spectroscopy. The rate was measured by monitor the ^1H integration of the product peak (OCH_3 δ 3.71ppm) signal, and the values were normalized against the internal standard. The k_{obs} was estimated from a first-order log-linear plot of $\ln[\text{product}]$ vs. reaction time. A normal deuterium isotope effect was observed for the $\text{C}_6\text{H}_5\text{NC}_4\text{H}_4$ and $\text{C}_6\text{H}_3\text{D}_2\text{NC}_4\text{H}_2\text{D}_2$. The pseudo-first order plots of the catalytic reaction of both $\text{C}_6\text{H}_5\text{NC}_4\text{H}_4$ and $\text{C}_6\text{H}_3\text{D}_2\text{NC}_4\text{H}_2\text{D}_2$ with the 4-ethynylanisole, at 95 °C in C_6D_6 led to $k_{\text{obs}} = 0.1424 \text{ h}^{-1}$ and $k_{\text{obs}} = 0.1392 \text{ h}^{-1}$ (Figure 6) respectively, from which a $k_{\text{CH}}/k_{\text{CD}} = 1.0 \pm 0.1$ was calculated. This is different from the predicted value of $k_{\text{CH}}/k_{\text{CD}}$, which should be larger than 1, if the C-H bond cleavage is the rate-limiting step. This low KIE values suggest the C-H bond cleavage in the α -position of the pyrrole is not the rate-limiting step. And the isotope effect of $k_{\text{CH}}/k_{\text{CD}} = 1.0 \pm 0.1$ was observed from the coupling reactions of $\text{C}_6\text{H}_5\text{CCH}$ and $\text{C}_6\text{H}_5\text{CCD}$ with the $\text{C}_6\text{H}_5\text{NC}_4\text{H}_4$ (Figure 6) and this means C-H bond cleavage in the alkyne is not the rate-limiting step. Based on these isotope effect data, we concluded that the C-H bond cleavage of both the pyrrole and the alkyne is not the rate-limiting step.

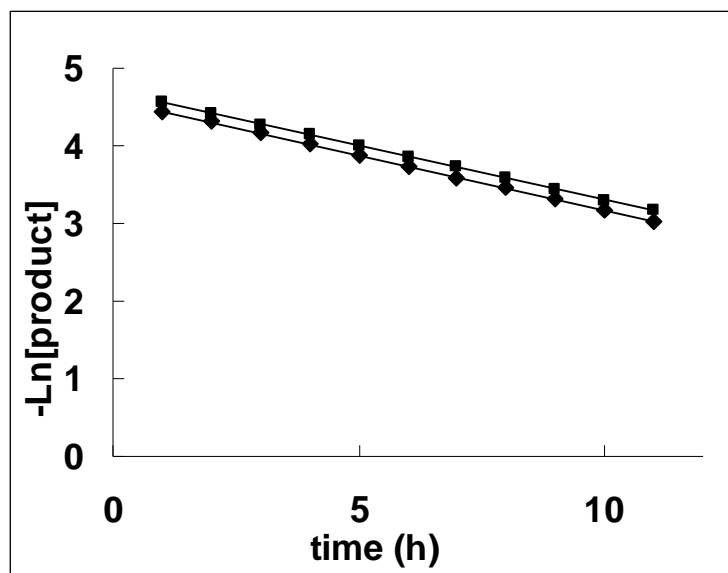
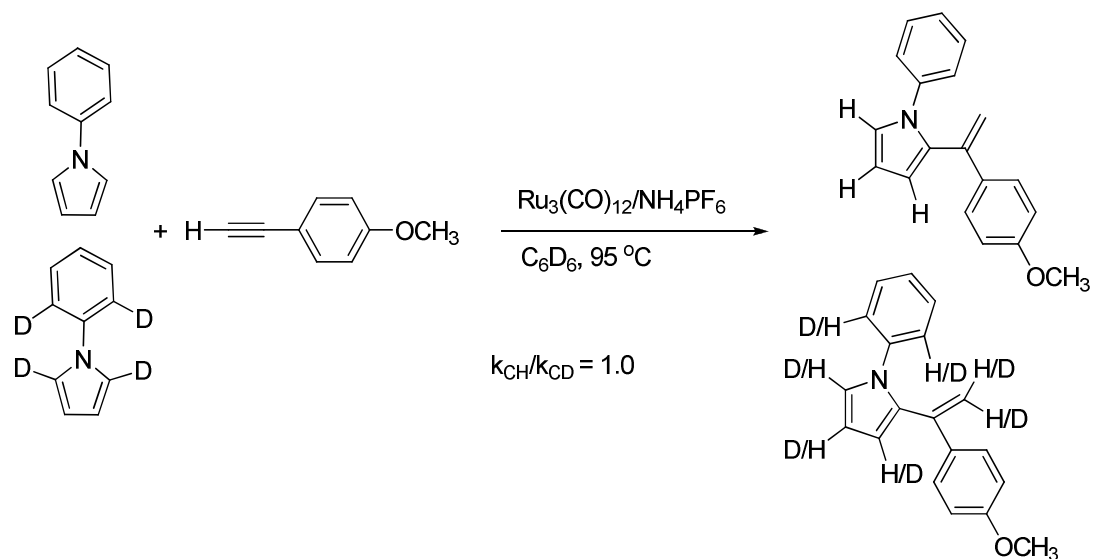
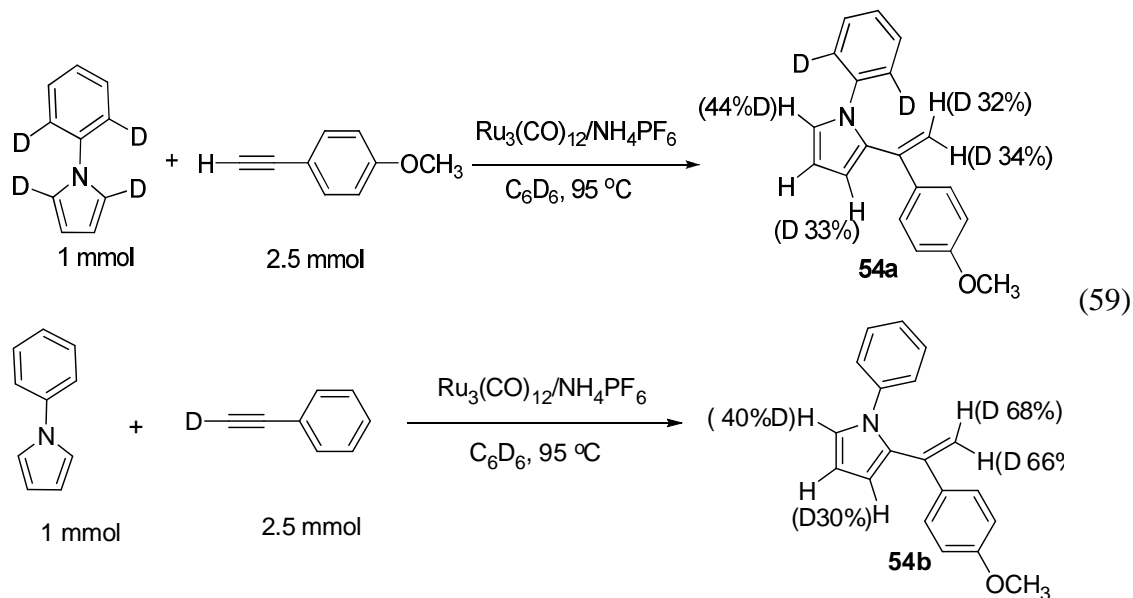


Figure 6. First Order Plot of $-\ln[\text{product}]$ vs Reaction Time for the Coupling Reaction; \blacklozenge -Phenyl pyrrole- d_4 ; \blacksquare -Phenyl pyrrol

2.3.3 Deuterium Labeling Studies

Though the isotope effect studies indicated that the C-H bond cleavage of the pyrrole and the alkyne was not the rate-limiting step, the mechanism is still largely

unknown. To learn more about the reaction mechanism, the following deuterium labeling studies were performed (Eq 59).



The reaction of the $C_6H_3D_2NC_4H_2D_2$ with excess 4-ethynylanisole (2.5 equiv.) and $Ru_3(CO)_{12}/NH_4PF_6$ (1:3 molar ratio) in benzene at 95 °C for 15 hours yielded product **54a** with extensive deuterium incorporation at terminal alkene (D 32% and 34%) and at the β position (D 33%) of the phenyl pyrrole as well as on the α position (D 44%) of the phenyl pyrrole as measured by both 1H and 2H NMR. Conversely, 68% and 66% on the terminal alkene and 30% on the β position of the phenyl pyrrole as well as 44% on the α position of the phenyl pyrrole were found to contain the deuterium when phenyl pyrrole was reacted with 2.5 equiv. of phenyl acetylene- d_1 in benzene at 95 °C for 15 hours yielded product **54b**.

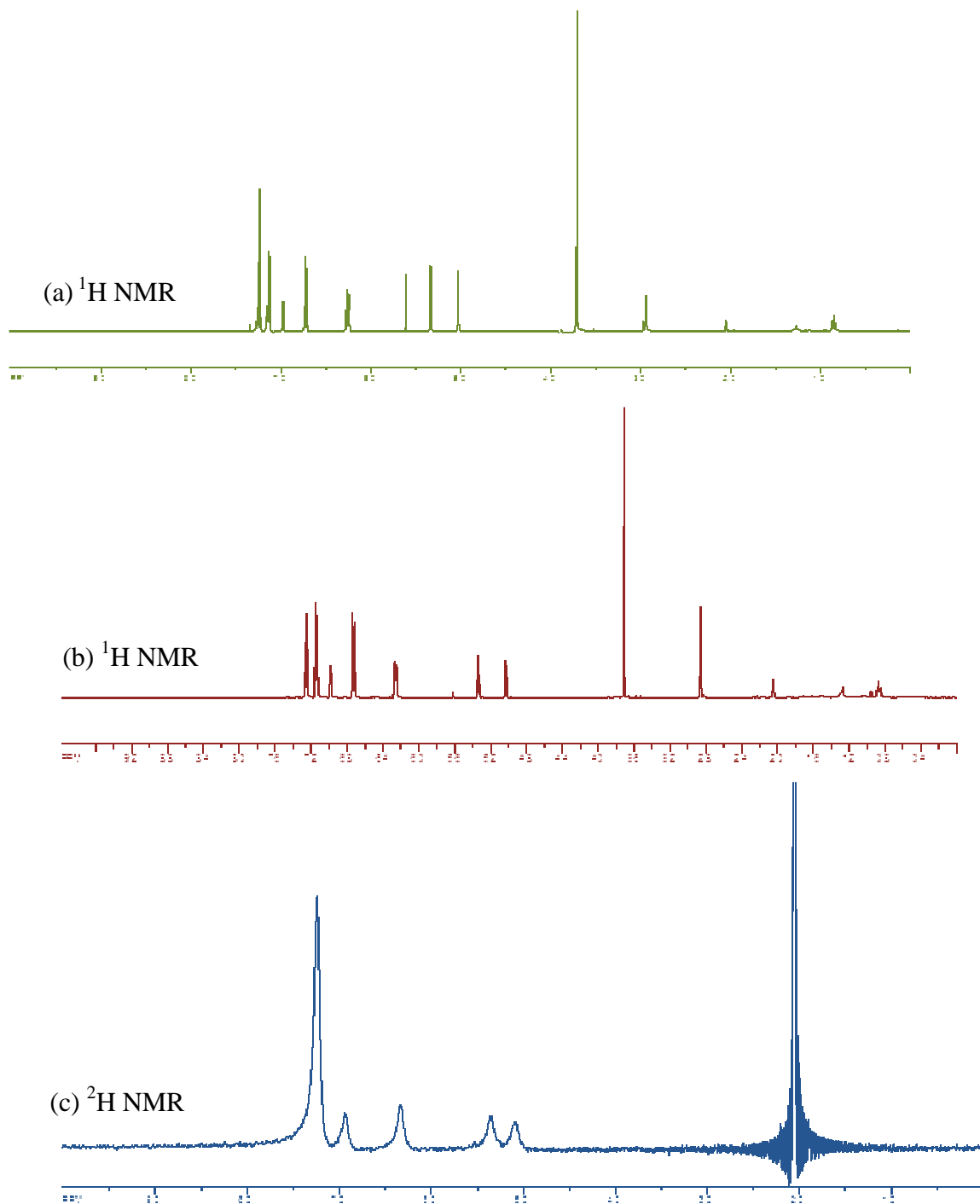


Figure 7. (a) ^1H NMR Spectrum of the Undeuterated Compound; (b) ^1H NMR Spectrum of the Compound **54a**; (c) ^2H NMR Spectrum of the Compound **54a**.

Figure 7a is the ^1H NMR spectrum of the non-deuterated compound and Figure 7b is the ^1H NMR spectrum of the compound **54a**. The intensities of the peaks at δ 5.33 ppm, 5.02 ppm and 6.25 ppm corresponds to vinyl and β position of the phenyl pyrrole resonances, respectively, which were significantly decreased due to extensive deuterium incorporation. As show in Figure 7c), the existence of deuterium at each position was further confirmed by ^2H NMR.

There are two possibilities for the proton and deuterium exchange: one is that the rate of deuterium and proton exchange is faster than the rate of the formation of the coupling products and the other one is the rate of deuterium and proton exchange is slower than the rate of forming the coupling products. If the rate of exchange is slower than the rate of product formation, there should be little D/H exchange between reagents, which would give less amount of deuterium in the product. However, from the studies, we can see that there are large amount of D in the coupling products. This faster D and H exchanges indicate that C-H bonds activation step in both alkyne and pyrrole are reversible.

2.3.4 Carbon Isotope Effect Study

In order to get information about the rate-determining step, experiments based on carbon isotope effect study were also performed. In a glove box, $\text{Ru}_3(\text{CO})_{12}$ (0.03 mmol), NH_4PF_6 (0.1 mmol), *N*-phenylpyrrole (1.0 mmol) and 4-ethynylanisole (2.5 mmol) were dissolved in 3 mL benzene solution in a 25 mL Schlenk tube equipped with a magnetic stirring bar. The tube was brought out of the glove box. The reaction tube was heated in an oil bath at 95 °C for 15 h. The tube was opened to air at room temperature, and the crude product mixture was analyzed by GC/MS (75% conversion). And the solvent was removed under a rotary aspirator, and the unreacted *N*-phenylpyrrole was isolated by a column chromatograph on silica gel ($\text{CH}_2\text{Cl}_2/n$ -hexanes).

The ^{13}C NMR analysis of the recovered and virgin samples of *N*-phenylpyrrole was performed according to Singleton's method.⁹⁴ The NMR sample of virgin and recovered *N*-phenylpyrrole was prepared identically by adding *N*-phenylpyrrole (75 mg) in CDCl_3 (0.5 mL) in a 5 mm high precision NMR tube. The ^{13}C $\{^1\text{H}\}$ NMR spectra were recorded with H-decoupling and 45 degree pulses. A 60 s delay between pulses was imposed to minimize T_1 variations (d1 = 60 s, at = 5.0 s, np = 245098, nt = 512). The average ^{13}C integration ratio of the recovered and virgin samples of *N*-phenylpyrrole is shown in Table 4.

Table 4. Average ^{13}C Integration of the Recovered and Virgin Samples of N-phenylpyrrole

C#	Virgin	Recovered (75% conv.)	Recovered/Virgin	Change (%)
1	0.998(5)	1.017(5)	1.019(5)	1.90(5)
2	1.020(3)	1.025(3)	1.005(3)	0.49(3)
3	1.009(4)	1.008(4)	0.999(4)	0.11(4)
4(ref)	1.000	1.000	1.000	0.00
5	0.469(3)	0.468(3)	0.998(3)	0.22(3)

C#	Virgin	Recovered (70% conv.)	Recovered/Virgin	Change (%)
1	0.998(5)	1.011(5)	1.013(5)	1.30(5)
2	1.020(3)	1.025(3)	1.005(3)	0.47(3)
3	1.009(4)	1.007(4)	0.998(4)	0.19(4)
4(ref)	1.000	1.000	1.000	0.00
5	0.469(3)	0.468(3)	0.998(3)	0.24(3)

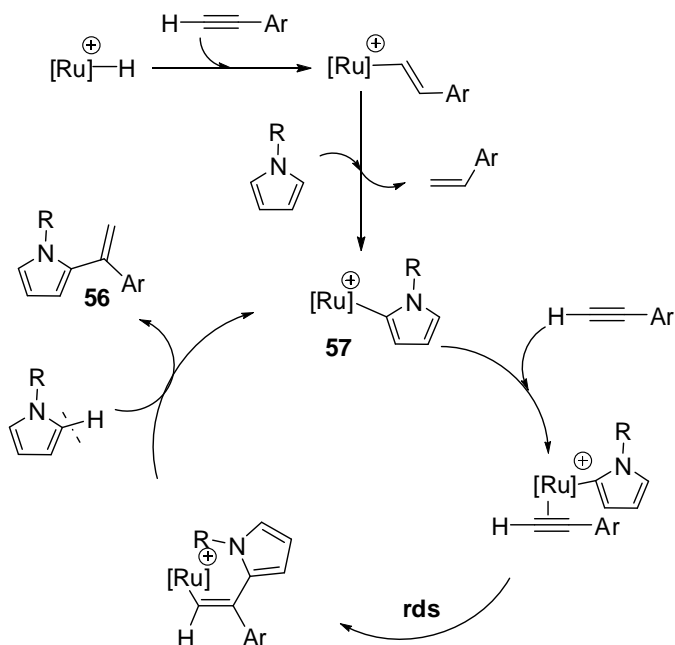
From this study, the most significant carbon isotope effect was observed at the α -position carbon of the phenyl pyrrole. This isotope effect indicates that the reaction step involving α -position carbon of the phenyl pyrrole is slow. Since ^{13}C is heavier than

^{12}C , and in the slow reaction step, the migration rate of ^{13}C should be slower than that of ^{12}C , thus results in that the abundance of ^{13}C α -position carbon of the recovered phenyl pyrrole would be more than the unused phenyl pyrrole. The experimental data agrees well with the theory. With the isotope effect studies, which indicated that the C-H bond cleavage is not the rate-limiting step and deuterium labeling studies, which showed the H and D exchange is faster than the formation of the coupling product, we reached the conclusion: C-C bond formation involving in the α -position carbon of the phenyl pyrrole should be the rate-limiting step.

2.3.5 Proposed Mechanism of the Coupling Reactions of Pyrroles and Alkynes

We provided a mechanistic rationale for the coupling reaction based on these results (Scheme 17). Here, we propose that the catalytically active cationic Ru-pyrrole species **57** is initially formed from an *ortho*-metallation followed by the elimination of an arylalkene. In support of this hypothesis, catalytic coupling reaction of *N*-phenylpyrrole with $\text{PhC}\equiv\text{CH}$ was performed.

The formation of styrene (3%) was detected by both ^1H NMR and GC-MS. Both negligible $k_{\text{H}}/k_{\text{D}}$ isotope effect and rapid H/D exchange pattern on the coupling reaction are consistent with a rapid and reversible C-H bond activation step.



Scheme 17. Proposed Mechanism for the Coupling Reactions of Pyrrole and Alkynes

The observation of a significant α -carbon isotope effect on the pyrrole substrate provides a strong evidence for the rate-limiting C–C bond formation step. A relatively strong negative Hammett ρ value from the correlation of *para*-substituted *N*-arylpyrroles also supports that the C–C bond formation step is promoted by the nucleophilicity of the pyrrole substrate. The regioselective insertion of pyrrole to the internal alkynyl carbon would be dictated by the formation of sterically less demanding Ru–vinyl species to yield the 1,1-disubstituted vinylpyrrole product **56**. The C–C bond forming step has been commonly observed as the rate determining step in other C–H insertion reactions.

2.4 Conclusions

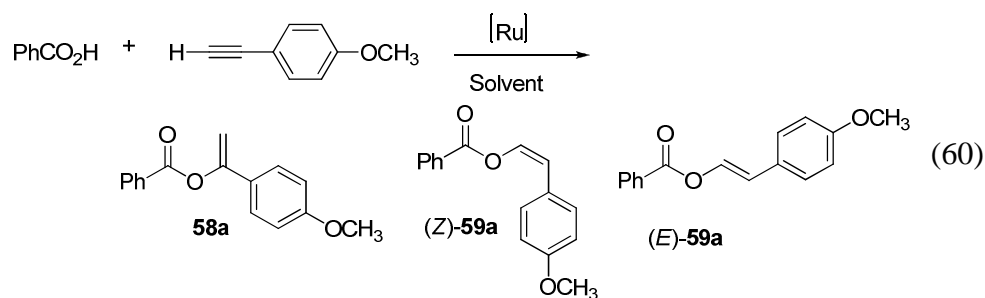
In summary, the cationic ruthenium catalyst $\text{Ru}_3(\text{CO})_{12}/\text{NH}_4\text{PF}_6$ was found to be effective for the regioselective intermolecular coupling reaction of pyrroles and terminal alkynes to give α -vinylpyrroles. The mechanistic studies on the coupling reaction revealed a rate-limiting C-C bond formation step and electronic origin of the regioselective formation of the coupling products. This catalytic method provides a predictable way to introduce synthetically useful *gem*-vinyl group to pyrroles and related nitrogen heterocycles.

Chapter 3. Scope and Mechanistic Investigations on the Solvent-Controlled Regio- and Stereoselective Formation of Enol Esters from the Ruthenium-Catalyzed Coupling Reaction of Terminal Alkynes and Carboxylic Acids

Enol esters are a versatile class of precursors for a variety of synthetically important organic transformations such as cycloaddition,⁹⁵ asymmetric hydrogenation,⁹⁶ C-C bond coupling,⁹⁷ and Aldol- and Mannich-type of condensation reactions.⁹⁸ Since enol esters can also serve as a synthon for aldehydes and ketones, much research efforts has been devoted to develop efficient catalytic methods to control both regio- and stereoselectivity in forming substituted enol esters. From an industrial perspective of increasing synthetic efficiency and tolerating functional groups as well as reducing waste byproducts, catalytic methods for producing enol esters are highly desired compared to the classical methods that utilize stoichiometric amounts of strong base or toxic Hg salts.⁹⁹

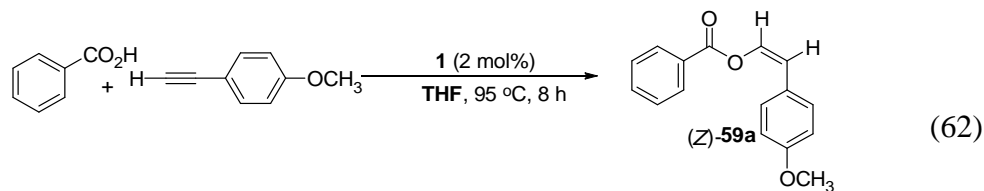
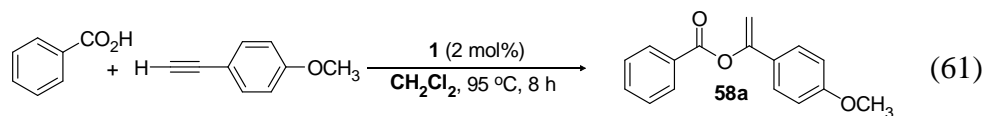
Transition metal-catalyzed alkyne-to-carboxylic acid coupling reaction offers an attractive route to enol esters, but its synthetic potential has not been fully realized, in part because this catalytic method typically produces a mixture of *gem*- and (*E*)/(*Z*)-enol ester products.¹⁰⁰ Considerable research has been devoted to control both regio- and stereoselectivity in forming the enol ester products by modulating steric and electronic nature of the metal catalysts. Generally, late transition metal catalysts have been found to

be effective for the coupling reaction to produce a mixture of (*E*)- and (*Z*)-enol esters from *anti*-Markovnikov addition of carboxylic acids to terminal alkynes over *gem*-enol ester products,¹⁰¹ though the regioselective formation of *gem*-enol esters has recently been achieved by using cationic Rh catalysts.¹⁰² Despite considerable synthetic and mechanistic progress, however, neither the nature of reactive intermediate species nor controlling factors for the formation of *gem*- vs (*E*)/(*Z*)-enol esters have been clearly established. Here we report the coordinatively unsaturated ruthenium-hydride complex (PCy₃)₂(CO)RuHCl (**1**) as a highly effective catalyst for the alkyne-to-carboxylic acid coupling reaction to form synthetically useful enol esters.¹⁰³ This chapter delineates kinetic and mechanistic insights as well as the solvent-controlled regio- and stereoselective formation of the enol ester products that are mediated by the ruthenium-hydride catalyst (Eq 60).



3.1 Results and Discussion

We found that the ruthenium hydride complex $(\text{PCy}_3)_2(\text{CO})\text{RuHCl}$ (**1**) showed the high activity on the coupling reaction of carboxylic acid with terminal alkynes to give product in a 1:1 ratio, and in different solvent it can give different product. For example, treating benzoic acid (122 mg, 1 mmol) with excess 4-ethynylanisole (1.5 mmol) in the presence of complex **1** in 3 mL dichloromethane at 95 °C for 8 hours could cleanly produce germinal olefin with 98% yield (Eq 61). When using THF as the solvent, the *cis*-olefin (*Z*)-**59a** was isolated as product (Eq 62).

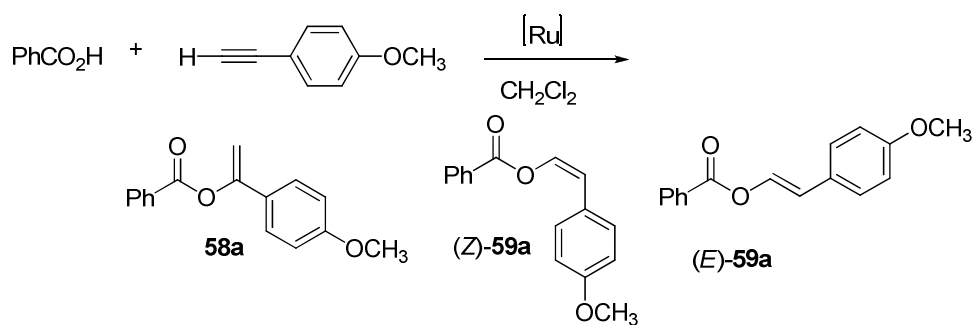


3.2 Optimization Studies for the Coupling of Carboxylic acid with Terminal Alkynes

3.2.1 Catalyst Activity Survey

The catalytic activity of selected ruthenium complexes was initially screened for the coupling reaction of benzoic acid and 4-ethynylanisole.

Table 5. Catalyst Survey on the Coupling Reaction of Benzoic Acid and 4-Ethynylanisole.^a



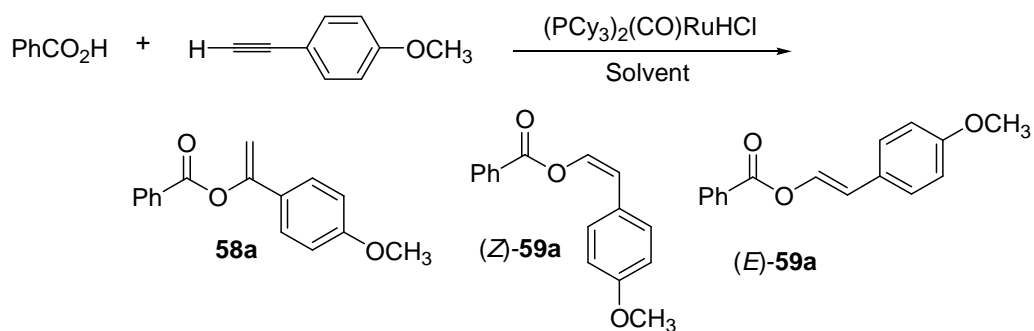
Entry	Catalyst	Yield (%) ^b	58a:(Z)-59a:(E)-59a
1	None	0	
2	(PCy ₃) ₂ (CO)RuHCl	>95	100:0:0
3	(PPh ₃) ₃ (CO)RuH ₂	0	
4	(PPh ₃) ₃ RuCl ₂	0	
5	RuCl ₃ ·3H ₂ O	0	
6	[RuCl ₂ (COD)] _x	0	
7	Ru ₃ (CO) ₁₂	90	8:17:75
8	Cp* ₂ Ru(PPh ₃) ₃ Cl	50	15:50:35
9	Cp* ₂ Ru(COD)Cl	60	27:78 ^c
10	PCy ₃	0	
11	(PCy ₃) ₂ (CO)(CH ₃ CN) ₂ HRu ⁺ BF ₄ ⁻	0	
12	(p-Cymene)RuCl ₂	0	

^a Reaction condition: benzoic acid (0.10 mmol), 4-ethynylanisole (0.15 mmol), catalyst (2 mol %), CH₂Cl₂ (2 mL), 95 °C, 8 h. ^b GC yields based on benzoic acid. ^c The ratio of 58a and 1:2 coupling products.

Among the selected ruthenium catalysts, complex **1** exhibited uniquely high catalytic activity and selectivity, giving the *gem*-enol ester product **58a** exclusively in CH₂Cl₂ within 5 h at 95 °C (Table 5). Both Ru₃(CO)₁₂ and Cp*Ru(PPh₃)₂Cl showed significant activity, but suffered from low selectivity. The catalyst Cp*Ru(COD)Cl, on the other hand, produced a mixture of 1:1 and 1:2 coupling products, which is in line with the previously reported results on the formation of 1:2 coupling products.

3.2.2 Solvent Effects

Solvent effect on catalyst activity and selectivity in coupling reaction of benzoic acid and 4-ethynylanisole was examined (Table 6). A remarkably strong solvent influence on the ruthenium catalyst **1** was observed in modulating the selectivity of the enol ester products. Thus, the coupling reaction in a relatively non-polar and non-coordinating solvent tended to favor formation of germinal coupling product **58a** over (*E*)- and (*Z*)-**59a**, of which CH₂Cl₂ was found to be the best in producing the germinal product **58a** among these non-coordinating solvents (entry 4, Table 6).

Table 6. Solvent Effect on the Coupling Reaction of Benzoic Acid and 4-Ethynylanisole^a

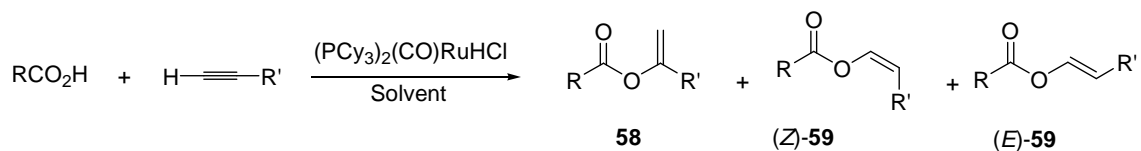
entry	solvent	58a:(Z)-59a:(E)59a	yield ^b
1	benzene	51:40:9	80
2	toluene	68:26:6	70
3	<i>n</i> -hexane	71:18:11	75
4	CH₂Cl₂	99:1:0	>99
5	Et ₂ O	13:20:67	60
6	CH ₃ CN	33:55:13	55
7	DME	5:74:21	50
8	DMSO	2:48:50	53
9	H ₂ O	3:44:53	73
10	THF	0:100:0	>99

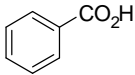
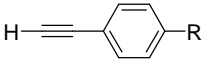
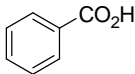
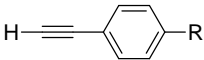
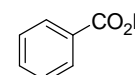
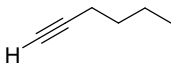
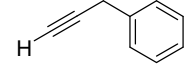
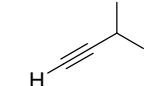
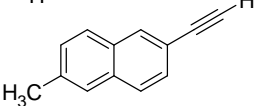
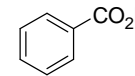
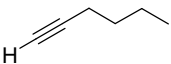
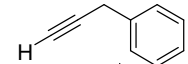
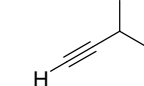
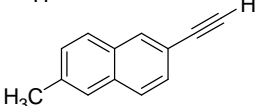
^a Reaction conditions: benzoic acid (0.10 mmol), 4-ethynylanisole (0.15 mmol), **1** (14 mg, 2 mol %), solvent (2 mL), 95 °C, 8 h. ^b GC yields based on benzoic acid.

In contrast, among polar coordinating solvents, which tended to favor the formation of (*Z*)-enol ester product (*Z*)-**59a**, THF was found to be the most selective in giving (*Z*)-**59a** (entry 10). It should be emphasized that the formation of 1:2 coupling products was not observed in the coupling reaction catalyzed by **1**. Other ruthenium catalysts such as Ru₃(CO)₁₂, Cp*Ru(PPh₃)₂Cl and Cp*Ru(COD)Cl surveyed in Table 5 did not exhibit similar degree of solvent control in forming the coupling products. It is imperative to mention about the recent research progress in controlling the activity and selectivity of products by using solvents with different polarity and coordinating ability. Coordinately unsaturated transition metal complexes have been found to be particularly sensitive to the nature of solvents in mediating unreactive bond activation reactions. For example, Milstein discovered a remarkable solvent effect of electrophilic pincer-ligated (PCP)Rh complexes in directing C-H vs. C-C bond activation and C-I vs C-CN reductive elimination reactions.¹⁰⁴ Jones studied the mechanistic aspects of solvent effects in C-C vs. C-H bond cleavage of butenenitriles by using well-defined Ni-diphosphine complexes.¹⁰⁵ The regioselectivity of a number of synthetically useful catalytic coupling reactions of alkenes and alkynes such as Heck-type coupling and allylic substitution reactions, has been successfully controlled by using different solvents.¹⁰⁶

3.3 Reaction Scope

The scope of the coupling reaction was surveyed by using the catalyst **1** in both CH₂Cl₂ and THF (Table 7). Excellent solvent-control in regio- and stereoselective formation of the enol ester products was observed in the coupling reaction of both aryl- and aliphatic terminal alkynes with carboxylic acids. Thus, the coupling reaction in CH₂Cl₂ led to the exclusive formation of the *gem*-enol ester product **58** for both aliphatic and aryl-substituted terminal alkynes. In contrast, the coupling reaction in THF predominantly gave the (*Z*)-enol ester product (*Z*)-**59** for aryl-substituted alkynes. The electronic nature of the alkynes was found to be an important factor in dictating regioselective formation of *gem*-enol ester products **58** from the reaction with the aliphatic terminal alkynes, even when the reaction was performed in THF (Table 7, entries 15, 30, 32). In most cases, a relatively low catalyst loading (1-2 mol %) was used to obtain the enol ester products, which were readily isolated in high yields after a simple column chromatography on silica gel. The coupling reactions in CH₂Cl₂ show the high selectivity for the formation of the germinal product. In this system, a variety of alkynes were tested, such as phenylacetylene, the linear alkynes 1-hexyne (Table 7, entry 13), bulky alkynes 2-ethynyl-6-methoxynaphthalene (entry 16) and both the electron withdrawing substitutes (entry 1 and 2) and electron donating substitutes (entry 4 and 5) only generate germinal coupling products.

Table 7. Alkyne-to-Carboxylic Acid Coupling Reaction Catalyzed by Complex **1**.^a

Entry	Acid	Alkyne	Solvent	Product Ratio 58 :(<i>Z</i>)- 59 :(<i>E</i>)- 59	Yield (%) ^b	
1				R = OMe 58a :(<i>Z</i>)- 59a :(<i>E</i>)- 59a = 100:0:0	91	
2			CH₂Cl₂	R = Me 58b :(<i>Z</i>)- 59b :(<i>E</i>)- 59b = 100:0:0	87	
3				R = H 58c :(<i>Z</i>)- 59c :(<i>E</i>)- 59c = 100:0:0	98	
4				R = Br 58d :(<i>Z</i>)- 59d :(<i>E</i>)- 59d = 100:0:0	98	
5				R = CF ₃ 58e :(<i>Z</i>)- 59e :(<i>E</i>)- 59e = 100:0:0	98	
6				R = F 58f :(<i>Z</i>)- 59f :(<i>E</i>)- 59f = 100:0:0	98	
7						R = OMe 58a :(<i>Z</i>)- 59a :(<i>E</i>)- 59a = 0:100:0
8			CH₂Cl₂	R = Me 58b :(<i>Z</i>)- 59b :(<i>E</i>)- 59b = 0:86:14	90	
9				R = H 58c :(<i>Z</i>)- 59c :(<i>E</i>)- 59c = 0:87:13	98	
10				R = Br 58d :(<i>Z</i>)- 59d :(<i>E</i>)- 59d = 0:94:6	89	
11				R = CF ₃ 58e :(<i>Z</i>)- 59e :(<i>E</i>)- 59e = 0:93:7	90	
12				R = F 58f :(<i>Z</i>)- 59f :(<i>E</i>)- 59f = 0:90:10	87	
13						
14				58h :(<i>Z</i>)- 59h :(<i>E</i>)- 59h = 100:0:0	96	
15			CH₂Cl₂	58i :(<i>Z</i>)- 59i :(<i>E</i>)- 59i = 100:0:0	97	
16				58j :(<i>Z</i>)- 59j :(<i>E</i>)- 59j = 100:0:0	89	
17			THF	58g :(<i>Z</i>)- 59g :(<i>E</i>)- 59g = 100:0:0	97	
18					58h :(<i>Z</i>)- 59h :(<i>E</i>)- 59h = 100:0:0	96
19					58i :(<i>Z</i>)- 59i :(<i>E</i>)- 59i = 100:0:0	97
20					58j :(<i>Z</i>)- 59j :(<i>E</i>)- 59j = 0:100:0	89

Entry	Acid	Alkyne	Solvent	Product Ratio 58:(Z)-59:(E)-59	Yield (%) ^b
21				R = OMe 58k :(Z)- 59k :(E)- 59k = 100:0:0	83
22			CH₂Cl₂	R = Me 58l :(Z)- 59l :(E)- 59l = 100:0:0	90
23				R = Br 58m :(Z)- 59m :(E)- 59m = 100:0:0	68
24				R = CN 58n :(Z)- 59n :(E)- 59n = 100:0:0	89
25				R = CF ₃ 58o :(Z)- 59o :(E)- 59o = 100:0:0	90
26				R = OMe 58k :(Z)- 59k :(E)- 59k = 0:90:10	95
27			THF	R = Me 58l :(Z)- 59l :(E)- 59l = 0:90:10	93
28				R = Br 58m :(Z)- 59m :(E)- 59m = 0:92:8	90
29				R = CN 58n :(Z)- 59n :(E)- 59n = 3:92:5	83
30				R = CF ₃ 58o :(Z)- 59o :(E)- 59o = 8:81:11	85
31			CH₂Cl₂	58p :(Z)- 59p :(E)- 59p = 100:0:0	90
32				58q :(Z)- 59q :(E)- 59q = 100:0:0	93
33			THF	58p :(Z)- 59p :(E)- 59p = 100:0:0	97
34				58q :(Z)- 59q :(E)- 59q = 100:0:0	96
35			CH₂Cl₂	58r :(Z)- 59r :(E)- 59r = 88:12:0	90
36			THF	58r :(Z)- 59r :(E)- 59r = 0:97:3	93
37			CH₂Cl₂	58s :(Z)- 59s :(E)- 59s = 89:11:0	91
38			THF	58s :(Z)- 59s :(E)- 59s = 0:90:10	91

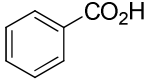
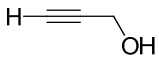
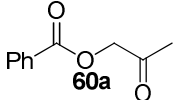
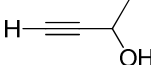
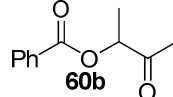
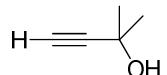
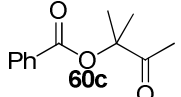
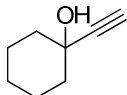
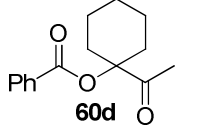
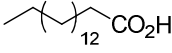
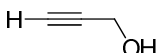
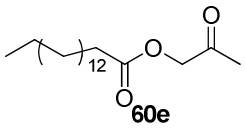
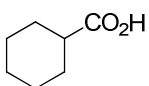
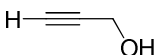
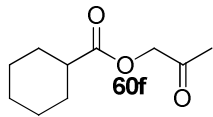
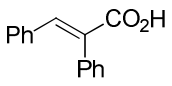
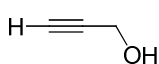
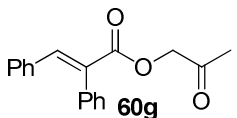
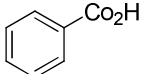
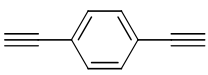
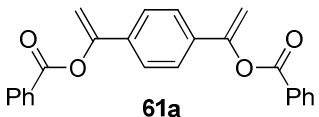
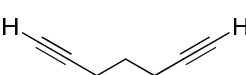
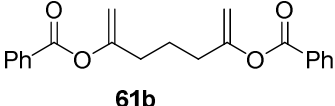
^a Reaction conditions: acid (1.0 mmol), alkyne (2.0 mmol), **1** (14 mg, 2 mol %), solvent (2-3 mL), 90-95 °C, 8-12 h. ^b Isolated yield.

Internal alkynes such as 1-phenyl-1-propyne show no reactivity in the coupling reactions. Most carboxylic acid reactants give the germinal product, but when unbranched linear aliphatic carboxylic acids is used (entry 37), we detected the formation of the (Z)-59s isomer as a minor product. In THF, the reactions favor the anti-Markovnikov addition to generate the (E) and (Z) isomers, with the (Z) isomer is the major coupling product, but the less bulky alkynes such as 1-hexyne (entry 17), 3-phenyl-1-propyne (entry 18) and 3-methyl-3-buten-1-yne (entry 19), only generate the germinal coupling products. For *para*-substituted benzoic acid reactants, electron-donating substituents strongly favor anti-Markovnikov addition. For *para*-substituted benzoic acid with strongly electron withdrawing substituents (entry 29 and 30), a small amount of the germinal was also detected.

To further demonstrate the synthetic utility of the ruthenium catalyst **1**, we next examined the coupling reaction of carboxylic acids with both propargylic alcohols and diynes (Table 8).

Catalyst **1** was found to catalyze coupling reactions of carboxylic acids with propargylic alcohols to give acetomethyl ester products **60** in high yields. In this case, the ketone product was formed exclusive from the Markovnikov-selective hydration of the alkynes. Such Markovnikov-selectivity has been generally preferred for the hydration of terminal alkynes,¹⁰⁷ though *anti*-Markovnikov selective hydration of alkynes has been achieved more recently by using late transition metal catalysts.

Table 8. Coupling Reaction of Carboxylic Acids with Propargyl Alcohols and Diynes.^a

entry	acid	alkyne	product	yield(%) ^b
1				98
2				95
3				97
4				90
5				89
6				83
7				85
8 ^c				90
9 ^c				94

^a Reaction conditions: carboxylic acid (1.0 mmol), alkyne (2.0 mmol), **1** (14 mg, 2 mol %), CH₂Cl₂ (2-3 mL), 90-95 °C, 8-12 h. ^b Isolated yield. ^c 48 h of the reaction time.

The analogous coupling reaction with an aryl-substituted diyne, 1,4-diethynylbenzene, in CH₂Cl₂ predictably yielded the corresponding *gem*-dienol diester product **61a** (entry 8), while a mixture of *gem*-, (*E*)- and (*Z*)-dienol diester products were formed in THF (*gem*:(*E*):(*Z*) = 18:32:50, 91% combined yield). In contrast, an aliphatic diyne produced *gem*-dienol diester **61b** exclusively in both CH₂Cl₂ and THF (entry 9).

3.4 Mechanistic Study

3.4.1 Phosphine Inhibition Study

We performed a series of PCy₃ inhibition experiments to gain further insight into the mechanism of coupling reaction of alkynes and carboxylic acid. It is well documented that PCy₃ ligands reversibly dissociates from the reactive metal centers. This reversible association/dissociation occurs more rapidly at higher temperature, creating vacant coordination sites on the catalyst. Under such conditions, PCy₃ is most likely to inhibit substrate coordination to the active metal sites. In order to observe this phenomenon, experiments analogous to the substrate rate dependence experiments were performed.

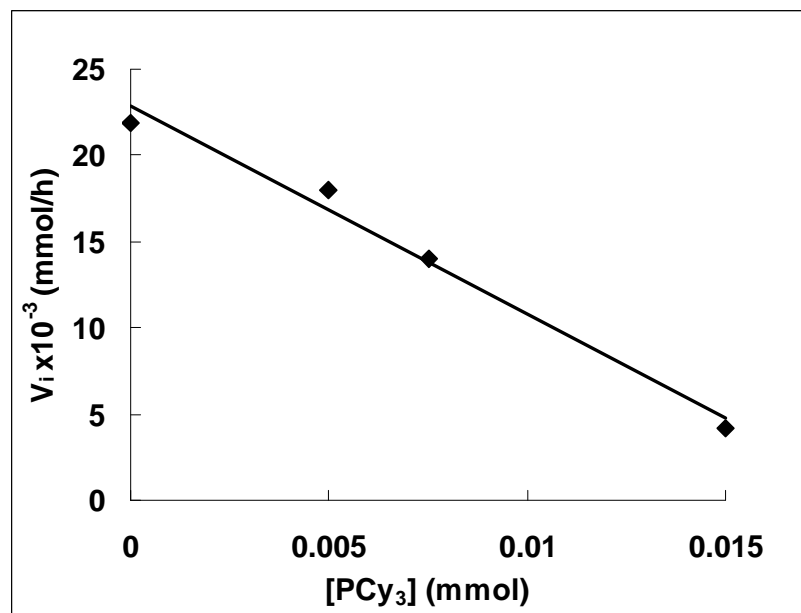
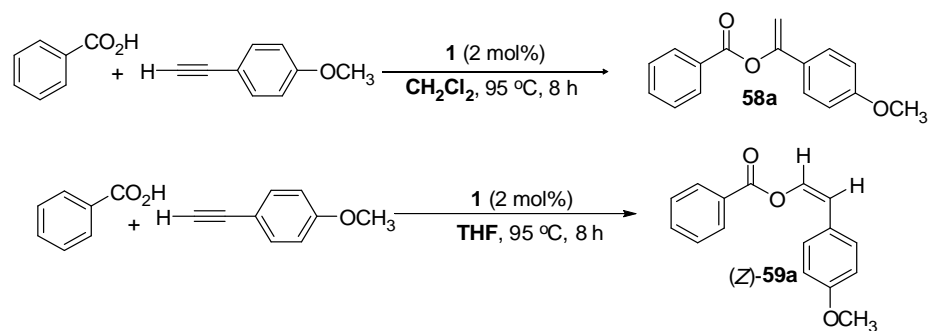


Figure 8. Plot of the Initial Rate (v_i) vs. $[\text{PCy}_3]$ for the Coupling Reaction of Benzoic Acid and Phenylacetylene. Reaction conditions: benzoic acid (0.20 mmol), phenylacetylene (0.40 mmol), **1** (3 mg, 2 mol %), CDCl_3 (0.5 mL).

The initial rate method was used to monitor the rate of formation of enol ester in the presence of increasing PCy_3 concentration of inhibitor. Benzoic acid (0.20 mmol), phenylacetylene (0.40 mmol), **1** (3 mg, 2 mol %) and C_6Me_6 (2 mg, internal standard) were dissolved in 0.5 mL of CDCl_3 solution and transferred into a J-Young NMR tube with a Teflon screw cap. A solution of PCy_3 in CDCl_3 (5 μL , 1.0 M) was added to the tube via

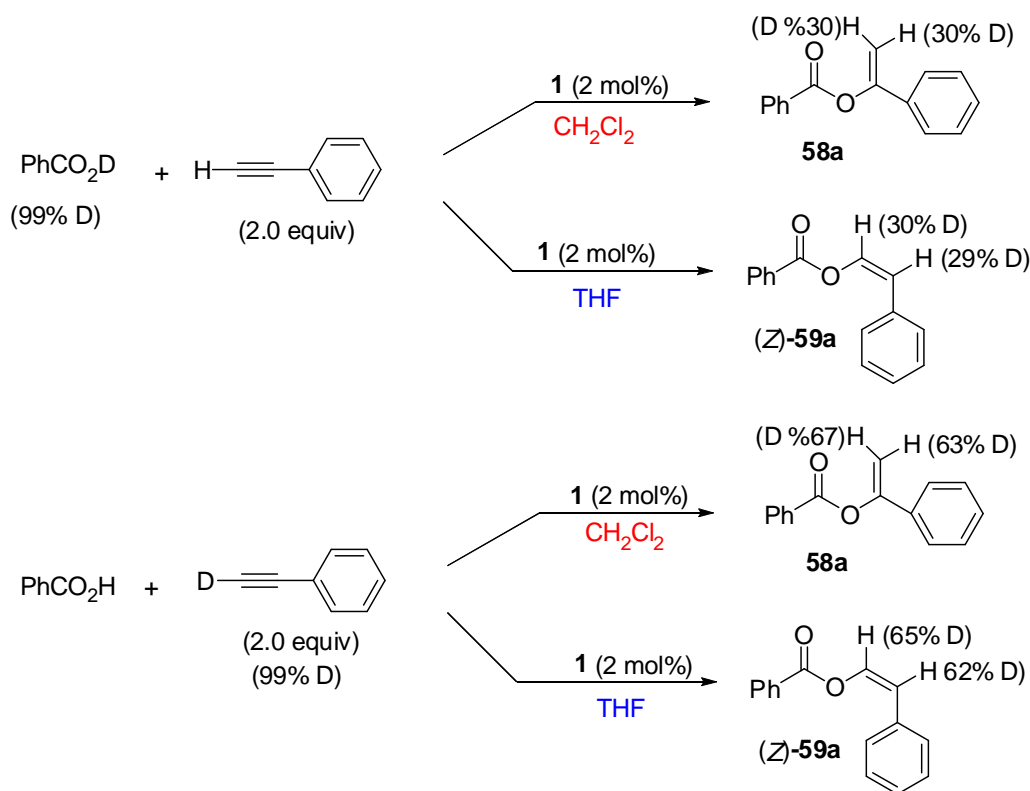
syringe. The tube was brought out of the glove box and was heated in oil bath at 95 °C. The reaction was monitored by ^1H NMR spectroscopy in 30 min intervals. The rate was measured by the ^1H integration of the product peak at δ 5.61 ppm ($=\text{CH}_2$), and was normalized against the internal standard peak.

The initial rates (v_i) were estimated from a first-order plot of $\ln[\text{product}]$ vs. reaction time. The plot of the initial rates (v_i) as a function of $[\text{PCy}_3]$ showed a linear dependency on $[\text{PCy}_3]$ (Figure 8). Addition of PCy_3 (5-15 μmol , 2.5-7.5 mol %) to the reaction mixture under otherwise similar conditions led to a steady decrease of k_{obs} from $1.8 \times 10^{-2} \text{ h}^{-1}$ (without PCy_3) to $4.0 \times 10^{-3} \text{ h}^{-1}$ (15 μmol of PCy_3). These results indicate that the active Ru catalyst is formed by an initial dissociation of the phosphine ligand.

3.4.2 Deuterium Labeling Study

In order to determine the possibility of a rate-limiting step of the catalytic reaction, the following experiments on the deuterium labeling study were performed. The treatment of PhCO_2D with $\text{PhC}\equiv\text{CH}$ (2.0 equiv.) and **1** (2 mol %) in CH_2Cl_2 at 95 °C yielded the *gem*-enol ester product **58a** with 30% D on both vinyl positions as determined by both ^1H and ^2H NMR spectroscopy (Scheme 18). The analogous reaction in THF also formed the product (*Z*)-**59a** with a similar amount of deuterium on the vinyl positions. On

the other hand, the reaction of PhCO₂H with PhC≡CD (2 equiv.) in CH₂Cl₂ produced the *gem*-enol ester product **58a** with nearly equal amount of the deuterium (63-67%) at the vinyl positions, while the reaction in THF resulted in the production of (*Z*)-**59a** with the similar H/D exchange at the vinyl positions. In a separate experiment, the H/D exchange reaction between PhCO₂D with PhC≡CH (2.0 equiv.) and **1** (2 mol %) was almost complete within 10 min at 95 °C prior to the product formation.



Scheme 18. Deuterium Labeling Study on the Coupling Reaction of Alkyne and Carboxylic Acid

The ruthenium catalyst was found to facilitate the H/D exchange, since no significant H/D exchange between PhCO₂D with PhC≡CH was observed in the absence of **1** under otherwise similar conditions. These results indicate that the H/D exchange between the acid and alkynyl hydrogen is rapid and reversible, and that the alkynyl C–H bond activation step is not a rate-limiting step of the coupling reaction.

3.4.3 Hammett Study

To discern the electronic effects on the product formation, the Hammett ρ values were measured for the coupling reaction in both CDCl₃ and THF. In a glove box, a *para*-substituted acid *p*-X-C₆H₄CO₂H (X = OMe, CH₃, H, CF₃) (0.20 mmol), phenylacetylene (40 mg, 0.4 mmol), **1** (3 mg, 2 mol %) and C₆Me₆ (2 mg, internal standard) were dissolved in CDCl₃ (0.5 mL) solution and transferred into a J-Young NMR tube with a Teflon screw cap. The tube was then heated in 95 °C oil bath. The reaction was monitored in 10 min intervals by ¹H NMR spectroscopy. The k_{obs} was estimated from a first-order plot of ln[product] vs. reaction time by measuring the ¹H integration of the product peak (=CH₂, δ 5.61 ppm), which was normalized against the peak of internal standard. For the reaction in THF, *para*-substituted acid *p*-X-C₆H₄CO₂H (X = OMe, CH₃, H, CF₃ and CN) (1.0 mmol), phenylacetylene (200 mg, 2.0 mmol) and **1**

(14 mg, 2 mol %) and C_6Me_6 (26 mg, internal standard) were dissolved in 3 mL of THF solution in a 25 mL Schlenk tube equipped with a Teflon stopcock and a magnetic stirring bar. The tube was then heated in 95 °C oil bath. The reaction was monitored by GC in 10 min intervals.

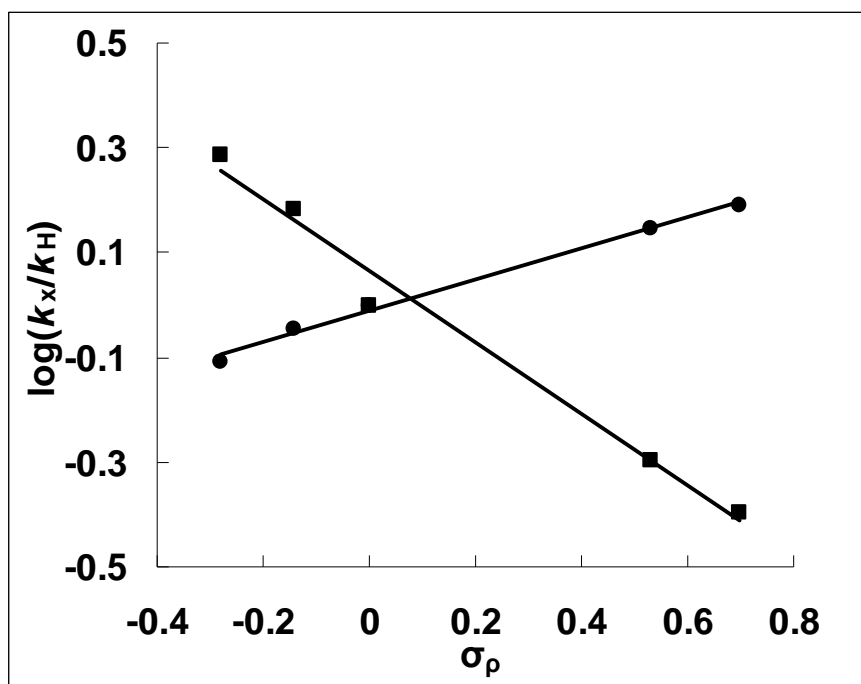
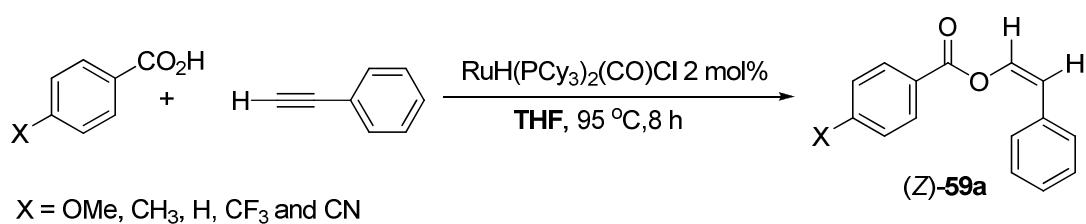
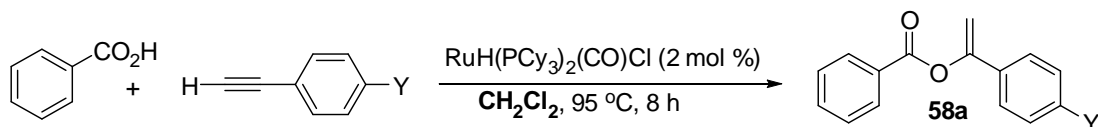
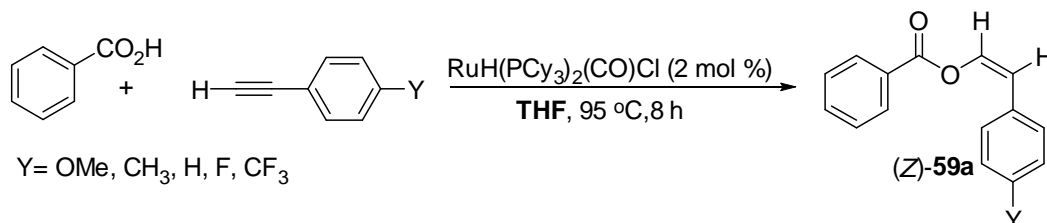


Figure 9. Hammett Plot of the Coupling Reaction of *para*-Substituted p -X- $C_6H_4CO_2H$ (X = OMe, CH₃, H, CF₃, CN) with Phenylacetylene in CDCl₃ (●) and in THF (■)



Y = OMe, CH₃, H, F, CF₃



Y = OMe, CH₃, H, F, CF₃

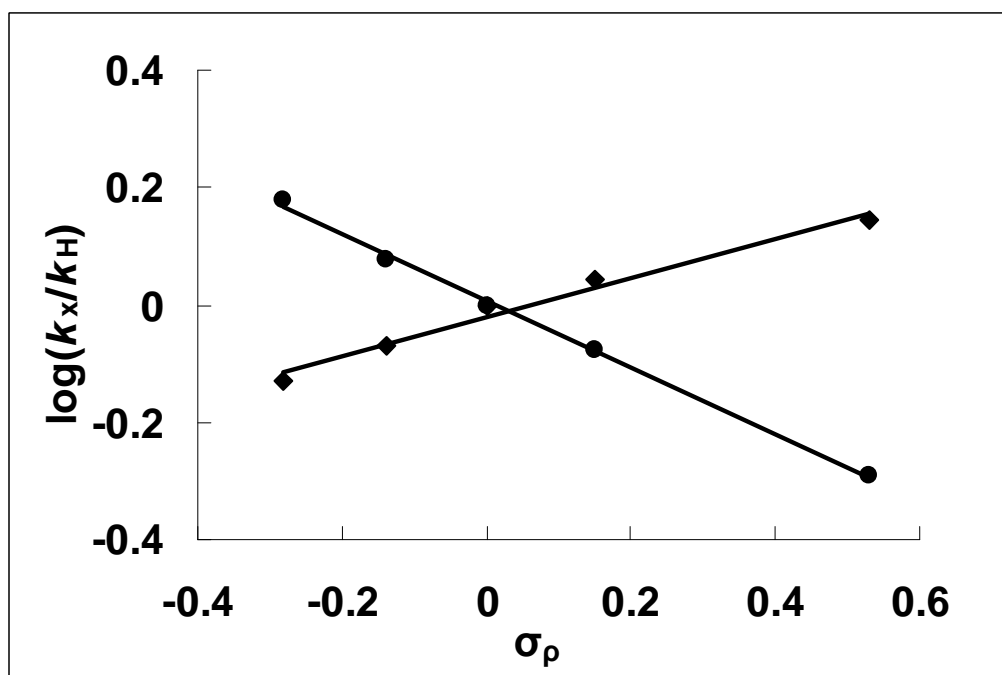


Figure 10. Hammett Plot of the Coupling Reaction of *para*-Substituted *p*-X-C₆H₄C≡CH (X = OMe, CH₃, H, CF₃, F) with Benzoic Acid in CDCl₃ (●) and in THF (■)

The k_{obs} was estimated from a first-order plot of $\ln[\text{product}]$ vs. reaction time by measuring the amount of the products against the internal standard. Thus, correlation of the relative rates with ρ for a series of *para*-substituted benzoic acids *p*-X-C₆H₄CO₂H (X = OMe, CH₃, H, CF₃, CN) with phenylacetylene in the presence **1** (2 mol %) at 95 °C led to

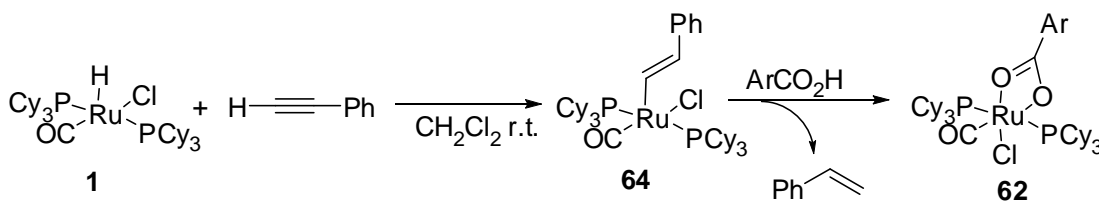
the opposite trend between the reaction in CDCl_3 ($\rho = +0.30$) and in THF ($\rho = -0.68$, Figure 9). An analogous correlation of the reaction rates of benzoic acid with a series of *para*-substituted alkynes $p\text{-Y-C}_6\text{H}_4\text{C}\equiv\text{CH}$ (Y = OMe, CH₃, H, F, CF₃) also resulted in the opposite slope between two solvents ($\rho = -0.57$ in CDCl_3 vs $\rho = +0.33$ in THF, Figure 10).

The opposite Hammett ρ value indicates a different mechanistic pathway for the coupling reaction between CDCl_3 and THF. The positive ρ value observed from the correlation of *para*-substituted benzoic acids $p\text{-X-C}_6\text{H}_4\text{CO}_2\text{H}$ in CDCl_3 matches well with the nucleophilicity of the carboxylic oxygen atom due to a developing negative charge on the carbonyl oxygen, resulted from the direct migratory insertion of the acid to the coordinated terminal alkyne.

On the other hand, a negative ρ value from the reaction in THF indicates considerable cationic character build-up on the transition state, and this can be explained via formation of Ru-vinylidene species, where α -vinylidene carbon has been well known to be electrophilic. The analogous opposite trend from the correlation of the alkynes $p\text{-Y-C}_6\text{H}_4\text{C}\equiv\text{CH}$ can be explained similarly in terms of charges development on the alkynyl carbon. Thus, a negative ρ value in CDCl_3 is consistent with the positive charge build-up on the internal alkynyl carbon, while the positive ρ value in THF suggests a partial positive charge build-up on the terminal alkynyl carbon. Once again, the latter case is consistent with the formation of a Ru-vinylidene species and the addition of the carboxylate group to the electrophilic α -vinylidene carbon in the transition state.

3.4.4 Synthesis of Catalytically Relevant Ruthenium-Carboxylate

A catalytically relevant ruthenium-carboxylate complex was successfully isolated from the reaction of **1** with a carboxylic acid. Thus, the treatment of **1** (72 mg, 0.10 mmol) with phenylacetylene in CH₂Cl₂ (2 mL) at room temperature for 10 min form the complex **64** in 95% isolated yield. And the treatment of complex **64** (0.1 mmol) with *p*-OMe-C₆H₄CO₂H (0.11 mmol) in CH₂Cl₂ (2 mL) at room temperature for 10 h led to the clean formation of ruthenium-carboxylate complex **62**, which was isolated in 87% yield after recrystallization in CH₂Cl₂/*n*-hexanes (Scheme 19).



Scheme 19. Synthesis of Ruthenium Vinylidene and Carboxylate Complexes

Complex **62** exhibited two sets of aryl protons at δ 7.88 (d, $J = 8.7$ Hz) and 6.89 (d, $J = 8.7$ Hz) in ¹H NMR spectroscopy, as well as two carbonyl peaks at δ 208.8 (t, $J_{\text{PH}} = 13.3$ Hz, CO) and 179.0 (s, CO₂) in ¹³C {¹H} NMR spectroscopy. A single phosphine peak at δ 28.7 was also observed by ³¹P {¹H} NMR spectroscopy.

The structure of **62** was further established by X-ray crystallography (Figure 11).

The molecular structure showed a relatively acute *cis* geometry between CO and Cl⁻ ligands (bond angle = 96.4°) to accommodate κ^2 -bonding mode of the carboxylate ligand. Isolated complex **62** was found to be an active catalyst for coupling reactions of alkyne.

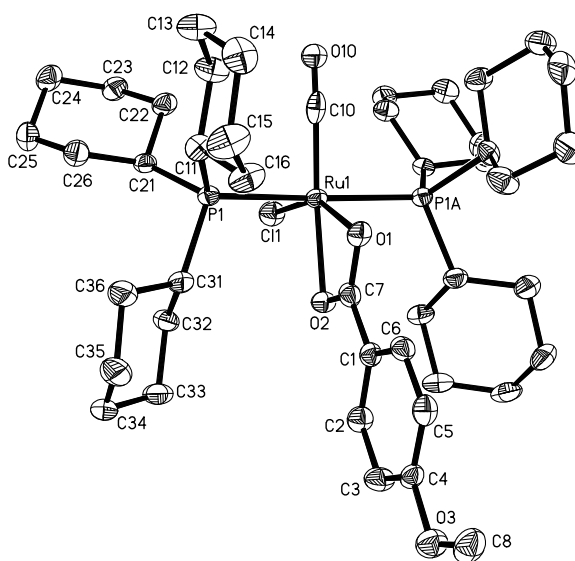


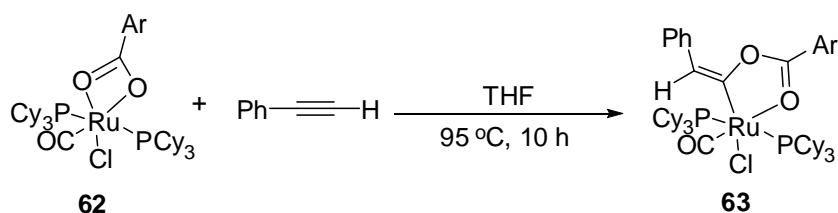
Figure 11. Molecular Structure of **62**

3.4.5 Synthesis of Catalytically Relevant Ruthenium–Vinylidene–Carboxylate Complexes

The reaction of the ruthenium-carboxylate complex **62** with terminal alkynes was performed in THF to form a catalytically relevant ruthenium-vinylidene complex.

Complex **62** (44 mg, 0.050 mmol) was heated with phenylacetylene (1.2 equiv) in THF to 95 °C for 10 h led to the coupling product **63**, which was isolated in 85% yield as a yellow-colored solid (Scheme 20).

^1H NMR of complex **63** showed a diagnostic vinyl peak at δ 6.24 (br s), and two distinct K-carbonyl peaks at δ 208.8 (t, $J_{\text{PH}} = 14.4$ Hz, Ru-CO) and 190.2 (t, $J_{\text{PH}} = 12.1$ Hz, Ru-C(O)CHPh) were also observed in the $^{13}\text{C}\{^1\text{H}\}$ NMR spectroscopy.



Scheme 20. Synthesis of Catalytically Relevant Ruthenium -Vinylidene-Carboxylate Complexes

The Structure of **63** was further established by X-ray crystallography (Figure 12). The molecular structure of **63** showed a *syn* orientation between the carboxylate oxygen atom and the phenyl group, which was resulted from the coupling between the carboxylate and the vinylidene ligand. The structure clearly implicates the formation of the (*Z*)-enol ester product (*Z*)-**59k** from the protonation by another carboxylic acid. To show the enol ester product formation, complex **63** was treated with an equivalent of

benzoic acid in THF at 90 °C, which produced carboxylate complex **62** and (*Z*)-**59k** along with another unidentified ruthenium complexes. Furthermore, catalytic activity of **63** for the coupling reaction was found to be virtually identical as **1**.

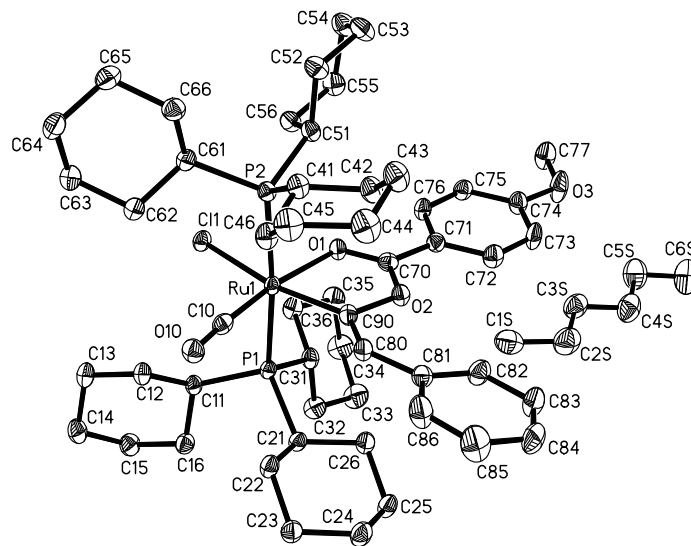
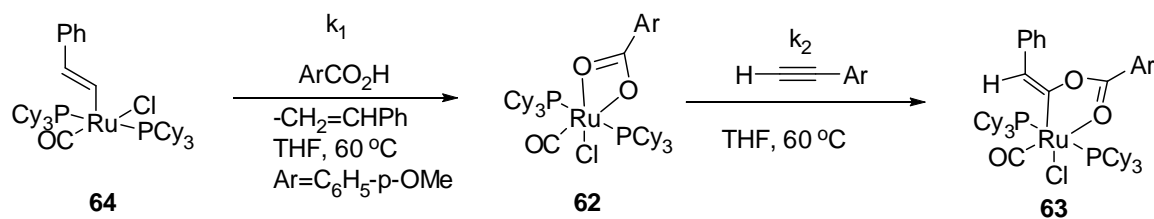


Figure 12. Molecular Structure of **63**

3.4.6 Kinetic Experiments on the Conversion of Complex **64** to Complex **62** and Complex **63**



Scheme 21. Synthesis of Complex **62** and Complex **63** from Complex **64**

The successful isolation of the catalytically relevant complexes **62** and **63** enabled us to further examine the kinetics of the formation of these complexes. The treatment of **1** (14 mg, 0.02 mmol) with an excess amount of *p*-OMe-C₆H₄CO₂H (10 equiv.) and HC≡CPh (15 equiv.) in THF was followed by ¹H and ³¹P NMR spectroscopy (Scheme 21).

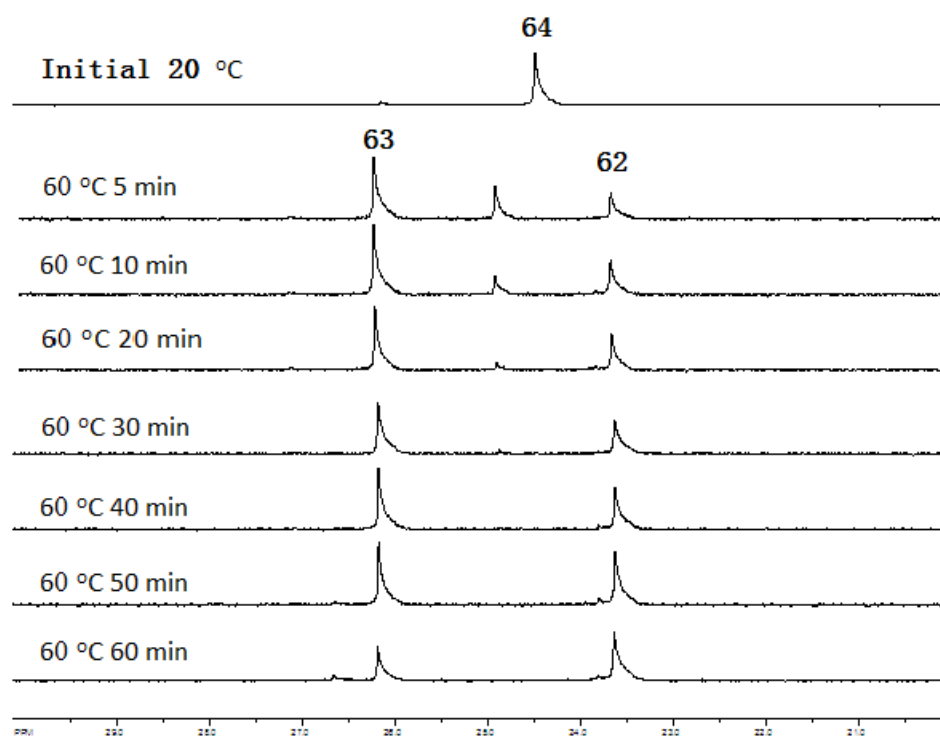


Figure 13. High-temperature VT-NMR of the Conversion of Complex **62** and **63** from Complex **64**

As expected, the formation of the previously synthesized ruthenium-vinyl complex **64** was observed after 15 min at room temperature.¹⁰⁹ For ³¹P NMR, there was only one peak at 24.5 ppm in THF. The formation of complex **62** can happen at 20 °C,

but it is slow. Upon warming up to 60 °C, the vinyl complex **64** was converted to carboxylate complex **62** within 30 min along with formation of styrene. And the signal (P2 at 26.3 ppm) due to vinylidene-carboxylate complex **63** gradually appeared at the expense of carboxylate complex **62**. Formation of complex **63** from complex **62** went smoothly and took couple hours (Figure 13). At these periods the formation of coupling product was not detected. After 3 hours, the mixtures was heated up to 90 °C for 2 hour, formation of the coupling product (Z)-**59k** was detected by ¹H NMR spectroscopy and about 10% of Cy₃PH⁺PhCO₂⁻ was detected by ³¹P NMR spectroscopy.

3.4.7 Derivation of the Kinetic Equation of the Conversion of **64** to **63**

The derivation for two consecutive first-order reactions was followed as described¹⁰⁸.

$$d[\mathbf{64}]/dt = -k_1t$$

$$d[\mathbf{62}]/dt = k_1[\mathbf{64}] - k_2[\mathbf{62}]$$

$$d[\mathbf{63}]/dt = k_2[\mathbf{62}]$$

$$[\mathbf{64}] = [\mathbf{64}]_0 e^{-k_1t}$$

$$d[\mathbf{62}]/dt = k_1[\mathbf{64}]_0 e^{-k_1t} - k_2[\mathbf{62}]$$

$$[\mathbf{62}] = [\mathbf{64}]_0 k_1 (e^{-k_1t} - e^{-k_2t}) / (k_2 - k_1)$$

$$d[\mathbf{64}]/dt + d[\mathbf{62}]/dt + d[\mathbf{63}]/dt = 0$$

Since:

$$[\mathbf{64}] + [\mathbf{62}] + [\mathbf{63}] = [\mathbf{64}]_0$$

$$[\mathbf{62}]_0 = [\mathbf{63}]_0 = 0$$

$$[\mathbf{63}] = [\mathbf{64}]_0 - [\mathbf{64}] - [\mathbf{62}]$$

$$= [\mathbf{64}]_0 [1 + (k_2 e^{-k_1 t} - k_1 e^{-k_2 t}) / (k_1 - k_2)]$$

$$d[\mathbf{63}]/dt = [\mathbf{64}]_0 k_1 k_2 [(e^{-k_1 t} - e^{-k_2 t}) / (k_1 - k_2)]$$

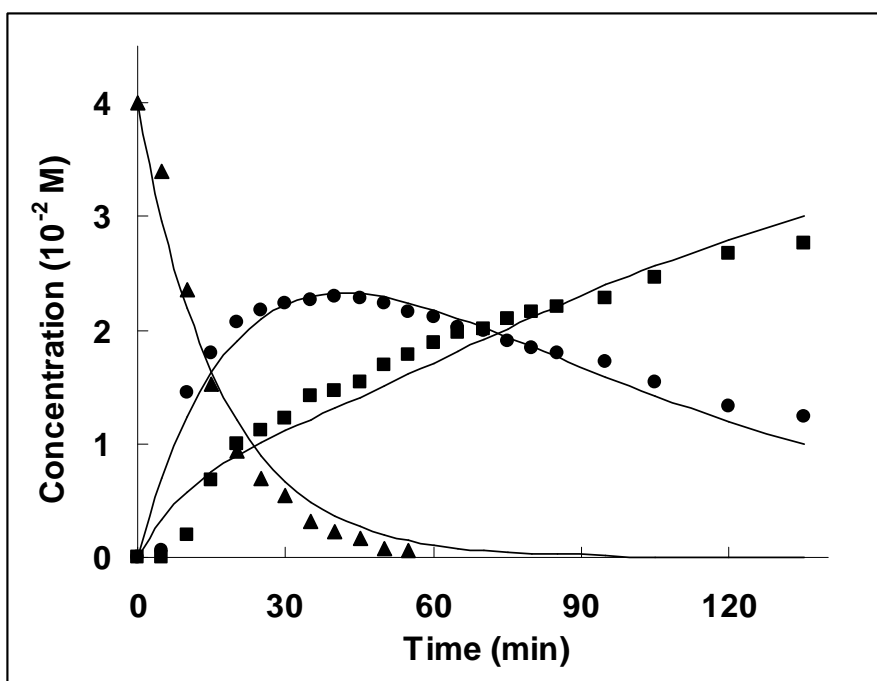


Figure 14. Kinetic Profile of the Conversion of **64** to **63**. Notations: **64** (▲), **62** (●), **63** (■)

The experimental data was globally fitted to the kinetic equation by non-linear regression techniques (Sigmaplot V. 10). The rate constants $k_1 = 0.039 \text{ min}^{-1}$ and $k_2 = 0.013 \text{ min}^{-1}$ were obtained and from this analysis, which led to

$$\begin{aligned} d[\mathbf{63}]/dt &= [\mathbf{64}]_0 * 0.039 * 0.013 * (e^{-0.039t} - e^{-0.013t}) / (0.039 - 0.013) \\ &= [\mathbf{64}]_0 * 0.0195 * (e^{-0.039t} - e^{-0.013t}) \end{aligned}$$

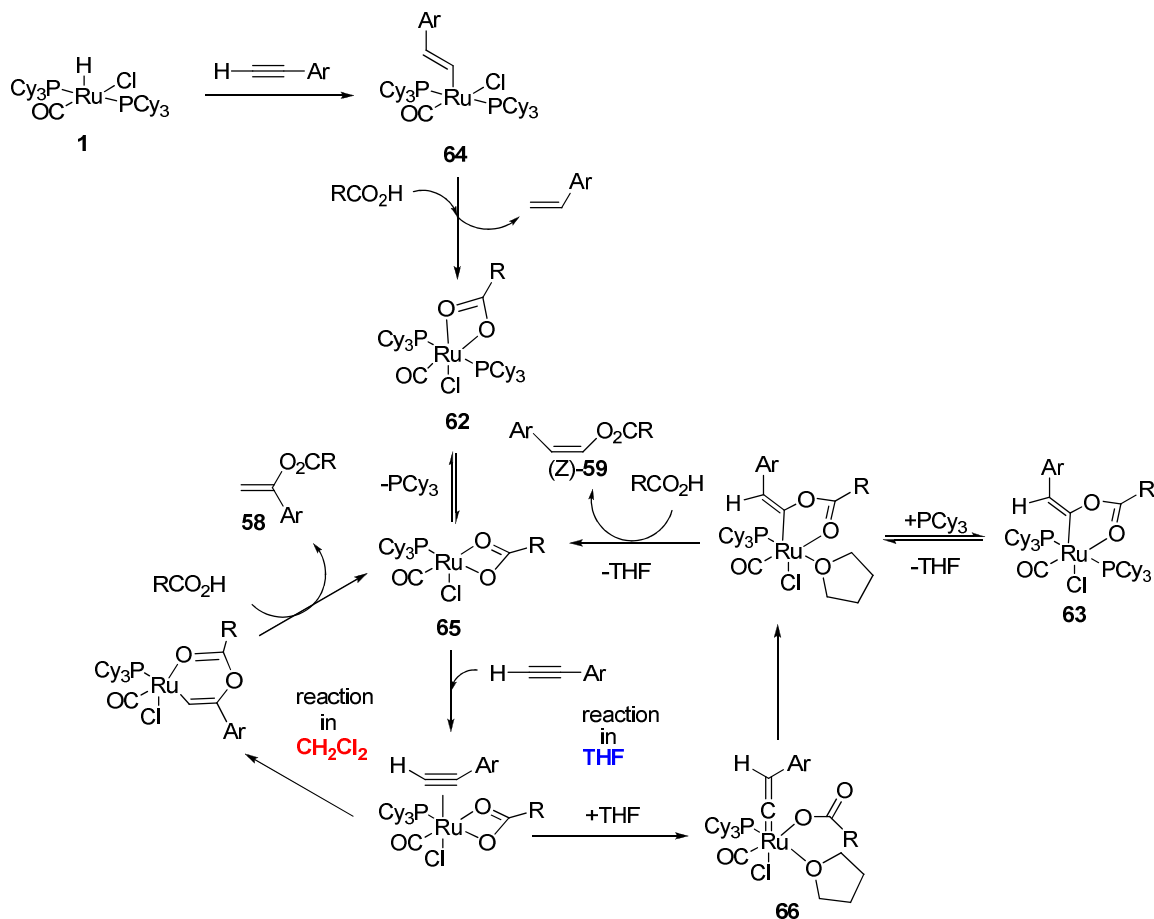
The kinetics of the conversion of the vinyl complex **64** to the carboxyl complex **63** was followed by ^{31}P NMR spectroscopy (Figure 14). In a J-Young NMR tube, **1** (14 mg, 0.020 mmol), 4-methoxybenzoic acid (30 mg, 0.20 mmol) and phenylacetylene (31 mg, 0.30 mmol) in THF was dissolved in THF (0.5 mL). Formation of the vinyl complex **64** was completed within 10 min at room temperature. The appearance of **62** and **63** was monitored by ^{31}P NMR spectroscopy at 60 °C in 5 min intervals.

The experimental data was globally fitted to the kinetic equation for two consecutive reactions kinetics by non-linear regression techniques for the conversion from **64** to **63** (Sigmaplot Version 10). The rate constants $k_1 = 0.039 \text{ min}^{-1}$ and $k_2 = 0.013 \text{ min}^{-1}$ were obtained and from this analysis. A relatively smaller value of k_2 compared to k_1 is consistent with the rate-limiting C-O bond formation step.

3.4.8 Proposed Mechanism

We proposed a mechanism for the coupling reaction involving a coordinative unsaturated ruthenium-carboxylate complex **65** as one of the key intermediate species (Scheme 22). The phosphine inhibition study suggests that the catalytically active 16 e⁻ complex **65** is formed from the Ru-carboxylate complex **62** by reversible phosphine dissociation. For the coupling reactions in a non-coordinating solvent such as CH₂Cl₂, direct migratory insertion of the carboxylate oxygen atom to an internal carbon of the alkyne substrate is preferred over the terminal ones to give the germinal ester product **58**. The dative coordination of carboxylic oxygen atom would promote such insertion by stabilizing the intermediate species.

On the other hand, formation of (*Z*)-enol ester product (*Z*)-**59** is rationalized via formation of Ru-vinylidene species **66**. It is well-established that the acetylene-to-vinylidene rearrangement is relatively facile for aryl-substituted alkynes. The X-ray crystal structure of **63** provided a direct evidence for the *cis* addition of carboxylate oxygen to the Ru-vinylidene ligand. The ability to promote the acetylene-to-vinylidene rearrangement for the ruthenium-catalyst in a coordinating solvent such as THF appears to be an important factor for the stereoselective formation of (*Z*)-enol ester products.



Scheme 22. Proposed Mechanism of the Coupling Reaction of Carboxylic Acids and Terminal Alkynes

The Hammett study suggested that C-O bond formation in catalytic coupling reaction is strongly influenced by the electronic nature of the substrates. For the coupling reaction in CH_2Cl_2 , this implies a direct migratory insertion of the coordinated terminal alkyne to the Ru-carboxylic oxygen bond, where both steric and electronic factors dictate the Markovnikov-selective formation of the gem-enol ester product **58**. The dative coordination of the carbonyl oxygen to the Ru center would also facilitate this

transformation by avoiding the formation of a high-energy 14-electron species. The successful isolation of **62** and **63** and their kinetic reaction profile provided a mechanistic rationale for the formation of (*Z*)-enol ester products (*Z*)-**59**. It is reasonable to extrapolate that the coordinating THF solvent promotes the acetylene-to-vinylidene rearrangement for aryl-substituted alkynes by stabilizing unsaturated Ru-vinylidene complex **66**. The reversible dissociation of PCy₃ from both complexes **62** and **63** would form the catalytically active species for the coupling reaction. A slow formation of Cy₃PH⁺ apparently from the protonation reaction with the carboxylic acid substrate would also prohibit the re-coordination of the dissociated PCy₃ ligand. The *syn* geometry of the vinylidene-carboxylate ligand of **63** clearly indicates that the formation of (*Z*)-enol ester product (*Z*)-**3** is electronically controlled during the addition of carboxylate group to the vinylidene ligand of the ruthenium-vinylidene species **66**. From a purely steric perspective, such *syn* addition step would be favored over the anti- Markovnikov addition due to sterically demanding Ru center, and would also be facilitated by the dative coordination of the carboxylate oxygen atom. Since these catalytically active species are not easily detected by spectroscopic methods, corresponding computational study on related catalytic coupling reactions would be prudent in identifying these catalytically active intermediate species.

3.5 Conclusions

The ruthenium-hydride complex **1** was found to be a highly effective catalyst for the alkyne-to-carboxylic acid coupling reaction to give synthetically valuable enol esters. Regio- and stereoselective pattern of the catalyst **1** was successfully controlled by using CH_2Cl_2 and THF. The salient features of the ruthenium catalyst **1** are: its ability to control the activity and selectivity on the enol ester products as well as a broad substrate scope and mild reaction condition. A detailed mechanism of the coupling reaction has been established from the kinetic and mechanistic investigations as well as the successful isolation of ruthenium-carboxylate and -vinylidene complexes **62** and **64**. The mechanistic knowledge gained from these studies should provide new insights in designing the next generation of the metal catalysts.

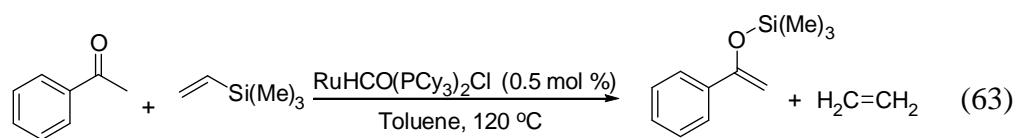
Chapter 4. Catalytic Formation of Silyl Enol Ethers from the Reaction of Ketones with Vinylsilanes and Their Use in Aldol-Type Condensation and Fluorination Reactions

Enol silyl ethers are widely employed in the organic synthesis as the reactive precursors for for a number of synthetically useful C-C and C-heteroatom bond forming reactions. They are useful in various synthetic transformations in the various region-, chemo- and stereoselective reactions. Silyl enol ethers have been commonly utilized as precursors for Aldol-type condensations and other α -functionalization reactions of ketones and bulk material synthesis.¹⁰⁹ Over the past decades, methods have been developed to generate the enol silyl ethers. One of the early and still one of the mostly frequently used route to (*E*) or (*Z*)-silyl enol ethers is trapping ketone or aldehyde enolates generated under the kinetics or equilibrium controlled conditions. Another widely used method to generate enol silyl ethers is by deprotonation of acidic α -proton of carbonyl compounds and trapping the corresponding enolates with R_3SiCl . Since a stoichiometric amount of strong base is required to form enolates, the method is generally incompatible with highly functionalized ketone substrates and controlling stereochemistry of *E/Z* mixture of the enol ethers has often been a problematic. The transition metal catalyzed silylation methods offer significant advantages in forming silyl enol ethers, because these methods do not require strong base and generate less waste. The most widely used catalyst for the formation of enol silyl ether is iridium complexes,

but the problem is that the reaction conditions require high temperature, high pressure and high catalyst loading. We are working on the methods to generate the enol silyl ether in the mild conditions by the ruthenium complexes. We previously reported that the well-defined ruthenium-hydride complex $(PCy_3)_2(CO)RuHCl$ (**1**) is an effective catalyst precursor for oxidative silylation of terminal alkenes and alkynes.¹¹⁰ Here we report a highly regioselective formation of silyl enol ethers from the coupling reaction of ketones and vinylsilanes. The synthetic utility of the silyl enol ethers formed in this reaction has been demonstrated by Mukaiyama Aldol condensation and fluorination reactions. More details on the mechanistic study will allow to be discussed.

4.1 Results and discussion

Recently, we found that the ruthenium hydride complex **1** was effective for the coupling reactions of ketones and vinylsilane to generate the enol silyl ether. From the initial study, the treatment of acetophenone (1 mmol) with excess vinyltrimethylsilane (2 mmol) in the presence of **1** (0.5 mol %) in toluene at 120 °C for 12 hours cleanly produced the enol silyl ether in 95% conversion and the ethylene gas as byproduct (Eq 63).

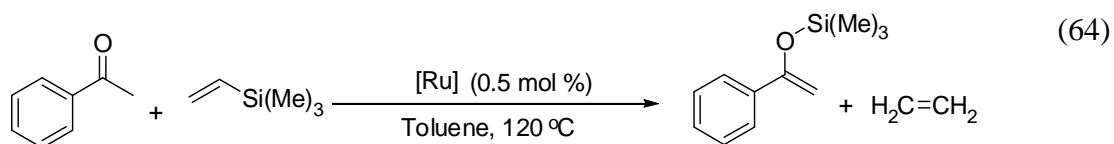


The details on the reactions scope, the synthetic utility for the silyl enol ethers and more details on the mechanistic study will be discussed.

4.2 Optimization Studies for the Coupling of Ketones with Vinylsilane

4.2.1 Catalyst Activity Survey

The catalytic activity of selected ruthenium complexes were initially screened for the coupling reaction of phenyl acetone and vinyltrimethylsilane (Eq 64).



The survey of the catalysts showed that ruthenium hydride complex **1** has the highest activity in the formation of the enol ether among selected ruthenium complexes (Table 9, entry 5). $(\text{PCy}_3)_2(\text{CO})\text{RuHCl}$ (**1**) complex exhibited uniquely high activity for silylation reaction, giving >99% conversion with less than 0.5 mol % catalyst loading (Table 9). The ruthenium complex $\text{RuH}_2(\text{CO})(\text{PPh}_3)_3$ (entry 7) showed a modest activity,

giving the coupling product in 20% yield under similar reaction condition. Other commonly ruthenium complexes such as $\text{Ru}_3(\text{CO})_{12}$, $\text{Ru}(\text{CO})\text{H}_2(\text{PPh}_3)_3$, $\text{RuCl}_3 \cdot 3\text{H}_2\text{O}$, $[(\text{COD})\text{RuCl}_2]_x$ and $[(\text{PCy}_3)_2(\text{CO})(\text{MeCN})_2\text{RuH}]^+\text{BF}_4^-$, were not effective in giving coupling products under similar reaction condition.

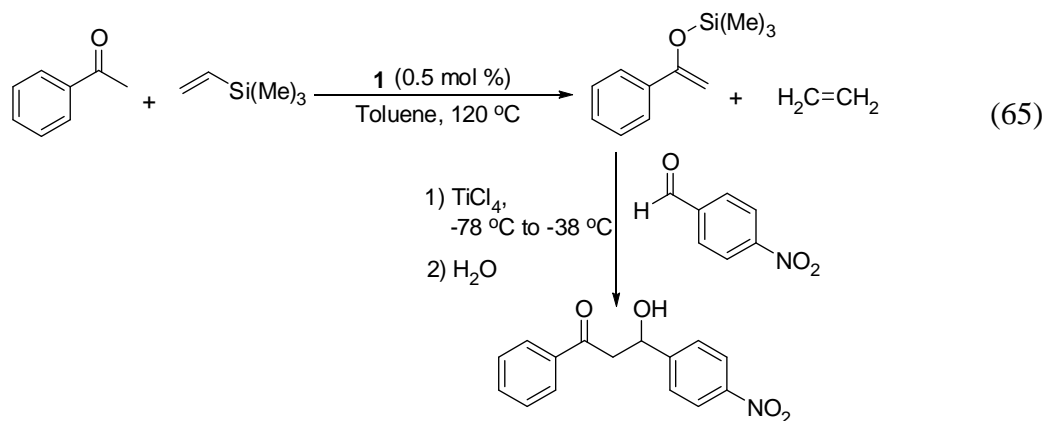
Table 9. Catalyst Activity Survey for the Coupling Reaction of Vinyltrimethylsilane and Acetophenone.^a

Entry	Catalyst	Additive	Yield (%) ^b
1	None	None	0
2	$\text{Ru}_3(\text{CO})_{12}$	None	0
3	$\text{Ru}_3(\text{CO})_{12}$	NH_4PF_6	0
4	$\text{RuCl}_3 \cdot 3\text{H}_2\text{O}$	None	0
5	$(\text{PCy}_3)_2(\text{CO})\text{RuHCl}$	None	99
6	$(\text{PCy}_3)_2(\text{CO})\text{RuHCl}$	HBF_4OEt_2	<5
7	$(\text{PPh}_3)_3(\text{CO})\text{RuH}_2$	None	0
8	$(\text{PPh}_3)_3\text{RuCl}_2$	None	0
9	$(\text{PPh}_3)_3(\text{CO})\text{RuHCl}$	None	0
10	$[\text{RuCl}_2(\text{COD})]_x$	None	0
11	$[(\text{PCy}_3)_2(\text{CO})(\text{CH}_3\text{CN})_2\text{HRu}]^+\text{BF}_4^-$	None	<3
12	$(p\text{-Cymene})\text{RuCl}_2$	None	0
13	PCy_3	None	0

^a Reaction conditions: 0.1 mmol of acetophenone, 0.2 mmol vinyltrimethylsilane, catalyst (0.5 mol %), toluene (2 mL), 120 °C, 12 h. ^b GC yields based on acetophenone.

4.3 The Scope for the Reactions of Ketones with Vinylsilane and the Reaction of Enol Ether with Aldehyde under the Titanium (IV) Chloride

To demonstrate the synthetic utility of the catalyst $(\text{PCy}_3)_2(\text{CO})\text{RuHCl}$ on the reactions of ketones and vinylsilane, the scope of the reaction was explored by using $(\text{PCy}_3)_2(\text{CO})\text{RuHCl}$ (**1**) as the catalyst (Table 10). A variety of ketones was explored in this reaction; both alkyl- and aryl-substituted ketones were found reacting smoothly with vinyltrimethylsilane to give enol silyl ether products. In general, the conversion the products determined by GC-MS was found to be quite high with a relatively small catalyst loading (0.5-1 mol % of Ru). Since many of silyl enol ether products were found to be thermally unstable and could not be isolated by column chromatography, isolated yields of the products were determined from the Mukaiyama Aldol condensation reaction with an aldehyde. Thus, treatment of the silyl enol ether (entry 7) product with $p\text{-NO}_2\text{-C}_6\text{H}_4\text{CHO}$ in the presence of a stoichiometric amount of TiCl_4 led to β -hydroxyketone products (Eq 65).¹¹¹



In a typical reaction, after evaporating the solvent from the silyl enol ether solution under high vacuum, and the crude product was dissolved in CH_2Cl_2 (2-3 mL). In a separate 100 mL Schlenk flask, TiCl_4 (3 mmol) was added to a cooled CH_2Cl_2 solution (5 mL) of 4-nitrobenzaldehyde (3 mmol) at $0\text{ }^\circ\text{C}$. After stirring for about 15 min, the solution was cooled to $-78\text{ }^\circ\text{C}$, and the CH_2Cl_2 solution of crude silyl enol ether was added dropwise via a syringe to the reaction flask. After stirring at $-40\text{ }^\circ\text{C}$ for 1 h, water (3 mmol) was added to the reaction flask, and the resulting mixture was stirred at $0\text{ }^\circ\text{C}$ for 8 h. The reaction mixture was quenched by adding saturated Na_2CO_3 solution (10 mL), and the organic layer was extracted with Et_2O ($3 \times 20\text{ mL}$). The ether solution was dried with anhydrous MgSO_4 , and the Aldol product was isolated by a column chromatograph on silica gel (*n*-hexanes/ CH_2Cl_2) and the product was characterized by NMR in Figure 15.

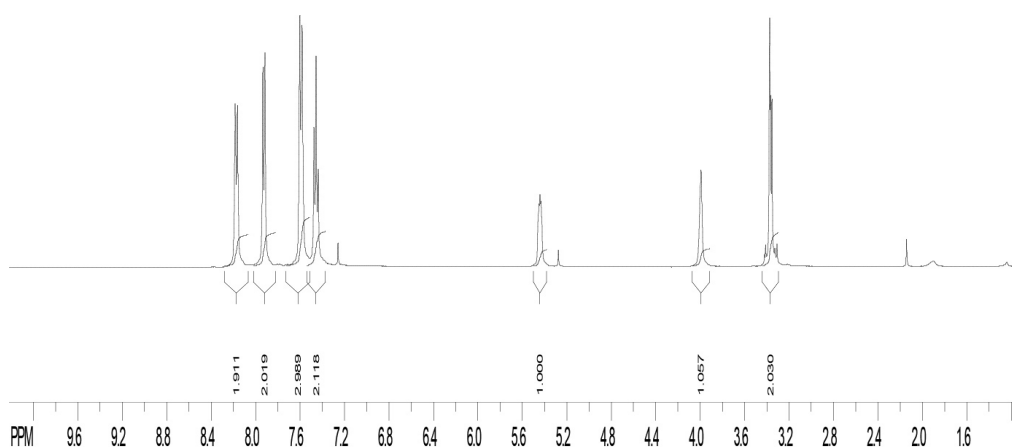
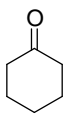
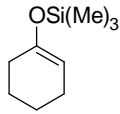
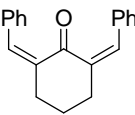
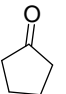
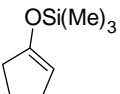
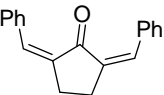
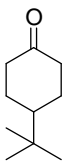
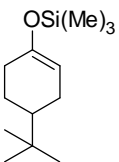
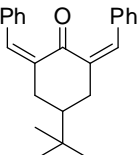
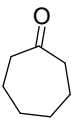
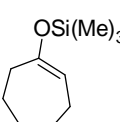
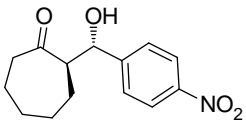
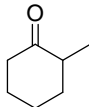
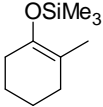
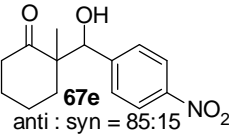
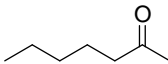
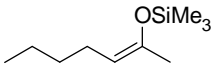
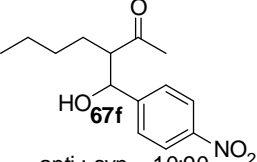
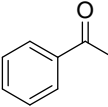
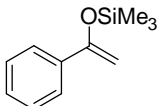
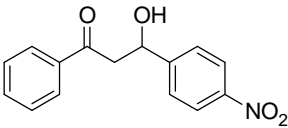
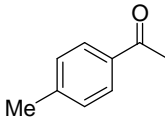
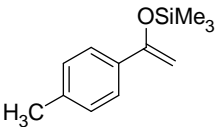
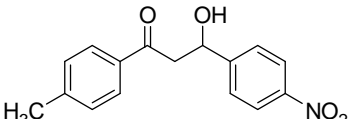
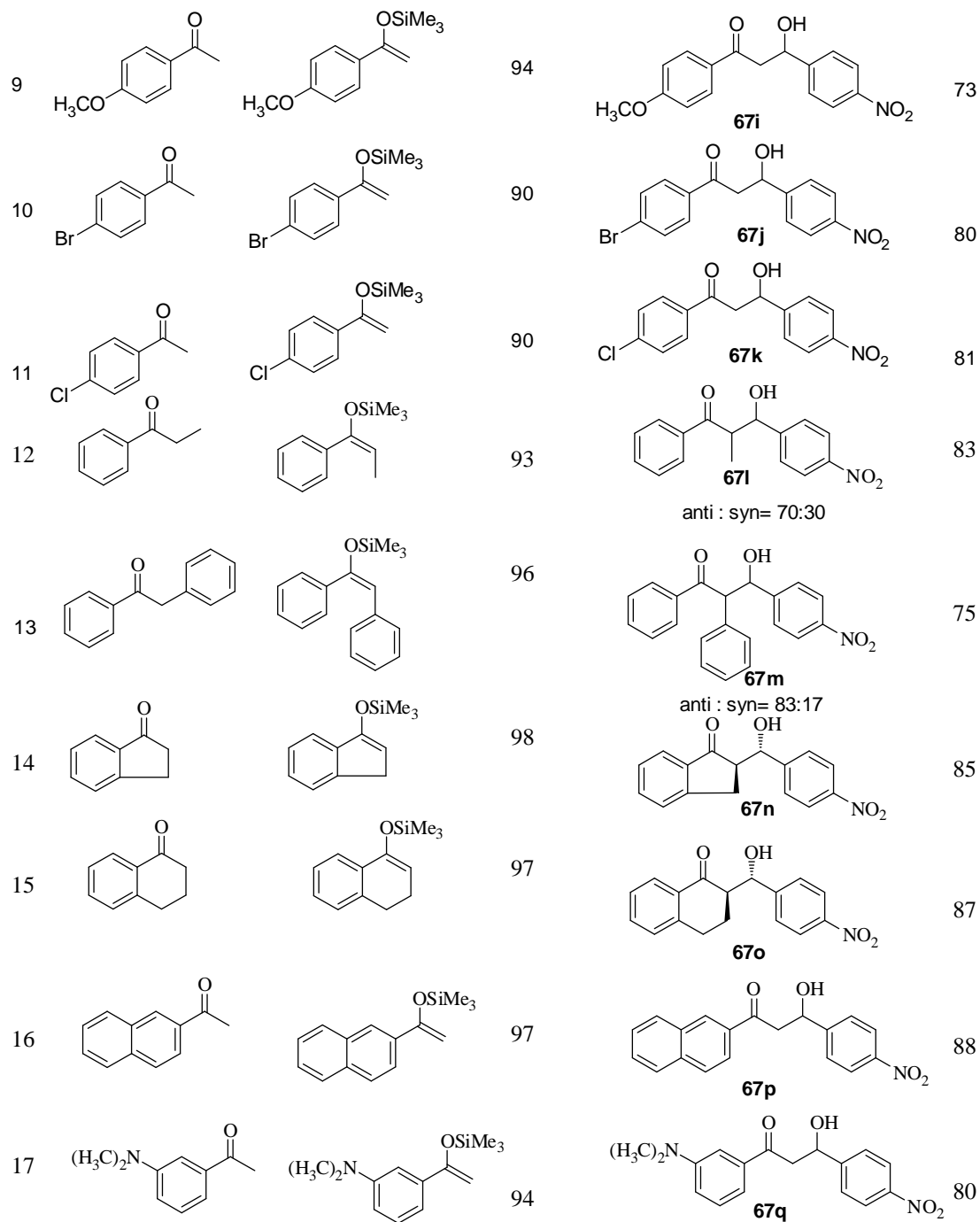


Figure 15. ^1H NMR Spectroscopy of Product **67g**

For aliphatic ketones, enone products were obtained under similar reaction conditions. Regioselective formation of silyl enol ether with more substituted α -carbon was implicated in the formation of products **67i** and **67m** (Table 10, entries 16, 17). These both substrates produce enol silyl ether in high conversion level according to GC-MS data. For Mukaiyama Aldol condensation reaction with an aldehyde, they generate *syn*- and *anti*- mixtures and the *anti*- product was the major. But for 2-heptanone (entry 6), the reaction generated the *syn*-isomer as the major product. For 1-indanone and α -tetralone (entry 14 and 15), the reaction gave the highly *anti*-diastereoselective formation of β -hydroxyketones was resulted from the condensation to the α -carbon of the ketones. Other ketones showed high diastereoselectivity of the formation of β -hydroxyketone products on Mukaiyama Aldol condensation reaction. Cyclohexanone, cyclopentanone and 4-*tert*-butylcyclohexanone (Table 10, entry 1, 2 and 3), with the treatment of enol silyl ether with benzaldehyde under Mukaiyama Aldol condensation reaction conditions generate dienes as products.

Table 10. Coupling Reaction of ketones with Vinyltrimethylsilane^a and the Reaction of Enol Ether with Aldehyde under the Titanium (IV) Chloride.^b

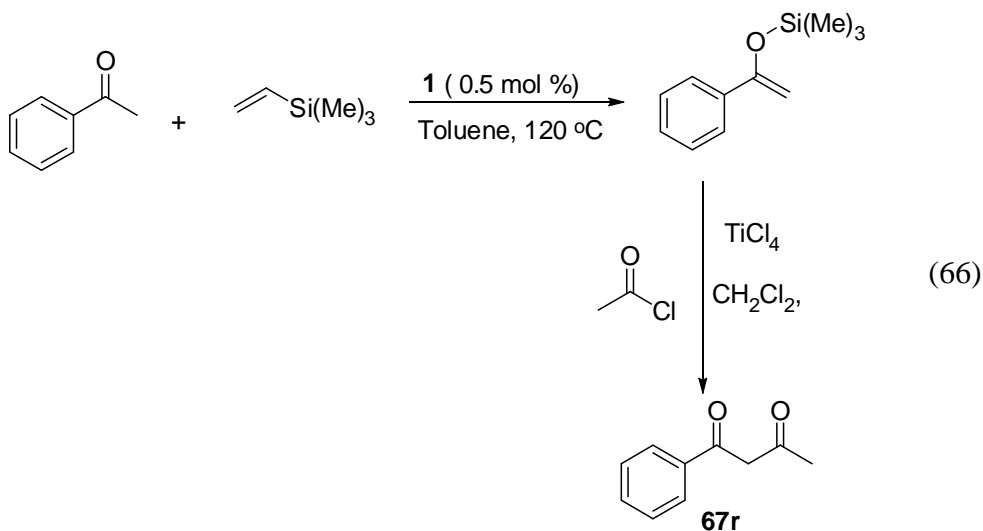
Entry	Ketone	Enol	Conv(%) ^c	Product	Yield(%) ^d
1			99	 67a	93
2			97	 67b	83
3			99	 67c	85
4			95	 67d	89
5			85	 67e anti : syn = 85:15	65
6			90	 67f anti : syn = 10:90	78
7			98	 67g	85
8			95	 67h	75



^a Reaction conditions: ketone (1.0 mmol), vinyltrimethylsilane (2.0 mmol), **1** (0.5 mol %), toluene (3 mL), 120 °C, 12-15 h. ^b Reaction conditions enol ether (2.0 mmol), aldehyde (3.0 mmol), TiCl₄ (3.0 mmol), CH₂Cl₂ (10 mL). ^c Conversion based on ketone by GC-MS. ^d Isolated yield based on the ketones.

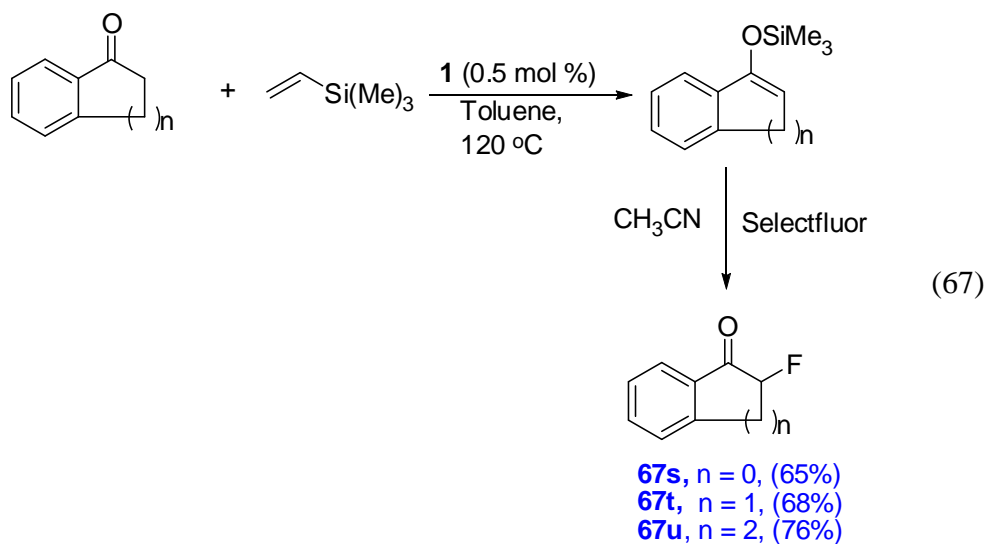
4.3.1 The Use of Enol Silyl Ether in Fluorination Reactions and Diketone Reactions

To further demonstrate the synthetic utility of the silyl enol ether formation, we next performed a set of C-C and C-F bond forming reactions. For example, acetophenone was treated with vinyltrimethylsilane in the presence of the catalyst **1** to produce the enol ether product, as indicated in Table entry **7**. The crude product of enol silyl ether (1.0 mmol) was subsequently reacted with acetyl chloride (80 mg, 1.1 mmol) in the presence of TiCl₄ (1.1 mmol) to form the 1,3-diketone product in 43 % yield (Eq 66). The other substrates were treated with this reaction, but only acetophenone can generate the diketone product.



In an analogous fashion, in a 50 mL Schlenk flask, the crude silyl enol ether product residue (2.0 mmol) was dissolved in CH₃CN (2 mL), and the solution was cooled to 0 °C in an ice bath. Selectfluor[®] (2.0 mmol) was added in several portions to the

solution under N₂ purge. The reaction mixture was stirred while it was allowed to gradually warm to room temperature over 8 h. The solvent was evaporated, water (10 mL) was added to the residue, and the organic layer was extracted with Et₂O (3 × 20 mL). The combined organic layers were washed with brine solution, dried over anhydrous Na₂SO₄, and the solvent was evaporated. The pure product **67s** was isolated by a column chromatography on silica gel (EtOAc/*n*-hexanes) in 65% isolated yield after silica chromatography (Et₂O/*n*-hexane) (Eq 67)¹¹².



The products were characterized by NMR in Figure 16, which show 46.9 Hz as the coupling constant between F and H.

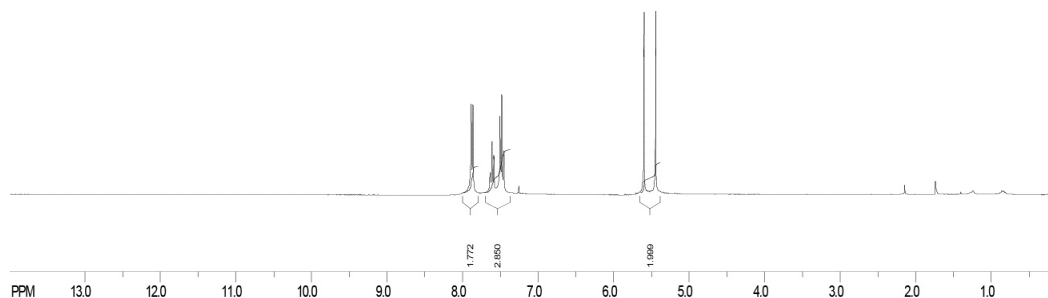
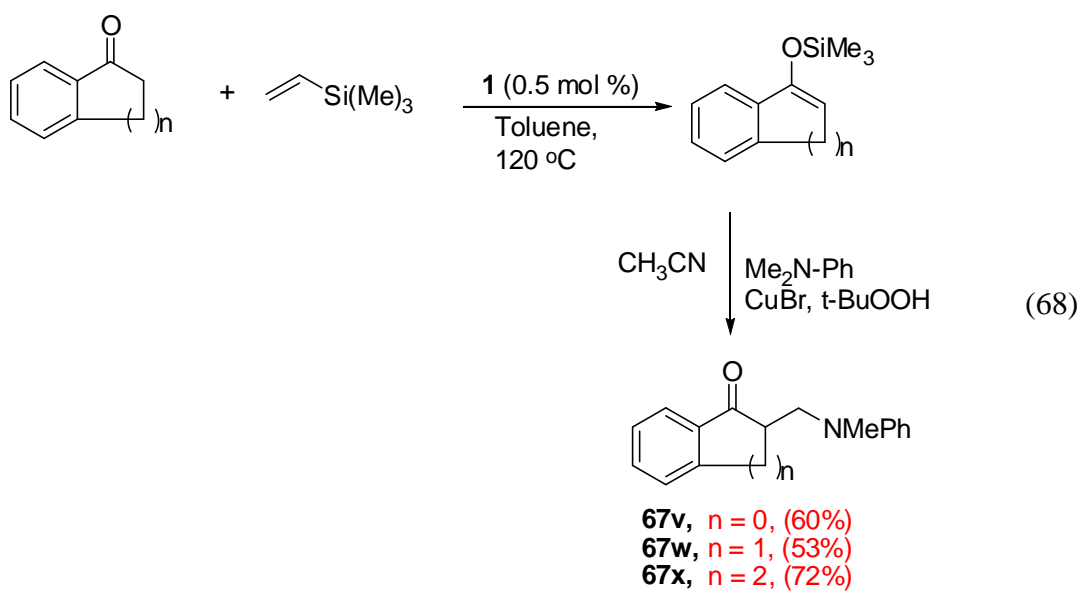


Figure 16. ^1H NMR Spectroscopy for complex **67s**

In both cases, the reaction can be carried out in tandem in a one-pot without isolating the enol ether products.



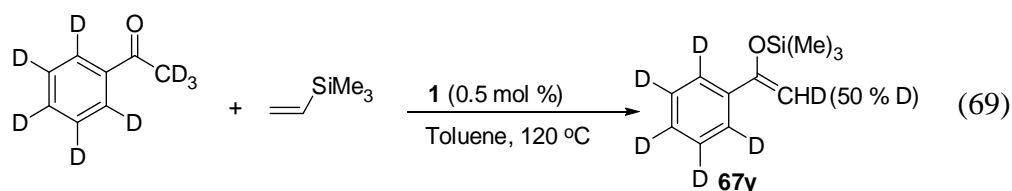
Next, the aminomethylation reaction of the silyl enol ethers was performed by following a recently reported procedure (Eq 68). Thus, in a 100 mL Schlenk flask, *t*-BuOOH (0.10 mL, 5-6 M in decane) was added dropwise to a mixture of *N,N*-dimethylanilines (1.5 mmol), CuBr (4 mg, 0.025 mmol), crude silyl enol ether product (0.5 mmol) and CH₃CN (5 mL) at room temperature. The resulting mixture was stirred at 50 °C for 12 h. The mixture was filtered

through a pad of celite, and the solvent was removed under a reduced pressure. The residue was purified by a column chromatography on silica gel to afford the desired product **67v-67x** in 60-72% isolated yields.

4.4 Mechanistic Study on the Reaction of Ketones and Vinylsilanes

4.4.1 Deuterium Labeling Study

We performed the following kinetic experiments to gain mechanistic insights on this coupling reaction. First, the deuterium labeling experiment was performed from treatment of PhCOCD_3 with $\text{CH}_2=\text{CHSiMe}_3$ (2 equiv.) and **1** (0.5 mol %) in toluene (3 mL) at 120 °C (Eq 69).



The NMR spectroscopy of the product **67y** was acquired, and the crude coupling product showed 50% D on the vinyl positions as determined by both ^1H and ^2H NMR spectroscopy (Figure 17).

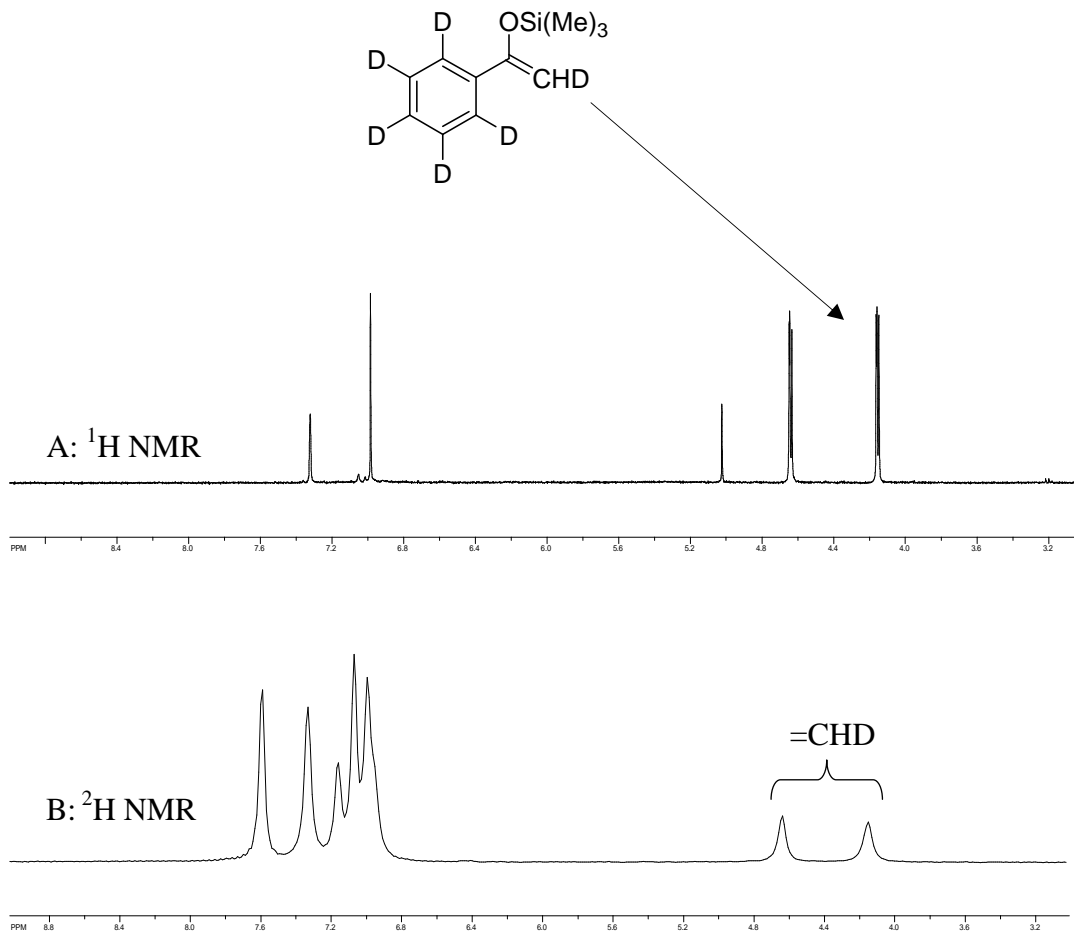


Figure 17. A- ¹H NMR Spectroscopy of the Reaction Mixtures; B- ²H NMR Spectroscopy of the Reaction Mixtures.

The two vinyl protons of enol silyl ether were assigned to 4.34 ppm and 4.86 ppm in the ¹H NMR spectroscopy (Figure 17A), in the same region, there are deuterium signals which were assigned to vinyl protons of enol silyl ether in the ²H NMR spectroscopy (Figure 17B). In the ²H NMR spectroscopy, there are deuterium signals assigned to

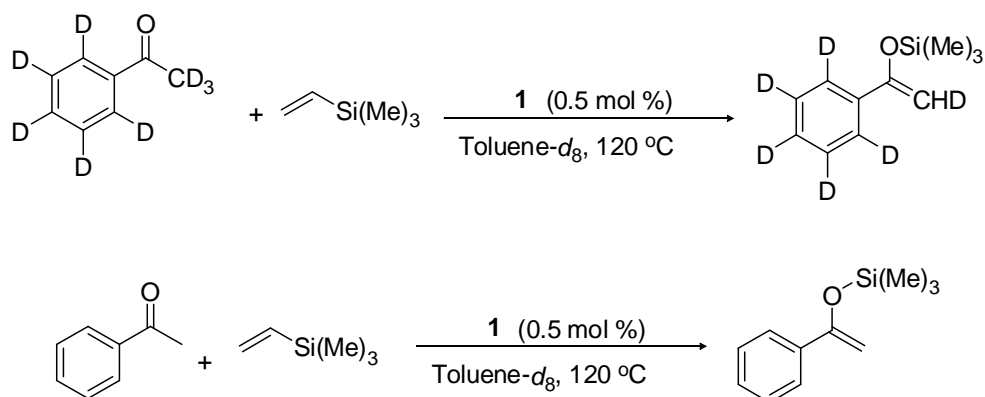
unreacted vinyltrimethylsilane. In addition, the deuterium signal at 5.3 ppm was assigned to ethylene gas.

These results show that D/H exchange happens between $C_6D_5COCD_3$ and vinyltrimethylsilane. This exchange should be rapid and reversible, and should be done before the formation of the enol silyl ether. The extensive H/D exchange pattern at the vinyl positions is consistent with the rapid and reversible keto-enol tautomerization of the ketone substrate and its exchange with the vinyl group of $CH_2=CHSiMe_3$.

4.4.2 Deuterium Isotope Effect Study

Experiments based on kinetic isotope effect were performed on the reaction of ketone and vinylsilanes to determine the possibility of a rate-determining C-H bond cleavage step. Again, the initial rate method was used to determine the rate of each reaction. Thus, $RuH(CO)(PCy_3)_2Cl$ (**1**) (0.5 mol %), acetophenone- d_8 (0.2 mmol) and vinyltrimethylsilane (0.4 mmol, 2.0 equiv.) and hexamethylbenzene (26 mg as the internal standard) were dissolved in 0.5 ml toluene- d_8 solution in a Wilmad J-Young NMR tube with a Teflon screw cap. The tube was kept stirred in oil bath set at 120 °C. The reaction mixture was monitored every 30 min by NMR spectroscopy. The rate was measured by 1H integration of the product peak vinyl protons signal which shows 4.34

ppm in the ^1H NMR spectroscopy and the data were normalized vinyl protons against the internal standard. The k_{obs} was estimated from a first-order plot of $\ln[\text{product}]$ vs. reaction time and gave $k_{\text{obs}} = 0.1237 \text{ h}^{-1}$. The other reaction of acetophenone with vinyltrimethylsilane was setup and monitored under the similar condition as the former reaction, and this reaction gave $k_{\text{obs}} = 0.1265 \text{ h}^{-1}$ which translated to $k_{\text{CH}}/k_{\text{CD}} = 1.0 \pm 0.1$ (Scheme 23).

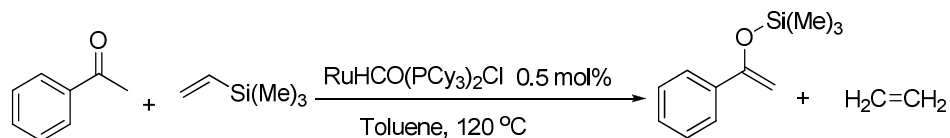


Scheme 23. The Kinetics Study on the Reaction of Ketone and Vinylsilane

This low KIE value suggests that the keto-enol tautomerization involving C-H bond cleavage of is fast and not the rate-limiting step. This deuterium isotope effect study also supported the notion of rapid H/D exchange in deuterium labeling study.

4.4.3 Phosphine Inhibition Study

We next performed a series of phosphine inhibition experiments to gain further insight into the mechanism of the reaction of ketone and vinylsilanes. Experiments analogous to the PCy₃ rate dependence experiments were performed. The initial rate method was used to monitor the rate of the reactions. Therefore, the treatment of acetophenone and vinyltrimethylsilane with various concentrated PCy₃ (5-15 μmol) in the presence of the catalyst **1** (0.5 mol %) in toluene-*d*₈ at 120 °C was monitored by ¹H NMR spectroscopy every 30 min intervals at room temperature.



The initial rate (v_i) of each reaction was constructed from the first-order plot of $\ln[\text{product}]$ vs reaction time. The initial rate (v_i) as a function of added [PCy₃] showed a linear rate dependence on [PCy₃] (Figure 18). The addition of PCy₃ (5-15 μmol, 1.5-7.0 mol %) to the reaction mixture under otherwise similar conditions led to a steady decrease from $k_{\text{obs}} = 8.34 \times 10^{-2} \text{ h}^{-1}$ (without PCy₃) to $4.38 \times 10^{-2} \text{ h}^{-1}$ (15 μmol of PCy₃). These results indicate that the active Ru catalyst is formed by the initial dissociation of the phosphine ligand. Reaction conditions: acetophenone (0.20 mmol), vinyltrimethylsilane (0.40 mmol) with various concentrations of PCy₃ in the presence of the catalyst **1** (0.5 mol %) in toluene-*d*₈ at 120 °C.

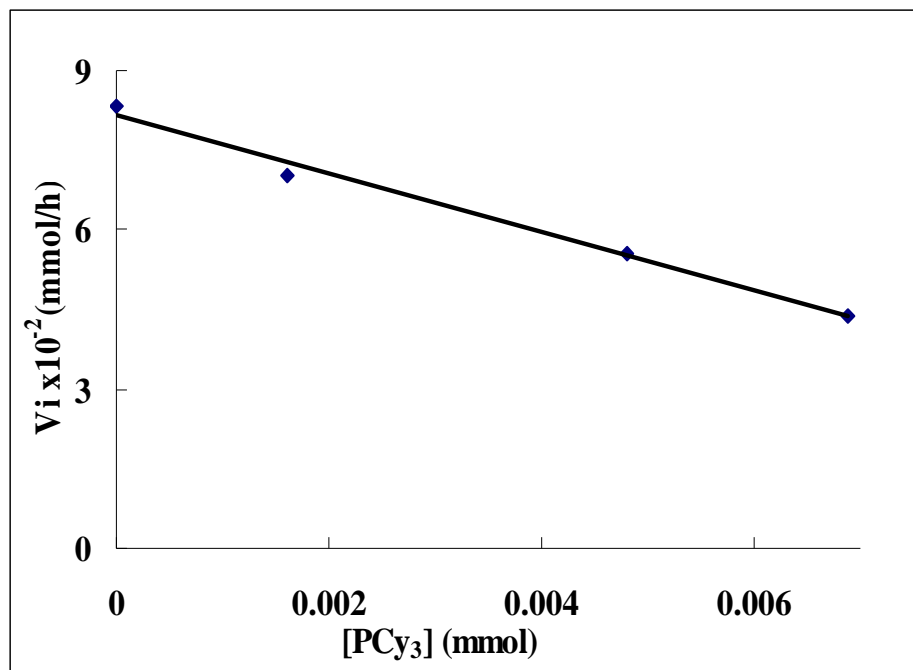
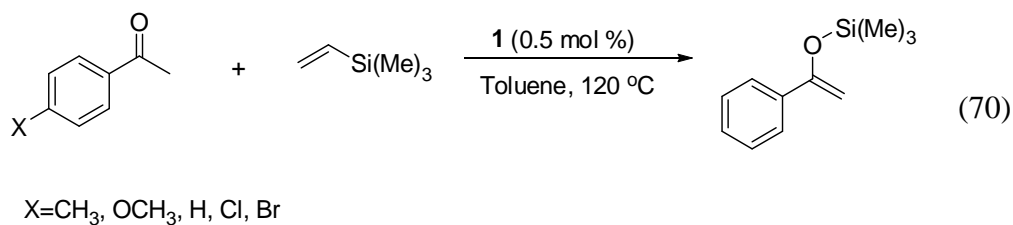


Figure 18. Plot of the Initial Rate (v_i) vs. $[\text{PCy}_3]$ for the Coupling Reaction of Acetophenone and Vinyltrimethylsilane

4.4.4 Hammett Study

Hammett studies of *para*-substituted acetophenones were performed in order to determine the electronic effects on the reaction mechanism. Therefore, in the glove-box, $(\text{PCy}_3)_2(\text{CO})\text{RuHCl}$ (1 mg 0.5 mol %), *para*-substituted acetophenones (0.2 mmol), Vinyltrimethylsilane (0.4 mmol) and hexamethylbenzene (26 mg as the internal standard) were dissolved in 0.5 ml toluene- d_8 solution in a Wilmad J-Young NMR tube with a Teflon screw cap (Eq 70).



The tube was taken out and was heated in oil bath at 120 °C. ¹H NMR of the reactions mixtures were monitored every 30 min at room temperature. The initial rate method was used to determine the rate of each reaction. The rates were measured by integration of the vinyl protons peak of the product (=CH₂), which gives 4.34 ppm on ¹H NMR spectroscopy, and these were normalized against vinyl protons of the internal standard. The *k*_{obs} was estimated from a first-order plot of ln[product] vs reaction time.

Other reactions were monitored under the same condition. A Hammett plot was constructed by plotting the log (*k*_x/*k*_H) vs σ_p and a positive Hammett value of ρ = 0.97 was obtained from the correlation of *para*-substituted *p*-X-C₆H₄COCH₃ (X = OMe, CH₃, H, Cl, Br) with Vinyltrimethylsilane (Figure 19).

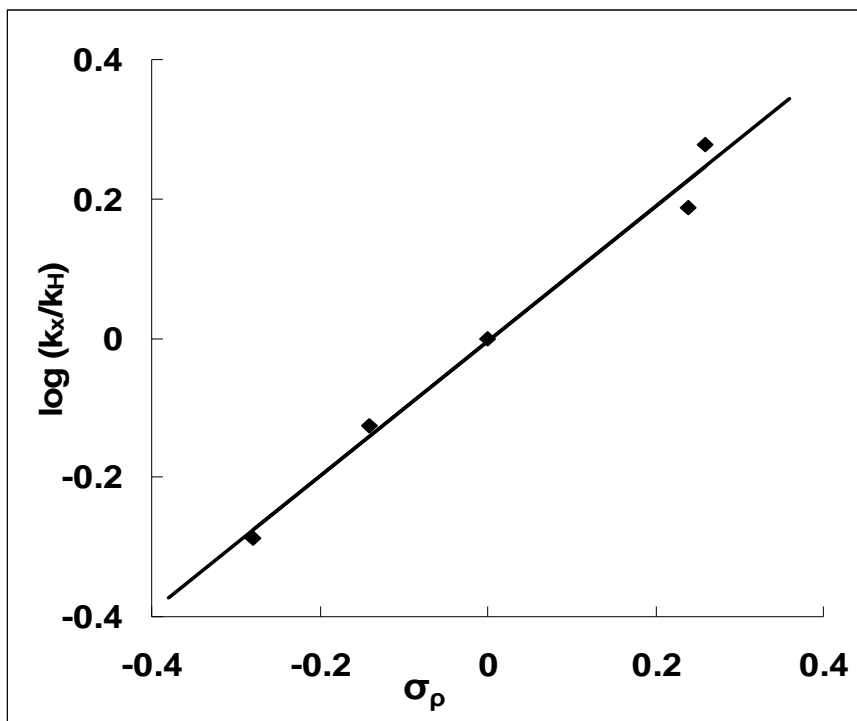
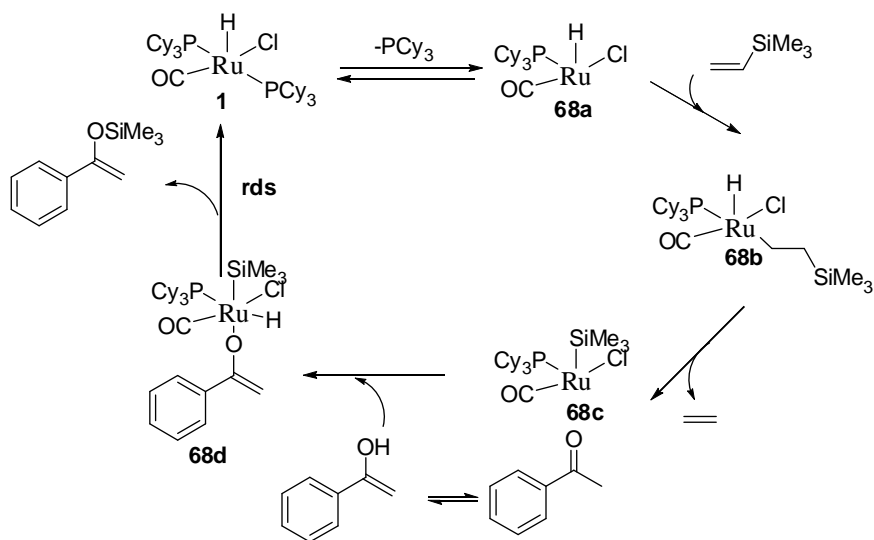


Figure 19. Hammett Plot of the Reaction of *para*-Substituted $p\text{-X-C}_6\text{H}_4\text{COCH}_3$ (X = OMe, CH₃, H, Cl, Br) with Vinyltrimethylsilane

The rate of the reaction can be accelerated by adding electron-withdrawing group on the acetophenone and the promotional effect by electron-withdrawing group is indicative of an electrophilic nature of the carbonyl carbon which is stabilized by the Ru catalyst. The results are consistent with the notion that a buildup of negative charge on transition state of C-Si bond formation step.

4.5 Proposed Mechanism of the Reaction of Ketone and Vinylsilanes

A plausible mechanistic rationale for the silyl enol ether formation is illustrated on the basis of these results (Scheme 24).



Scheme 24. Proposed Mechanism of the Coupling Reaction of Ketones and Vinyltrimethylsilane

From the phosphine inhibition study, we learned that PCy_3 ligand show strong inhibition on enol silyl ether formation, the dissociation of phosphine ligand is necessary to give the open active site to the substitutes to coordinate to the ruthenium center. And the dissociation of PCy_3 should be the first step and at high temperature this step is rapid and reversible. With the dissociation of PCy_3 from the ruthenium complex **1**, there is one open active site in the ruthenium center in the ruthenium complex **68a**, so complex **68a** is active. We proposed that the catalytically active cationic Ru-silyl species **68c** was

initially formed from an alkene insertion followed by the elimination of ethylene molecule. The elimination of ethylene happened before the formation of the enol silyl ether and was detected by ^1H NMR spectroscopy. The ^{13}C isotope effect study also indicates that elimination of ethylene and form ruthenium-silyl complex is not the rate-limiting step. But we did not detect the formation of ruthenium-silyl species, which hints this step to be reversible and rapid. Next step is the keto-enol tautomerization and insertion of an enol substrate to the ruthenium-silyl complex to form a Ru-enolate species. The low KIE value from the kinetic isotope effect study on the reaction of acetophenone and vinyltrimethylsilane indicates that the keto-enol tautomerization which involves the C-H bond cleavage is not the rate-limiting step. The Ru-enolate species **68d** would then undergo reductive elimination to yield the silyl enol ether product **68e**. A relatively positive high Hammett value from the correlation of *para*-substituted arylketones supports the notion that a buildup of negative charge on transition state of the Ru-enolate species **68d** and the O-Si bond formation step the rate-limiting step.

4.6 Conclusions

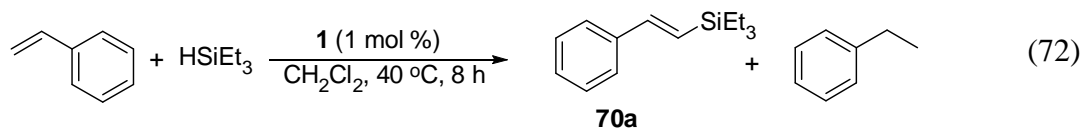
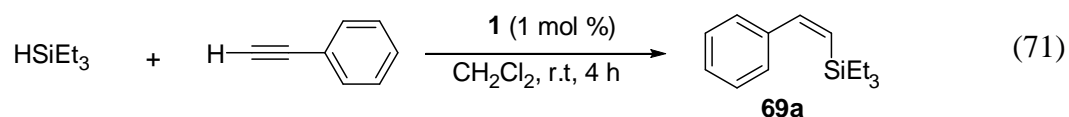
We successfully developed an effective catalytic method to produce synthetically useful vinylsilyl ethers through coupling reaction of ketones and vinylsilane by using well-defined ruthenium-hydride catalyst **1**. As demonstrated from both Mukaiyama Aldol condensation and aminomethylation reactions, the catalytic method of silyl enol ether formation should find useful applications in α -functionalization reactions of ketones. Phosphine inhibition and kinetics studies give the useful information on the mechanism. The highly positive Hammett value from the correlation of *para*-substituted arylketones on vinyltrimethylsilanes support the O-Si bond formation step being the rate-limiting step.

Chapter 5. Highly Stereoselective and Regioselective Hydrosilylation of Alkynes and Alkenes Catalyzed by $(\text{PCy}_3)_2(\text{CO})\text{RuHCl}$

Vinylsilanes have emerged as versatile building blocks in organic synthesis. Because of their low toxicity, low cost, high stability, and innocuous byproduct, vinylsilanes play an increasingly important role in the synthesis and particularly in metal-catalyzed cross-coupling reactions. Over the past decades, many groups have been working on routes to synthesize vinylsilanes, and among them, hydrosilylation of alkynes catalyzed by transition metals is the most straightforward and atom-economical method. Generally, the hydrosilylation of alkynes generates a mixture of three compounds. There are still things to improve in such hydrosilylation reactions. Though recently the selectivity of the germinal products has been improved by using Pd catalyst, Firstly, generation of highly selective *cis* or *trans* coupling products remains difficult. Moreover, the high catalyst loading is typically required in these reactions and mechanism of the hydrosilylation is still unclear. Here, we have been working to improve the selectivity on the formation of *cis* and *trans* vinylsilane, as well as learning the factor to the selectivity of vinylsilanes formation and the mechanism of the hydrosilylation reactions.

5.1 Results and Discussion

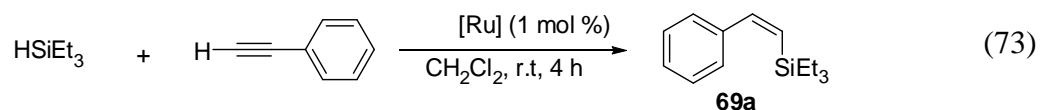
Due to the synthetic utility of vinylsilane, we have been working on the methods to generate selective vinylsilanes by transition metal catalysts. Recently, we observed that $(\text{PCy}_3)_2(\text{CO})\text{RuHCl}$ (**1**) shows a considerably high selectivity and reactivity toward hydrosilylation of alkynes and alkenes. For example, the treatment of phenylacetylene (1.0 mmol) and triethylsilane (2.0 mmol) in the presence of 1 mol % ruthenium catalyst **1** in CH_2Cl_2 generated (*Z*)- vinylsilanes **69a** in 99% yield (Eq 71). On the other hand, the treatment of styrene with 2.0 equiv. triethylsilane at 40 °C forms the (*E*)-vinylsilanes **70a** at a high yield (Eq 72). More details on experimental conditions, reaction scope, and mechanism of these reactions, will be discussed in this chapter.



5.2 Scope of the Hydrosilylation of Alkynes

5.2.1 Catalyst Survey

The catalytic activity of selected ruthenium complexes was initially screened for the coupling reaction of phenylacetylene and triethylsilane (Eq 73). The survey of catalysts showed that ruthenium hydride complex $(\text{PCy}_3)_2(\text{CO})\text{RuHCl}$ (**1**) has the highest activity in the formation of the vinylsilanes among selected ruthenium complexes in 4 hours at room temperature with 99 % conversion determined by GC-MS and NMR (Table 11, entry 5).



Under similar conditions, $\text{Ru}_3(\text{CO})_{12}$ (entry 4) and $[(p\text{-cymene})\text{RuCl}_2]_2$ (entry 12) showed some activity on the hydrosilylation products, but the conversion is low (around 5%). Other commonly ruthenium complexes such as $\text{Ru}(\text{CO})\text{H}_2(\text{PPh}_3)_3$, $\text{RuCl}_3 \cdot 3\text{H}_2\text{O}$, $[(\text{COD})\text{RuCl}_2]_x$ and $[(\text{PCy}_3)_2(\text{CO})(\text{MeCN})_2\text{RuH}]^+\text{BF}_4^-$, were not effective in giving coupling products under similar reaction conditions.

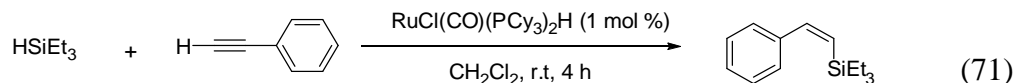
Table 11. Catalyst Activity Survey for the Coupling Reaction of Phenylacetylene and Triethylsilane

Entry	Catalyst	Additive	yield(%) ^b
1	None	None	0
2	Ru ₃ (CO) ₁₂	None	3
3	Ru ₃ (CO) ₁₂	NH ₄ PF ₆	4
4	RuCl ₃ ·3H ₂ O	None	0
5	(PCy₃)₂(CO)RuHCl	None	99
6	(PCy ₃) ₂ (CO)RuHCl	HBf ₄ OEt ₂	< 5
7	(PPh ₃) ₃ (CO)RuH ₂	None	0
8	(PPh ₃) ₃ RuCl ₂	None	0
9	(PPh ₃) ₃ RuHCl	None	0
10	[RuCl ₂ (COD)] _x	None	0
11	(PCy ₃) ₂ (CH ₃ CN) ₂ (CO)Ru [⊕] H BF ₄ [⊖]	None	0
12	[(p-cymene)RuCl ₂] ₂	None	5

^a Reaction conditions: 1.0 mmol of phenylacetylene, 2.0 mmol triethylsilane, [Ru] 1 mol %, CH₂Cl₂ 2 mL, room temperature, 4 hours. ^b GC yields based on phenylacetylene.

5.2.2 Scope of the Hydrosilylation of Alkynes

To demonstrate the synthetic utility of the catalyst **1**, we explored the scope of the hydrosilylation of alkynes. The reactions of phenylacetylene with different silanes such as triethylsilane, diethylmethylsilane, the more bulky substituted triphenyl silane were tested under the similar conditions and all gave only (*Z*)-vinylsilane isomers (Eq 71).

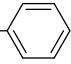
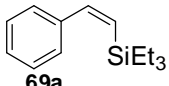
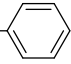
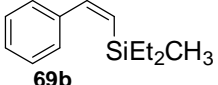
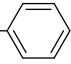
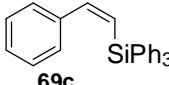
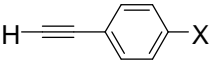
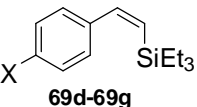
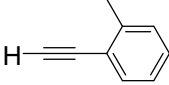
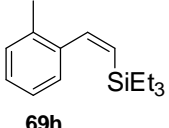
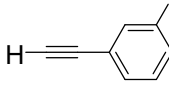
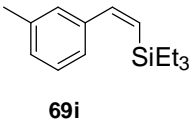
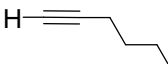
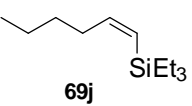
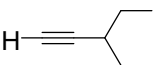
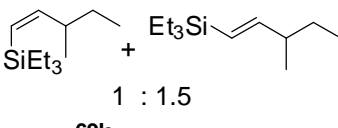
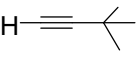
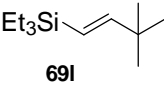
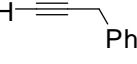
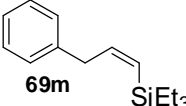
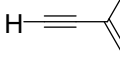
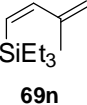


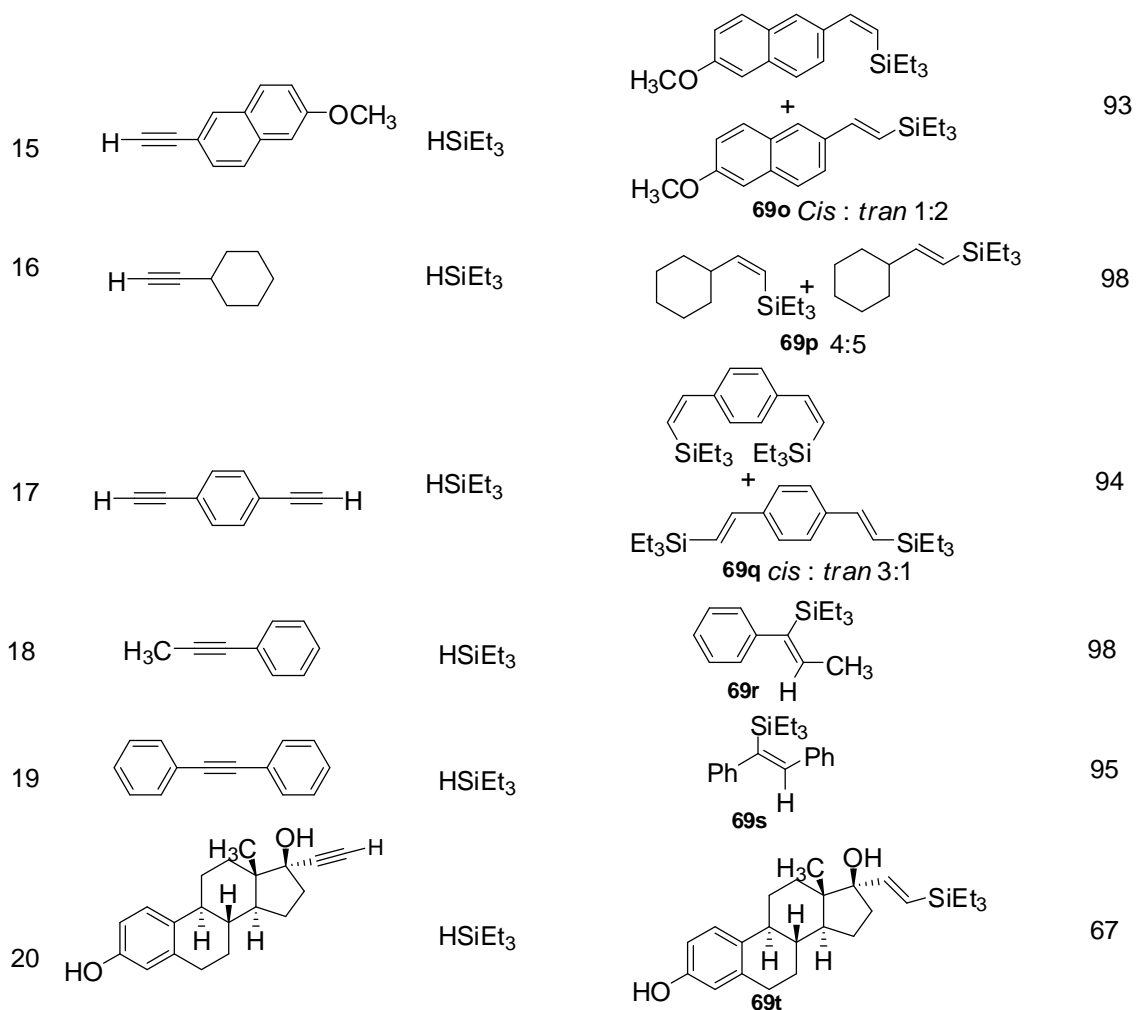
A variety of terminal and internal alkynes were proven to be amenable for the hydrosilylation reaction. We found that these alkynes showed a strong steric effect on the selectivity of the coupling products. For phenylacetylene (entry 1) and 1-hexyne (entry 10), (*Z*)-vinylsilanes were detected by ^1H NMR. But for the steric bulky alkynes as 3-methyl-1-butyne (entry 11), a mixture of both (*Z*) and (*E*) isomers at a ratio of 3:2 was detected. When we treated the more bulky substrate 3,3-dimethyl-1-butyne in entry 21, only *trans* vinylsilanes was formed. So the selectivity of formation of vinylsilane has significant dependence on alkynes. Bulky substrates generally favor formation of *trans* vinylsilane (Table 12), which may due to the steric hindrance between the alkynes and the ruthenium complex.

We also tried to explore the utility of these hydrosilylation reactions by some internal alkynes (entry 17 and 18). They all showed the high activity and conversion to vinylsilane products. For prop-1-yne benzene (entry 17), we determined the product to be the (*E*)-isomer based on NOSEY and ^1H NMR data. We also detected a signal of the

methyl with the ethyl group, and for ^1H NMR the signals signed to methyl show the doublet with a small coupling constant (1.7 Hz). This result is also consistent with the prediction based on stereo effect, in which the bulky group favors formation of *trans* product. So, at this point, the reaction of diphenylethyne with triethylsilane should give *trans* vinylsilane. For 1,4-diethynylbenzene (entry 16), it generates a mixture of *cis* and *trans* products at a ratio of 3:1. We also tried 1, 6-heptadiyne, but the selectivity of the reaction was poor, as multiple isomers were detected.

Table 12. The Coupling Reaction of Alkynes and Triethylsilane ^a

Entry	Alkyne	Silane	Product	Yield (%)
1		HSiEt ₃	 69a	99
2		HSiEt ₂ CH ₃	 69b	98
3		HSiPh ₃	 69c	95
4		HSiEt ₃	 69d-69g	X=CH ₃
5				X=OCH ₃
6				X=F
7				X=CF ₃
8		HSiEt ₃	 69h	98
9		HSiEt ₃	 69i	98
10		HSiEt ₃	 69j	98
11		HSiEt ₃	 69k	90
12		HSiEt ₃	 69l	91
13		HSiEt ₃	 69m	96
14		HSiEt ₃	 69n	85

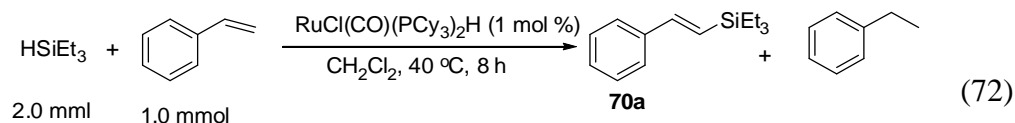


^a Reaction conditions: alkyne (1.0 mmol), hydrosilane (1.5 mmol), **1** (1 mg, 1 mol %), CH₂Cl₂ (2-3 mL), room temperature, 6 h. ^b Isolated yield. ^c 60 °C, 15 h.

5.2.3 The Scope of the Hydrosilylation of Alkenes

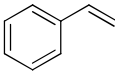
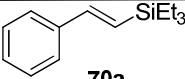
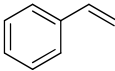
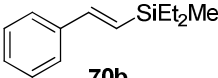
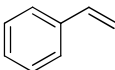
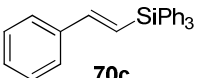
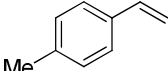
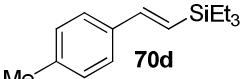
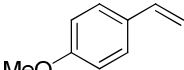
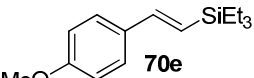
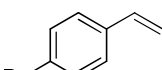
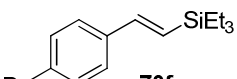
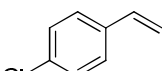
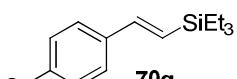
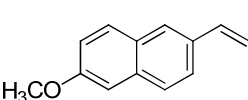
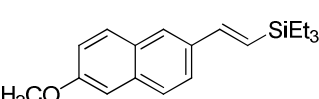
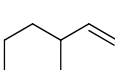
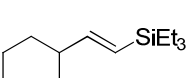
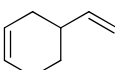
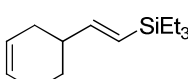


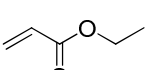
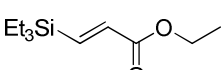


In another case, the treatment of 1.0 mmol styrene with 2.0 mmol triethylsilane in the presence of 1 mol % catalyst **1** in CH₂Cl₂ at 40 °C for 8 h smoothly generates *trans*

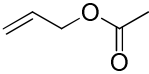
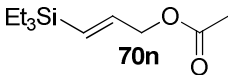
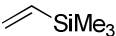
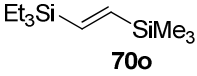
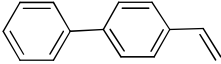
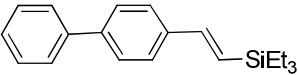
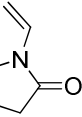
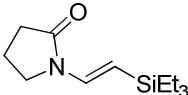
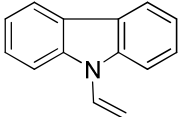
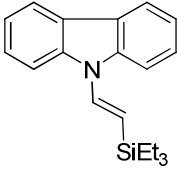
vinylsilane **70a** as coupling product along with one equiv. of ethyl benzene as the byproduct (Eq 72).



To demonstrate the synthetic utility of the catalyst $(\text{PCy}_3)_2(\text{CO})\text{RuHCl}$ on the hydrosilylation of alkenes, we explored the reaction scope. Firstly, triethylsilane, diethylmethylsilane and triphenylsilane were explored by the reaction with styrene, which all give *trans*-vinylsilane. Triethoxy(vinyl)silane show the low conversion under similar conditions. A variety of alkenes was used in this reaction. The Table 13 shows that both less bulky substitutes as 1-hexene (entry 11) and more bulky substitutes as 2-methoxy-6-vinylnaphthalene (entry 8) and vinylcyclohexane (entry 9) give only *trans* products. So unlike the hydrosilylation of alkynes, there is no steric effect on the formation of coupling products. On the other hand, those internal alkenes showed no reactivity in the hydrosilylation reactions.

Table 13. The Coupling Reaction of Alkenes and Hydrosilane. ^a

Entry	Alkene	Silane	Product	Yield(%) ^b
1		HSiEt ₃	 70a	98
2		HSiEt ₂ Me	 70b	96
3		HSiPh ₃	 70c	87
4		HSiEt ₃	 70d	97
5		HSiEt ₃	 70e	95
6		HSiEt ₃	 70f	94
7		HSiEt ₃	 70g	95
8		HSiEt ₃	 70h	90
9		HSiEt ₃	 70i	96
10		HSiEt ₃	 70j	95
11		HSiEt ₃	 70k	87
12		HSiEt ₃	 70l	93
13		HSiEt ₃	 70m	92

14		HSiEt ₃		83
15		HSiEt ₃		93
16		HSiEt ₃		69
17		HSiEt ₃		73
18		HSiEt ₃		85

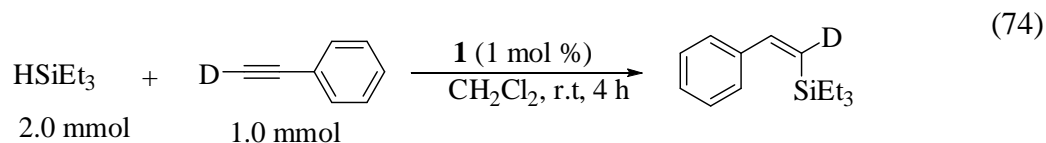
^a Reaction conditions: alkenes (2.0 mmol), HSiEt₃ (1.0 mmol), **1** (1 mg, 1 mol %), CH₂Cl₂ (2-3 mL), 40 °C, 8 h. ^b Isolated yield.

We explored the reaction scope by using some functional substituents such as ethyl arylate (entry 12), carbazole (entry 18) and 1-vinylpyridin-2-one (entry 17). They all show very high selectivity towards *trans* products. However, in the reactions of but-3-en-2-one, isoprene, and but-3-en-2-ol, only a trace amount of *trans*-product was detected. This may result from the fact that these substituents are highly reactive, thus favoring self-isomerization.

5.3 Mechanistic Study on the Hydrosilylation of Alkynes

5.3.1 Deuterium Labeling Study on the Hydrosilylation of Alkynes

In order to get insight on the mechanism of these reactions, we performed a series of deuterium labeling study experiments. The treatment of triethylsilane (2.0 mmol) with PhC≡CD (1.0 mmol) in the presence of **1** (1 mol %) in CH₂Cl₂ at room temperature yielded coupling product **69a** without H/D exchange and **69a** was determined by both ¹H and ²H NMR (Eq 74 and Figure 20).



In Figure 19, there are only two deuterium signal, one (2.05 ppm) was the reference acetone-*d*₆ and the other (5.81 ppm) the vinyl proton of complex **69a**. Since no signal at this position was observed in ¹H NMR spectroscopy. It is clear that this deuterium is from PhC≡CD, and there should be no H/D exchange between phenylacetylene and triethylsilane during this reaction. This indicated that for phenylacetylene, there should be no C-H bond cleavage during the reaction.

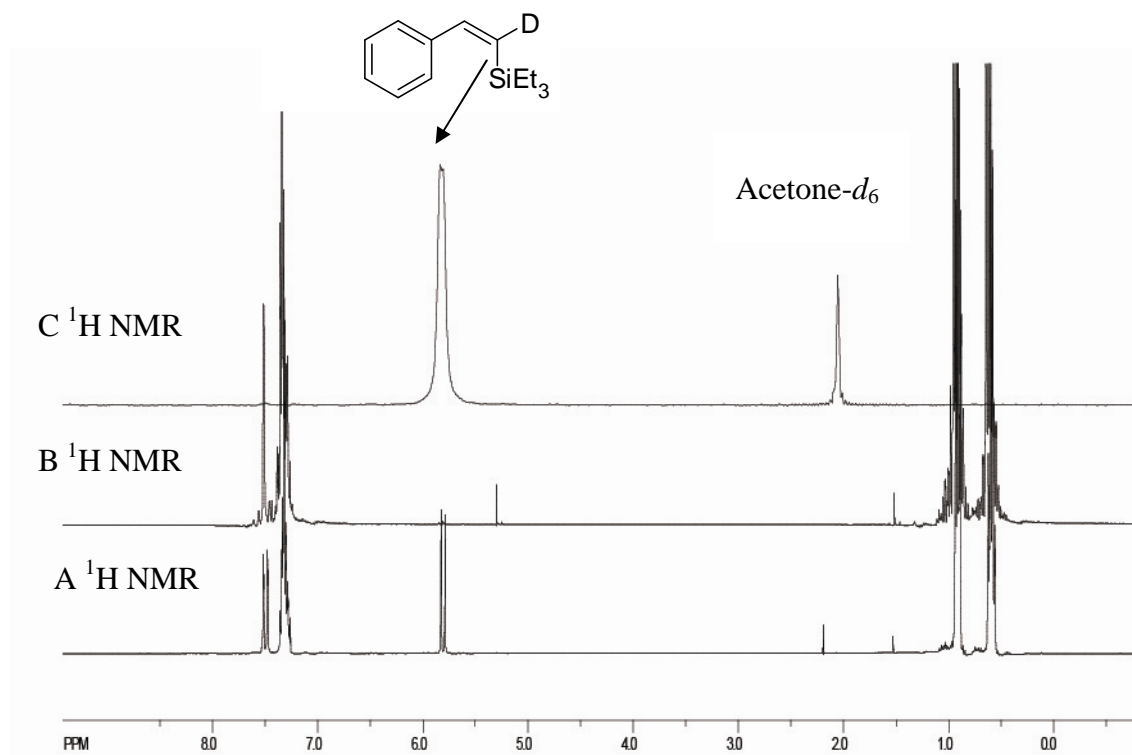


Figure 20. ^1H and ^2H NMR for the Deuterated Complex **69a**. A- ^1H NMR Spectroscopy of *cis*-vinylsilane **69a**; B- ^1H NMR Spectroscopy of Deuterium Vinylsilane; C- Deuterium NMR Spectroscopy of Deuterium Product and Acetone- d_6 is the Reference.

5.3.2 Phosphine Inhibition Study on the Hydrosilylation of Alkynes.

We next performed a series of phosphine inhibition experiments to gain further insight into the reaction mechanism. Therefore, in order to observe such phosphine inhibition, phenylacetylene (0.20 mmol), triethylsilane (0.40 mmol), **1** (2 mg, 1 mol %) and C_6Me_6 (2 mg, internal standard) were dissolved in 0.5 mL of CDCl_3 solution in a J-Young NMR tube with a Teflon screw cap. A pre-dissolved PCy_3 in CDCl_3 solution (5 μL , 1.0 M) was added to the tube via syringe. The reaction was monitored by ^1H NMR

spectroscopy with 30 min interval at room temperature. The initial rate method was used to measure the rate of each reaction. The rate was measured by the ^1H integration of the product peak at δ 5.81 (=CHSi), and was normalized against the internal standard peak. The k_{obs} was estimated from the first order plot of $\ln[\text{product}]$ vs. reaction time.

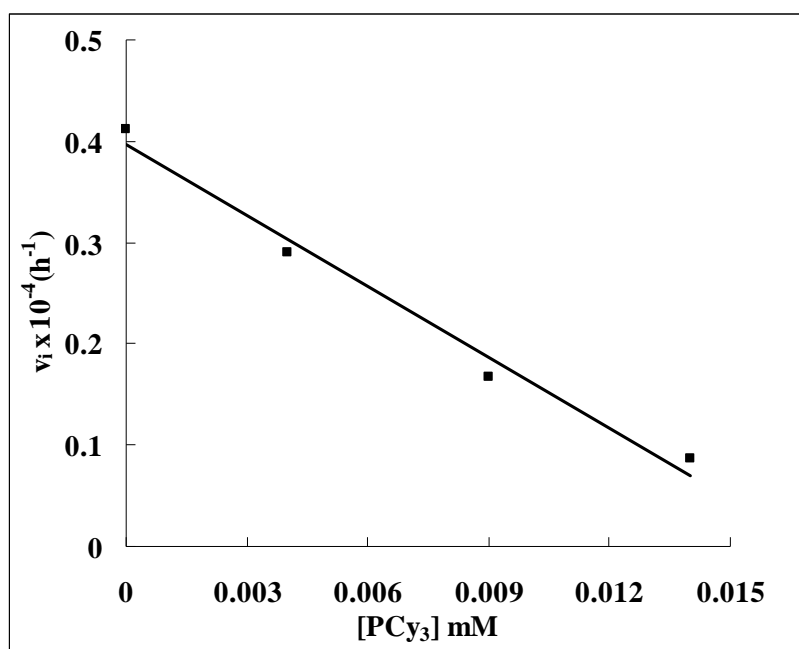


Figure 21. The Phosphine Inhibition for the Coupling Reaction of Phenylacetylene and Triethylsilane; ^a Reaction conditions: phenylacetylene (0.20 mmol), triethylsilane (0.40 mmol), **1** (1 mol %), PCy₃ (0.0-0.014 mM).

The catalytic reaction was found to be strongly inhibited by the phosphine ligand.

The initial rate was estimated from [product] vs. time plots for each sample with different [PCy₃] (Figure 21). The addition of PCy₃ (2.7-8.3 mol, 2.7-8.3 mol %) to the reaction

mixture under otherwise similar conditions led the rate to a steady decrease from $4.1 \times 10^{-5} \text{ h}^{-1}$ (without PCy_3) to $8.7 \times 10^{-6} \text{ h}^{-1}$ (0.014 M of PCy_3). These results indicate that active Ru catalyst formed by initial dissociation of a phosphine ligand.

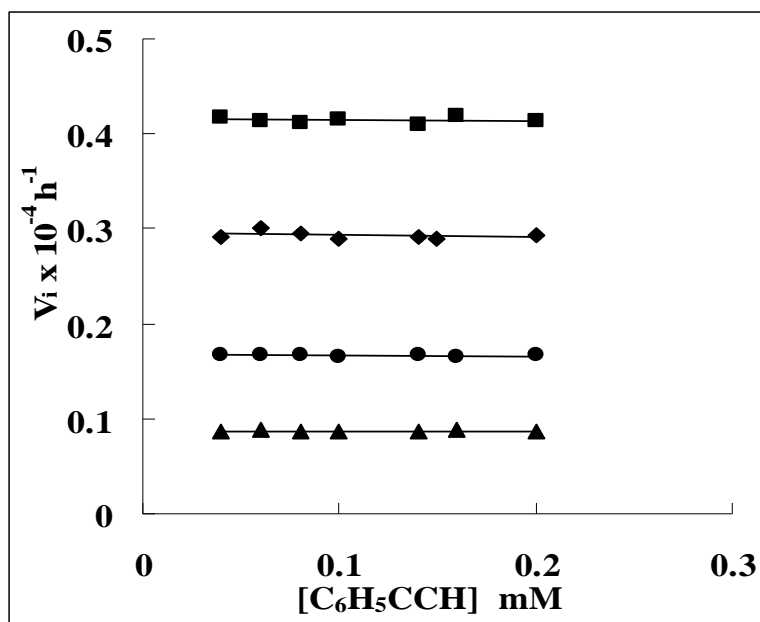


Figure 22. Plot of the Initial Rate vs. $[\text{PhC}\equiv\text{CH}]$ at different PCy_3 Concentrations
 No PCy_3 (■); 0.004 mM (0.8 equiv.) PCy_3 (◆); 0.009 mM (1.8 equiv.) PCy_3 (●); 0.014 mM (2.8 equiv.) PCy_3 (▲).

In order to determine the nature of such inhibition, a series of kinetic experiments were performed. Therefore the reaction of phenylacetylene (0.04-0.2 mmol) and excess amount of triethylsilane with various concentrations of PCy_3 (0-0.14 M, 0-2.8 equiv. compared to **1**) in presence of **1** (1 mol %) in CDCl_3 at room temperature was monitored using ^1H NMR over the internal standard. Rate vs. the concentration of phenylacetylene

plot (Figure 22) was constructed from a linear, pseudo-first order plot of product formation vs. time.

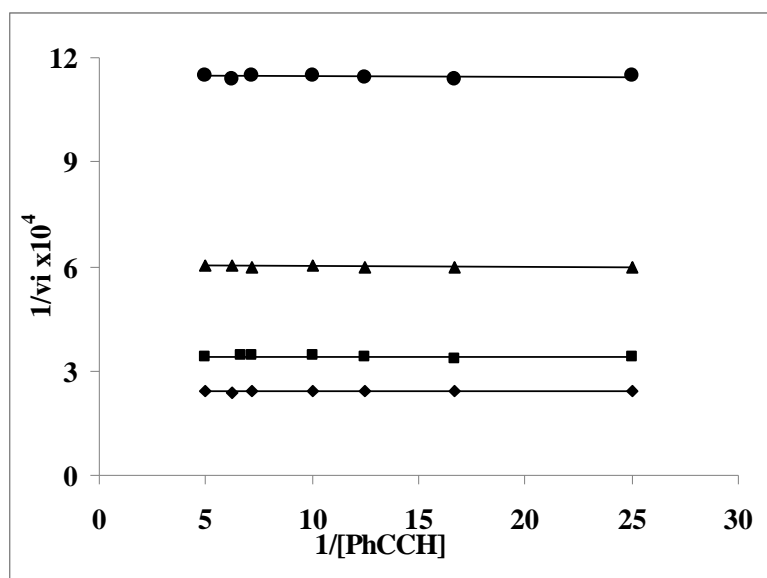


Figure 23. Lineweaver-Burke Plot of $1/v_i$ vs. $1/[\text{PhCCH}]$

In order to determine the nature of the inhibition, the inhibition data was fitted to Michaelis-Menten equation to determine the kinetic parameters for the addition. A series of Lineweaver-Burke plot (Figure 23) were constructed.

The rate dependence on alkynes would provide valuable insights into the mechanism for hydrosilylation of alkynes. The initial rate method was used to determine the rate of reaction. The treatment of 0.06-0.8 M phenylacetylene with excess amount of triethylsilane in the presence of 2 mg of **1** at room temperature in CDCl_3 was monitored by ^1H NMR spectroscopy. The initial rates of the reactions were determined from linear, pseudo-first order plots of product formation rate vs. time.

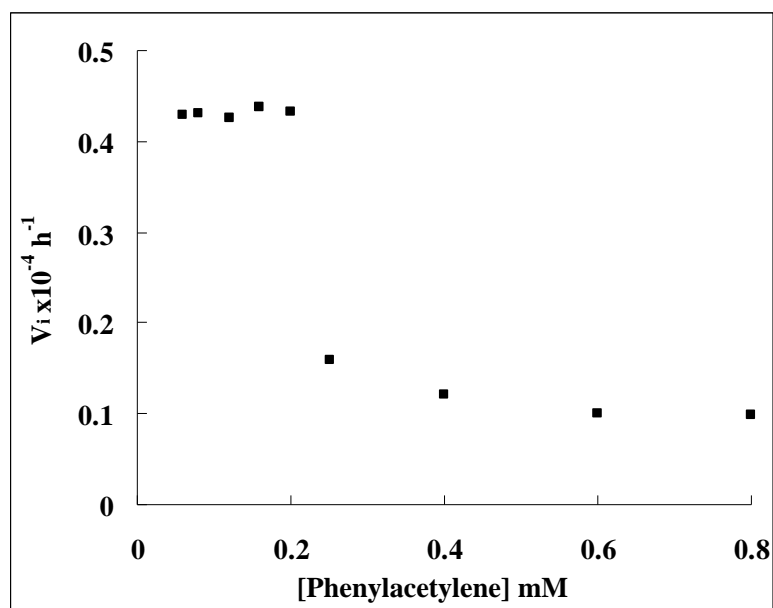


Figure 24. Plot of the Initial Rate vs. $[\text{PhC}\equiv\text{CH}]$

In Figure 24, the rate does not show any dependence on the concentration of phenylacetylene in 0.06 M-0.20 M, the k_{obs} is $4.3 \times 10^{-5} \text{ h}^{-1}$. However, from 0.2 M, with the concentration of phenylacetylene to 0.8 M, the k_{obs} was decreased from $4.3 \times 10^{-5} \text{ h}^{-1}$

(0.2 M) to $1.0 \times 10^{-5} \text{ h}^{-1}$ (0.8 M). These results indicate that the rate of reaction shows no dependence on concentration of phenylacetylene under the dilute condition. However, with the concentration increasing, the phenylacetylene coordinates to the catalyst center by creating inactive catalytic species and will eventually prevent the substrate from the coordination to the ruthenium center to generate the products.

We next performed a kinetic study on the rate dependency on triethylsilane.

Treatment of 0.06-0.8 M of phenylacetylene with excess amount of triethylsilane in the presence of 2 mg of **1** at room temperature in CDCl_3 was monitored by ^1H NMR spectroscopy. The initial rate method was used to determine the rate of the reactions. The initial rates of the reactions were determined from linear, pseudo-first order plots of rate of the product formation vs. time.

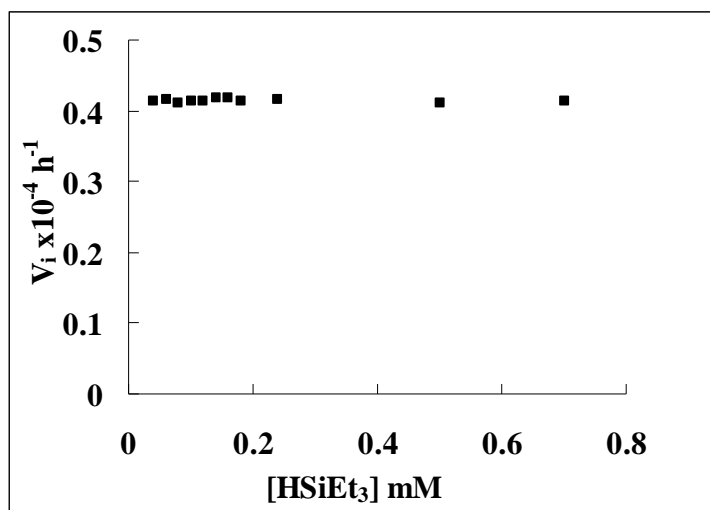


Figure 25. Plot of the initial rate vs. $[\text{HSiEt}_3]$

Figure 25 indicated that the rates of reaction of hydrosilylation of alkynes showed no dependence on the concentration of triethylsilane. We monitored the rate of the reactions with the different concentration of triethylsilane from 0.04 M to 0.7 M at similar conditions, and found all the reactions giving similar k_{obs} value as $4.3 \times 10^{-5} \text{ h}^{-1}$.

5.3.4 Rate Dependence on the Catalyst Concentration

In order to get insight into the mechanism, the rate dependence of ruthenium hydride concentration was performed. The treatment of 1.4-11 mM ruthenium hydride **1** with 0.4 M triethylsilane and 0.2 M phenylacetylene at room temperature in CDCl_3 was monitored by ^1H NMR spectroscopy. The initial rate method was used to determine the rates of the reactions. The initial rates of the reactions were determined from linear, pseudo-first order plots of rate of the product formation vs. time.

The rate of the reactions of hydrosilylation of alkynes showed dependence on the concentration of catalyst. We monitored the rates of reaction with different concentration of catalyst from 1.4 mM to 11 mM under similar conditions, and we found that the k_{obs} increased from $7.5 \times 10^{-6} \text{ h}^{-1}$ to $6.8 \times 10^{-5} \text{ h}^{-1}$. The plot of v_i vs. concentration of ruthenium hydride is linear, which indicated that there was a first order rate dependence

on the concentration of catalyst. So in the dilution, we can drive the kinetics equation rate

$$= k [\text{Ru}]^1 [\text{Alkyne}]^0 [\text{silane}]^0.$$

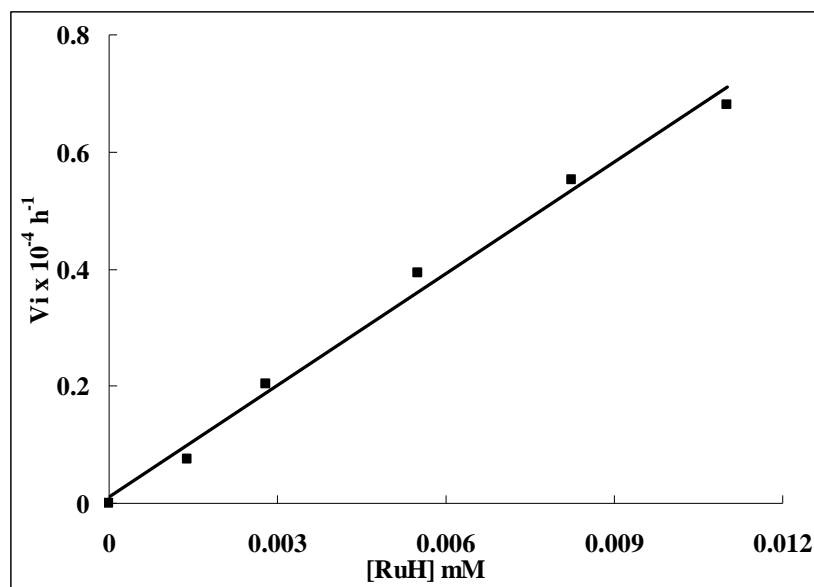


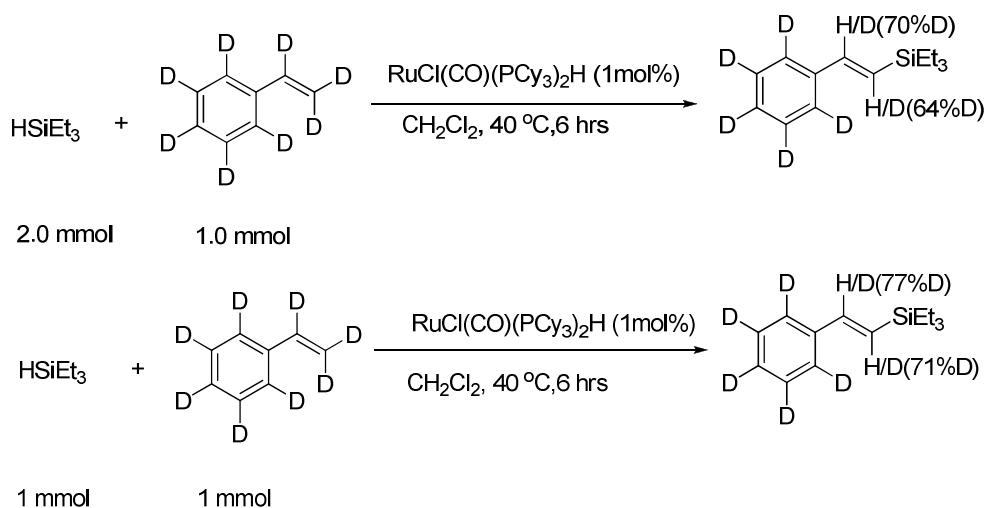
Figure 26. Plot of the initial rate vs. [RuH]

5.4 Mechanistic Study on the Hydrosilylation of Alkenes

5.4.1 Deuterium Labeling Study on the Hydrosilylation of Alkenes

To explore the mechanism of hydrosilylation of alkenes, we first performed deuterium labeling study experiments. The treatment of triethylsilane (1.0 mmol) and styrene- d_8 (1.0 mmol) in CH_2Cl_2 at 40 °C was monitored by ^1H NMR spectroscopy. The

coupling product **70a** was characterized by ^1H and ^2H NMR spectroscopy. For the product **70a**, a similar amount of deuterium on the two vinyl positions was detected by ^1H and ^2H NMR spectroscopy which gives the 77% and 71% deuterium (Scheme 26). Under similar conditions, the reaction of styrene- d_8 (1.0 mmol) with triethylsilane (2.0 mmol) gave the product with 70% and 64% deuterium on the vinyl positions.



Scheme 26. Deuterium Labeling Study on the Hydrosilylation of Alkenes

As shown in Figure 27, A is the ^1H NMR spectroscopy of trans-vinylsilane; B is the ^1H NMR of deuterium vinylsilane and C is ^2H NMR spectroscopy of deuterium product two deuterium signals at 2.6 ppm and 0.8 ppm were detected, which were assigned to the ethylbenzene. In ^1H NMR spectroscopy, two signals were detected at the same chemical shift. In addition, there was also a deuterium signal assigned to the unused

triethylsilane. These H/D exchange results indicate that the H/D exchange is rapid and done before the formation of the coupling products.

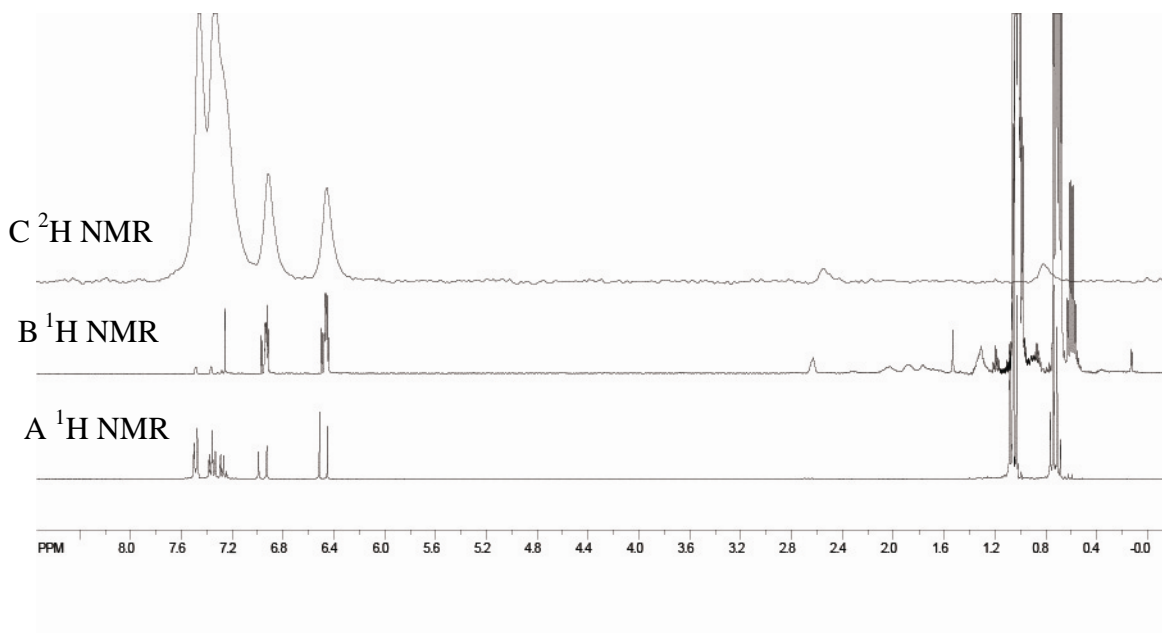


Figure 27. ^1H and ^2H NMR for the complex **70a**

5.4.2 Isotope Effect Study on the Hydrosilylation of Alkenes

In order to determine the possibility of a rate-limiting C-H bond cleavage step, the kinetic isotope effect for the hydrosilylation of alkenes was performed. Again, the initial rate method was used in order to determine the reaction rates. Here, the treatment of styrene (0.1 mmol) and triethylsilane (0.2 mmol) in the presence of 1.0 mol % of **1** in CDCl_3 was monitored by ^1H NMR spectroscopy at 40 °C (Scheme 27).

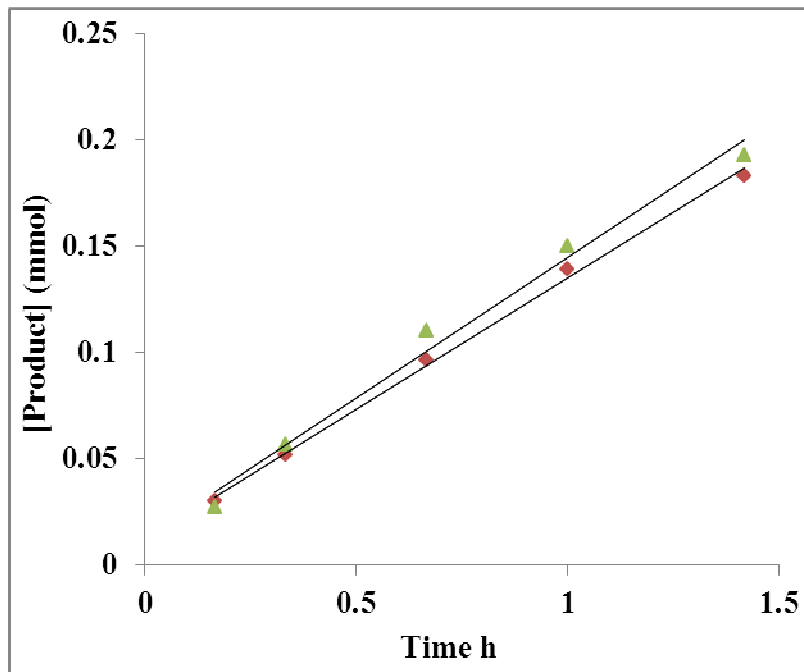
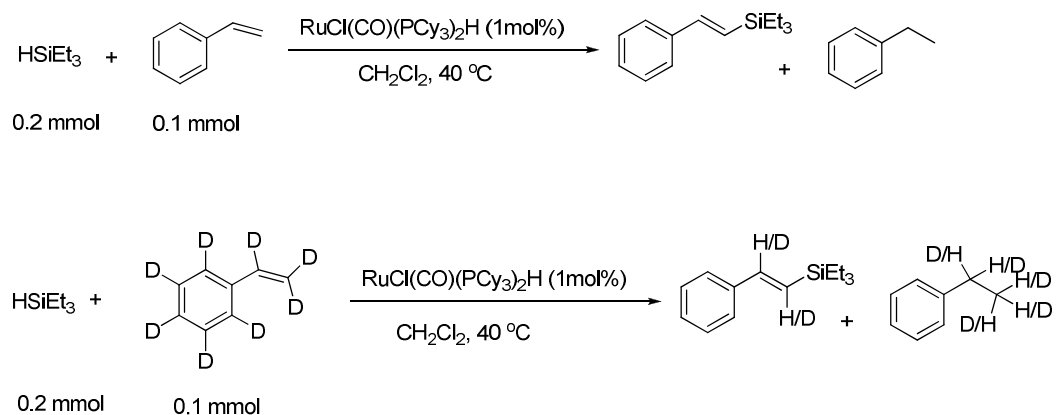


Figure 28. Kinetics Plot of the Reaction of Styrene and HSiMe₃

The rate of reaction was then determined from linear, pseudo-first order plots of the product formation vs. time (Figure 28), which gave the k_{obs} as $1.1 \times 10^{-5} \text{ h}^{-1}$. Under similar conditions, the reaction of deuterated styrene- d_8 (0.1 mmol) and triethylsilanes (0.2 mmol) was monitored by NMR spectroscopy at 40 °C, and gave the k_{obs} as $9.8 \times 10^{-6} \text{ h}^{-1}$. The kinetic isotope effect study gave us a similar k_{obs} value for the deuterated and regular reactions, which gave the $k_{\text{CH}}/k_{\text{CD}}$ as 1.1 ± 0.1 . This low KIE value suggested that C-H bond cleavage of the styrene is not the rate-limiting step.

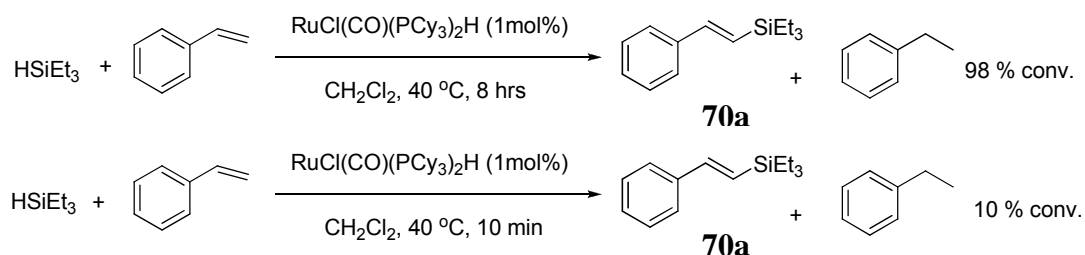


Scheme 27. Kinetic Isotope Effect Study on the Hydrosilylation of Alkenes

5.4.3 Carbon Isotope Effect Study

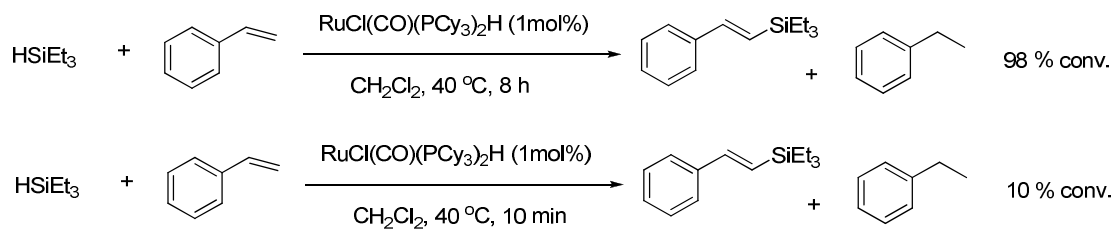
In order to get more information on the rate limiting step, we used singleton's method in carbon isotope effect study. In glove box, styrene (2.0 mmol), triethylsilane (3.0 mmol), **1** (14 mg, 1 mol %) were dissolved in 3 mL CH_2Cl_2 solution in two 25 mL Schlenk tubes equipped with a magnetic stirring bar. The reaction tube was then heated in oil bath at 40 °C for 10 min and was opened to air at room temperature, and the crude product mixture was analyzed by GC/MS (10 % conversion). The other reaction tube was heated in an oil bath at 40 °C for 8 hr and was opened to the air at room temperature. The crude product mixture was analyzed by GC/MS (98 % conversion). The solvent was

removed under a rotary aspirator, and the product *trans* vinylsilane was isolated by a column chromatograph on silica gel (*n*-hexanes) (Scheme 28).



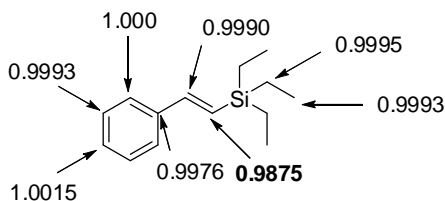
Scheme 28. Carbon Isotope Effect Study on the Hydrosilylation of Styrene

The ^{13}C NMR analysis of *trans* vinylsilane of both 98% conversion and 15% conversion was performed by following Singleton's ^{13}C NMR method. The NMR samples were prepared identically by adding *trans* vinylsilane (198 mg) in CDCl_3 (0.5 mL) in a 5 mm high precision NMR tube. The ^{13}C $\{^1\text{H}\}$ NMR spectra were recorded with H-decoupling and 45 degree pulses. A 60 s delay between pulses was imposed to minimize T_1 variations (d1 = 60 s, at = 5.0 s, np = 245098, nt = 512). The average ^{13}C integration ratio of the samples of *trans* vinylsilane **70a** is shown in Table 14.

Table 14. Average ^{13}C Integration of the Samples of trans-vinylsilane **70a**

C#	98% conv.	18% conv.	18% conv./98% conv.	change (%)
1	2.9936 (3)	2.9925 (3)	0.9996 (3)	0.04 (3)
2	2.9827 (4)	2.9823 (4)	0.9998 (4)	0.02 (4)
3	0.9314 (5)	0.9208 (5)	0.9886 (5)	1.14 (5)
4	1.0084 (3)	1.0060 (3)	0.9976 (3)	0.24 (3)
5	0.9288 (4)	0.9272 (4)	0.9983 (4)	0.17 (4)
6	2.0000 (5)	2.0000 (5)	1.0000 (5)	0.00 (5)
7	1.9892 (3)	1.9884 (3)	0.9996 (5)	0.04 (5)
8	0.9938 (3)	0.9923 (3)	0.9985 (3)	0.15 (3)
C#	98% conv.	10% conv.	10% conv./98% conv.	change (%)
1	2.9936 (4)	2.9915 (4)	0.9993 (4)	0.07 (4)
2	2.9827 (4)	2.9813 (3)	0.9995 (3)	0.05 (3)
3	0.9314 (5)	0.9198 (5)	0.9875 (5)	1.25 (5)
4	1.0084 (3)	1.0074 (3)	0.9990 (3)	0.10 (3)
5	0.9288 (4)	0.9266(4)	0.9976 (4)	0.24 (4)
6	2.0000 (5)	2.0000 (5)	1.0000 (5)	0.00 (5)
7	1.9892 (3)	1.9879(3)	0.9993 (5)	0.07 (5)
8	0.9938 (3)	0.9953 (3)	1.0015 (3)	0.15 (3)

In Table 14, the most significant carbon isotope effect was observed at the CH=CH-Si of the product. We can see that at 10 % conversion, the integration of the carbon **3** which was signed to CH=CH-Si is 0.9198 at five runs, comparing with 0.9314 at 98% conversion the integration of carbon **3** is change by 1.25 %. But other carbons change by 0.05 %-0.15%. At 18 % conversion, the results is similar, the carbon **3** changed by 1.14 %, and others changes even less. This result indicates that the reaction step involving this C-Si carbon is slow and should be rate limiting. This is based on an assumption that the migration of ^{13}C is slower than the migration of ^{12}C in such slow steps, which results that the abundance of ^{13}C of the product at low conversion will become less than the ^{13}C of the product from the completed reaction.

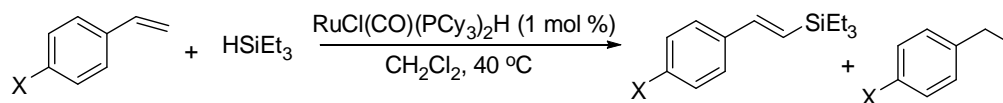


Compound **70a**

5.4.4 Hammett Study on the Hydrosilylation of Alkenes

Hammett studies of *para*-substituted styrene were performed to determine the electronic effects on the alkene substrates for the hydrosilylation of alkenes. The treatment of the *para*-substituted styrene $p\text{-X-C}_6\text{H}_4\text{CH=CH}$ ($\text{X} = \text{OMe}, \text{CH}_3, \text{H}, \text{Br}, \text{Cl}$)

(0.2 mmol), Triethylsilane (0.3 mmol) and hexamethylbenzene (26 mg as the internal standard) was monitored by ^1H NMR spectroscopy at 40 °C.



X = OMe, CH₃, H, Br, Cl

Scheme 29. The Hammett Study on the Hydrosilylation of Alkenes

The initial rate method was used to determine the rate of each of reactions. The rates were measured by the integration of the products vinyl peak (6.48 ppm). The integration of product peak was normalized against the internal standard. The k_{obs} was estimated from a pseudo first-order plot of $\ln[\text{product}]$ vs reaction time. The Hammett plot of the $\log(k_x/k_H)$ vs the σ_p gave the Hammett ρ value of 0.59 (Figure 31).

In Figure 29, the Hammett plot of the $\log(k_x/k_H)$ vs the σ_p gave a positive Hammett ρ value of 0.59, which indicated that the rate of the reaction increased with the electron-withdrawing substitutes. By using styrene, the reaction gave $k_{\text{obs}} = 1.1 \times 10^{-5} \text{ h}^{-1}$. The reaction with the electron-donating substitutes as 4-methoxyl styrene, gave $k_{\text{obs}} = 7.3 \times 10^{-6} \text{ h}^{-1}$. But when using the electron-withdrawing substitutes as the 4-bromo-styrene, the reaction gave a $1.5 \times 10^{-5} \text{ h}^{-1}$ as the k_{obs} value. This positive Hammett ρ value indicated that possible anionic nature of the transition state.

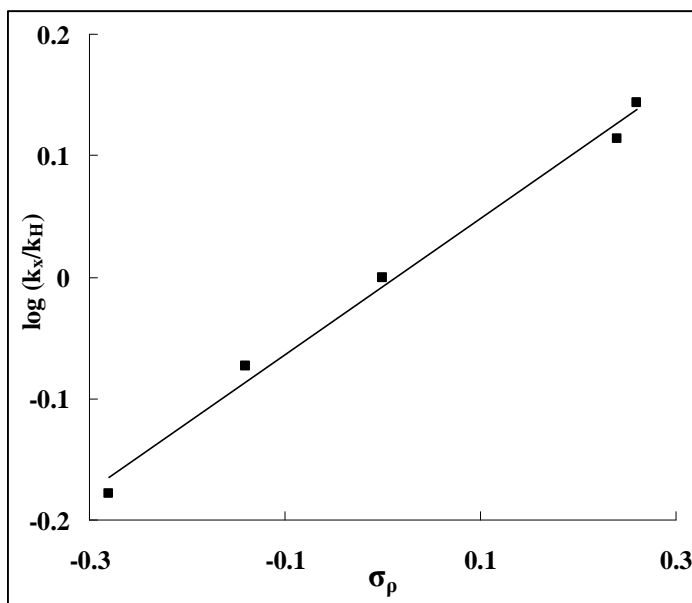


Figure 29. Hammett Plot of the Coupling Reaction of *para*-Substituted $p\text{-X-C}_6\text{H}_4\text{CH=CH}_2$ (X = OMe, CH₃, H, Cl, F) with Triethylsilane

Here, we propose the structure of possible transition state of the intermediate (Figure 30), where X can be either electron-withdrawing or the electron-donating substitutes. When X are electron-withdrawing substitutes, the Ru-C bond will become weak and easy to break. Besides, the electrophonic addition of silyl group to the carbon will become easy. So in this case, the rate of the reaction will increase. These results indicate that the transition state is stable and the formation of C-Si bond is slow and rate-determining. These results are also consistent with the carbon isotope effect study, which suggests that the formation of the C-Si bond is the rate-determining step.

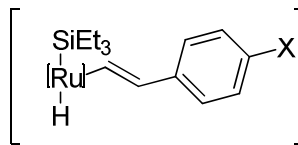


Figure 30. Possible Transition State for the Intermediate of the Hydrosilylation of Alkenes

5.4.5 Phosphine Inhibition Study on the Hydrosilylation of Alkenes

We next performed a series of phosphine inhibition experiments to gain the further insights into the reaction mechanism. The phosphine inhibition is common in our ruthenium hydride catalyst system, we observed a strong phosphine inhibition in the reaction of alkynes with triethylsilane and the reaction of alkynes with carboxylic acid. This phenomenon may also happen in the hydrosilylation of the alkenes. Therefore, to observe this phosphine inhibition, the mixtures of styrene (0.20 mmol), triethylsilane (0.40 mmol), **1** (2 mg, 1 mol %) and C₆Me₆ (2 mg, internal standard) were dissolved in 0.5 mL of CDCl₃ solution in a J-Young NMR tube with a Teflon screw cap. A pre-dissolved PCy₃ in CDCl₃ solution (5 μL, 1.0 M) was added to the tube via syringe. The tube was brought out of the glove box. The reaction was monitored by ¹H NMR at 10 min interval at 40 °C. The initial rate method was used to measure the rate of each reaction. The rate was measured by integration of product peak at δ 5.81 ppm (=CHSi), and was normalized against the internal standard peak. The *k*_{obs} was estimated from the first order plot of *ln*[product] vs. reaction time.

The catalytic reaction was found to be strongly inhibited by the phosphine ligand. The initial rate was estimated from the [product] vs. time for each added [PCy₃] (Figure 31). Addition of PCy₃ (2.7-1.0 μmol, 2.7-1.0 mol %) to the reaction mixture under the similar conditions led the rate to a steady decrease from 3.6 × 10⁻⁵ h⁻¹ (without PCy₃) to 1.2 × 10⁻⁶ h⁻¹ (1.0 mM of PCy₃). These results indicated that active Ru catalyst formed by initial dissociation of one phosphine ligand.

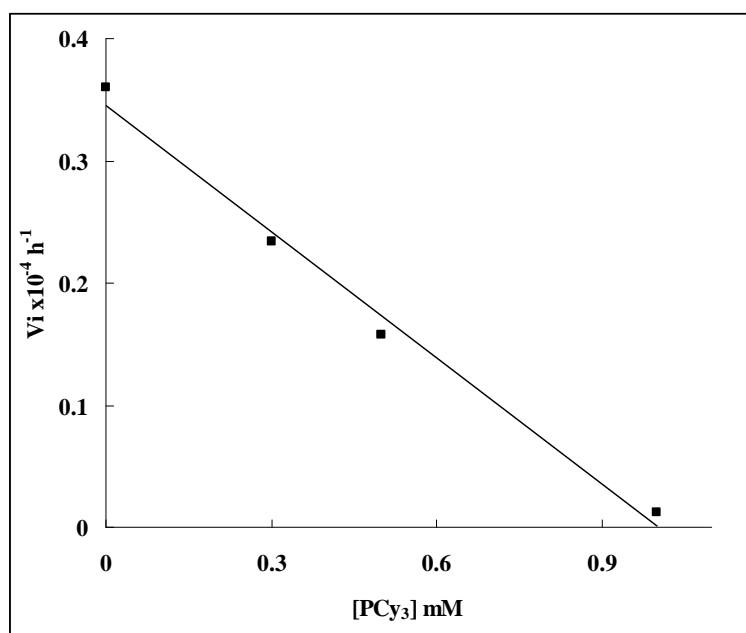


Figure 31. The Phosphine Inhibition for the Reaction of Styrene and Triethylsilane

In order to determine the type of inhibition, a series of kinetic experiments were performed. The treatment of styrene (0.05-1.0 mmol) and excess amount of triethylsilane with various concentrations of PCy₃ (0-1.0 mM, 0-2.2 equiv. compared to **1**) in presence

of **1** (1 mol %) in CDCl_3 at room temperature was monitored by ^1H NMR. The rate vs. [styrene] plot (Figure 32) was constructed from linear, pseudo-first order plot of product formation vs. time.

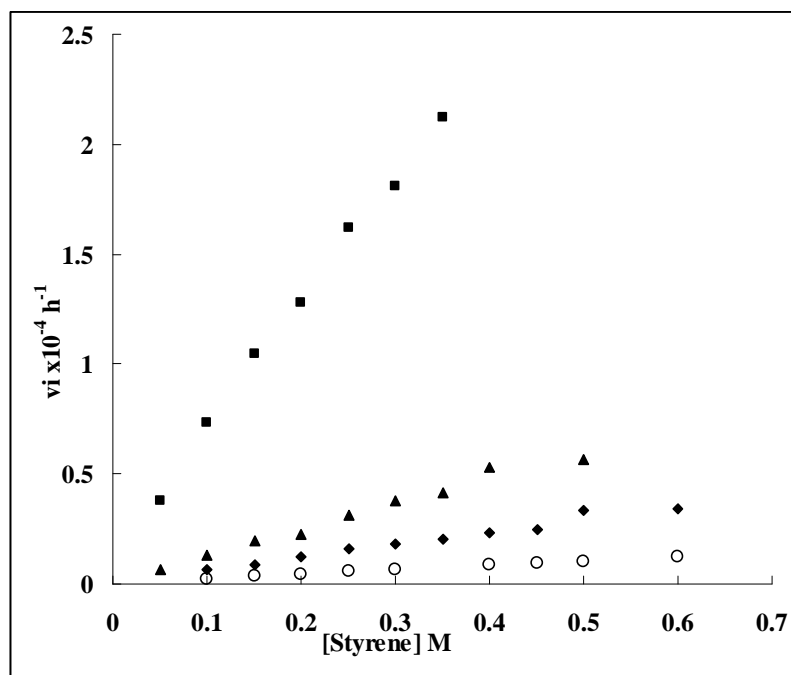
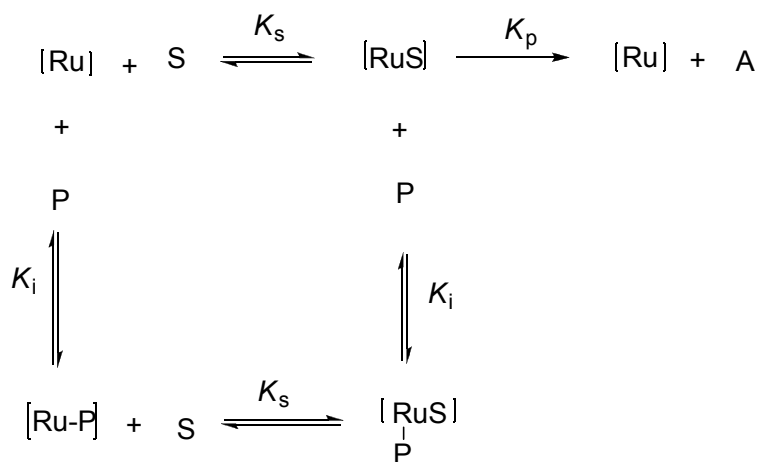


Figure 32. Plot of the Initial Rate vs. [styrene] at Different PCy_3 Concentrations. Without PCy_3 (■); 0.21 mM (0.4 equiv) PCy_3 (▲); 0.42 mM (0.8 equiv) PCy_3 (◆); 1.01 mM (1.8 equiv) PCy_3 (○);

The inhibition data was fitted to the Michaelis-Menten equation to determine the kinetic parameters. A series of Lineweaver-Burke plots (Scheme 30) were constructed. The reciprocal plots indicated that PCy_3 acts as a noncompetitive inhibitor, as illustrated

in Scheme 30, where [Ru] is the catalytic active species, [S] is the substrate, P is PCy₃ ligand and A is the vinylsilane product.



Scheme 30. General Kinetic Scheme for the Noncompetitive Inhibitor¹¹⁴

In order to conform this, replot of the slope and Dixon plot of $1/v$ vs. [PCy₃] were constructed (Figure 33 and 34).

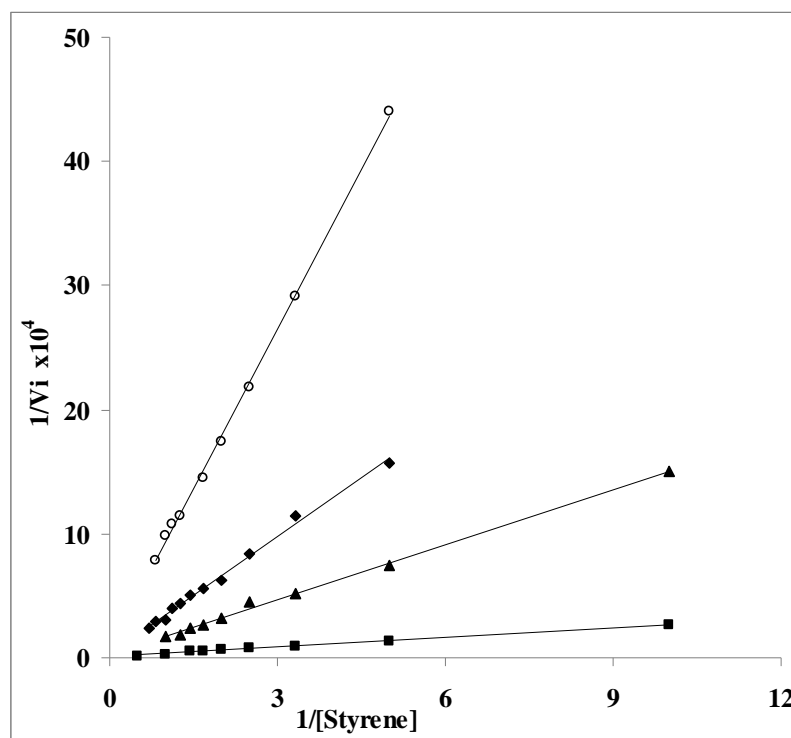


Figure 33. Lineweaver-Burke Plot of $1/v_i$ vs. $1/[\text{styrene}]$. No PCy_3 (\blacksquare); 0.21 mM (0.4 equiv.) PCy_3 (\blacktriangle); 0.42 mM (0.8 equiv.) PCy_3 (\blacklozenge); 1.01 mM (1.8 equiv.) PCy_3 (\circ);

The following reciprocal equation is for noncompetitive inhibition.

$$\frac{1}{v} = \frac{K_m}{V_{\max}} \left(1 + \frac{[I]}{K_i}\right) \frac{1}{[S]} + \frac{1}{V_{\max}} \left(1 + \frac{[I]}{K_i}\right)$$

And this equation may be rearranged to:

$$\frac{1}{v} = \left(1 + \frac{K_m}{[S]}\right) \frac{[I]}{V_{\max} K_i} + \frac{1}{V_{\max}} \left(1 + \frac{K_m}{[S]}\right)$$

A plot of $1/v$ versus $[I]$ will be a straight line. The slope of the Dixon plot is given

by

$$\text{slope} = \frac{K_m}{V_{\max} K_i} \frac{1}{[S]} + \frac{1}{V_{\max} K_i}$$

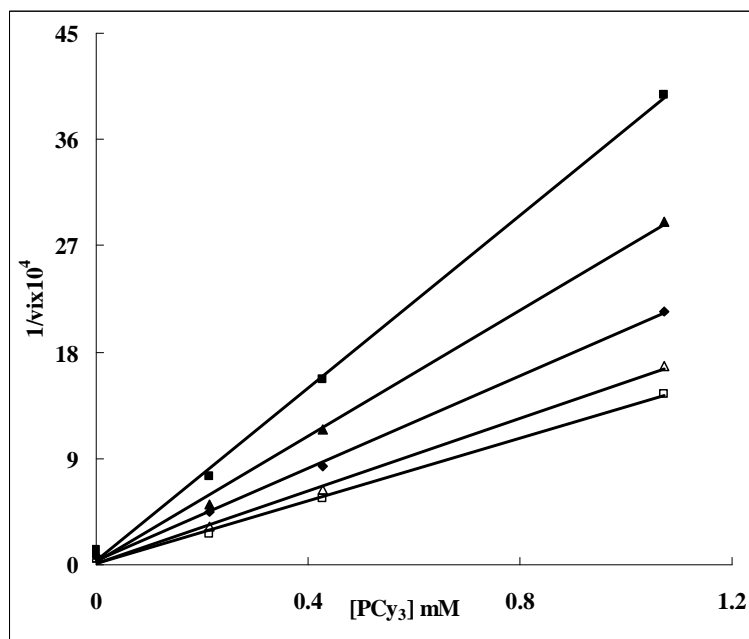


Figure 34. Dixon plot of $1/v$ versus $[PCy_3]$

From the equations, the replot of slope vs. $1/[S]$ should be a straight line with a slope of $K_m/V_{\max}K_i$, and an intercept of $1/V_{\max}K_i$. So K_m can be figured out from Figure 35 by slope/intercept which gave 3.033. The value of K_i is from the Figure 34. The plot of $1/v$ vs. $[I]$ gave a straight line with a slope of $(1+K_m/[S])/V_{\max}K_i$ and an intercept of $(1+K_m/[S])/V_{\max}$. So $K_i = \text{intercept/slope}$ which gave 0.16 and V_{\max} is 10.42. Therefore the kinetic equation can be derived by using these parameters.

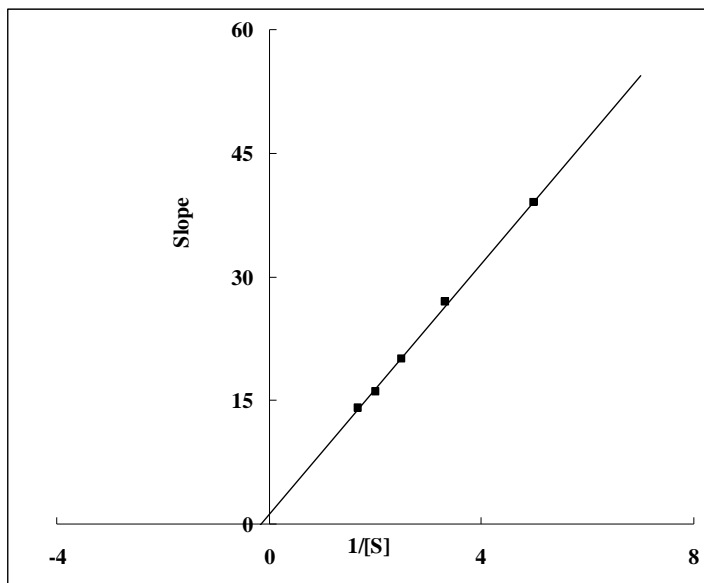
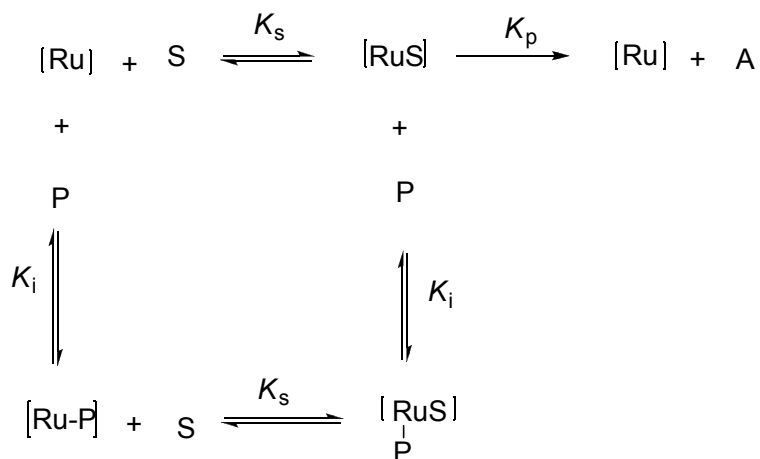


Figure 35. The replot of slope vs. $1/[S]$



Scheme 31. General Kinetic Scheme for the Non-competitive Inhibitor¹¹⁵

Where [Ru] is the catalytically active species, [S] is the substrate, P is PCy₃ ligand and A is the vinylsilane products. In this scheme, the inhibitor reversibly coordinates to the catalyst-substrate complex [RuS], creating inactive catalyst-substrate-inhibitor

complex [RuSP]. The catalyst-substrate-inhibitor complex [RuSP] can release the S to form the catalyst-inhibitor complex [RuP], which can generate the catalytically active species [Ru] by the dissociation of inhibitor PCy₃.

Kinetics data for the hydrosilylation of alkenes can be explained using a non-competitive inhibitor model. The Lineweaver-Burke plots, Dixon plot and slope secondary plot are consistent with this non-competitive inhibitor model: A non-competitive inhibitor has no effect on the affinity the [RuP] complex has for the coordination of alkene. The overall effect for a non-competitive inhibitor is to lower the V_{\max} of the reaction.

5.4.6 Rate Dependence on the Substrate Concentration

The rate dependence on alkenes would provide valuable insights into the mechanism for the hydrosilylation of alkynes. The initial rate method was used to determine the rate of reactions. The treatment of 0.06-0.8 M styrene with excess amount of triethylsilane in the presence of 2 mg **1** at 40 °C in CDCl₃ was monitored by ¹H NMR spectroscopy. The initial rates of the reactions were determined from linear, pseudo-first order plots of product formation rate vs. time.

In Figure 36, the rate showed the linear dependence on the concentration of styrene as first order.

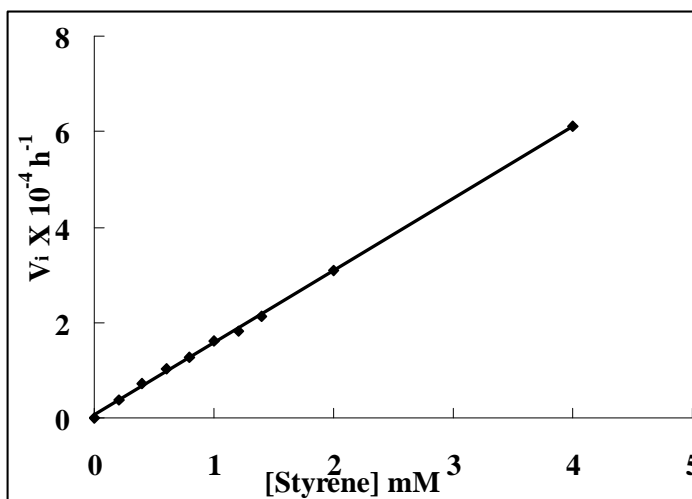


Figure 36. Plot of the initial rate vs. [styrene]

We next performed a kinetic study on the rate dependency on triethylsilane. Treatment of 0.04 M to 0.7 M triethylsilane with excessive amount styrene in the presence of 2 mg **1** at room temperature in CDCl_3 was monitored by ^1H NMR spectroscopy. The initial rate method was used to determine the rate of the reactions. The initial rates of the reactions were determined from linear, pseudo-first order plots of rate of the product formation vs. time.

The Figure 37 indicated that the rates of reaction of hydrosilylation of alkynes showed no dependence on the concentration of silane. We monitored the rate of the

reactions with the different concentration of silanes from 0.04 M to 0.7 M at similar conditions, and found all the reactions giving similar k_{obs} value as $7.3 \times 10^{-5} \text{ h}^{-1}$.

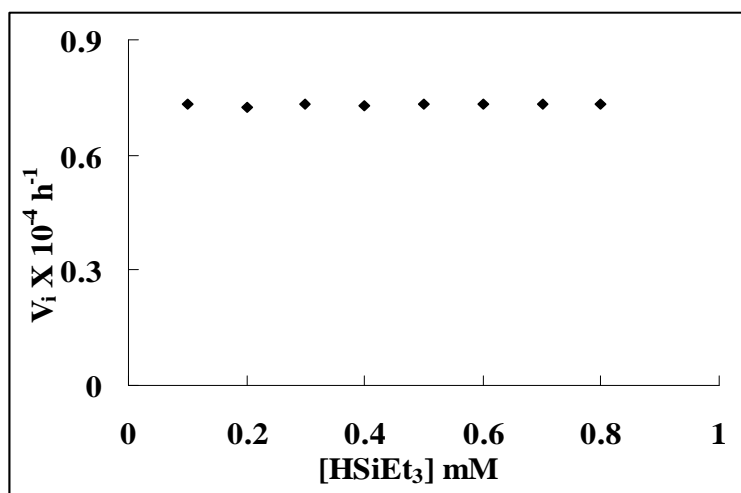


Figure 37. Plot of the initial rate vs. [HSiEt₃]

5.4.7 Rate Dependence on the Catalyst Concentration

In order to get insight into the mechanism, the rate dependence on ruthenium hydride concentration was performed. The treatment of 1.4-11 mM of ruthenium hydride **1** with 0.4 M of triethylsilane and 0.2 M of phenylacetylene at room temperature in CDCl₃ was monitored by ¹H NMR spectroscopy. The initial rate method was used to determine the rates of the reactions. The initial rates of the reactions were determined from linear, pseudo-first order plots of rate of the product formation vs. time.

The rate of the reactions of hydrosilylation of alkenes showed dependence on the concentration of catalyst. We monitored the rates of reaction with different concentration of catalyst from 0.0014 M to 0.011 M at similar conditions, and find the k_{obs} increasing from $5.0 \times 10^{-5} \text{ h}^{-1}$ to $3.82 \times 10^{-4} \text{ h}^{-1}$. The plot of v_i vs. concentration of ruthenium hydride is linear, which indicates that there was a first order rate dependence on the concentration of catalyst.

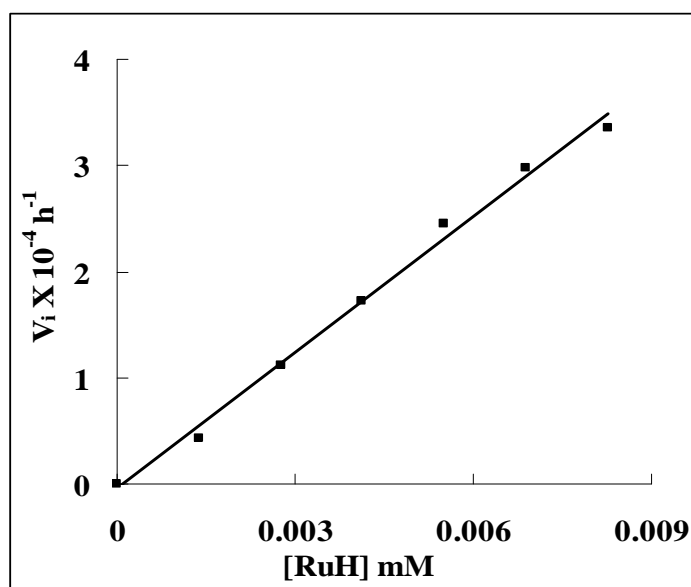
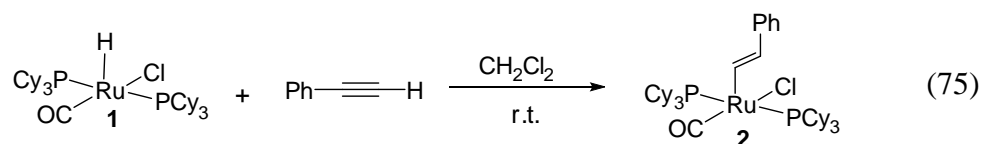


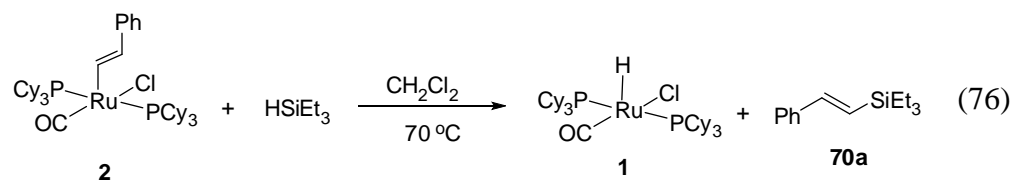
Figure 38. Plot of the initial rate vs. [RuH]

5.5 The Reaction of Triethylsilane with Ruthenium Vinyl Complex

In order to get insight into the mechanism, we made the immediate species ruthenium vinyl complex in Eq 75. Thus, in glove box, 100 mg ruthenium complex **1**, excess amount of phenylacetylene were dissolved in 3 mL CH₂Cl₂ solution in two 25 mL Schlenk tubes equipped with a magnetic stirring bar, at room temperature for 30 min this reaction led to the clean formation of the ruthenium-vinyl complex **2**, which was isolated in 87% yield after recrystallization in CH₂Cl₂/*n*-hexanes (Eq 75).



We tested the activity of complex **2** for both the reaction of triethylsilane with styrene and the reaction of triethylsilane with phenylacetylene, they showed the same activity as the complex **1**, for the hydrosilylation of phenylacetylene, the reaction generates *cis* product, for the styrene case, it generates *trans* product. We performed the reaction of complex **2** (0.1mmol) with styrene (0.2 mmol) in the CDCl₃, and monitored the reaction by the VT-NMR from -40 °C to 80 °C, and observed no change on both the ¹H NMR and ³¹P NMR. On the other hand, we also observed by VT-NMR that no reaction of complex **2** with triethylsilane took place at temperatures below 70 °C. However, when heated above 70 °C, the formation of the *trans* vinylsilane was detected, and the complex **2** was detected to turn back to complex **1** (Eq 76).



The Figure 39 showed the ^{31}P NMR signal change at 70 °C, before the reaction, there was only one signal at 27.8 ppm, which belonged to ruthenium vinyl complex **2**. And then we observed ruthenium hydride signal at 45.8 ppm and for the ^1H NMR, we observed the formation of complex **70a**. After 3hr the reaction was done, all the complex **2** converts to the ruthenium hydride complex **1**.

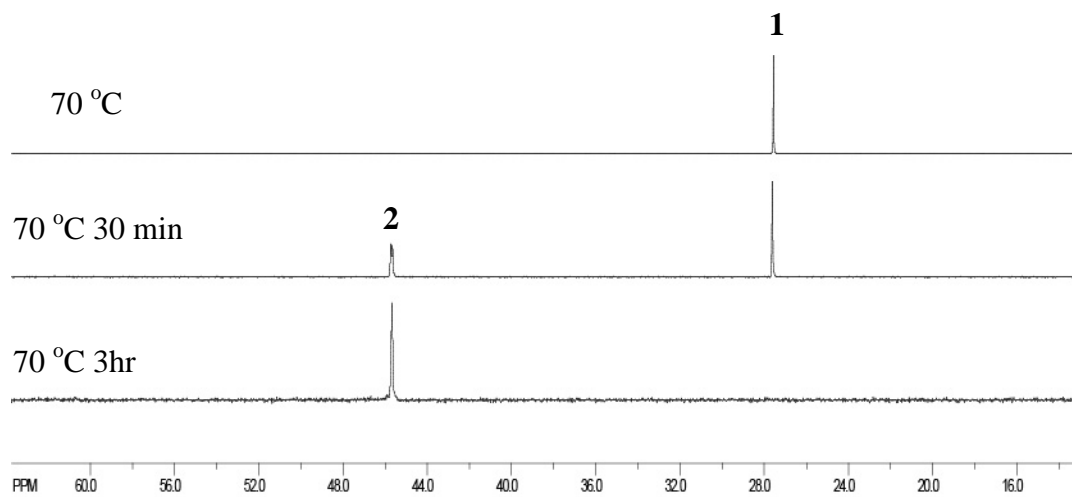


Figure 39. ^{31}P NMR of the Formation of Ruthenium Hydride Complex **1** from Rutheniumvinyl Complex **2**

Since this reaction is slower than the catalytic reactions, which can generate the product at room temperature, the following kinetic experiments are performed to get more information on this reaction. In a glove box, triethylsilane (0.3 mmol) with complex

2 (0.2 mmol), C_6Me_6 (2 mg, internal standard) were dissolved in 0.5 mL $CDCl_3$ in J-Young tube. This tube was taken out and was monitored by the 1H NMR, The rate was measured by integration of the product 1H peak at δ 5.81 ($=CHSi$), and was normalized against the internal standard peak. The k_{obs} was estimated from the first order plot of [product] vs. reaction time. Under similar conditions, we monitored the rate change by adding PCy_3 and by adding styrene. We found that this reaction shows the strong phosphine inhibition (Figure 40).

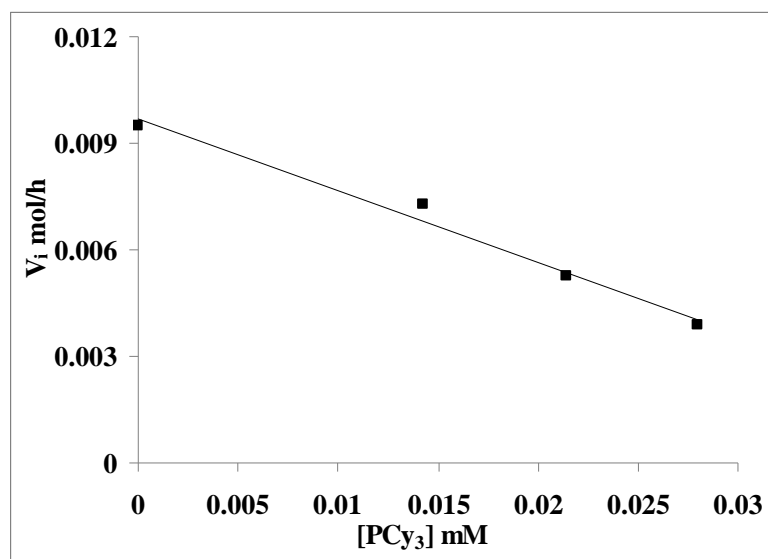


Figure 40. The Plot of the Reaction Rate vs the Concentration of PCy_3

The k_{obs} of this reaction of triethylsilane with ruthenium vinyl complex is 0.0095 mol/h. By adding 0.005 mmol PCy_3 the reaction gives a k_{obs} 0.007 mmol/h. These

results are consistent with the catalytic reactions which were observed the strong phosphine inhibition.

Meanwhile, we observed that the reaction can be promoted by adding styrene. By adding the styrene, k_{obs} of the reaction are 0.016 mmol/h (0.01 mmol styrene), 0.016 mmol/h (0.035 mmol styrene) 0.016 mmol/h (0.046 mmol styrene) (Figure 41).

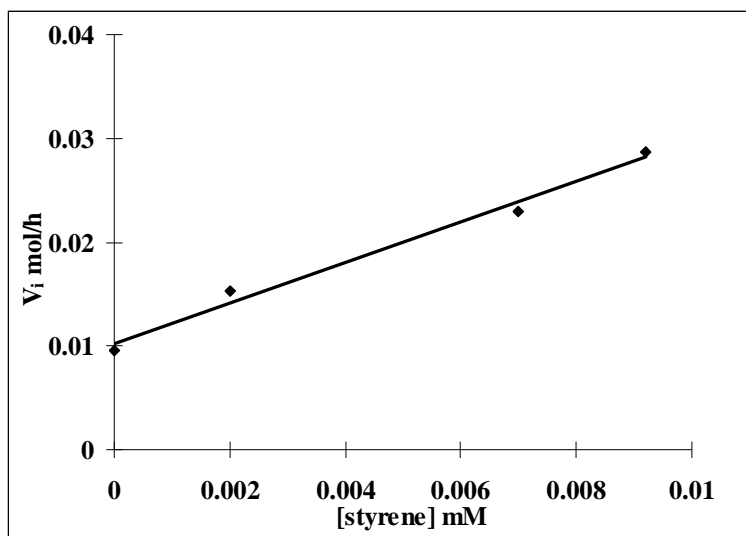


Figure 41. The Plot of Reaction Rate vs the Concentration of Styrene

So these indicated that the formation of intermediate **72c** (Eq 77) through the intermediate **72b** requires phosphine dissociation and styrene addition, as styrene can be coordinated to the ruthenium center and promote the dissociation of PCy_3 . Without styrene, the dissociation of the PCy_3 does not favor. This can explain that the reaction of

complex **2** with triethylsilane needs being heated to 70 °C to generate the product but a catalytic reaction can finish just at room temperature.

5.6 Computation Studies on the Hydrosilylation of Alkynes

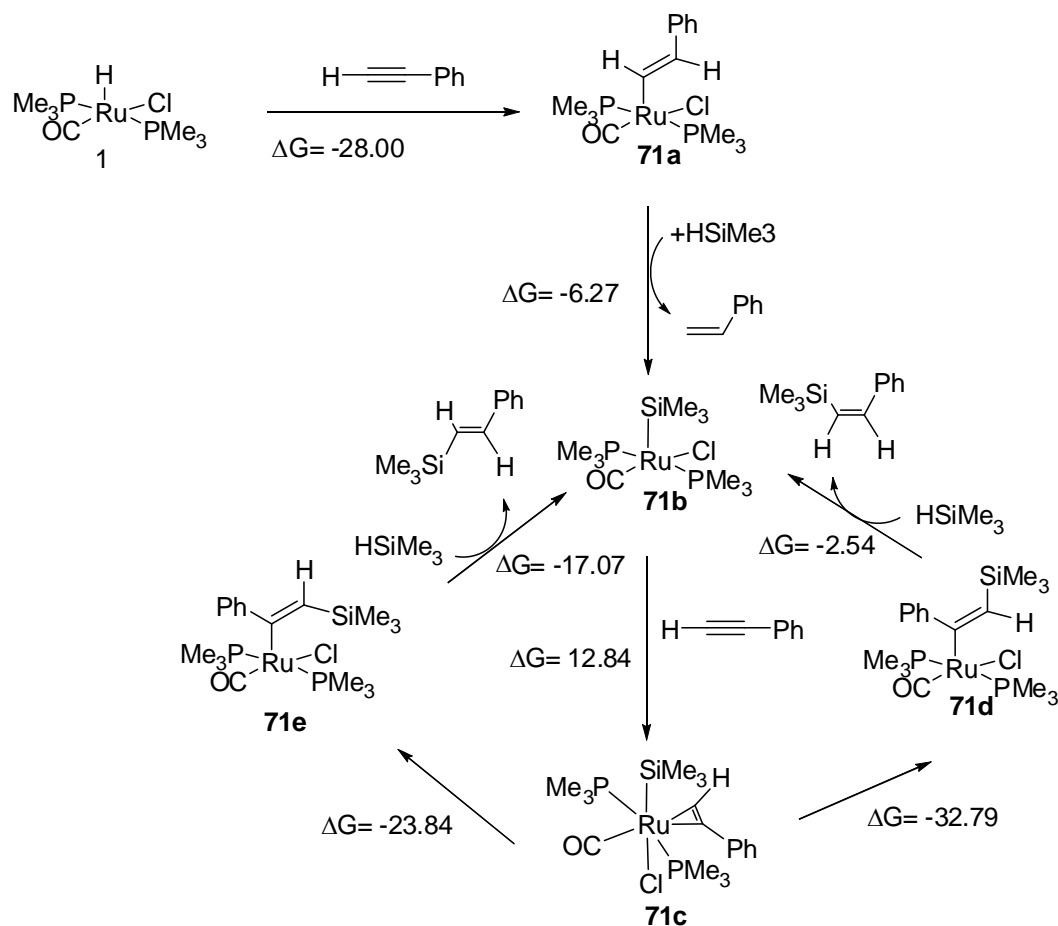
For the mechanism of the hydrosilylation of alkynes, deuterium labeling study was carried out and the results indicated that there was no D/H exchange during the reaction, which means there should not be C-H cleavage of the alkynes during the reaction. We also detected the formation of ruthenium vinyl complex, which showed similar activity and selectivity as complex **1** on the hydrosilylation of alkyne. So we proposed that the catalytic reaction starts at the formation of the ruthenium vinyl complex by adding alkyne to the ruthenium center. Then with the coordination of silane to the ruthenium center, the key intermediate ruthenium-silyl complex was generated by the eliminating styrene. This step was monitored by ^1H NMR and ^{31}P NMR, only the formation of styrene was detected, there was no information on the formation of ruthenium silyl complex. This may be due to the high reactivity of 14 electron ruthenium silyl complex. In order to get more details on the selectivity and mechanism of the hydrosilylation of alkynes, density functional calculations were carried out. All calculations were carried out with Gaussian 09 program. First of all, all geometries of the

reactants, transition structures and intermediates were fully optimized by B3LYP method. The 6-31G (d) basis set was used for H, C, O, P, Si and Cl atoms, while the Lanl2dz basis set and ECP were used for Ru atom. The Ru atom was augmented with f-polarization functions. The harmonic vibration frequency calculation was performed for each structure, from which the zero-point energy, thermal energy, entropy and free energy were derived. In order to minimize computation time, RuH(PMe₃)₂Cl(CO) was chosen to be the catalyst, with trimethylsilane and phenylacetylene as the reacting silane and alkyne.

First we considered two mechanism pathways: two phosphine ligand system (Scheme 32) and one phosphine ligand system (Scheme 33).

In the two phosphine ligands system (Scheme 32), there was no phosphine ligand dissociation during the reaction, while the one phosphine ligand system with the dissociation of phosphine ligand. The reaction started at the formation of ruthenium vinyl complex **71a**, and this step gave $\Delta G = -28.00 \text{ kcal mol}^{-1}$. Then ruthenium silyl complex **71b** was formed with the elimination of styrene by giving negative ΔG . With the alkyne coordination the ruthenium center, complex **71c** was generated, which was followed by the migration of silyl group and elimination to give the *cis* or *trans* vinyl silane. But this mechanism cannot explain the strong phosphine inhibition which was detected by experiments and indicated that there should be the dissociation of phosphine ligand or one more phosphine ligand coordinating to the ruthenium center. Due to the steric

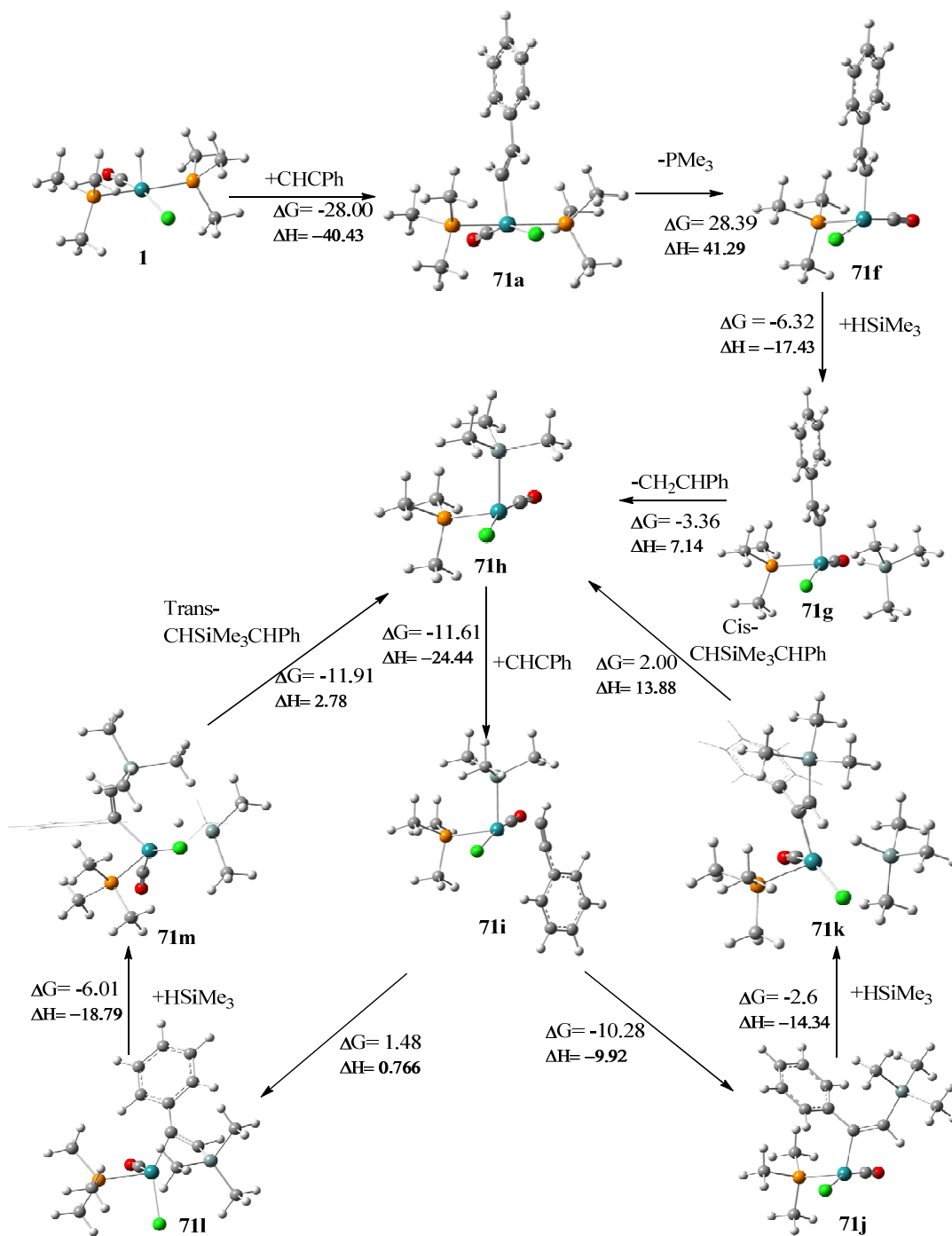
hindrance between the ligands, there was no way to build up the ruthenium complex with three phosphine ligands based on the computational studies.



Scheme 32. Proposed Mechanism of the Hydrosilylation of Alkyne with Two Phosphine Ligand

Here we proposed the other mechanism which involves the dissociation of the phosphine ligand (Scheme 33) and our computational results, with the computed reaction free energies given in kcal mol^{-1} were shown in Scheme 34.

In this monophosphine catalytic cycle, the first step was the formation of ruthenium vinyl complex **71a** by the addition of alkyne to ruthenium center. This step was done in seconds at room temperature by mixing ruthenium hydride with alkyne. For complex **71a**, the ruthenium center was coordinated by five ligands and there was strong steric hindrance between the ligands. Due to there was no active site left, so complex **71a** was stable and inactive. Complex **71a** was isolated and characterized by ^1H NMR and ^{31}P NMR. With the dissociation of one phosphine ligand active complex **71f** was generated, and then trimethylsilane coordinated to ruthenium center to form complex **71g**. Next, the high active 14 electron ruthenium silyl complex **71h** was formed with the elimination of styrene, which was detected by NMR. And then the alkyne coordinated to the ruthenium center to form complex **71i** with the π -bonding between ruthenium and alkyne. Next step was the silyl group migration to the alkyne to form η^2 - vinyl complex **71j** or **71l**.

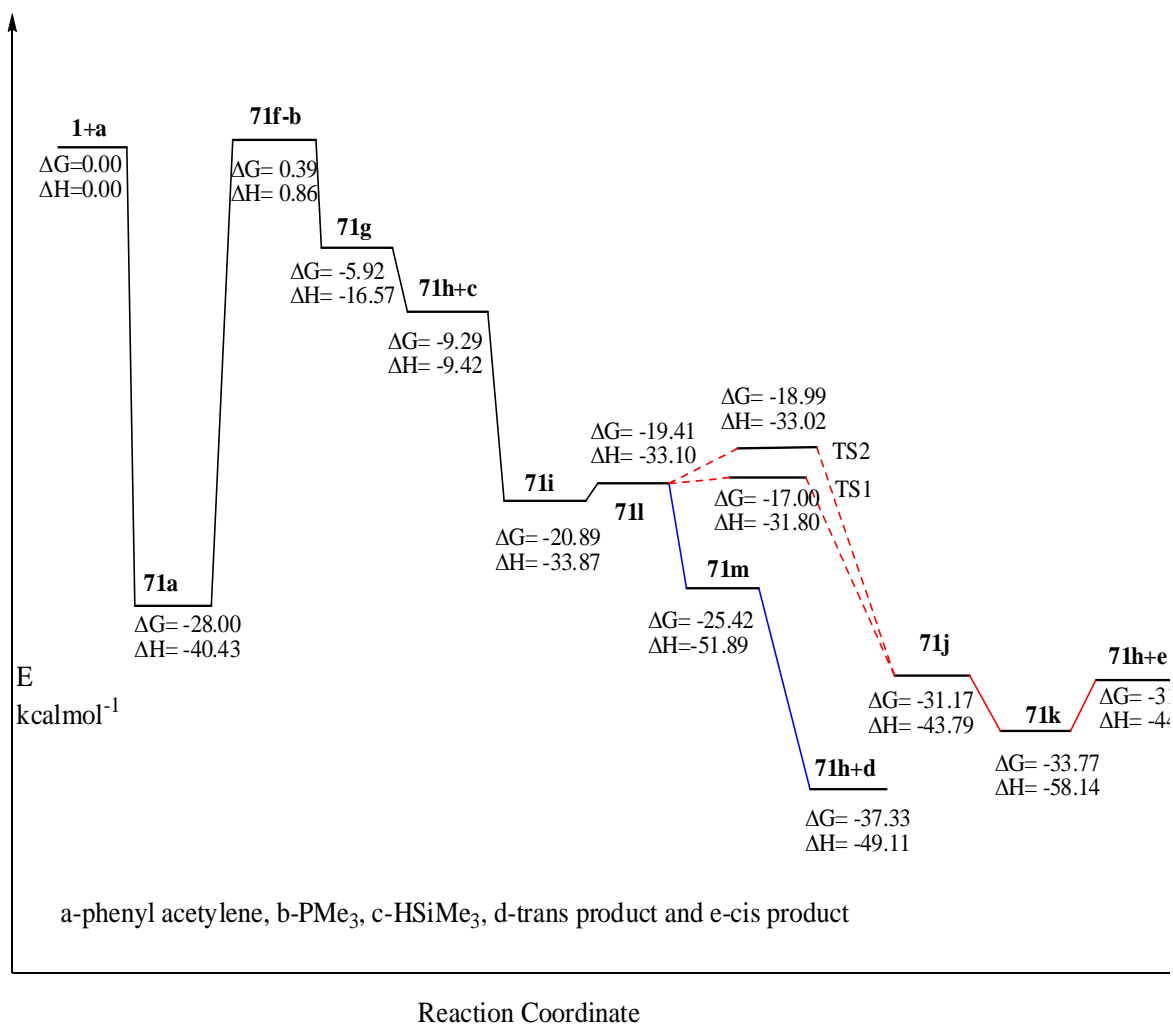


Scheme 34. Proposed Mechanism of the Hydrosilylation of Alkyne with the Dissociation of Phosphine

Based on the experimental results, this reaction has high selectivity, when R was less steric group as phenyl, there was only *cis* complex formed, while R was bulky group as t-butyl, there was trans product formed. In order to get the details on the selectivity factors, the computational studies were performed. First of all, all the stable intermediate species in Scheme 34 were optimized by B3LYP method by Gaussian 09 and the harmonic vibration frequency calculation was performed for each structure, from which the zero-point energy, thermal energy, entropy and free energy were derived and the ΔG and ΔH of each step was calculated and showed in Scheme 35.

In Scheme 35, which showed the entropy and free energy of all the structure, the entropy and free energy of ruthenium with phenylacetylene were considered as zero. The ruthenium vinyl complex **71a** has low entropy and free energy, and this was constant with the experimental results. And with the dissociation of one phosphine ligand, more active intermediate **71f** formed and the free energy increased to $0.39 \text{ kcalmol}^{-1}$. Based on Scheme 34 and Scheme 35, it was clear that, the first step which gave $-28.00 \text{ kcalmol}^{-1}$ as the Gibbs free energy was thermal favor while the dissociation of phosphine gave the $28.39 \text{ kcalmol}^{-1}$. Comparing with other steps, the dissociation of phosphine which needs more energy should be the rate-determining step. We tried to look for the transition state for the phosphine dissociation, unfortunately we failed. Here we proposed that the high active intermediate **71h** was the real starting catalyst for the catalytic cycle, with the

alkyne coordinating to the ruthenium center, the intermediate **7li** was more stable and this step was thermal favor.



Scheme 35. Calculated Energy of the Reaction Pathway

The silyl group migration was the key step for the formation the selective product.

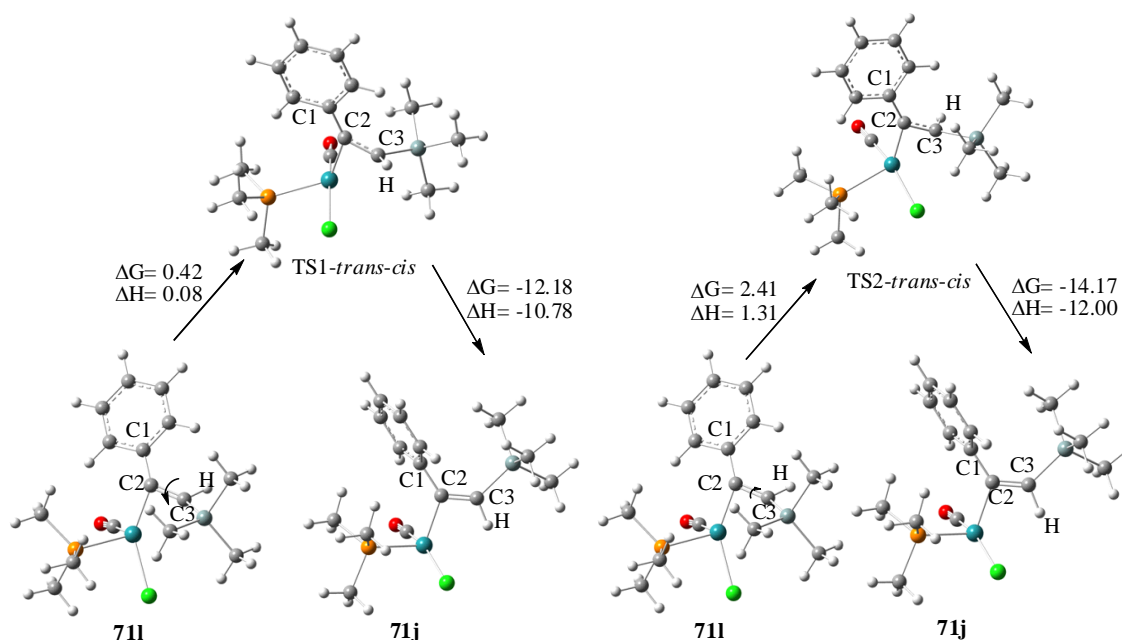
We proposed two pathways to form the selective product. One is that the silyl group

migration determining the selectivity of the product by directly forming the *cis* η^2 -vinyl species **71j** or *trans* η^2 -vinyl species **71i** which was determined by the steric hindrance between the ligands. We tested this possibility by using phenylacetylene as alkyne, but we could not get the *cis* η^2 -vinyl by the silyl group migration, what we got was only the *trans* η^2 -vinyl species **71i**. Based on these computational results, if the silyl group migration was the selectivity demanding step, there should be only *trans* product formation without *cis* product. But there was only *cis* product formed as the experimental results. So the step of the silyl group migration should not be the selectivity determining step.

Based on these, we proposed the other possibility: intermediate **71i** went through the silyl group migration to form the *trans* η^2 -vinyl species **71i** first and then **71i** went through the isomerization to form *cis* η^2 -vinyl species **71j**. The intermediates **71i** and **71i**, had close entropy and free energy and the ΔG for the silyl group migration to form the *trans* η^2 -vinyl species **71i** was only 1.48 kcalmol⁻¹. The free energy of *trans* η^2 -vinyl species **71i** was higher than the *cis* η^2 -vinyl species **71j** by 11.78 kcalmol⁻¹ and the isomerization from *trans* η^2 -vinyl species **71i** to *cis* η^2 -vinyl species **71j** step gave -11.78 kcalmol⁻¹ and was thermal favored. After the isomerization, the trimethylsilane coordinates to the ruthenium center by forming the hydrogen bridge bond to form more stable species which had -33.77 kcalmol⁻¹ as free energy. Finally, the *cis* product was generated by the elimination with 2.00 kcalmol⁻¹ as free energy, and the catalyst came

back to the 14 electron high active ruthenium silyl intermediate **71h**. Although the *cis* product was only detected, the pathway to form the *trans* vinylsilane product was also calculated and the results were summarized in Scheme 35 (in blue). The Gibbs free energy for the formation of **71m** from *trans* η^2 -vinyl species **71l** was $-25.42 \text{ kcalmol}^{-1}$, comparing with the Gibbs free energy for the isomerization, it was higher by $5.75 \text{ kcalmol}^{-1}$. So after the formation of *trans* η^2 -vinyl species **71l**, it was favorite to go through the isomerization to generate the *cis* product. These computational results were constant with our experimental results and can explain that in phenyl acetylene case, there was only *cis* product formed.

One of the importances of this catalytic pathway is that how the isomerization happened. In order to get more details, more computational work was done on looking for the transition state of the isomerization. Firstly, we considered the phenylacetylene as the alkyne. We monitored the rotation of silyl group and vinyl proton and we found that the rotation of vinyl proton related to the isomerization. The transition state between complex **71l** and complex **71j** (Scheme 36) was detected by scanning the dihedral angle.



Scheme 36. Model I for the Isomerization of the Hydrosilylation of Phenylacetylene

In this model, the transition state (TS1) was figured out by scanning the anti-clockwise rotation of the dihedral angle of C1, C2, C3 and H. Here we considered the free energy and entropy of the *cis* complex **71j** as 0.00 kcalmol⁻¹, so the *trans* complex **71i** gave $\Delta G = 11.76$ kcalmol⁻¹ while the transition state (TS1) gave 12.18 kcalmol⁻¹ in Figure 43 which indicated the formation of *cis* complex was thermal favor. In the Scheme 36, the *trans* complex **71i** went through the rotation to reach the transition state (TS1) by giving a smooth energy barrier as 0.42 kcalmol⁻¹, but there was -12.18 kcalmol⁻¹ between the transition state and the *cis* complex **71j**. So based on these

computational results, it was clear that the isomerization from *trans* η^2 -vinyl species **71i** to *cis* η^2 -vinyl species **71j** was thermal and dynamic favorite.

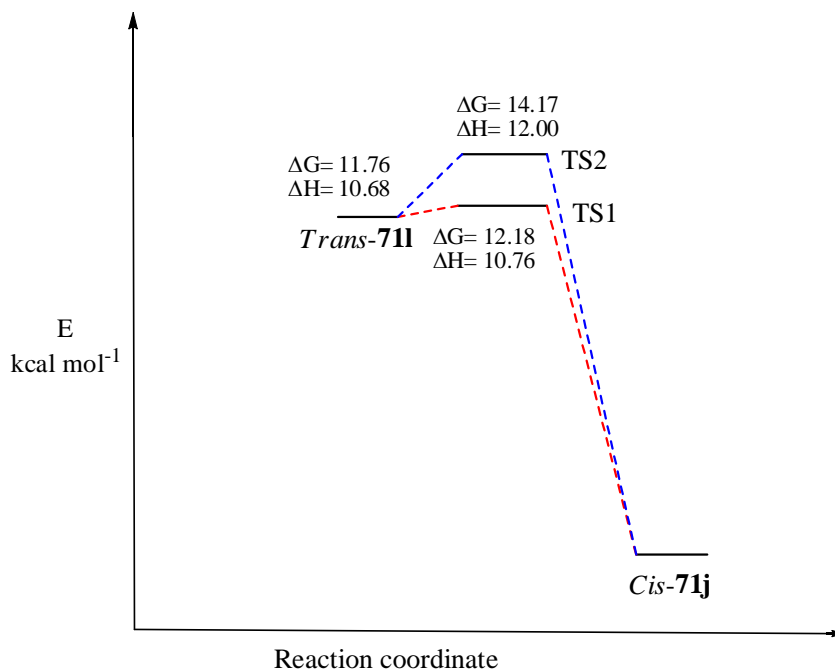


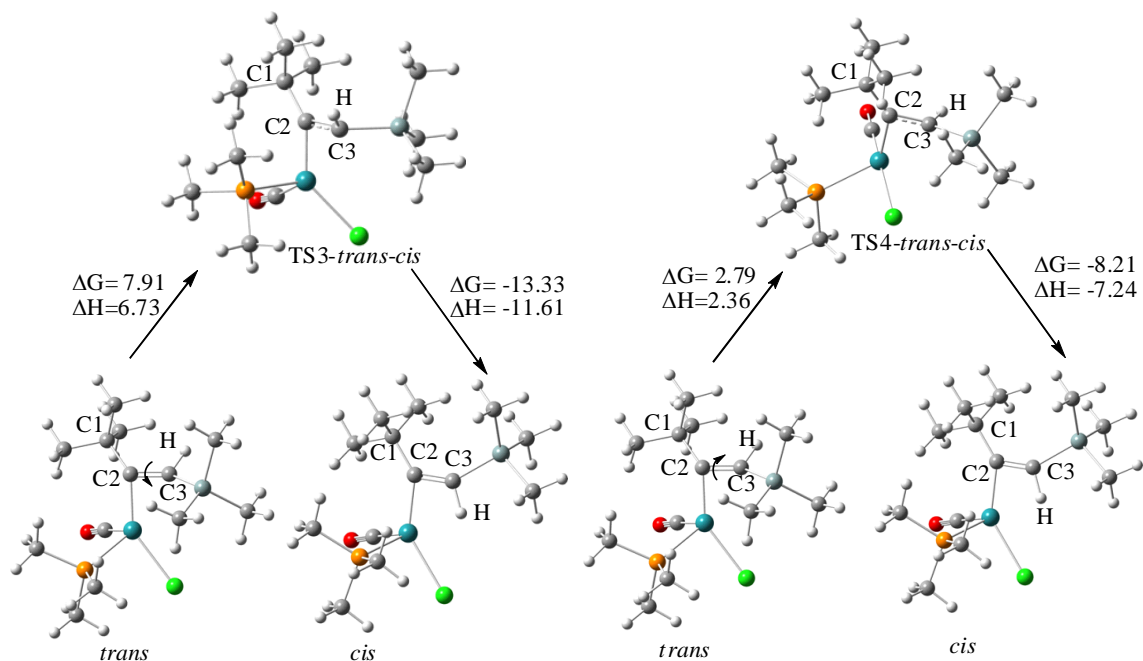
Figure 42. The Energy of intermediate **71i**, **71j** and Transition State 1 and Transition State 2

On the other hand, the clockwise rotation of dihedral angle was considered which gave transition state (TS2) with higher energy comparing with transition state 1 (TS1). In Figure 42 (in blue), the transition state had free energy as $14.17 \text{ kcal mol}^{-1}$ which was higher than TS1 by $2.0 \text{ kcal mol}^{-1}$. The Scheme 36 demonstrated that activation energy of the isomerization, in the transition state 2, *trans* η^2 -vinyl species **71i** need to go through an energy barrier as $2.41 \text{ kcal mol}^{-1}$ to reach the transition state and activation energy for the

transition state to the *cis* η^2 -vinyl species **71j**. These results indicated that the isomerization going through the transition state 2 was thermal and dynamic favorite. Comparing with transition state 1, *trans* η^2 -vinyl species **71i** need around 2 kcalmol⁻¹ more than in Scheme 36 to reach the transition state. Although the model of transition state 2 can indicated that the isomerization was thermal and dynamic favorite, it required higher energy barrier to reach the transition state comparing with the model of transition state 1. So we chose the model of transition state 1 as the isomerization transition state.

Comparing with phenylacetylene, 3,3-dimethylbutyne gave only the *trans* vinylsilane when reacting with trimethylsilane, we also did the computational studies on finding the transition state of the isomerization. The same scan method was used to get the crude transition state structure and then the structure was optimized to get the transition state structure.

The model II in Scheme 37 demonstrated the two transition states of the isomerization for 3,3-dimethylbutyne, the transition state (TS3) was figured out by scanning the anti-clockwise rotation of the dihedral angle of C1, C2, C3 and H. Here we considered the free energy and entropy of the *cis* η^2 -vinyl species as 0.00 kcalmol⁻¹, so the *trans* η^2 -vinyl species gave free energy $\Delta G = 5.42$ kcalmol⁻¹ while the transition state (TS3) gave 13.33 kcalmol⁻¹ in Figure 43.



Scheme 37. Model II for the Isomerization

On the other hand, the clockwise rotation of dihedral angle (C1, C2, C3 and H) was considered which gave transition state (TS4) with lower energy comparing with transition state 3 (TS3). In Figure 44 (in red), the transition state had free energy as 8.21 kcalmol⁻¹ which was higher than TS3 by 5.21 kcalmol⁻¹. The Scheme 37 demonstrated that activation energy of the isomerization, *trans* η²-vinyl species need to go through a energy barrier as 2.79 kcalmol⁻¹ to reach the transition state and activation energy for the transition state to the *cis* η²-vinyl species was -13.33 kcalmol⁻¹, which indicated that the step to form the *cis* η²-vinyl species from transition state 4 was thermal favorite. Due to

the lower energy barrier comparing with TS3, TS4 was considered as the transition state of the isomerization from *trans* η^2 -vinyl species *cis* η^2 -vinyl species.

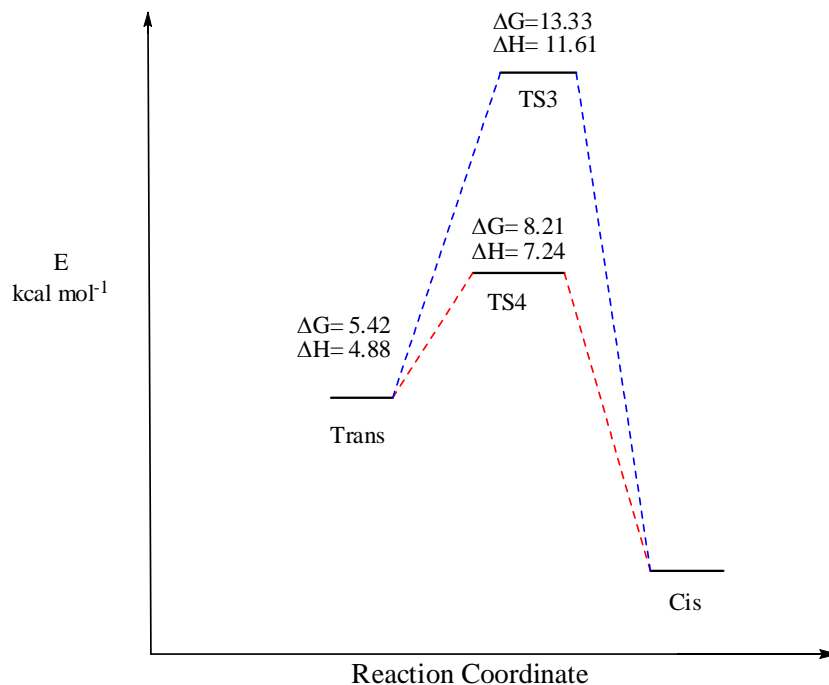


Figure 43. The Energy of *cis* and *trans* Intermediate and Transition State 1 and Transition State 2 for 3,3-Dimethylbutyne

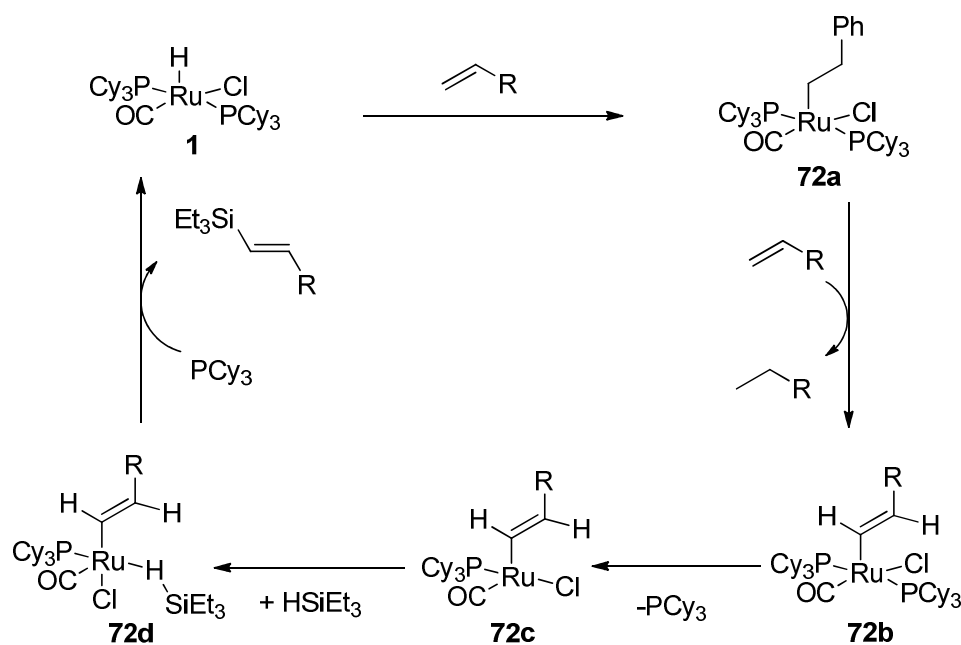
For 3, 3-dimethyl butyne, there was only *trans* product detected by the experiment. There was 2.79 kcalmol⁻¹ energy barrier for the isomerization, although it is not significant, comparing to the phenyl acetylene case with 0.42 kcalmol⁻¹ energy barrier, it still can explain the isomerization is less favor in 3,3-dimethylbutyne case, and the reaction attends to form to *trans* product. One more important thing is that all the computation calculation was done in gas phase while the experiment was done in solvent,

which would cause the difference between the experimental results and computational results. On the other hand, for the computation calculation, we used PMe_3 as the phosphine ligand in order to save computation time, and can also cause the difference. So we can see that the computation results can match the experimental results.

5.7 Proposed Mechanism of the Hydrosilylation of Alkenes

Here, we propose a mechanism for the coupling reaction of alkenes and triethylsilane (Scheme 38). This catalytic cycle starts at the coordination of styrene to the ruthenium center. Then, the alkenes add to the metal center to form complex **72a**. This addition of alkene to the ruthenium center should be rapid and reversible. We tried to detect the formation of complex **72a** by VT NMR from $-40\text{ }^\circ\text{C}$ to $60\text{ }^\circ\text{C}$. Unfortunately, we did not detect any signal of complex **72a**. But when we treated the ruthenium hydride complex with excess amount ethylene, we detected a new phosphine peak (26.5 ppm), which was assigned to the ruthenium-ethyl complex. This ruthenium-ethyl complex was active for the reaction of alkene and triethylsilane to generate the *trans* vinylsilane product. Next, another equiv. styrene was added to ruthenium center by eliminating one equiv. ethylbenzene to form the ruthenium vinyl complex and this step should be rapid. We syntheses this ruthenium vinyl complex **72b** by using phenylacetylene with

ruthenium hydride complex, this complex **72b** showed a similar activity as the ruthenium hydride (**1**) on the coupling reaction of styrene and triethylsilane to generate the *trans*-vinylsilane product under the similar conditions. In order to get insight into the mechanism of this step, we treated the complex **72b** and styrene as 1:3 ratios, and monitored the mixture by VT NMR from -40 °C to 60 °C. However, we observed no reaction between them. On the other hand, when complex **72b** is treated with excess amount of triethylsilane, a slow formation of *trans* vinylsilane was detected at 70 °C. These results are consistent with the carbon isotope effect study which indicated that the formation of the Si-C bond is the rate-determining step.



Scheme 38. Proposed Mechanism of the Coupling Reaction of Alkene and Triethylsilane

We also detected the strong phosphine inhibition on the reaction of intermediate **72b** with triethylsilane, which indicated that the formation of the intermediate **72d** involved the phosphine dissociation. Then, with the migration of silyl to the alkene, the *trans* vinylsilane product was generated and the ruthenium complex comes back to complex **1**. Recovered ruthenium complex was identified by ^1H NMR and ^{31}P NMR spectroscopy, and they are all consistent with that of the ruthenium hydride complex. The step of the migration of silyl group to the alkene to form the Si-C bond which involving the intermediate **72d** should be the rate limiting step. The observation of the carbon isotope effect study on the products provides the strong evidence for this, which showed significant abundance change of ^{13}C of the product. Moreover, the reaction of ruthenium vinyl complex and triethylsilane also supported this step to be rate-determining. Besides, the relatively positive Hammett value from the *para*-substituted styrene also proved this conclusion.

5.8 Conclusions

The ruthenium–hydride complex **1** was found to be a highly effective catalyst for hydrosilylation of the alkynes and alkenes to form selective vinylsilane under mild conditions. The mechanistic studies on the coupling reactions of alkenes with triethylsilane revealed C-Si bond formation as the rate-limiting step. The Hammett study, carbon isotope effect study, and the treatment of the ruthenium vinyl complex with triethylsilane also gave the strong evidence for this conclusion. For the mechanism study on hydrosilylation of alkyne, the isomerization of η^2 -vinyl complex was key point for the selectivity determining by the computation calculation. Other kinetics studies provided important and useful information on the mechanism. Hereby, we believe our catalytic method provides a promising way to generate synthetically useful vinylsilane in a highly selective fashion.

Chapter 6. Experimental Sections

6.1 General Information

All operations were carried out in an inert-atmosphere glove box or by using standard high vacuum and Schlenk techniques. Benzene, tetrahydrofuran were distilled from purple solution of sodium and benzophenone immediately prior to use. Hexane and dichloromethane were distilled from CaH_2 . The NMR solvent was dried from the activated molecular sieves (4\AA). All the ketones and vinyltrimethylsilane were received from commercial sources and used without further purification. The ^1H , ^2H and ^{13}C NMR spectra were recorded on a Varian Mercury 300 MHz or 400 MHz FT-NMR spectrometer. Mass spectras were recorded from a Hewlett-Packard HP 5970 GC/MS spectrometer. Elemental analyses were performed at the Midwest Microlab, Indianapolis, IN. High-resolution FAB mass spectra were obtained at the center of Mass Spectrometry, Washington University, St, Louis, MO.

6.2 For Chapter 2

6.2.1 Typical Procedure of the Catalytic Reaction

In a glove box, $\text{Ru}_3(\text{CO})_{12}$ (0.03 mmol), NH_4PF_6 (0.1 mmol), pyrrole (1.0 mmol) and alkyne (2.0 mmol) were dissolved in 3ml benzene solution in a thick-walls 25 mL Schlenk tube equipped with a magnetic stirring bar. The tube was brought out of the glove box. The reaction tube was heated in an oil bath at 95 °C for 8-15 hours. The tube was opened to the air at room temperature, and the crude product mixture was analyzed by GC/MS. The solvent was removed under a rotary aspirator, and the organic product was isolated by a column chromatograph on silica gel (*n*-hexane/dichloromethane).

6.2.2 Hammett Study of the Catalytic Reaction

$\text{Ru}_3(\text{CO})_{12}$ (3 μmol), NH_4PF_6 (0.01 mmol), pyrrole (0.1 mmol), 4-ethynylanisole (0.25 mmol) and hexamethylbenzene (26 mg as the internal standard) were dissolved in 0.5 mL benzene- d_6 solution in a Wilmad J-Young NMR tube with a Teflon screw cap. The tube was cooled in liquid nitrogen bath, and degassed for three times. The tube was gradually warmed to the room temperature and was heated in an oil bath at 95 °C. The reaction was monitored every hour by ^1H NMR spectroscopy. The rate was measured by monitor the ^1H integration of the product peak (OCH_3 δ 3.71 ppm) signal, and these were normalized against the internal standard. The k_{obs} was estimated from a first-order plot of $\ln[\text{product}]$ vs. reaction time.

6.2.3 Isotope Effect Study

$\text{Ru}_3(\text{CO})_{12}$ (0.003 mmol), NH_4PF_6 (0.01 mmol), phenylpyrrole- d_4 (0.1 mmol), 4-ethynylanisole (0.25 mmol) and hexamethylbenzene (26 mg as the internal standard) were dissolved in 0.5 mL benzene- d_6 solution in a Wilmad J-Young NMR tube with a Teflon screw cap. The tube was cooled in the liquid nitrogen bath, and degased for three times. The tube was gradually warmed to room temperature and was heated in an oil bath at 95 °C. The reaction was monitored every hour by NMR. The rate was measured by monitor the ^1H integration of the product peak (OCH_3 δ 3.71 ppm) signal, and these were normalized against the internal standard. The k_{obs} was estimated from a first -order plot of $\ln[\text{product}]$ vs reaction time.

6.2.4 Preparation of the Phenylpyrrole- d_4

Phenylpyrrole- d_4 was prepared form the following procedure: 1.0 mmol phenylpyrrole was dissolved in 25 mL dry THF in the Schlenk flask, $n\text{-BuLi}$ (2 mmol, 2.5 M in hexane) was added in this solution under nitrogen gas in the acetone-dry ice bath, and then the mixtures were warmed to room temperature and kept stirring for 30 min. Then, the excess amount of D_2O was added in to the solution in the acetone-dry ice

bath, and this solution was stirred by the magnetic stirring bar for 3 hours at room temperature until the solution became clear. The reaction was quenched by adding water. The organic layer was extracted from ether, and the water solution was washed for three times by ether. The organic product was isolated by a column chromatograph on silica gel (hexane/dichloromethane), and was characterized by ^1H NMR spectroscopy and ^2H NMR spectroscopy.

6.2.4.1 Deuterium Labeling Study

In a glove box, $\text{Ru}_3(\text{CO})_{12}$ (22 mg, 0.030 mmol), NH_4PF_6 (16 mg, 0.10 mmol), pyrrole (1.0 mmol) and $\text{DC}\equiv\text{CPh}$ (2.5 mmol, 2.5 equiv.) were dissolved in 3.0 mL benzene solution in a 25 mL Schlenk tube equipped with a magnetic stirring bar. The tube was brought out of the glove box, and was stirred in an oil bath set at 95 °C for 8-15 h. The tube was cooled to room temperature, and the crude product mixture was analyzed by GC-MS. The solvent was removed under a rotary aspirator, and analytically pure organic product was isolated by a column chromatograph on silica gel (*n*-hexanes/ CH_2Cl_2). The ^1H and ^2H NMR was taken at room temperature.

6.2.4.2 Carbon Isotope Effect Study

In a glove box, $\text{Ru}_3(\text{CO})_{12}$ (0.03 mmol), NH_4PF_6 (0.1 mmol), phenylpyrrole (1.0 mmol) and 4-ethynylanisole (2.5 mmol) were dissolved in 3 mL benzene solution in a thick-wall 25 mL Schlenk tube equipped with a magnetic stirring bar. The tube was brought out of the glove box. The reaction tube was heated in an oil bath at 95 °C for 15 hours. The tube was opened to the air at room temperature, and the crude product mixture was analyzed by GC/MS and the conversion was 75%. The solvent was removed under a rotary aspirator, and the unreacted phenylpyrrole was isolated by a column chromatograph on silica gel (*n*-hexane/dichloromethane).

The ^{13}C NMR analysis of the recovered and virgin samples of N-phenylpyrrole was performed by following Singleton's ^{13}C NMR method. The NMR sample of virgin and recovered N-phenylpyrrole was prepared identically by N-phenylpyrrole (75 mg) in CDCl_3 (0.5 mL) in a 5 mm high precision NMR tube. The $^{13}\text{C}\{^1\text{H}\}$ NMR spectra were recorded with H-decoupling and 45 degree pulses. A 60 s delay between pulses was imposed to minimize T_1 variations ($d_1 = 60$ s, $at = 5.0$ s, $np = 245098$, $nt = 2400$).

C#	Virgin	Recovered (75% conv.)	Recovered/Virgin	Change (%)
1	0.998(5)	1.017(5)	1.019(5)	1.90(5)
2	1.020(3)	1.025(3)	1.005(3)	0.49(3)
3	1.009(4)	1.008(4)	0.999(4)	0.11(4)
4(ref)	1.000	1.000	1.000	0.00
5	0.469(3)	0.468(3)	0.998(3)	0.22(3)
C#	Virgin	Recovered (70% conv.)	Recovered/Virgin	Change (%)
1	0.998(5)	1.011(5)	1.013(5)	1.30(5)
2	1.020(3)	1.025(3)	1.005(3)	0.47(3)
3	1.009(4)	1.007(4)	0.998(4)	0.19(4)
4(ref)	1.000	1.000	1.000	0.00
5	0.469(3)	0.468(3)	0.998(3)	0.24(3)

6.3 Characterization Data of Selected Organic Products

For **53a**: ^1H NMR (400 MHz, acetone- d_6) δ 7.25 and 6.92 (m, 4H), 6.70 (m, 1H), 6.05 (m, 2H), 5.46 and 5.15 (d, $J = 1.6$ Hz, 2H), 3.81 (s, 3H), 3.30 (s, 3H); $^{13}\text{C}\{^1\text{H}\}$ NMR (75 MHz, acetone- d_6) δ 160.5, 142.4, 134.6, 134.4, 129.1, 114.8, 124.4, 113.8, 110.9, 107.9, 55.4, 35.1 (CH_3); HREI (m/z): Calcd for $\text{C}_{14}\text{H}_{15}\text{NO}$ (M) $^+$ 213.1154. Found 213.1144.

For **53b**: ^1H NMR (400 MHz, acetone- d_6) δ 7.70- 7.15 (m, 6H), 6.80 (m, 1H), 6.30 (m, 2H), 5.65 and 5.33 (d, $J = 1.6$ Hz, 2H), 3.39 (s, 3H), 3.13 (s, 3H); $^{13}\text{C}\{^1\text{H}\}$ NMR (75 MHz, acetone- d_6) δ 159.5, 143.1, 137.7, 135.9, 134.9, 131.0, 130.2, 128.2, 127.2, 125.0, 120.4, 115.8, 111.5, 108.4, 107.0, 56.1, 35.6; GC-MS $m/z = 263$ (M^+); Anal. Calcd for $\text{C}_{18}\text{H}_{17}\text{NO}$: C, 82.10; H, 6.51. Found C, 81.98; H, 6.59.

For **53c**: ^1H NMR (400 MHz, acetone- d_6) δ 7.25, 7.15 and 6.73 (m, 9H), 6.98 (m, 1H), 6.26 (m, 2H), 5.34 and 5.03 (d, $J = 1.6$ Hz, 2H), 3.71 (s, 3H); $^{13}\text{C}\{^1\text{H}\}$ NMR (75 MHz, acetone- d_6) δ 160.3, 142.4, 141.6, 134.4, 134.2, 129.7, 129.3, 127.2, 125.6, 124.7.9, 114.2, 114.1, 113.4, 109.6, 55.6; GC-MS $m/z = 275$ (M^+); Anal. Calcd for $\text{C}_{19}\text{H}_{17}\text{NO}$: C, 82.88; H, 6.22. Found C, 82.92; H, 6.27.

For **53d**: ^1H NMR (300 MHz, CDCl_3) δ 7.25- 6.73 (m, 8H), 6.98 (m, 1H), 6.26 (m, 2H), 5.21 and 4.90 (d, $J = 1.6$ Hz, 2H), 3.71 (s, 3H), 2.21 (s, 3H); $^{13}\text{C}\{^1\text{H}\}$ NMR (75 MHz, CDCl_3) δ 159.3, 140.7, 138.3, 136.2, 133.8, 129.4, 128.7, 125.0, 124.0, 114.2, 113.4, 112.5, 108.5, 55.3, 21.1; GC-MS $m/z = 289$ (M^+); Anal. Calcd for $\text{C}_{20}\text{H}_{19}\text{NO}$: C, 83.01; H, 6.62. Found C, 82.92; H, 6.71.

For **53e**: ^1H NMR (400 MHz, CDCl_3) δ 7.15-6.73 (m, 8H), 6.91 (m, 1H), 6.22 (m, 2H), 5.31 and 4.98 (d, $J = 1.6$ Hz, 2H), 3.73 (s, 3H), 3.72 (s, 3H); $^{13}\text{C}\{^1\text{H}\}$ NMR (75 MHz, acetone- d_6) δ 160.3, 159.1, 142.1, 134.7, 134.4, 134.3, 129.4, 127.0, 124.8, 114.7, 114.1, 114.0, 112.8, 109.1, 55.7, 55.5; HREI (m/z): Calcd for $\text{C}_{14}\text{H}_{15}\text{NO}$ (M^+) 305.1416, found 305.1408.

For **53f**: ^1H NMR (300 MHz, CDCl_3) δ 7.25-6.73 (m, 8H), 6.98 (m, 1H), 6.26 (m, 2H), 5.41 and 5.18 (d, 2H, $J = 1.6\text{Hz}$), 3.71 (s, 3H); ^{13}C $\{^1\text{H}\}$ NMR (75 MHz, CDCl_3) δ 159.3, 140.7, 139.3, 134.0, 133.4, 132.0, 129.0, 128.6, 123.8, 114.6, 113.5, 113.0, 109.2, 55.3; GC-MS $m/z = 309$ (M^+); Anal. Calcd for $\text{C}_{19}\text{H}_{16}\text{ClNO}$: C, 73.66; H, 5.21. Found C, 72.68; H, 5.15.

For **53g**: ^1H NMR (300 MHz, CDCl_3) δ 7.25 - 6.73 (m, 8H), 6.98 (m, 1H), 6.43 (m, 2H), 5.43 and 5.18(d, 2H, $J = 1.6\text{Hz}$), 3.78 (s, 3H); ^{13}C $\{^1\text{H}\}$ NMR (75 MHz, CDCl_3) δ 162.2, 159.8, 140.7, 136.8, 134.4.0 133.4, 128.5, 126.6, 128.6, 123.8, 115.6, 114.6, 113.5, 112.6, 108.9, 55.3; GC-MS $m/z = 293$ (M^+).

For **53h**: ^1H NMR (400 MHz, CDCl_3) δ 7.70-7.15 (m, 11H), 6.98 (m, 1H), 6.30 (m, 2H), 5.48 and 5.28 (d, 2H, $J = 1.6\text{Hz}$), 3.89 (s, 3H); ^{13}C $\{^1\text{H}\}$ NMR (75 MHz, CDCl_3) δ 157.9, 141.3, 140.8, 136.4, 134.2, 134.0, 129.9, 128.9, 127.8, 126.7, 126.6, 126.2, 125.3, 124.2, 119.0, 115.7, 112.9, 108.9, 105.7, 56.1; GC-MS $m/z = 325$ (M^+); Anal. Calcd for $\text{C}_{23}\text{H}_{19}\text{NO}$: C, 84.89; H, 5.89. Found C, 85.09; H, 6.05.

For **53i**: ^1H NMR (400 MHz, CDCl_3) δ 7.70-7.15, 6.78 (m, 10H), 6.98 (m, 1H), 6.26 (m, 2H), 5.51 and 5.15 (d, 2H, $J = 1.6\text{Hz}$), 3.89 (s, 3H), 3.66 (s, 3H); ^{13}C $\{^1\text{H}\}$ NMR (75 MHz, CDCl_3) δ 159.4, 159.3, 143.0, 137.4, 135.6, 134.8, 130.9 129.9, 127.7, 127.5, 127.4, 127.0, 125.3, 120.0, 115.9, 115.1, 113.4, 109.7, 106.9, 56.1; GC-MS $m/z = 355$ (M^+); Anal. Calcd for $\text{C}_{24}\text{H}_{21}\text{NO}_2$: C, 81.10; H, 5.96. Found C, 80.88; H, 6.02.

For **53j**: ^1H NMR (300 MHz, CDCl_3) δ 7.40-7.28 (m, 4H), 6.77 (m, 1H), 6.23-6.21 (m, 2H), 5.62 and 5.41 (d, 2H, $J = 1.6\text{Hz}$), 3.82 (t, 2H, $J = 7.0\text{Hz}$), 2.43 (t, 2H, $J = 7.0\text{Hz}$); $^{13}\text{C}\{^1\text{H}\}$ NMR (75 MHz, CDCl_3) δ 141.9, 141.3, 133.5, 129.2, 128.6, 127.6, 123.3, 118.0, 116.7, 111.7, 108.7, 43.5, 19.9; GC-MS $m/z = 222$ (M^+); Anal. Calcd for $\text{C}_{15}\text{H}_{14}\text{N}_2$: C, 81.05; H, 6.35. Found C, 81.25; H, 6.30.

For **53k**: ^1H NMR (400 MHz, acetone- d_6) δ 7.24 -7.18 (m, 4H), 6.91 (m, 1H), 6.15 (m, 2H), 5.62 and 5.40 (d, 2H, $J = 1.6\text{Hz}$), 3.91 (t, 2H, $J = 7.0\text{ Hz}$), 2.64 (t, 3H, $J = 7.0\text{Hz}$), 2.34 (s, 3H); $^{13}\text{C}\{^1\text{H}\}$ NMR (75 MHz, acetone- d_6) δ 141.9, 138.8, 138.7, 133.9, 130.1, 127.7, 123.3, 118.3, 116.1, 111.7, 108.7, 43.5, 21.2, 19.9; GC-MS $m/z = 236$ (M^+); Anal. Calcd for $\text{C}_{16}\text{H}_{16}\text{N}_2$: C, 81.32; H, 6.82. Found C, 81.47; H, 7.02.

For **53l**: ^1H NMR (400 MHz, acetone- d_6) δ 7.25 - 6.92 (m, 4H), 6.92 (m, 1H), 6.15 (m, 2H), 5.56 and 5.26 (d, 2H, $J = 1.6\text{ Hz}$), 3.91 (t, 2H, $J = 7.0\text{Hz}$), 3.81 (s, 3H), 2.64 (t, 2H, $J = 7.0\text{Hz}$); $^{13}\text{C}\{^1\text{H}\}$ NMR (75 MHz, acetone- d_6) δ 160.3, 141.1, 133.5, 133.4, 128.4, 114.3, 123.0, 117.8, 114.3, 111.2, 108.3, 55.4, 43.5, 19.9; GC-MS $m/z = 252$ (M^+); Anal. Calcd for $\text{C}_{16}\text{H}_{16}\text{N}_2$: C, 76.16; H, 6.39. Found C, 75.73; H, 6.45.

For **53m**: ^1H NMR (300 MHz, CDCl_3) δ 7.25- 6.64 (m, 4H), 6.67 (m, 1H), 6.23 (m, 2H), 5.45 and 5.21 (d, 2H, $J = 1.6\text{Hz}$), 3.88 (t, 2H, $J = 7.0\text{Hz}$), 2.99 (s, 6H), 2.46 (t, 2H, $J = 7.0\text{Hz}$); $^{13}\text{C}\{^1\text{H}\}$ NMR (75 MHz, CDCl_3) δ 150.7, 140.6, 133.8, 128.1, 127.9, 112.3, 122.2, 117.5, 113.7, 111.4, 108.6, 43.2, 40.6, 19.9; GC-MS $m/z = 265$ (M^+).

For **53n**: ^1H NMR (300 MHz, CDCl_3) δ 7.70 - 7.15 (m, 6H), 6.80 (m, 1H), 6.30 (m, 2H), 5.72 and 5.45 (d, 2H, $J = 1.6\text{Hz}$), 3.93 (s, 3H), 3.84 (t, 2H, $J = 7.0\text{Hz}$), 2.46 (t, 2H, $J = 7.0\text{Hz}$); ^{13}C $\{^1\text{H}\}$ NMR (75 MHz, CDCl_3) δ 159.2, 142.1, 136.7, 135.6, 134.0, 130.7, 128.1, 126.7, 126.2, 120.1, 116.7, 123.5, 118.3, 111.9, 109.0, 106.6, 55.7, 43.8, 20.2; GC-MS $m/z = 302$ (M^+); Anal. Calcd for $\text{C}_{20}\text{H}_{18}\text{N}_2\text{O}$: C, 79.43; H, 6.00. Found C, 78.93; H, 5.99.

For **53o**: ^1H NMR (400 MHz, CDCl_3) δ 7.25 (m, 6H), 6.60 (d, 2H, $J = 2.03\text{Hz}$), 6.00 and 5.36 (d, 2H, $J = 1.6\text{ Hz}$), 3.22 (s, 3H), 2.36 (s, 3H); ^{13}C $\{^1\text{H}\}$ NMR (75 MHz, CDCl_3) δ 193.2, 140.3, 139.8, 135.5, 128.6 128.4, 128.2, 126.8, 124.8, 117.5, 110.4, 43.9, 35.6, 27.0, 21.1; GC-MS $m/z = 225$ (M^+); Anal. Calcd for $\text{C}_{15}\text{H}_{15}\text{NO}$: C, 79.97; H, 6.71. Found C, 79.89; H, 6.48.

For **53p**: ^1H NMR (300 MHz, CDCl_3) δ 7.80 (s, 1H), 7.61- 6.85 (m, 8H), 5.62 and 5.42 (d, $J = 1.6\text{ Hz}$), 3.86 (s, 3H), 2.26 (s, 3H); $^{13}\text{C}\{^1\text{H}\}$ NMR (75 MHz, CDCl_3) δ 160.0, 141.1, 135.5, 134.2, 133.0, 129.8, 129.4, 122.6, 119.6, 119.2, 115.1, 114.1, 110.9, 110.8, 55.6, 10.1; GC-MS $m/z = 288$ (M^+); Anal. Calcd for $\text{C}_{18}\text{H}_{17}\text{NO}$: C, 82.09; H, 6.50. Found C, 81.99; H, 6.42.

For **53q**: ^1H NMR (300 MHz, CDCl_3) δ 7.80 (s, 1H), 7.65 - 7.05 (m, 10H), 5.67 and 5.42 (d, $J = 1.6\text{ Hz}$), 3.86 (s, 3H), 2.26 (s, 3H); $^{13}\text{C}\{^1\text{H}\}$ NMR (75 MHz, CDCl_3) δ 160.0, 141.1, 137.4, 135.5, 134.2, 133.0, 130.9, 129.8, 129.4, 127.7, 127.5, 127.4, 127.0,

122.6, 119.6, 119.2, 115.1, 114.1, 110.9, 110.8, 55.6, 10.1; GC-MS $m/z = 313$ (M^+);

Anal. Calcd for $C_{22}H_{19}NO$: C, 84.31; H, 6.11. Found C, 84.49; H, 6.14.

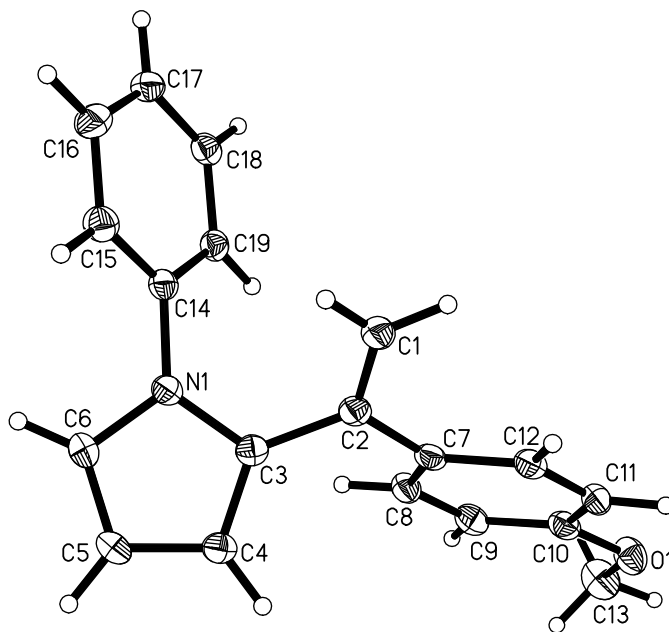
For **53r**: 1H NMR (400 MHz, $CDCl_3$) δ 7.46-6.95 (m, 12H), 6.53 (s, 1H), 3.70 (s, 6H), 2.40 (s, 6H); $^{13}C\{^1H\}$ NMR (75 MHz, $CDCl_3$) δ 145.4, 138.0, 135.1, 128.4, 128.0,

127.1, 123.6, 122.5, 118.6, 109.5, 43.9, 32.9, 29.4, 21.1; GC-MS $m/z = 378$ (M^+); Anal.

Calcd for $C_{18}H_{17}N$: C, 85.67; H, 6.92. Found C, 85.69; H, 6.82.

For **53s**: 1H NMR (300 MHz, $CDCl_3$) δ 7.46 and 6.95 (m, 13H), 6.53 (s, 2H), 3.70 (s, 3H), 2.40 (s, 3H); $^{13}C\{^1H\}$ NMR (75 MHz, $CDCl_3$) δ 148.6, 138.0, 128.4, 128.0,

127.1, 126.0, 123.6, 122.5, 121.3, 118.6, 109.5, 43.9, 32.9, 29.4; GC-MS $m/z = 363$ (M^+).



Molecular Structure of **53**

Crystal Data and Structure Refinement for **53c**.

Identification code	yis	
Empirical formula	C ₁₉ H ₁₇ NO	
Formula weight	275.34	
Temperature	100(2) K	
Wavelength	1.54178 Å	
Crystal system	Monoclinic	
Space group	P21/c	
Unit cell dimensions	a = 19.3228(3) Å	= 90°.
	b = 17.3708(2) Å	= 96.4510(10)°.
	c = 8.83840(10) Å	= 90°.
Volume	2947.85(7) Å ³	
Z	8	
Density (calculated)	1.241 Mg/m ³	
Absorption coefficient	0.596 mm ⁻¹	
F(000)	1168	
Crystal size	0.50 x 0.40 x 0.20 mm ³	
Theta range for data collection	3.43 to 67.84°.	
Index ranges	-23 ≤ h ≤ 23, 0 ≤ k ≤ 20, 0 ≤ l ≤ 10	
Reflections collected	24399	
Independent reflections	5215 [R(int) = 0.0186]	
Completeness to theta = 67.84°	97.20%	
Absorption correction	Semi-empirical from equivalents	
Max. and min. transmission	0.8901 and 0.7548	
Refinement method	Full-matrix least-squares on F ²	
Data / restraints / parameters	5215 / 0 / 516	
Goodness-of-fit on F ²	0.993	
Final R indices [I > 2σ(I)]	R1 = 0.0310, wR2 = 0.0768	
R indices (all data)	R1 = 0.0335, wR2 = 0.0787	
Extinction coefficient	0.00105(10)	
Largest diff. peak and hole	0.194 and -0.165 e.Å ⁻³	

6.4 For Chapter 3

6.4.1 General Procedure of the Catalytic Reaction

In a glove box, a carboxylic acid (1.0 mmol), a terminal alkyne (2.0 mmol) and the ruthenium catalyst **1** (14 mg, 2 mol %) were dissolved in 3 mL of CH₂Cl₂ (or THF) in a 25 mL Schlenk tube equipped with a Teflon stopcock and a magnetic stirring bar. The reaction tube was brought out of the glove box, and was stirred in an oil bath at 90-95 °C for 10-12 h. The tube was opened to the air at room temperature, and the crude product mixture was analyzed by GC-MS. Analytically pure organic product was isolated by a column chromatography on silica gel (*n*-hexane/EtOAc).

6.4.1.1 Hammett Study

In a glove box, a *para*-substituted acid *p*-X-C₆H₄CO₂H (X = OMe, CH₃, H, CF₃) (0.20 mmol), phenylacetylene (40 mg, 0.4 mmol), **1** (3 mg, 2 mol %) and C₆Me₆ (2 mg, internal standard) were dissolved in CDCl₃ (0.5 mL) solution in a J-Young NMR tube with a Teflon screw cap. The tube was brought out of the glove box and was heated in an oil bath set at 95 °C. The reaction was monitored in 10 min intervals by ¹H NMR. The *k*_{obs} was estimated from a first-order plot of ln[product] vs. reaction time by measuring the ¹H integration of the product peak (=CH₂, δ 5.61 ppm), which was normalized against

the internal standard peak. For the THF system, in a glove box, *para*-substituted acid $p\text{-X-C}_6\text{H}_4\text{CO}_2\text{H}$ ($\text{X} = \text{OMe}, \text{CH}_3, \text{H}, \text{CF}_3$) (1.0 mmol), phenylacetylene (200 mg, 2.0 mmol) and **1** (14 mg, 2 mol %) and C_6Me_6 (26 mg, internal standard) were dissolved in 3 mL of THF solution in a 25 mL Schlenk tube equipped with a Teflon stopcock and a magnetic stirring bar. The tube was brought out of the glove box, and was heated in an oil bath at 95 °C. The reaction was monitored by GC in 10 min intervals. The k_{obs} was estimated from a first-order plot of $\ln[\text{product}]$ vs. reaction time by measuring the amount of the products against the internal standard.

6.4.1.2 Isotope Labeling Study

In a glove box, benzoic acid (122 mg, 1.0 mmol) and $\text{DC}\equiv\text{CPh}$ (206 mg, 2.0 mmol) were added via a syringe to a 25 mL Schlenk tube equipped with a magnetic stirring bar and Teflon stopcock. The catalyst **1** (14 mg, 2 mol %) and the solvent (3 mL) were added to the reaction tube. The reaction tubes were brought out of the box and were stirred in an oil bath at 95 °C for 10 h. The solvent was removed from a rotary evaporator, and the organic product was isolated by a column chromatography on silica gel (*n*-hexanes/ $\text{CH}_2\text{Cl}_2 = 3:2$). The deuterium content of the product was measured by

both ^1H NMR (CDCl_3 with 10 mg cyclohexane as the external standard) and ^2H NMR (CH_2Cl_2 with 50 μL CDCl_3).

6.4.1.3 Phosphine Inhibition Study

In a glove box, benzoic acid (0.20 mmol), phenylacetylene (0.40 mmol), **1** (3 mg, 2 mol %) and C_6Me_6 (2 mg, internal standard) were dissolved in 0.5 mL of CDCl_3 solution in a J-Young NMR tube with a Teflon screw cap. A pre-dissolved PCy_3 in CDCl_3 solution (5 μL , 1.0 M) was added via syringe to the tube via the syringe. The tube was brought out of the glove box and was heated in an oil bath at 95 $^\circ\text{C}$. The reaction was monitored by ^1H NMR in 30 min intervals. The rate was measured by the ^1H integration of the product peak at δ 5.61 ($=\text{CH}_2$), and was normalized against the internal standard peak. The k_{obs} was estimated from the first order plot of $\ln[\text{product}]$ vs reaction time.

6.4.1.4 Kinetic Profile Experiment

In a glove box, **1** (14 mg, 0.02 mmol), 4-methoxybenzoic acid (30 mg, 0.20 mmol) and $\text{HC}\equiv\text{CPh}$ (31 mg, 0.30 mmol) in THF were dissolved in THF in a J-Young NMR tube with a Teflon screw cap (0.5 mL). The tube was brought out of the glove box,

and was placed in NMR probe which was preset at 60 °C. The appearance and disappearance of the phosphine signals for **64** ($\delta = 24.4$ ppm), **62** ($\delta = 25.9$ ppm) and **63** ($\delta = 23.4$ ppm) were monitored by ^{31}P NMR at 60 °C in 5 min intervals. The rate of the product formation was determined by measuring the integration of the product peaks against the disappearance of the complex **64**. The experimental data was globally fitted to the kinetic equation by using a non-linear regression technique (Sigmaplot V. 10). The rate constants $k_1 = 0.039 \text{ min}^{-1}$ and $k_2 = 0.013 \text{ min}^{-1}$ were obtained and from this analysis.

6.4.1.5 Synthesis of $(\text{PCy}_3)_2(\text{CO})(\text{Cl})\text{Ru}(\text{K}^2\text{-O}_2\text{CC}_6\text{H}_4\text{-p-OMe})$ (**62**)

In a glove box, 4-methoxybenzoic acid (13 mg, 0.10 mmol), phenylacetylene (10 mg, 0.10 mmol), and complex **1** (72 mg, 0.10 mmol) were dissolved in CH_2Cl_2 (3 mL) in a 25 mL Schlenk tube equipped with a Teflon screw cap stopcock and a magnetic stirring bar. The tube was brought out of the box, and was stirred for 10 h at room temperature. The solvent was evaporated and the residue was washed with hexanes (3 mL \times 3 times) to obtain **62** in 87% yields. Single crystals suitable for X-ray crystallographic study were obtained from hexanes/ CH_2Cl_2 .

For **62**: ^1H NMR (300 MHz, CDCl_3) δ 7.88 (d, $J = 8.7$ Hz, 2H), 6.89 (d, $J = 8.7$ Hz, 2H), 3.86 (s, 3H), 2.30-1.01 (m, 72H); $^{13}\text{C}\{^1\text{H}\}$ NMR (100 MHz, CDCl_3) δ 208.8 (t,

$J_{\text{PH}} = 13.3 \text{ Hz}$), 179.0, 162.9, 130.3, 125.1, 113.6, 55.5, 34.1, 30.2, 29.7, 28.3, 26.8;

$^{31}\text{P}\{^1\text{H}\}$ NMR (161 MHz, CDCl_3) δ 28.7 (s, PCy_3); IR (KBr) $\nu_{\text{CO}} = 1913 \text{ cm}^{-1}$.

Crystal Data and Structure Refinement for 62.

Identification code	yi1ka	
Empirical formula	$\text{C}_{45} \text{H}_{73} \text{Cl} \text{O}_4 \text{P}_2 \text{Ru}$	
Formula weight	876.49	
Temperature	100(2) K	
Wavelength	1.54178 Å	
Crystal system	Orthorhombic	
Space group	$A b m 2$	
Unit cell dimensions	$a = 9.7750(2) \text{ Å}$	$a = 90^\circ$.
	$b = 24.8661(4) \text{ Å}$	$b = 90^\circ$.
	$c = 17.6805(3) \text{ Å}$	$c = 90^\circ$.
Volume	$4297.53(13) \text{ Å}^3$	
Z	4	
Density (calculated)	1.355 Mg/m^3	
Absorption coefficient	4.543 mm^{-1}	
F(000)	1864	
Crystal size	0.12 x 0.09 x 0.04 mm^3	
Theta range for data collection	3.55 to 67.20°.	
Index ranges	$-11 \leq h \leq 0, -22 \leq k \leq 27, -17 \leq l \leq 21$	
Reflections collected	10054	
Independent reflections	3201 [$R(\text{int}) = 0.0231$]	
Completeness to $\theta = 67.20^\circ$	98.20%	
Absorption correction	Numerical	
Max. and min. transmission	0.8392 and 0.6117	
Refinement method	Full-matrix least-squares on F ²	
Data / restraints / parameters	3201 / 1 / 263	
Goodness-of-fit on F ²	1.015	
Final R indices [$I > 2\sigma(I)$]	$R_1 = 0.0323, wR_2 = 0.0793$	
R indices (all data)	$R_1 = 0.0349, wR_2 = 0.0808$	
Absolute structure parameter	0.450(8)	
Largest diff. peak and hole	d -0.422 e.Å ⁻³	

6.4.1.6 Synthesis of (PCy₃)₂(CO)(Cl)RuC(=CHPh)OC(O)C₆H₄-p-OMe (63)

In a glove box, the Ru-carboxylate complex **62** (44 mg, 50 μmol) and phenylacetylene (6 mg, 60 μmol) were dissolved in THF (3 mL) in a 25 mL Schlenk tube equipped with a Teflon screw cap stopcock and a magnetic stirring bar. The tube was brought out of the glove box and was heated in an oil bath at 95 °C for 10 h. The solvent was removed under high vacuum, and the residue was washed with hexanes (3 mL × 3 times) to obtain analytically pure **63** in 85% yield. Single crystals suitable for X-ray crystallographic study were obtained from hexanes/CH₂Cl₂.

For **63**: ¹H NMR (400 MHz, C₆D₆) δ 8.44 (d, *J* = 8.7 Hz, 2H), 7.76 (d, *J* = 7.7 Hz, 2H), 7.36-6.63 (m, 5H), 6.24 (s, 1H), 2.98 (s, 3H), 2.71-0.8 (m, 72H); ¹³C{¹H} NMR (100 MHz, CDCl₃) 209.8 (t, *J*_{PC} = 14.4 Hz), 190.2 (t, *J*_{PC} = 12.2 Hz), 173.8, 167.9, 165.4, 138.4, 133.8, 129.1, 125.0, 122.5, 120.0, 115.1, 55.4, 35.2, 31.1, 30.6, 29.8, 28.8, 27.3; ³¹P{¹H} NMR (400 MHz, CDCl₃) δ 27.0 (PCy₃); IR (KBr) ν_{CO} = 1922 cm⁻¹.

Table 15. Crystal Data and Structure Refinement for **63**

Identification code	yl1na
Empirical formula	C ₅₉ H ₉₃ Cl O ₄ P ₂ Ru
Formula weight	1064.79
Temperature	100(2) K
Wavelength	1.54178 Å
Crystal system	Triclinic
Space group	P -1

Unit cell dimensions	a = 10.9925(2) Å a= 103.0180(10)° b = 12.9129(2) Å c = 21.9786(5) Å
Volume	2815.46(9) Å ³
Z	2
Density (calculated)	1.256 Mg/m ³
Absorption coefficient	3.558 mm ⁻¹
F(000)	1140
Crystal size	0.40 x 0.23 x 0.17 mm ³
Theta range for data collection	3.74 to 67.81°.
Index ranges	-13<=h<=12, -15<=k<=15, 0<=l<=26
Reflections collected	23248
Independent reflections	9565 [R(int) = 0.0242]
Completeness to theta = 67.81°	93.50%
Absorption correction	Numerical
Max. and min. transmission	0.5897 and 0.3317
Refinement method	Full-matrix least-squares on F ²
Data / restraints / parameters	9565 / 0 / 607
Goodness-of-fit on F ²	1.012
Final R indices [I>2sigma(I)]	R1 = 0.0295, wR2 = 0.0722
R indices (all data)	R1 = 0.0321, wR2 = 0.0735

6.5 Characterization Data of Selected Organic Products

For **58a**: ¹H NMR (300 MHz, CDCl₃) δ 8.15-6.70 (m, 9H), 5.37 (d, 1H, *J* = 2.1 Hz), 4.98 (d, 1H, *J* = 2.1 Hz), 3.69 (s, 3H); ¹³C{¹H} NMR (75 MHz, CDCl₃) δ 165.1, 160.5, 153.2, 133.8, 130.4, 129.8, 128.8, 127.2, 126.6, 114.2, 100.7, 55.5; GC-MS *m/z* = 254 (M⁺).

For **58b**: ^1H NMR (300 MHz, CDCl_3) δ 8.25-7.10 (m, 9H), 5.57 (d, 1H, $J = 2.1$ Hz), 5.14 (d, 1H, $J = 2.1$ Hz), 2.37 (s, 3H); ^{13}C $\{^1\text{H}\}$ NMR (100 MHz, CDCl_3) δ 164.9, 153.3, 139.0, 133.6, 131.6, 130.1, 129.6, 129.3, 128.5, 124.8, 100.4, 21.3; GC-MS $m/z = 238$ (M^+).

For **58c**: ^1H NMR (300 MHz, CDCl_3) δ 8.05-7.10 (m, 10H), 5.57 (d, 1H, $J = 1.9$ Hz), 5.09 (d, 1H, $J = 1.9$ Hz); $^{13}\text{C}\{^1\text{H}\}$ NMR (75 MHz, CDCl_3) δ 164.9, 153.3, 134.4, 133.8, 130.2, 129.5, 129.1, 128.8, 128.7, 125.0, 102.5; GC-MS $m/z = 224$ (M^+).

For **58d**: ^1H NMR (300 MHz, CDCl_3) δ 8.25-7.38 (m, 9H), 5.60 (d, 1H, $J = 2.4$ Hz), 5.21 (d, 1H, $J = 2.4$ Hz); $^{13}\text{C}\{^1\text{H}\}$ NMR (75 MHz, CDCl_3) δ 165.1, 152.5, 134.0, 133.6, 132.0, 130.4, 129.5, 126.8, 123.4, 103. ($\text{CH}_2=\text{C}$); GC-MS $m/z = 303$ (M^+).

For **58e**: ^1H NMR (400 MHz, CDCl_3) δ 8.25-7.38 (m, 9H), 5.69 (d, 1H, $J = 2.4$ Hz), 5.30 (d, 1H, $J = 2.4$ Hz); $^{13}\text{C}\{^1\text{H}\}$ NMR (100 MHz, CDCl_3) δ 163.8, 153.2, 135.4, 135.0, 134.1, 132.8, 130.7, 129.4, 128.8, 125.9, 122.4, 102.8; GC-MS $m/z = 292$ (M^+).

For **58f**: ^1H NMR (300 MHz, CDCl_3) δ 8.25-7.00 (m, 9H), 5.53 (d, 1H, $J = 2.4$ Hz), 5.16 (d, 1H, $J = 2.4$ Hz); $^{13}\text{C}\{^1\text{H}\}$ NMR (75 MHz, CDCl_3) δ 165.1, 161.7, 152.5, 133.9, 130.8, 130.3, 129.5, 128.9, 127.1, 115.7, 102.4; GC-MS $m/z = 242$ (M^+); Anal. Calcd for $\text{C}_{15}\text{H}_{11}\text{FO}_2$: C, 74.37; H, 4.58. Found: C, 73.27; H, 4.50.

For **58g**: ^1H NMR (300 MHz, CDCl_3) δ 8.15-7.38 (m, 5H), 4.87 (s, 2H), 4.83 (s, 2H), 2.34 (t, 2H), 1.53 (m, 2H), 1.39 (m, 2H), 0.92 (t, 3H); $^{13}\text{C}\{^1\text{H}\}$ NMR (75 MHz,

CDCl_3) δ 164.8, 156.9, 133.3, 130.0, 129.6, 128.5, 101.3, 33.2, 28.7, 22.2, 13.9; GC-MS $m/z = 204$ (M^+).

For **58h**: ^1H NMR (400 MHz, CDCl_3) δ 8.15-7.30 (m, 10H), 5.08 (d, 1H, $J = 2.4$ Hz), 4.90 (d, 1H, $J = 2.4$ Hz), 3.75 (s, 2H); $^{13}\text{C}\{^1\text{H}\}$ NMR (100 MHz, CDCl_3) δ 164.8, 155.8, 137.0, 133.5, 130.0, 129.8, 129.6, 128.6, 126.9, 103.6, 40.1; GC-MS $m/z = 238$ (M^+).

For **58i**: ^1H NMR (300 MHz, CDCl_3) δ 8.20-7.38 (m, 5H), 5.22 (d, 1H, $J = 2.4$ Hz), 5.03 (d, 1H, $J = 2.4$ Hz), 2.0 (s, 3H); $^{13}\text{C}\{^1\text{H}\}$ NMR (75 MHz, CDCl_3) δ 164.6, 153.7, 136.6, 133.5, 130.0, 129.5, 128.6, 113.9, 103.6, 19.4; GC-MS $m/z = 188$ (M^+).

For **58j**: ^1H NMR (300 MHz, CDCl_3) δ 8.35-7.10 (m, 11H), 5.70 (d, 1H, $J = 2.4$ Hz), 5.23 (d, 1H, $J = 2.4$ Hz), 3.90 (s, 3H); $^{13}\text{C}\{^1\text{H}\}$ NMR (75 MHz, CDCl_3) δ 165.2, 158.4, 153.5, 135.0, 133.8, 130.3, 129.7, 129.6, 128.8, 127.4, 124.1, 123.4, 119.4, 105.9, 102.1, 55.5 (OCH_3); GC-MS $m/z = 304$ (M^+); Anal. Calcd for $\text{C}_{16}\text{H}_{14}\text{O}_2$: C, 78.93; H, 5.30. Found: C, 78.76; H, 5.37.

For **58k**: ^1H NMR (300 MHz, CDCl_3) δ 8.25-6.95 (m, 9H), 5.62 (d, 1H, $J = 2.4$ Hz), 5.19 (d, 1H, $J = 2.4$ Hz), 3.87 (s, 3H); $^{13}\text{C}\{^1\text{H}\}$ NMR (75 MHz, CDCl_3) δ 164.6, 164.0, 153.3, 134.5, 132.3, 129.0, 128.6, 125.0, 121.8, 114.2, 102.3, 55.5; GC-MS $m/z = 254$ (M^+).

For **58l**: ^1H NMR (400 MHz, CDCl_3) δ 8.20-7.32 (m, 9H), 5.66 (d, 1H, $J = 2.1$ Hz), 5.23 (d, 1H, $J = 2.1$ Hz), 2.48 (s, 3H); $^{13}\text{C}\{^1\text{H}\}$ NMR (100 MHz, CDCl_3) δ 164.9,

153.3, 144.5, 134.4, 132.2, 130.1, 129.6, 129.0, 128.5, 126.8, 102.4, 21.8; GC-MS m/z = 238 (M^+)

For **58m**: ^1H NMR (300 MHz, CDCl_3) δ 8.00-7.20 (m, 9H), 5.50 (d, 1H, J = 2.4 Hz), 5.07 (d, 1H, J = 2.4 Hz); $^{13}\text{C}\{^1\text{H}\}$ NMR (75 MHz, CDCl_3) δ 164.3, 153.2, 134.2, 132.2, 131.8, 129.3, 129.0, 128.8, 128.5, 125.0, 102.7; GC-MS m/z = 303 (M^+).

For **58n**: ^1H NMR (400 MHz, CDCl_3) δ 8.30-7.00 (m, 9H), 5.52 (d, 1H, J = 2.4 Hz), 5.10 (d, 1H, J = 2.4 Hz, = CH_2); $^{13}\text{C}\{^1\text{H}\}$ NMR (100 MHz, CDCl_3) δ 163.3, 153.2, 133.9, 133.3, 132.7, 130.7, 129.3, 128.8, 128.5, 125.0, 118.0, 117.1, 102.7; GC-MS m/z = 249 (M^+); Anal. Calcd for $\text{C}_{16}\text{H}_{11}\text{NO}_2$: C, 77.10; H, 4.45. Found: C, 77.30; H, 4.47.

For **58o**: ^1H NMR (300 MHz, CDCl_3) δ 8.38-7.32 (m, 9H), 5.64 (d, 1H, J = 2.4 Hz), 5.20 (d, 1H, J = 2.4 Hz); $^{13}\text{C}\{^1\text{H}\}$ NMR (75 MHz, CDCl_3) δ 163.8, 153.2, 135.4, 135.0, 134.1, 132.8, 130.7, 129.5, 128.8, 125.9, 122.4, 102.8; GC-MS m/z = 292 (M^+); Calcd for $\text{C}_{16}\text{H}_{11}\text{F}_3\text{O}_2$: C, 65.76; H, 3.80. Found: C, 65.51; H, 3.82.

For **58p**: ^1H NMR (400 MHz, CDCl_3) δ 7.92 (s, 1H), 7.40-6.90 (m, 15H), 5.38 (d, 1H, J = 2.4 Hz), 5.01 (d, 1H, J = 2.4 Hz); $^{13}\text{C}\{^1\text{H}\}$ NMR (100 MHz, CDCl_3) δ 166.1, 153.4, 142.1, 135.7, 134.5, 134.4, 132.0, 131.0, 129.9, 129.6, 129.0, 128.9, 128.6, 128.4, 125.0, 102.8; GC-MS m/z = 326 (M^+); Calcd for $\text{C}_{23}\text{H}_{18}\text{O}_2$: C, 84.64; H, 5.56. Found: C, 84.40; H, 5.55.

For **58q**: ^1H NMR (300 MHz, CDCl_3) δ 7.97 (s, 1H), 7.47-7.08 (m, 15H), 4.86 (d, 1H, J = 2.4 Hz), 4.79 (d, 1H, J = 2.4 Hz), 2.43 (t, 2H), 1.55 (m, 4H), 1.03 (t, 3H);

$^{13}\text{C}\{^1\text{H}\}$ NMR (75 MHz, CDCl_3) δ 166.1, 157.0, 141.3, 135.7, 134.5, 132.4, 130.8, 129.9, 129.3, 128.7, 128.4, 101.0, 33.1, 28.7, 14.0, 2.1; GC-MS m/z = 306 (M^+).

For **58r**: ^1H NMR (400 MHz, CDCl_3) δ 7.52-7.30 (m, 5H), 5.53 (d, 1H, J = 2.4 Hz), 5.01 (d, 1H, J = 2.4 Hz), 2.56 (m, 1H), 2.09-1.83 (m, 4H), 1.7-1.2 (m, 6H); $^{13}\text{C}\{^1\text{H}\}$ NMR (100 MHz, CDCl_3) δ 174.2, 153.1, 134.7, 129.0, 128.6, 125.0, 102.0, 43.4, 29.1, 25.8, 25.5; GC-MS m/z = 230 (M^+); Calcd for $\text{C}_{15}\text{H}_{18}\text{O}_2$: C, 78.22; H, 7.87. Found: C, 78.09; H, 7.66.

For **58s**: ^1H NMR (400 MHz, CDCl_3) δ 7.52-7.30 (m, 5H), 5.48 (d, 1H, J = 2.4 Hz), 5.01 (d, 1H, J = 2.4 Hz), 2.56 (t, 2H), 1.74 (m, 2H), 1.44-1.20 (m, 24H), 0.89 (t, 3H); $^{13}\text{C}\{^1\text{H}\}$ NMR (100 MHz, CDCl_3) δ 172.2, 153.1, 134.7, 129.0, 128.6, 125.0, 102.4, 34.5, 31.2, 30.0, 29.9, 29.8, 29.7, 29.6, 29.5, 29.4, 29.3, 25.1, 22.9, 14.3; GC-MS m/z = 230 (M^+); Calcd for $\text{C}_{24}\text{H}_{38}\text{O}_2$: C, 80.40; H, 10.68. Found: C, 80.55; H, 10.46.

For (*Z*)-**59a**: ^1H NMR (300 MHz, CDCl_3) δ 8.10-6.63 (m, 9H), 7.38 (d, 1H, J = 7.4 Hz), 5.71 (d, 1H, J = 7.4 Hz), 3.73 (s, 3H); $^{13}\text{C}\{^1\text{H}\}$ NMR (75 MHz, CDCl_3) δ 163.8, 159.1, 133.8, 133.0, 130.8, 130.3, 129.3, 129.0, 127.1, 114.2, 112.5, 55.5; GC-MS m/z = 254 (M^+).

For (*Z*)-**59b**: ^1H NMR (400 MHz, CDCl_3) δ 8.05-7.05 (m, 9H), 7.98 (d, 1H, J = 12.8 Hz), 6.47 (d, 1H, J = 12.8 Hz), 2.25 (s, 3H); $^{13}\text{C}\{^1\text{H}\}$ NMR (75 MHz, CDCl_3) δ 163.7, 137.4, 135.9, 133.7, 133.6, 131.1, 130.0, 129.5, 129.0, 128.6, 115.8, 21.3; GC-MS m/z = 238 (M^+); Anal. Calcd for $\text{C}_{16}\text{H}_{14}\text{O}_2$: C, 80.65; H, 5.92. Found: C, 80.74; H, 5.99.

For (Z)-**59c**: ^1H NMR (300 MHz, CDCl_3) δ 8.05-7.10 (m, 10H), 7.40 (d, 1H, $J = 7.4$ Hz), 5.76 (d, 1H, $J = 7.4$ Hz); $^{13}\text{C}\{^1\text{H}\}$ NMR (75 MHz, CDCl_3) δ 163.5, 134.2, 134.1, 133.8, 130.2, 129.2, 128.9, 128.8, 128.5, 127.4, 112.7; GC-MS $m/z = 224$ (M^+).

For (Z)-**59d**: ^1H NMR (300 MHz, CDCl_3) δ 8.15-7.24 (m, 9H), 7.50 (d, 1H, $J = 7.4$ Hz), 5.80 (d, 1H, $J = 7.4$ Hz); $^{13}\text{C}\{^1\text{H}\}$ NMR (75 MHz, CDCl_3) δ 163.8, 159.1, 133.8, 133.0, 130.8, 130.3, 129.3, 129.0, 127.1, 114.2, 112.5, 55.5; GC-MS $m/z = 303$ (M^+); Calcd for $\text{C}_{15}\text{H}_{11}\text{BrO}_2$: C, 59.42; H, 3.66. Found: C, 59.06; H, 3.64.

For (Z)-**59e**: ^1H NMR (400 MHz, CDCl_3) δ 8.20-7.50 (m, 9H), 7.53 (d, 1H, $J = 7.4$ Hz), 5.89 (d, 1H, $J = 7.4$ Hz); $^{13}\text{C}\{^1\text{H}\}$ NMR (75 MHz, CDCl_3) δ 163.8, 159.1, 133.8, 133.0, 130.8, 130.3, 129.3, 129.0, 127.1, 114.2, 112.5, 55.5; GC-MS $m/z = 292$ (M^+).

For (Z)-**59f**: ^1H NMR (400 MHz, CDCl_3) δ 8.24-7.00 (m, 9H), 7.50 (d, 1H, $J = 7.4$ Hz), 5.83 (d, 1H, $J = 7.4$ Hz); $^{13}\text{C}\{^1\text{H}\}$ NMR (100 MHz, CDCl_3) δ 163.6, 163.2, 160.8, 134.1, 134.0, 131.1, 130.3, 129.0, 128.8, 115.7, 111.7; GC-MS $m/z = 242$ (M^+); Calcd for $\text{C}_{15}\text{H}_{11}\text{FO}_2$: C, 74.37; H, 4.58. Found: C, 73.27; H, 4.50.

For (E)-**59b**: ^1H NMR (400 MHz, CDCl_3) δ 8.05-7.05 (m, 9H), 7.98 (d, 1H, $J = 12.8$ Hz), 6.47 (d, 1H, $J = 12.8$ Hz), 2.25 (s, 3H); $^{13}\text{C}\{^1\text{H}\}$ NMR (75 MHz, CDCl_3) δ 163.7, 137.4, 135.9, 133.7, 133.6, 131.1, 130.0, 129.5, 129.0, 128.6, 115.8, 21.3; GC-MS $m/z = 238$ (M^+).

For (*E*)-**59c**: ^1H NMR (300 MHz, CDCl_3) δ 8.05-7.10 (m, 10H), 8.05 (d, 1H, $J = 12.8$ Hz), 5.76 (d, 1H, $J = 12.8$ Hz); ^{13}C $\{^1\text{H}\}$ NMR (75 MHz, CDCl_3) δ 163.7, 136.1, 133.7, 133.5, 130.1 130.0, 128.9, 128.6 127.5, 126.3, 115.9; GC-MS $m/z = 224$ (M^+).

For (*E*)-**59d**: ^1H NMR (300 MHz, CDCl_3) δ 8.15-7.24 (m, 9H), 8.09 (d, 1H, $J = 12.8$ Hz), 6.53 (d, 1H, $J = 12.8$ Hz); ^{13}C $\{^1\text{H}\}$ NMR (75 MHz, CDCl_3) δ 163.7, 137.4, 134.7, 134.0, 133.2, 132.0, 130.9, 130.2, 128.8, 127.9, 111.5; GC-MS $m/z = 303$ (M^+).

For **60a**: ^1H NMR (300 MHz, CDCl_3) δ 8.08-7.38 (m, 5H), 4.84 (s, 2H), 2.18 (s, 3H); ^{13}C $\{^1\text{H}\}$ NMR (75 MHz, CDCl_3) δ 201.9, 165.9, 133.5, 129.9, 129.2, 128.5, 68.8, 26.6; GC-MS $m/z = 178$ (M^+).

For **60b**: ^1H NMR (300 MHz, CDCl_3) δ 8.10-7.38 (m, 5H), 5.29 (m, 1H), 2.22 (s, 3H), 1.53 (d, 3H, $J = 7.1$ Hz); ^{13}C $\{^1\text{H}\}$ NMR (75 MHz, CDCl_3) δ 205.9, 165.9, 133.5, 129.9, 129.5, 128.5, 75.6, 25.8, 16.2; GC-MS $m/z = 192$ (M^+).

For **60c**: ^1H NMR (300 MHz, CDCl_3) δ 8.10-7.38 (m, 5H), 2.12 (s, 3H), 1.55 (s, 6H); ^{13}C $\{^1\text{H}\}$ NMR (75 MHz, CDCl_3) δ 206.7, 165.9, 133.5, 129.7, 129.5, 128.5, 84.2, 23.6, 23.4; GC-MS $m/z = 206$ (M^+).

For **60d**: ^1H NMR (300 MHz, CDCl_3) δ 8.10-7.38 (m, 5H), 2.14 (m, 2H), 2.06 (s, 3H), 1.74-1.50 (m, 8H); ^{13}C $\{^1\text{H}\}$ NMR (75 MHz, CDCl_3) δ 206.9, 165.9, 133.3, 129.7, 129.5, 128.5, 85.5, 30.8, 25.5, 23.5, 21.3; GC-MS $m/z = 247$ (M^+).

For **60f**: ^1H NMR (300 MHz, CDCl_3) δ 4.60 (s, 2H), 2.60 (m, 2H), 2.40 (s, 3H), 2.15 (m, 26H), 0.85 (t, 3H); ^{13}C $\{^1\text{H}\}$ NMR (75 MHz, CDCl_3) δ 201.8, 175.2, 68.3, 51.9,

34.1, 34.0, 32.1, 29.9, 29.8, 29.7, 29.6, 29.5, 29.4, 29.3, 26.2, 22.9, 25.0, 14.3; GC-MS $m/z = 276$ (M^+).

For **60g**: ^1H NMR (300 MHz, CDCl_3) δ 4.60 (s, 2H), 2.40 (m, 1H), 2.13 (s, 3H), 2.0-1.10 (m, 10H); ^{13}C $\{^1\text{H}\}$ NMR (75 MHz, CDCl_3) δ 202.2, 175.5, 68.2, 42.9, 29.1, 26.3, 25.5, 25.9 (COCH_3); GC-MS $m/z = 184$ (M^+).

For **60h**: ^1H NMR (300 MHz, CDCl_3) δ 7.93 (s, 1H), 7.40-7.08 (m, 10H), 4.75 (s, 2H), 2.10 (s, 3H); $^{13}\text{C}\{^1\text{H}\}$ NMR (75 MHz, CDCl_3) δ 201.6, 166.8, 141.4, 135.4, 134.3, 131.5, 130.6, 129.9, 129.2, 128.5, 128.1, 127.8, 68.8, 25.9; GC-MS $m/z = 280$ (M^+).

For **61a**: ^1H NMR (300 MHz, CDCl_3) δ 8.25-7.45 (m, 14H), 5.6 (d, 2H, $J = 2.4$ Hz), 5.22 (d, 2H, $J = 2.4$ Hz); $^{13}\text{C}\{^1\text{H}\}$ NMR (75 MHz, CDCl_3) δ 164.9, 152.7, 135.0, 133.8, 130.3, 129.4, 128.8, 125.3, 103.1; GC-MS $m/z = 370$ (M^+).

For **61b**: ^1H NMR (300 MHz, CDCl_3) δ 8.10-7.35 (m, 10H), 4.91 (d, 4H, $J = 2.4$ Hz), 2.45 (t, 4H, $J = 7.5$ Hz), 1.78 (m, 2H); $^{13}\text{C}\{^1\text{H}\}$ NMR (75 MHz, CDCl_3) δ 164.7, 155.8, 133.4, 130.0, 129.8, 128.5, 102.2, 32.7, 23.5; GC-MS $m/z = 336$ (M^+).

6.6 For Chapter 4

6.6.1 Typical Procedure of the Catalytic Reaction

In a glove box, $\text{RuH}(\text{CO})(\text{PCy}_3)_2\text{Cl}$ (0.5 mol %), ketone (2.0 mmol) and vinylsilane (3.0 mmol) were dissolved in 3 mL toluene solution in a thick-walls 25 mL Schlenk tube equipped with a magnetic stirring bar. The tube was brought out of the glove box. The reaction tube was heated in an oil bath at 120 °C for 8-15 hours. The tube was opened under nitrogen gas at room temperature and the crude product mixture was analyzed by GC-MS.

6.6.2 Typical Procedure of the Aldol-Type Condensation Reaction

When the catalytic reaction of ketone with vinylsilane was done, the toluene was evacuated, and the crude product was dissolved in 2 mL CH_2Cl_2 . 3.0 mmol 4-nitrobenzaldehyde was dissolved in 5 mL CH_2Cl_2 , when the solution was cool to 0 °C, 3.0 mmol TiCl_4 was added in, this mixture was stirred for about 15 min and then the crude silyl enol ether solution was added in by dropwise at -78 °C, and this mixture was warmed to -38 °C, and kept stirring for 1 hr, and added about 3 mmol water, the mixture was stirred in 0 °C for 8 hr. The reaction was quenched by adding the Na_2CO_3 solution, the oil lay was extracted with ethyl ether (20 mL), and the water lay was washed by ethyl ether (3 x 20 mL). The solution was dried by MgSO_4 , and the crude product was isolated by a column chromatograph on silica gel (hexane/dichloromethane).

6.6.3 Typical Procedure of the Fluorination Reaction

When the catalytic reaction of ketone with vinylsilane was done, the toluene was evacuated, and the crude product (2.0 mmol) was dissolved in 2 mL CH₃CN, and the solution was cooled to 0 °C. Selectfluor (0.708 g, 2.0 mmol) was added in several portions to the solution. After the addition of Selectfluor, the cold bath was removed and the reaction mixture was allowed to warm to room temperature over several hours. After the completion of the fluorination, the solvent was evaporated. Water (10 mL) was added to the residue, and the product was extracted with ethyl ether (3 x 20 mL). The combined organic layers were washed with brine and dried over anhydrous Na₂SO₄, and the solvent was evaporated. The pure product was isolated as a colorless liquid by flash chromatography using EtOAc/*n*-hexane.

6.6.4 Typical Procedure of the Diketone Reactions

When the catalytic reaction of ketone with vinylsilane was done, the toluene was evacuated, and the crude product (2.0 mmol) was dissolved in 2 mL CH₂Cl₂. Acetyl chloride (2.5 mmol) was dissolved in 5 mL CH₂Cl₂, and the solution was cooled to 0 °C, 3 mmol TiCl₄ was added in. This mixture was stirred for about 15 min and then the crude

silyl enol ether solution was added dropwise at $-78\text{ }^{\circ}\text{C}$, and this mixture was warmed to $-38\text{ }^{\circ}\text{C}$, and kept stirring for 1 hr. The reaction was quenched by adding the NH_4Cl solution, the oil layer was extracted with ethyl ether (20 mL), and the water layer was washed by ethyl ether (3 x 20 mL). The solution was dried by MgSO_4 , and the crude product was isolated by a column chromatograph on silica gel (*n*-hexane/ dichloromethane).

6.6.5 Typical Procedure of Aminomethylation Reaction

The experiment was performed by following a reported procedure. To a mixture of *N,N*-dimethylanilines (1.5 mmol), CuBr (4 mg, 0.025 mmol), crude product **2** (0.5 mmol) and CH_3CN (5 mL), *t*-BuOOH (0.10 mL, 5.0 M in decane) was added dropwise at room temperature. The resulting mixture was stirred at $50\text{ }^{\circ}\text{C}$ for 12 h. After the reaction, the mixture was filtered through a pad of celite, and the solvent was removed under reduced pressure. The residue was purified on a silica gel column to afford the desired product.

6.6.6 Hammett Study

In the glove box, $(\text{PCy}_3)_2(\text{CO})\text{RuHCl}$ (0.5 mol %), *para*-substituted acetophenones (0.2 mmol), vinyltrimethylsilane (0.4 mmol) and hexamethylbenzene (26 mg as the internal standard) were dissolved in 0.5 mL toluene- d_8 solution in a Wilmad J-Young NMR tube with a Teflon screw cap. The tube was taken out and was heated in an oil bath at 120 °C. The reaction was monitored every 30 min by ^1H NMR spectroscopy at room temperature. The rate was measured by monitor the ^1H integration of the product peak vinyl protons signal, and these were normalized vinyl protons against the internal standard. The k_{obs} was estimated from a first-order plot of $\ln[\text{product}]$ vs. reaction time.

6.7 Characterization Data of Organic Products

For **67a**: ^1H NMR (400 MHz, CDCl_3) δ 7.82 (s, 2H), 7.52-7.32 (m, 10H), 2.93 (t, $J = 6.1$ Hz, 4H), 1.78 (t, $J = 6.1$ Hz, 2H); $^{13}\text{C}\{^1\text{H}\}$ NMR (75 MHz, CDCl_3) δ 190.3, 137.0, 136.2, 136.0, 130.4, 128.4, 128.6, 28.5, 23.0; GC-MS $m/z = 274$ (M^+).

For **67b**: ^1H NMR (400 MHz, CDCl_3) δ 7.60-7.36 (m, 12H), 3.09 (s, 1H); $^{13}\text{C}\{^1\text{H}\}$ NMR (100 MHz, CDCl_3) δ 196.5, 137.5, 135.9, 134.0, 130.9, 128.9, 129.6, 26.7; GC-MS $m/z = 260$ (M^+).

For **67c**: ^1H NMR (300 MHz, CDCl_3) δ 7.82 (s, 2H), 7.52-7.32 (m, 10H), 3.15 (d, $J = 15.6$ Hz, 2H), 2.45 (t, $J = 13.8$ Hz, 2H), 1.48 (m, 1H), 0.96 (s, 9H); $^{13}\text{C}\{^1\text{H}\}$ NMR

(75 MHz, CDCl₃) δ 190.9, 137.0, 136.4, 136.2, 130.6, 128.8, 128.7, 44.6, 32.8, 29.8 and 27.5; GC-MS m/z = 330 (M⁺).

For **67d**: ¹H NMR (300 MHz, CDCl₃) δ 8.16 (d, 2H, J = 8.9 Hz), 7.50 (d, 2H, J = 8.9 Hz), 5.26 (s, 1H), 3.73 (s, 1H), 2.435 (m, J = 13.8 Hz, 1H), 2.60-2.40 and 1.80-1.20 (m, 10H); ¹³C{¹H} NMR (75 MHz, CDCl₃) δ 217.7, 149.8, 147.2, 126.9, 123.6, 72.6, 57.4, 44.0, 29.2, 128.7, 44.6, 29.3, 29.2, 24.0, 23.7.

For **67e** (*syn*): ¹H NMR (300 MHz, CDCl₃) δ 8.10 (d, 2H, J = 8.9 Hz), 7.32 (d, 2H, J = 8.9 Hz), 5.26 (s, 1H), 4.00 (s, 1H), 3.26-1.68 (m, 8H) and 1.37 (s, 3H); ¹³C{¹H} NMR (75 MHz, CDCl₃) δ 214.4, 148.1, 146.8, 130.1, 123.9, 77.7, 47.9, 42.9, 35.7, 34.7, 25.3 and 22.5.

For **67e** (*anti*): ¹H NMR (300 MHz, CDCl₃) δ 8.13 (d, 2H, J = 8.9 Hz), 7.47 (d, 2H, J = 8.9 Hz), 5.03 (s, 1H), 4.25 (s, 1H), 3.26-1.68 (m, 8H), 1.14 (s, 3H); ¹³C{¹H} NMR (75 MHz, CDCl₃) δ 219.0, 147.6, 146.8, 129.3, 123.0, 76.9, 52.7, 39.2, 37.1, 27.5, 20.7, 16.1.

For **67f** (*syn*): ¹H NMR (300 MHz, CDCl₃) δ 8.04 (d, J = 8.9 Hz, 2H), 7.41 (d, J = 8.9 Hz, 2H), 5.17 (s, 1H), 3.97 (s, 1H), 2.81 (m, 1H), 2.02 (s, 3H), 1.44 (m, 2H), 1.09 (m, 4H), 0.69 (t, J = 6.6 Hz, 3H) ppm. ¹³C{¹H} NMR (75 MHz, CDCl₃) δ 211.1, 150.6, 147.2, 126.5, 123.6, 69.0, 50.6, 43.6, 31.2, 23.1, 22.4, 13.9 ppm. GC-MS m/z = 265 (M⁺).

The ¹H and ¹³C NMR spectral data are in good agreement with the literature data.

For **67f** (*anti*): ^1H NMR (300 MHz, CDCl_3) δ 8.04 (d, $J = 8.9$ Hz, 2H), 7.41 (d, $J = 8.9$ Hz, 2H), 4.94 (s, 1H), 3.74 (s, 1H), 2.81 (m, 1H), 2.02 (s, 3H), 1.44 (m, 2H), 1.09 (m, 4H), 0.69 (t, $J = 6.6$ Hz, 3H) ppm. $^{13}\text{C}\{^1\text{H}\}$ NMR (75 MHz, CDCl_3) δ 213.1, 149.8, 147.1, 127.1, 123.4, 72.9, 58.8, 31.5, 27.3, 23.4, 13.8 ppm. GC-MS $m/z = 265$ (M^+). The ^1H and ^{13}C NMR spectral data are in good agreement with the literature data.

For **67g**: ^1H NMR (400 MHz, CDCl_3) δ 8.16 (d, 2H, $J = 8.9$ Hz), 7.92 (d, 2H, $J = 7.8$ Hz), 7.50 (d, 2H, $J = 8.9$ Hz), 7.50-7.43 (3H), 5.44 (s, 1H), 3.99 (s, 1H), 3.35 (m, 2H); $^{13}\text{C}\{^1\text{H}\}$ NMR (75 MHz, CDCl_3) δ 199.6, 150.5, 147.4, 136.3, 134.2, 129.0, 126.7, 123.9, 69.3, 47.2.

For **67h**: ^1H NMR (300 MHz, CDCl_3) δ 8.16 (d, 2H, $J = 8.9$ Hz), 7.81 (d, 2H, $J = 8.1$ Hz), 7.57 (d, 2H, $J = 8.9$ Hz), 7.23 (d, 2H, $J = 8.1$ Hz), 5.44 (q, 1H, $J = 4.0$ Hz), 4.04 (s, 1H), 3.33 (m, 2H) and 2.39 (s, 3H); $^{13}\text{C}\{^1\text{H}\}$ NMR (100 MHz, CDCl_3) δ 199.1, 150.5, 147.2, 145.0, 133.7, 129.5, 128.3, 126.6, 123.7, 69.3, 46.8, 21.7.

For **67i**: ^1H NMR (300 MHz, CDCl_3) δ 8.16 (d, 2H, $J = 8.9$ Hz), 7.88 (d, 2H, $J = 8.4$ Hz), 7.57 (d, 2H, $J = 8.9$ Hz), 6.90 (d, 2H, $J = 8.4$ Hz), 5.44 (m, 1H), 4.10 (s, 1H), 3.85 (s, 3H), 3.31 (m, 2H); $^{13}\text{C}\{^1\text{H}\}$ NMR (75 MHz, CDCl_3) δ 198.2, 164.4, 150.7, 147.4, 130.8, 129.5, 126.8, 124.0, 114.2, 69.6, 55.8, 46.8.

For **67j**: ^1H NMR (300 MHz, CDCl_3) δ 8.16 (d, 2H, $J = 8.9$ Hz), 7.88 (d, 2H, $J = 8.4$ Hz), 7.57 (d, 2H, $J = 8.9$ Hz), 6.90 (d, 2H, $J = 8.4$ Hz), 5.44 (m, 1H), 4.10 (s, 1H),

3.85 (s, 3H), 3.31(m, 2H); $^{13}\text{C}\{^1\text{H}\}$ NMR (75 MHz, CDCl_3) δ 198.2, 164.4, 150.7, 147.4, 130.8, 129.5, 126.8, 124.0, 114.2, 69.6, 47.3.

For **67k**: ^1H NMR (300 MHz, CDCl_3) δ 8.21 (d, 2H, $J = 8.8$ Hz), 7.88 (d, 2H, $J = 8.6$ Hz), 7.60 (d, 2H, $J = 8.8$ Hz), 7.44 (d, 2H, $J = 8.8$ Hz), 5.45 (m, 1H), 3.77 (s, 1H) and 3.33 (m, 2H); $^{13}\text{C}\{^1\text{H}\}$ NMR (75 MHz, CDCl_3) δ 198.4, 150.3, 147.6, 140.8, 134.7, 129.8, 129.4, 126.8, 124.1, 69.3, 47.3.

For **67l** (*syn*): ^1H NMR (400 MHz, CDCl_3) δ 8.16 (d, 2H, $J = 8.8$ Hz), 7.93 (d, 2H, $J = 8.9$ Hz), 7.62-7.44 (m, 5H), 5.34 (s, 1H), 4.08 (s, 1H), 3.79 (m, 1H) and 1.15 (d, 3H, $J = 7.2$ Hz); $^{13}\text{C}\{^1\text{H}\}$ NMR (75 MHz, CDCl_3) δ 205.3, 149.3, 147.1, 135.1, 134.0, 129.1, 128.7, 127.1, 123.7, 72.5, 46.8, 11.2.

For **67l** (*anti*): ^1H NMR (300 MHz, CDCl_3) δ 8.16 (d, 2H, $J = 8.8$ Hz), 7.93 (d, 2H, $J = 8.9$ Hz), 7.62-7.44 (m, 5H), 5.08 (d, $J = 7.2$ Hz), 4.08 (s, 1H), 3.82 (m, 1H) and 1.15 (d, 3H, $J = 7.2$ Hz); $^{13}\text{C}\{^1\text{H}\}$ NMR (75 MHz, CDCl_3) δ 204.4, 149.8, 147.6, 136.1, 133.8, 129.0, 128.6, 127.8, 123.8, 75.9, 47.8, 15.9.

For **67m** (*syn*): ^1H NMR (300 MHz, CDCl_3) δ 8.3-6.8 (m, 14H), 5.70 (d, $J = 3.4$ Hz 1H), 4.78 (d, $J = 3.4$ Hz, 1H), 3.90 (s, 1H) ppm. $^{13}\text{C}\{^1\text{H}\}$ NMR (75 MHz, CDCl_3) δ 202.1, 148.8, 147.6, 146.0, 138.1, 129.4, 133.4, 132.1, 130.4, 128.7, 128.3, 127.2, 124.1, 74.5, 60.0 ppm. GC-MS $m/z = 347$ (M^+). The ^1H and ^{13}C NMR spectral data are in good agreement with the literature data.

For **67m** (*anti*): ^1H NMR (300 MHz, CDCl_3) δ 8.10-6.85 (m, 14H), 5.55 (d, $J = 8.9$ Hz, 1H), 4.68 (d, $J = 3.4$ Hz, 1H), 3.50 (s, 1H) ppm. $^{13}\text{C}\{^1\text{H}\}$ NMR (75 MHz, CDCl_3) δ 198.1, 148.0, 147.0, 145.3, 137.9, 129.3, 133.5, 132.1, 130.4, 128.7, 128.4, 127.5, 124.3, 76.5, 62.3 ppm. GC-MS $m/z = 347$ (M^+). The ^1H and ^{13}C NMR spectral data are in good agreement with the literature data.

For **67n**: ^1H NMR (400 MHz, CDCl_3) δ 8.23-7.42 (m, 8H), 5.06 (s, 1H), 4.98 (d, 1H, $J = 8.9$ Hz), 3.00 (m, 1H), 2.73(m, 1H); $^{13}\text{C}\{^1\text{H}\}$ NMR (100 MHz, CDCl_3) δ 209.0, 153.6, 148.7, 148.0, 136.2, 136.1, 128.2, 128.0, 126.8, 124.5, 124.0, 75.0, 53.1, 29.7.

For **67o**: ^1H NMR (300 MHz, CDCl_3) δ 8.21 (d, 2H, $J = 8.8$ Hz), 8.05 (d, 1H, $J = 8.0$ Hz), 7.58 (d, 2H, $J = 8.8$ Hz), 7.54-7.23 (m, 3H), 5.11 (d, 1H, $J = 8.2$ Hz), 5.02 (s, 1H), 2.89 (m, 2H), 2.75 (m, 1H), and 1.68 (m, 2H); $^{13}\text{C}\{^1\text{H}\}$ NMR (75 MHz, CDCl_3) δ 201.6, 148.7, 147.8, 144.4, 134.6, 132.2, 129.0, 128.3, 127.8, 127.2, 123.8, 74.8, 53.9, 28.9, 26.2.

For **67p**: ^1H NMR (300 MHz, CDCl_3) δ 8.44 (s, 1H), 8.22 (d, 2H, $J = 8.8$ Hz), 7.93 (m, 4H), 7.64 (d, 2H, $J = 8.8$ Hz), 7.61 (m, 3H), 5.51 (t, 1H, $J = 4.0$ Hz), 3.97 (s, 1H) and 3.51 (m, 2H); $^{13}\text{C}\{^1\text{H}\}$ NMR (75 MHz, CDCl_3) δ 201.6, 148.7, 147.8, 144.4, 134.6, 132.2, 129.0, 128.3, 127.8, 127.2, 123.8, 74.8, 53.9, 28.9, 26.2.

For **67q**: ^1H NMR (300 MHz, CDCl_3) δ 8.23 (d, 2H, $J = 8.8$ Hz), 7.61 (d, 2H, $J = 8.8$ Hz), 7.26 (m, 3H), 6.95 (m, 1H), 5.43 (m, 1H), 3.95 (s, 1H), 3.35 (m, 2H) and 3.00 (s,

6H); $^{13}\text{C}\{^1\text{H}\}$ NMR (75 MHz, CDCl_3) δ 200.7, 150.9, 150.6, 147.5, 137.1, 129.7, 126.8, 124.0, 118.0, 116.6, 111.0, 69.6, 47.2, 40.7.

For **67r**: ^1H NMR (300 MHz, CDCl_3) δ 7.8-7.2 (m, 5H), 5.55 (d, $J_{\text{HF}} = 46.9$ Hz, 2H); $^{13}\text{C}\{^1\text{H}\}$ NMR (75 MHz, CDCl_3) δ 193.1 (d, $J_{\text{CF}} = 15.0$ Hz), 145.4, 132.4, 130.4, 127.6, 84.0 (d, $J_{\text{CF}} = 188.9$ Hz) ppm. GC-MS $m/z = 138$ (M^+).

For **67s**: ^1H NMR (300 MHz, CDCl_3) δ 7.70-7.30 (m, 4H), 5.14 (m, $J_{\text{HF}} = 51.0$ Hz, 1H), 3.35 (m, 1H), 3.08 (m, 1H) ppm. $^{13}\text{C}\{^1\text{H}\}$ NMR (75 MHz, CDCl_3) δ 199.9 (d, $J_{\text{CF}} = 14.9$ Hz), 149.7, 136.4, 133.7, 128.3, 126.9, 124.4, 91.7 (d, $J_{\text{CF}} = 189.9$ Hz), 33.2 (d, $J_{\text{CF}} = 21.4$ Hz) ppm. GC-MS $m/z = 150$ (M^+).

For **67t**: ^1H NMR (400 MHz, CDCl_3) δ 8.0-7.25 (m, 4H), 5.14 (ddd, $J_{\text{HF}} = 46.9$ Hz, $J_{\text{HH}} = 12.8, 5.2$ Hz, 1H), 3.12 (m, 2H), 2.56 (m, 1H), 2.34 (m, 1H) ppm. $^{13}\text{C}\{^1\text{H}\}$ NMR (100 MHz, CDCl_3) δ 193.6 (d, $J_{\text{CF}} = 14.8$ Hz), 143.2, 134.4, 131.4, 128.9, 128.0, 127.4, 91.2 (d, $J_{\text{CF}} = 188.4$ Hz), 30.4 (d, $J_{\text{CF}} = 19.4$ Hz), 27.1 (d, $J_{\text{CF}} = 11.6$ Hz) ppm. GC-MS $m/z = 164$ (M^+).

For **67u**: ^1H NMR (300 MHz, CDCl_3) δ 7.95-6.72 (m, 10H), 3.85 (t, $J = 7.0$ Hz, 2H), 3.24 (t, $J = 7.0$ Hz, 2H), 2.98 (s, 3H) ppm. $^{13}\text{C}\{^1\text{H}\}$ NMR (75 MHz, CDCl_3) δ 199.7, 148.8, 137.1, 133.4, 129.5, 128.8, 128.2, 116.7, 112.6, 48.1, 38.7, 35.3 ppm. GC-MS $m/z = 239$ (M^+).

For **67v**: ^1H NMR (300 MHz, CDCl_3) δ 7.26-6.75 (m, 5H), 3.89 (dd, $J = 15.1, 4.5$ Hz, 1H), 3.28 (dd, $J = 15.1, 8.0$ Hz, 1H), 2.96 (s, 3H), 2.53-2.45 (m, 1H), 2.37-1.63 (m,

6H) ppm. $^{13}\text{C}\{^1\text{H}\}$ NMR (75 MHz, CDCl_3) δ 220.2, 148.8, 129.3, 116.5, 112.3, 52.5, 48.4, 39.2, 38.1, 29.2, 20.8 ppm. GC-MS m/z = 203 (M^+).

For **67w**: ^1H NMR (300 MHz, CDCl_3) δ 7.30-6.70 (m, 5H), 3.89 (dd, J = 15.1, 5.6 Hz, 1H), 3.26 (dd, J = 15.3, 7.2 Hz, 1H), 3.02 (s, 3H), 2.78 (m, 1H), 2.50-1.42 (m, 8H) ppm. $^{13}\text{C}\{^1\text{H}\}$ NMR (75 MHz, CDCl_3) δ 212.5, 149.0, 129.2, 115.9, 111.7, 52.2, 49.2, 42.3, 39.6, 32.5, 27.9, 25.0 ppm. GC-MS m/z = 217 (M^+).

6.8 For Chapter 5

6.8.1 General Procedure of the Hydrosilylation of Alkynes

In a glove box, alkynes (1.0 mmol), triethylsilane (2.0 mmol) and the ruthenium catalyst **1** (7 mg, 1 mol %) were dissolved in 3 mL of CH_2Cl_2 in a 25 mL Schlenk tube equipped with a Teflon stopcock and a magnetic stirring bar. The reaction tube was brought out of the glove box, and was stirred at room temperature for 4-8 hours. The tube was opened to the air at room temperature, and the crude product mixture was analyzed by GC-MS. Analytically pure organic product was isolated by a column chromatography on silica gel (*n*-hexane/EtOAc).

6.8.2 General Procedure of the Hydrosilylation of Alkenes

In a glove box, alkenes (1.0 mmol), triethylsilane (2.0 mmol) and the ruthenium catalyst **1** (7 mg, 1 mol %) were dissolved in 3 mL of CH₂Cl₂ in a 25 mL Schlenk tube equipped with a Teflon stopcock and a magnetic stirring bar. The reaction tube was brought out of the glove box, and was stirred at 40 °C for 8 h. The tube was opened to the air at room temperature, and the crude product mixture was analyzed by GC-MS. Analytically pure organic product was isolated by a column chromatography on silica gel (*n*-hexane/EtOAc).

6.8.3 Hammett Study on the Hydrosilylation of Alkenes

In a glove box, a *para*-substituted styrene *p*-X-C₆H₄CCH (X = OMe, CH₃, Cl, Br) (0.20 mmol), triethylsilane (40 mg, 0.4 mmol), **1** (2 mg, 1 mol %) and C₆Me₆ (2 mg, internal standard) were dissolved in CDCl₃ (0.5 mL) solution in a J-Young NMR tube with a Teflon screw cap. The tube was brought out of the glove box and was heated in an oil bath set at 40 °C. The reaction was monitored in 10 min intervals by ¹H NMR. The *k*_{obs} was estimated from a first-order plot of *ln*[product] vs reaction time by measuring

the ^1H integration of the product peak ($=\text{CH}_2$, δ 5.81 ppm), which was normalized against the internal standard peak.

6.8.4 Isotope Labeling Study on the Hydrosilylation of Alkynes

In a glove box, triethylsilane (2.0 mmol) and $\text{DC}\equiv\text{CPh}$ (102 mg, 1.0 mmol) were added via a syringe to a 25 mL Schlenk tube equipped with a magnetic stirring bar and Teflon stopcock. The catalyst **1** (7 mg, 1 mol %) and the solvent (3 mL) were added to the reaction tube. The reaction tubes were brought out of the box was stirred at room temperature for 4 h. The solvent was removed from a rotary evaporator, and the organic product was isolated by a column chromatography on silica gel (*n*-hexanes). The deuterium content of the product was measured by both ^1H NMR (CDCl_3 with 10 mg cyclohexane as the external standard) and ^2H NMR (CH_2Cl_2 with 50 μL CDCl_3).

6.8.5 Phosphine Inhibition Study on the Hydrosilylation of Alkynes

In a glove box, triethylsilane (0.20 mmol), phenylacetylene (0.1mmol), **1** (3 mg, 2 mol %) and C_6Me_6 (2 mg, internal standard) were dissolved in 0.5 mL of CDCl_3 solution in a J-Young NMR tube with a Teflon screw cap. A pre-dissolved PCy_3 in CDCl_3

solution (5 μL , 1.0 M) was added via syringe to the tube via syringe. The tube was brought out of the glove box. The reaction was monitored by ^1H NMR in 30 min intervals. The rate was measured by the ^1H integration of the product peak at δ 5.81 (=CHSi), and was normalized against the internal standard peak. The k_{obs} was estimated from the first order plot of $\ln[\text{product}]$ vs reaction time.

6.8.6 Kinetic Studies on the Hydrosilylation of Alkenes

In the glove-box, the mixtures of styrene (0.006-0.2 M), triethyl silane (0.5 M), **1** (2 mg, 1 mol %) and C_6Me_6 (2 mg, internal standard) were dissolved in 0.5 mL of CDCl_3 solution in a J-Young NMR tube with a Teflon screw cap. A pre-dissolved PCy_3 in CDCl_3 solution (5 μL , 1.0 M) was added via syringe to the tube via syringe. The tube was brought out of the glove box. The reaction was monitored by ^1H NMR in 10 min intervals at 40 $^\circ\text{C}$. The initial rate method was used to measure the rate of each reaction. The rate was measured by the ^1H integration of the product peak at δ 5.81 ppm (=CHSi), and was normalized against the internal standard peak. The k_{obs} was estimated from the first order plot of $\ln[\text{product}]$ vs. reaction time.

6.8.7 Isotope Effect Study on the Hydrosilylation of Alkenes

In the glove-box, the mixtures of styrene (0.006-0.2 M), triethylsilane (0.5 M), **1** (2 mg, 1 mol %) and C₆Me₆ (2 mg, internal standard) were dissolved in 0.5 mL of CDCl₃ solution in a J-Young NMR tube with a Teflon screw cap. The tube was brought out of the glove box. The reaction was monitored by ¹H NMR in 10 min intervals at 40 °C. The initial rate method was used to measure the rate of each reaction. The rate was measured by the ¹H integration of the product peak at δ 5.81 ppm (=CHSi), and was normalized against the internal standard peak. The *k*_{obs} was estimated from the first order plot of *ln*[product] vs. reaction time. Under the similar reaction conditions, the reaction of deuterium styrene-*d*₈ (0.1 mmol) and triethylsilane (0.2 mmol) was monitored by ¹H NMR.

6.8.8 Carbon Isotope Effect Study on the Hydrosilylation of Alkenes

In the glove box, styrene (2.0 mmol), triethylsilane (3.0 mmol), **1** (14 mg, 1 mol %) were dissolved in 3 mL CH₂Cl₂ solution in two 25 mL Schlenk tubes equipped with a magnetic stirring bar. The tubes were brought out of the glove box. The reaction tube was heated in an oil bath at 40 °C for 10 min and was opened to air at room temperature, and the crude product mixture was analyzed by GC/MS (10 % conversion). The other reaction tube was heated in an oil bath at 40 °C for 8 h and was opened to the air at room

temperature. The crude product mixture was analyzed by GC/MS (98 % conversion). The solvent was removed under a rotary aspirator, and the product *trans* vinylsilane was isolated by a column chromatograph on silica gel (*n*-hexanes)

C#	98% conv.	18% conv.	18% conv./98% conv.	change (%)
1	2.9936 (3)	2.9925 (3)	0.9996 (3)	0.04 (3)
2	2.9827 (4)	2.9823 (4)	0.9998 (4)	0.02 (4)
3	0.9314 (5)	0.9208 (5)	0.9886 (5)	1.14 (5)
4	1.0084 (3)	1.0060 (3)	0.9976 (3)	0.24 (3)
5	0.9288 (4)	0.9272 (4)	0.9983 (4)	0.17 (4)
6	2.0000 (5)	2.0000 (5)	1.0000 (5)	0.00 (5)
7	1.9892 (3)	1.9884 (3)	0.9996 (5)	0.04 (5)
8	0.9938 (3)	0.9923 (3)	0.9985 (3)	0.15 (3)

C#	98% conv.	10% conv.	10% conv./98% conv.	change (%)
1	2.9936 (4)	2.9915 (4)	0.9993 (4)	0.07 (4)
2	2.9827 (4)	2.9813 (3)	0.9995 (3)	0.05 (3)
3	0.9314 (5)	0.9198 (5)	0.9875 (5)	1.25 (5)
4	1.0084 (3)	1.0074 (3)	0.9990 (3)	0.10 (3)
5	0.9288 (4)	0.9266(4)	0.9976 (4)	0.24 (4)
6	2.0000 (5)	2.0000 (5)	1.0000 (5)	0.00 (5)
7	1.9892 (3)	1.9879(3)	0.9993 (5)	0.07 (5)
8	0.9938 (3)	0.9953 (3)	1.0015 (3)	0.15 (3)

6.8.9 Synthesis of Carbonylchlorohydridotris(triphenyl-phosphine) Ruthenium (II)

A solution of 0.26 g (1.0 mmol) of hydrated ruthenium trichloride in 20 mL of 2-methoxyethanol and aqueous formaldehyde (20 ml, 40% w/v solution) are added rapidly and successively to a vigorously stirred, boiling solution of 1.58 g (6 mmol) of triphenylphosphine in 60 mL of 2-methoxyethanol. The mixture is heated under reflux for 10 min and allowed to cool. The precipitate which forms is separated and washed successively with ethanol, water, ethanol, and n-hexane and dried in vacuum.

6.8.10 Computational Study on Hydrosilylation of Alkynes

All calculations were carried out with Gaussian 09 program. First of all, all geometries of the reactants, transition structures and intermediates were fully optimized by B3LYP method. The 6-31G (d) basis set was used for H, C, O, P, Si and Cl atoms, while the Lanl2dz basis set and ECP were used for Ru atom. The Ru atom was augmented with f-polarization functions. The harmonic vibration frequency calculation was performed for each structure, from which the zero-point energy, thermal energy, entropy and free energy were derived. In order to minimize computation time,

$\text{RuH}(\text{PMe}_3)_2\text{Cl}(\text{CO})$ was chosen to be the catalyst, with trimethylsilane and phenylacetylene as the reacting silane and alkyne.

6.8.11 Characterization Data of Selected Organic Products of Hydrosilylation of Alkynes

For **69a**: ^1H NMR (400 MHz, CDCl_3) δ 7.50 (d, 1H, $J = 15.6$ Hz), 7.36-7.24 (m, 5H), 5.81 (d, 1H, $J = 15.6$ Hz), 0.91 (t, 9H), 0.59 (q, 6H); ^{13}C $\{^1\text{H}\}$ NMR (75 MHz, CDCl_3) δ 148.0, 140.8, 129.7, 128.1, 128.0, 127.6, 7.7, 5.0; GC-MS $m/z = 218$ (M^+).

For **69b**: ^1H NMR (400 MHz, CDCl_3) δ 7.46 (d, 1H, $J = 15.6$ Hz), 7.36-7.24 (m, 5H), 5.81 (d, 1H, $J = 15.6$ Hz), 0.91 (t, 6H), 0.59 (q, 4H), 0.01 (s, 3H); ^{13}C $\{^1\text{H}\}$ NMR (75 MHz, CDCl_3) δ 147.7, 140.6, 130.7, 128.2, 128.1, 127.6, 7.69, 6.8, -4.1; GC-MS $m/z = 204$ (M^+).

For **69c**: ^1H NMR (300 MHz, CDCl_3) δ 7.82 (d, 1H, $J = 15.6$ Hz), 7.70-6.94 (m, 20H), 6.44 (d, 1H, $J = 15.6$ Hz); ^{13}C $\{^1\text{H}\}$ NMR (75 MHz, CDCl_3) δ 150.6, 138.2, 135.2, 129.6, 128.9, 128.0, 127.9, 1125.5, 127.7; GC-MS $m/z = 376$ (M^+).

For **69d**: ^1H NMR (300 MHz, CDCl_3) δ 7.46 (d, 1H, $J = 15.6$ Hz), 7.18 (m, 4H), 5.74 (d, 1H, $J = 15.6$ Hz), 2.38 (s, 3H), 0.94 (t, 9H), 0.62 (q, 6H); ^{13}C $\{^1\text{H}\}$ NMR (75 MHz, CDCl_3) δ 147.9, 137.8, 137.3, 128.8, 128.0, 128.6, 21.5, 7.8, 5.0; GC-MS $m/z = 232$ (M^+).

For **69e**: ^1H NMR (300 MHz, CDCl_3) δ 7.42 (d, 1H, $J = 15.6$ Hz), 7.25 -6.86 (m, 4H), 5.67 (d, 1H, $J = 15.6$ Hz), 3.83 (s, 3H), 0.92 (t, 9H), 0.60 (q, 6H); ^{13}C $\{^1\text{H}\}$ NMR (75 MHz, CDCl_3) δ 147.9, 159.3, 133.3, 129.3, 113.5, 127.5, 55.4, 7.8, 5.0; GC-MS $m/z = 248$ (M^+).

For **69f**: ^1H NMR (300 MHz, CDCl_3) δ 7.40 (d, 1H, $J = 15.6$ Hz), 7.25 - 7.00 (m, 4H), 5.68 (d, 1H, $J = 15.6$ Hz), 0.88 (t, 9H), 0.58 (q, 6H); ^{13}C $\{^1\text{H}\}$ NMR (75 MHz, CDCl_3) δ 163.7, 161.3, 146.7, 136.8, 129.9, 129.7, 129.6, 115.1, 114.9, 7.7, 4.9; GC-MS $m/z = 238$ (M^+).

For **69g**: ^1H NMR (300 MHz, CDCl_3) δ 7.58-7.39 (d, 4H, $J = 8.5$ Hz), 7.46 (d, 1H, $J = 15.4$ Hz), 5.93 (d, 1H, $J = 15.4$ Hz), 0.89 (t, 9H), 0.57 (q, 6H); ^{13}C $\{^1\text{H}\}$ NMR (75 MHz, CDCl_3) δ 146.1, 144.0, 132.2, 129.3, 128.1, 124.9, 126.5, 125.6, 122.8, 120.2, 7.4, 4.6; GC-MS $m/z = 288$ (M^+).

6.8.12 Characterization Data of Selected Organic Products of Hydrosilylation of Alkenes

For **70a**: ^1H NMR (400 MHz, CDCl_3) δ 7.52-7.24 (m, 5H), 6.96 (d, 1H, $J = 19.4$ Hz), 6.48 (d, 1H, $J = 19.4$ Hz), 1.06 (t, 9H), 0.73 (q, 6H); ^{13}C $\{^1\text{H}\}$ NMR (75 MHz, CDCl_3) δ 145.1, 138.8, 128.7, 128.1, 126.0, 126.6, 7.7, 3.8; GC-MS $m/z = 218$ (M^+).

For **70b**: ^1H NMR (300 MHz, CDCl_3) δ 7.55-7.24 (m, 5H), 6.99 (d, 1H, $J = 19.4$ Hz), 6.54 (d, 1H, $J = 19.4$ Hz), 1.08 (t, 9H), 0.73 (q, 6H), 0.22 (s, 3H); ^{13}C $\{^1\text{H}\}$ NMR (75 MHz, CDCl_3) δ 145.1, 138.7, 128.8, 128.2, 127.4, 126.6, 7.7, 5.8, 5.3; GC-MS $m/z = 218$ (M^+).

For **70c**: ^1H NMR (300 MHz, CDCl_3) δ 7.70-6.94 (m, 20H), 7.02 (d, 1H, $J = 19.3$ Hz), 6.54 (d, 1H, $J = 19.3$ Hz); ^{13}C $\{^1\text{H}\}$ NMR (75 MHz, CDCl_3) δ 146.3, 138.1, 135.4, 129.5, 128.9, 128.0, 127.9, 1125.5, 126.2; GC-MS $m/z = 376$ (M^+).

For **70d**: ^1H NMR (400 MHz, CDCl_3) δ 7.38 (d, $J = 8.3$ Hz, 2H), 7.17 (d, $J = 8.3$ Hz, 2H), 6.91 (d, 1H, $J = 19.3$ Hz), 6.40 (d, 1H, $J = 19.3$ Hz), 2.38 (s, 3H), 1.04 (t, 9H), 0.70 (q, 6H); ^{13}C $\{^1\text{H}\}$ NMR (75 MHz, CDCl_3) δ 145.0, 137.9, 136.2, 129.1, 124.6, 126.5, 21.1, 7.7, 3.8; GC-MS $m/z = 232$ (M^+).

For **70e**: ^1H NMR (300 MHz, CDCl_3) δ 7.45 (d, $J = 8.8$ Hz, 2H), 6.92 (d, 2H, $J = 8.8$ Hz), 6.92 (d, 1H, $J = 19.4$ Hz), 6.33 (d, 1H, $J = 19.4$ Hz), 3.85 (s, 3H), 1.07 (t, 9H), 0.74 (q, 6H); ^{13}C $\{^1\text{H}\}$ NMR (75 MHz, CDCl_3) δ 144.5, 159.8, 131.8, 127.7, 114.1, 123.1, 55.5, 7.7, 3.8; GC-MS $m/z = 248$ (M^+).

For **70f**: ^1H NMR (400 MHz, CDCl_3) δ 7.46 (d, $J = 8.5$ Hz, 2H), 7.31 (d, $J = 8.5$ Hz, 2H), 6.83 (d, 1H, $J = 19.4$ Hz), 6.43 (d, 1H, $J = 19.4$ Hz), 1.00 (t, 9H), 0.67 (q, 6H); ^{13}C $\{^1\text{H}\}$ NMR (75 MHz, CDCl_3) δ 143.7, 137.6, 131.8, 128.0, 121.9, 127.3, 7.7, 3.6; GC-MS $m/z = 311$ (M^+).

For **70g**: ^1H NMR (400 MHz, CDCl_3) δ 7.39 and 7.31 (m, 4H, Ar), 6.87 (d, 1H, $J = 19.4$ Hz), 6.44 (d, 1H, $J = 19.4$ Hz), 1.02 (t, 9H), 0.69 (q, 6H); ^{13}C $\{^1\text{H}\}$ NMR (75 MHz, CDCl_3) δ 143.7, 137.2, 133.7, 128.9, 127.7, 127.1, 7.7, 3.7; GC-MS $m/z = 266$ (M^+).

For **70h**: ^1H NMR (400 MHz, CDCl_3) δ 7.75 and 7.18 (m, 5H, Ar), 7.10 (d, 1H, $J = 19.4$ Hz, $\text{CH}=\text{CHSi}$), 6.55 (d, 1H, $J = 19.4$ Hz), 3.94 (OCH_3), 1.09 (t, 9H), 0.76 (q, 6H); ^{13}C $\{^1\text{H}\}$ NMR (75 MHz, CDCl_3) δ 145.1, 158.0, 134.7, 134.2, 126.06, 125.2, 124.1, 119.2, 106, 127.2, 55.5, 7.7, 3.8. GC-MS $m/z = 298$ (M^+).

For **70i**: ^1H NMR (300 MHz, CDCl_3) δ 7.64-7.32 (m, 9H), 6.98 (d, 1H, $J = 19.5$ Hz), 6.52 (d, 1H, $J = 19.5$ Hz), 1.06 (t, 9H), 0.73 (q, 6H); ^{13}C $\{^1\text{H}\}$ NMR (75 MHz, CDCl_3) δ 144.6, 137.8, 129.0, 128.9, 128.5, 127.5, 127.3, 127.2, 126.4, 7.7, 3.8. GC-MS $m/z = 294$ (M^+).

References

- (1) Fischer, B. J.; Eisenberg, R. *Organometallics* **1983**, *2*, 764.
- (2) Sasaki, K.; Wada, K.; Tanaka, M. *Chem. Lett.* **1987**, 249.
- (3) Sasaki, K.; Wada, K.; Tanaka, M. *J. Am. Chem. Soc.* **1990**, *112*, 7221.
- (4) Kunin, A. J.; Eisenberg, R. *Organometallics* **1988**, *7*, 2124.
- (5) Liu, F.; Pak, E. B.; Singh, B.; Jensen, C.M. Goldman, A. S. *J. Am. Chem. Soc.* **1999**, *121*, 4086.
- (6) Jia, C.; Piao, D.; Oyamada, J.; Lu, W.; Fujiwara, Y. *Science*. **2000**, 287.
- (7) Murai, S.; Kakiuchi, F.; Sekine, S.; Tanaka, Y.; Kamatani, A.; Sonoda, M.; Charani, N. *Nature* **1993**, *366*, 529.
- (8) Lenges, C. P.; Brookhart, M. *J. Am. Chem. Soc.* **1999**, *121*, 6616.
- (9) Hani, A.; Mohammad, J. C.; Klaus, E.; Mack, G.; Speiser, B.; Novak, F.; Kaska, W.; Mayer, H. *Activation and Functionalization of C-H Bonds*, **2004**, 234, Chapter 14.
- (10) Filippini, M.; Rodriguez, J. *Org. Chem.* **1997**, *62*, 3034.
- (11) Lenges, C. P.; Brookhart, M. *J. Am. Chem. Soc.* **1999**, *121*, 6616.
- (12) Oi, S.; Ogino, Y.; Fukita.; Inoue, Y. *Org. Lett.* **2002**, *4*, 1783.
- (13) Wang, X.; Lane, B. S.; Sames, D. *J. Am. Chem. Soc.* **2005**, *127*, 4996.
- (14) (a) Stuart, D. R.; Villemure, E.; Fagnou, K. *J. Am. Chem. Soc.* **2007**, *129*, 12072.
(b) Maehara, A.; Tsurugi, H.; Satoh, T.; Miura, M. *Org. Lett.* **2008**, *10*, 1159.
- (15) Beck, E. M.; Grimster, N. P.; Hatley, R.; Gaunt, M. J. *J. Am. Chem. Soc.* **2006**, *128*, 2528.
- (16) Lu, W.; Jia, C.; Kitamura, T.; Fujiwara, Y. *Org. Lett.* **2000**, *2*, 2927.
- (17) Yang, Y.; Cheng, K.; Zhang, Y. *Org. Lett.* **2009**, *11*, 5606.
- (18) Zhuang, W.; Gathergood, N.; Hazel, R. G.; Jørgensen, K. A. *J. Org. Chem.* **2001**, *66*, 1009.
- (19) Palomo, C.; Oiarbide, M.; Kardak, B. G.; Garcia, J. M.; Linden, A. *J. Am. Chem. Soc.* **2005**, *127*, 4154.
- (20) Trost, B. M.; Muller, C. *J. Am. Chem. Soc.* **2008**, *130*, 2438.
- (21) Breno, K. L.; Pluth, M. D.; Tyler, D. R. *Organometallics* **2003**, *22*, 1203.
- (22) Gruber, S.; Zaitsev, A.; Worle, M.; Pregosin, P. S. *Organometallics* **2008**, *27*, 3796.
- (23) Hermatschweiler, R.; Fernandez, I.; Pregosin, P. S.; Watson, E. J.; Albinati, A.; Rizzato, S.; Veiros, L. F. *Organometallics* **2005**, *24*, 1809.
- (24) Grigg, R.; Savic, V. *Tetrahedron Lett.* **1997**, *38*, 5737.
- (25) Wang, X.; Lane, B. S.; Sames, D. *J. Am. Chem. Soc.* **2005**, *127*, 4996.
- (26) (a) Marrero, A.; Cueto, M.; Dcroz, L.; Darias, J. *Org. Lett.* **2008**, *10*, 3057
(b) Grundl, M.; Kennedy-Smith, J.; Trauner, D. *Organometallics* **2005**, *24*, 2831.
- (27) Yi, C. S.; Zhang, J. *Chem. Commun.* **2008**, 2349.

-
- (28) Li, Z.; Li, C. *Org. Lett.* **2004**, *6*, 4997.
- (29) Sezen, B.; Franz, R.; Sames, D. *J. Am. Chem. Soc.* **2002**, *124*, 13372.
- (30) Yanakawa, M.; Ito, H.; Noyoyi, R. *J. Am. Chem. Soc.* **2000**, *122*, 1466.
- (31) Lane, B. S.; Sames, D. *Org. Lett.* **2004**, *6*, 2897.
- (32) Murakami, M.; Hori, S. *J. Am. Chem. Soc.* **2003**, *125*, 4720.
- (33) (a) Li, W. J.; Nelson, D. P.; Jensen, M. S.; Hoerrner, R. S.; Javadi, G. J.; Cai, D.; Larsen, R. D. *Org. Lett.* **2003**, *5*, 4835. (b) Mori, A.; Sekiguchi, A.; Masui, K.; Shimada, T.; Horie, M.; Osakada, K.; Kawamoto, M.; Ikeda, T. *J. Am. Chem. Soc.* **2003**, *125*, 1700.
- (34) (a) Chaicharoenwimolkul, L.; Munmai, A.; Chairam, S.; Tewasekson, U.; Sapudom, S.; Lakliang, Y.; Somsook, E. *Tetrahedron Lett.* **2008**, *49*, 7299. (b) Sakurai, H.; Tsunoyama, H.; Tsukuda, T. *J. Organomet. Chem.* **2007**, *692*, 368.
- (35) Campeau, L. C.; Rousseaux, S.; Faugnou, K. Ahrendt, K. A.; Borths, C. J.; MacMillan, D. W. C. *J. Am. Chem. Soc.* **2005**, *127*, 18020.
- (36) Nakao, Y.; Kanyiva, K. S.; Hiyama, T. Ahrendt, K. A.; Borths, C. J.; MacMillan, D. W. C. *J. Am. Chem. Soc.* **2008**, *130*, 2448.
- (37) (a) Ireland, R. E.; Mueller, R. H.; Willard, A. K. *J. Am. Chem. Soc.* **1976**, *98*, 2868. (b) Rasmussen, J. K. *Synthesis* **1977**, 91. (c) Colvin, E. W. *Chem. Soc. Rev.* **1978**, *7*, 15. (d) Heathcock, C. H.; Buse, C. T.; Kleschick, W. A.; Pirrung, M. C.; Sohn, J. E.; Lampe, J. *J. Org. Chem.* **1980**, *45*, 1066. (e) Petrzilka, M.; Grayson, J. I. *Synthesis* **1981**, 753. (f) Brownbridge, P. *Synthesis* **1983**, 1 (g) Corey, E. J.; Gross, A. W. *Tetrahedron Lett.* **1984**, *25*, 495. (h) Cazeau, P.; Dubondin, F.; Moulines, F.; Babot, O.; Dunogues, J. *Tetrahedron* **1987**, *43*, 2075 and 2089. (i) Fleming, I.; Barbero, A.; Walter, D. *Chem. Rev.* **1997**, *97*, 2063.
- (38) Hall, P. L.; Glchrist, J. H.; Collum, D. B. *J. Am. Chem. Soc.* **1991**, *113*, 9571.
- (39) Tanabe, Y.; Misaki, T.; Kurihara, M.; Iida, A.; Nishii, Y. *Chem. Commun.* **2002**, 1628.
- (40) (a) Colquhoun, H. M.; Holton, J.; Thompson, D. J.; Twigg, M. V. *New Pathways for Organic Synthesis-Practical Applications of Transition Metals*; Plenum Press: London, 1984, 173. (b) McQuillin, F. J.; Parker, D. G.; Stephenson, G. R. *Transition Metal Organometallics for Organic Synthesis*; Cambridge University Press: New York, 1991, 27. (c) Otsuka, S.; Tani, K. *Synthesis* **1991**, 665.
- (41) (a) Boeckel, C. A. A.; Boom, J. M. *Tetrahedron Lett.* **1979**, 3561. (k) Carless, H. A. J.; Haywood, D. J. *Chem. Commun.* **1980**, 980. (b) Oltvoort, J. J.; Van Bockel, C. A. A.; De Koning, J. H.; van Boom, J. H. *Synthesis* **1981**, 305. (c) Sodeoka, M.; Yamada, H.; Shibasaki, M. *J. Am. Chem. Soc.* **1990**, *112*, 4906. (d) Takahashi, M.; Suzuki, H.; Moro-oka, Y.; Ikawa, T. *Chem. Lett.* **1981**, 1435. (e) Takahashi, M.; Suzuki, H.; Moro-oka, Y.; Ikawa, T. *J. Org. Chem.* **1991**, *56*, 4569. (f) Mitchell, T.

-
- N.; Gieselmann, F. *Synlett* **1996**, 475. (g) Wille, A.; Tomm, S.; Frauenrath, H. *Synthesis* **1998**, 305.
- (42) Chatani, N.; Yamaguchi, S.; Fukumoto, Y.; Murai, S. *J. Am. Chem. Soc.* **1992**, *114*, 9710.
- (43) Ohmura, T.; Yamamoto, Y.; Miyaura, N. *Organometallics* **1999**, *18*, 431.
- (44) Trost, B.; Surivet, J. P.; Toste, D. *J. Am. Chem. Soc.* **2001**, *123*, 2897.
- (45) Kownacki, I.; Marciniak, B.; Szubert, K.; Kubicki, M. *Organometallics* **2005**, *24*, 6179.
- (46) (a) Urabe, H.; Suzuki, D.; Sasaki, M.; Sato, F. *J. Am. Chem. Soc.* **2003**, *125*, 4036. (b) Hara, H.; Hirano, M.; Tanaka, K. *Org. Lett.* **2008**, *10*, 2537. (c) Nair, V.; Deepthi, A. *Chem. Rev.* **2007**, *107*, 1862.
- (47) (a) Brown, J. M. In *Comprehensive Asymmetric Catalysis*; Jacobsen, E. N., Pfaltz, A., Yamamoto, H., Eds.; Springer: Berlin, Germany, 1999. (b) Ohkuma, T.; Kitamura, M.; Noyori, R. In *Catalytic Asymmetric Synthesis*; Ojima, I., Ed.; Wiley-VCH: Weinheim, Germany, 2000. (c) Tang, W.; Zhang, X. *Chem. Rev.* **2003**, *103*, 3029.
- (48) Trost, B. M.; Toste, F. D.; Pinkerton, A. B. *Chem. Rev.* **2001**, *101*, 2067. (a) House, H. O. *Modern Synthetic Reactions*, 2nd Ed.; Benjamin/Cummings: Menlo Park, CA, 1972. (b) Smith, M. B.; March, M. *March's Advanced Organic Chemistry*, 5th Ed.; Wiley: New York, 2001.
- (49) (a) Isambert, N.; Cruz, M.; Arévalo, M. J.; Gómez, E.; Lavilla, R. *Org. Lett.* **2007**, *9*, 4199. (a) Isambert, N.; Cruz, M.; Arévalo, M. J.; Gómez, E.; Lavilla, R. *Org. Lett.* **2007**, *9*, 4199. (b) Yanagisawa, A.; Matusumoto, Y.; Asakawa, K.; Yamamoto, H. *J. Am. Chem. Soc.* **1999**, *121*, 892. (c) Karlsson, S.; Hogberg, H. E. *Tetradron Asymmetry* **2001**, *12*, 1977. (d) Isambert, N.; Cruz, M.; Arevalo, M. J.; Gomez, E.; Lavilla, R. *Org. Lett.* **2007**, *9*, 4199. (e) Clarke, P. A.; Zaytsev, A. V.; Morgan, T. W.; Whitwood, A. C.; Wilson, C. *Org. Lett.* **2008**, *10*, 2877.
- (50) (a) House, H. O. *Modern Synthetic Reactions*, 2nd Ed.; Benjamin Cummings: Menlo Park, CA, 1972. (b) Smith, M. B.; March, M. *March's Advanced Organic Chemistry*, 5th Ed.; Wiley: New York, **2001**.
- (51) (a) Wang, S.; Zhang, L. *J. Am. Chem. Soc.* **2006**, *128*, 8414. (b) Wang, S.; Zhang, L. *Org. Lett.* **2006**, *8*, 4585. (c) De Brabander, J. K.; Liu, B.; Qian, M. *Org. Lett.* **2008**, *10*, 2533. (d) Peng, Y.; Cui, L.; Zhang, G.; Zhang, L. *J. Am. Chem. Soc.* **2009**, *131*, 5062.
- (52) (a) Wang, S.; Zhang, L. *J. Am. Chem. Soc.* **2006**, *128*, 8414. (b) Wang, S.; Zhang, L. *Org. Lett.* **2006**, *8*, 4585. (c) De Brabander, J. K.; Liu, B.; Qian, M. *Org. Lett.* **2008**, *10*, 2533. (d) Peng, Y.; Cui, L.; Zhang, G.; Zhang, L. *J. Am. Chem. Soc.* **2009**, *131*, 5062.
- (53) DeBergh, J. R.; Spivey, K. M.; Ready, J. M. *J. Am. Chem. Soc.* **2008**, *130*, 7828.

-
- (54) Reviews: (a) Bruneau, C.; Dixneuf, P. H. *Acc. Chem. Res.* **1999**, *32*, 311. (b) Drozdak, D.; Allaert, B.; Ledoux, N.; Dragutan, I.; Dragutan, V.; Verpoort, F. *Adv. Synth. Cat.* **2005**, *347*, 1721.
- (55) Yoo, J. W.; Li, C. J. *J. Org. Chem.* **2006**, *71*, 6266.
- (56) Schaefer, C.; Fu, G. C. *Angew. Chem., Int. Ed.* **2005**, *44*, 4606.
- (57) Doucet, H.; Martin-Vaca, B.; Bruneau, C.; Dixneuf, P. H. *J. Org. Chem.* **1995**, *60*, 7247.
- (58) Mitsudo, T.; Hori, Y.; Yamakawa, Y. *J. Org. Chem.* **1987**, *52*, 2230.
- (59) Le Paih, J.; Monnier, F.; Dérien, S.; Dixneuf, P. H.; Clot, E.; Eisenstein, O. *J. Am. Chem. Soc.* **2003**, *125*, 11964.
- (60) Drozdak, D.; Allaert, B.; Ledoux, N.; Dragutan, I.; Dragutan, V.; Verpoort, F. *Adv. Synth. Cat.* **2005**, *347*, 1721.
- (61) (a) Bianchini, C.; Meli, A.; Peruzzini, M.; Zanobini, F.; Bruneau, C.; Dixneuf, P. H. *Organometallics* **1990**, *9*, 1155. (b) Doucet, H.; Höfer, J.; Bruneau, C.; Dixneuf, P. H. *Chem. Commun.* **1993**, 850. (c) Melis, K.; Opstal, T.; Verpoort, F. *Eur. J. Org. Chem.* **2002**, 3779. (d) Nakagawa, H.; Okimoto, Y.; Sakaguchi, S.; Ishii, Y. *Tetrahedron Lett.* **2003**, *44*, 103. (e) Hua, R.; Tian, X. *J. Org. Chem.* **2004**, *69*, 5782. (f) Doherty, S.; Knight, J. G.; Rath, R. K.; Clegg, W.; Harrington, R. W.; Newman, C. R.; Campbell, R.; Amin, H. *Organometallics* **2005**, *24*, 2633.
- (62) Cherry, K.; Parrain, J.-L.; Thibonnet, J.; Duchêne, A.; Abarbri, M. *J. Org. Chem.* **2005**, *70*, 6669.
- (63) Mitsudo, T.; Hori, Y.; Yamakawa, Y.; Watanabe, Y. *J. Org. Chem.* **1987**, *52*, 2230.
- (64) (a) Ho, J. H. H.; Black, D. S. Messerle, B. A.; Clegg, J. K.; Turner, P. *Organometallics* **2006**, *25*, 5800. (b) Mitsudo, T.; Hori, Y.; Yamakawa, Y. *J. Org. Chem.* **1987**, *52*, 2230.
- (65) Doucet, H.; Martin-Vaca, B.; Bruneau, C.; Dixneuf, P. H. *J. Org. Chem.* **1995**, *60*, 7247.
- (66) Le Paih, J.; Monnier, F.; Dérien, S.; Dixneuf, P. H.; Clot, E.; Eisenstein, O. *J. Am. Chem. Soc.* **2003**, *125*, 11964.
- (67) (a) Ueura, K.; Satoh, T.; Miura, M. *Org. Lett.* **2007**, *9*, 1407. (b) Kim, H.; Goble, S. D.; Lee, C. *J. Am. Chem. Soc.* **2007**, *129*, 1030.
- (68) Wang, Y.; Burton, D. J. *J. Org. Chem.* **2006**, *71*, 3859.
- (69) Ojima, I.; Li, Z.; Zhu, J. *In The Chemistry of Organosilicon Compounds*; Rappoport, S.; Apeloig, Y., Eds.; Wiley: New York, 1998; Laugkopf, E.; Schinzer, D. *Chem. Rev.* **1995**, *95*, 1375.
- (70) (a) Hatanaka, Y.; Hiyama, T. *Synlett* **1991**, 845. Hiyama, T. Organosilicon Compounds in Cross-Coupling reactions. In Metal-catalyzed Cross-Coupling reactions; (b) Diederich, F.; Stang, P. wiley-VCH: Weinheim, 1998. (c) Mowery, M. E.; DeShong, P. *Org. Lett.* **1999**, *1*, 2137; (d) Denmark, S. E.; Neuville, L., *Org. Lett.* **2000**, *2*, 3221.

-
- (71) Bunlaksananusorn, T.; Rodriguez, A. L.; Knochel, P. *Chem. Commun.* **2001**, 745.
- (72) Tamao, K.; Kumada, M.; Maeda, K. *Tetrahedron Lett.* **1984**, 25, 321.
- (73) Blumenkopf, T. A.; Overman, L. E. *Chem. Rev.* **1986**, 86, 857.
- (74) (a) Murai, S.; Sonoda, N. *Angew. Chem. Int. Ed. Engl.* **1979**, 18, 837. (b) Seki, Y.; Murai, S.; Hidaka, A.; Sonoda, N. *Angew. Chem. Int. Ed. Engl.* **1977**, 16, 881. (c) Seki, Y.; Hidaka, A.; Makino, S.; Murai, S.; Sonoda, N. *J. Organomet. Chem.* **1977**, 140, 361.
- (75) (a) Ikeda, S.; Chatani, N.; Kajikawa, Y.; Ohe, K.; Murai, S. *J. Org. Chem.* **1992**, 57, 2. (b) Seki, Y.; Kawamoto, K.; Chatani, N.; Hidaka, A.; Sonoda, N.; Ohe, K.; Kawasaki, Y.; Muri, S. *J. organomet. Chem.* **1991**, 403, 73.
- (76) (a) Matsuda, I.; Ogiso, A.; Sata, S.; Izumi, Y. *J. Am. Chem. Soc.* **1989**, 111, 2332. (b) Ojallima, I.; Ingallina, P.; Donovan, R.J. Clos, N. *Organometallics* **1991**, 10, 38.
- (77) Trost, B. M.; Ball, Z. T. *J. Am. Chem. Soc.* **2003**, 125, 30.
- (78) (a) Benkeser, R. A.; Burrous, M. L.; Nelson, L. E.; Swisher, J. V. *J. Am. Chem. Soc.* **1966**, 83, 4385. (b) Amrein, S.; Timmermann, A.; Studer, A. *Org. Lett.* **2001**, 3, 2357. (c) Asao, N.; Sudo, T.; Yamamoto, Y. *J. Org. Chem.* **1996**, 61, 7654. (d) Sudo, T.; Asao, N.; Gevorgyan, V.; Yamamoto, Y. *J. Org. Chem.* **1999**, 64, 2494.
- (79) Hamze, A.; Provot, O.; Alami, M.; Brion, J., D. *Org. Lett.* **2005**, 7, 5625.
- (80) Gelloz, G. B.; Schumers, J. M.; Bo, G.; Marko, I. E. *J. Org. Chem.* **2008**, 73, 4190.
- (81) Blug, M.; Goff, X.; Mezailles, N.; Floch, P. *Organometallics* **2009**, 28, 2360.
- (82) Seki, Y.; Takeshita, K.; kawamoto, K.; Murai, S. *J. Org. Chem.* **1986**, 51, 3890.
- (83) Na, Y.; Chang, S. *Org. Lett.* **2000**, 2, 1887.
- (84) Trost, B.; Ball, Z. *J. Am. Chem. Soc.* **2003**, 125, 30.
- (85) Kawanami, Y.; Sonoda, Y.; Mori, T.; Yamamoto, K. *Org. Lett.* **2002**, 4, 2825.
- (86) Dichers, H. M.; Haszeldine, R. N.; Mather, A. P.; Parish, R. V. *J. organomet. Chem.* **1978**, 161, 91.
- (87) Brady, K. A.; Nile, T. A. *J. organomet. Chem.* **1981**, 206, 299.
- (88) Ojima, I.; Clos, N.; Donovan, R. *Organometallics* **1990**, 9, 3127.
- (89) (a) Trofimov, B. A.; Sobenina, L. N.; Demenev, A. P.; Mikhaleva, A. I. *Chem. Rev.* **2004**, 104, 2481. (b) Cacchi, S.; Fabrizi, G. *Chem. Rev.* **2005**, 105, 2873.
- (90) (a) Murakami, M.; Horo, S. *J. Am. Chem. Soc.*, **2003**, 125, 4720. (b) Zaitsev, A. B.; Gruber, S.; Plss, P. A.; Pregosin, P. S.; Veiros, L. F.; Wrle, M. *J. Am. Chem. Soc.* **2008**, 130, 11604.
- (91) (a) Stuart, D. R.; Villemure, E.; Keith Fagnou, K. *J. Am. Chem. Soc.* **2007**, 129, 12072. (b) Maehara, A.; Tsurugi, H.; Satoh, T.; Miura, M. *Org. Lett.* **2008**, 10, 1159.
- (92) Gao, R.; Yi, S. C. *J. Org. Chem.* **2010**, 75, 3144.
- (93) Isaccs, M. *Phys. Org. Chem.* **1981**, 13, 4851.

-
- (94) (a) Singleton, D. A.; Thomas, A. A. *J. Am. Chem. Soc.* **1995**, *117*, 9357. (b) Frantz, D. E.; Singleton, D. A. *J. Am. Chem. Soc.* **1997**, *119*, 3383.
- (95) (a) Urabe, H.; Suzuki, D.; Sasaki, M.; Sato, F. *J. Am. Chem. Soc.* **2003**, *125*, 4036. (b) Hara, H.; Hirano, M.; Tanaka, K. *Org. Lett.* **2008**, *10*, 2537.
- (96) (a) Brown, J. M. In *Comprehensive Asymmetric Catalysis*; Jacobsen, E. N., Pfalts, A., Yamamoto, H., Eds.; Springer: Berlin, Germany, **1999**. (b) Ohkuma, T.; Kitamura, M.; Noyori, R. In *Catalytic Asymmetric Synthesis*; Ojima, I., Ed.; Wiley-VCH: Weinheim, Germany, **2000**. (c) Tang, W.; Zhang, X. *Chem. Rev.* **2003**, *103*, 3029.
- (97) Trost, B. M.; Toste, F. D.; Pinkerton, A. B. *Chem. Rev.* **2001**, *101*, 2067.
- (98) Isambert, N.; Cruz, M.; Arévalo, M. J.; Gómez, E.; Lavilla, R. *Org. Lett.* **2007**, *9*, 4199.
- (99) (a) House, H. O. *Modern Synthetic Reactions*, 2nd Ed.; Benjamin Cummings: Menlo Park, CA, 1972. (b) Smith, M. B.; March, M. *March's Advanced Organic Chemistry*, 5th Ed.; Wiley: New York, **2001**.
- (100) Reviews: (a) Bruneau, C.; Dixneuf, P. H. *Acc. Chem. Res.* **1999**, *32*, 311. (b) Drozdak, D.; Allaert, B.; Ledoux, N.; Dragutan, I.; Dragutan, V.; Verpoort, F. *Adv. Synth. Cat.* **2005**, *347*, 1721.
- (101) Doherty, S.; Knight, J. G.; Rath, R. K.; Clegg, W.; Harrington, R. W.; Newman, C. R.; Campbell, R.; Amin, H. *Organometallics* **2005**, *24*, 2633.
- (102) Ho, J. H. H.; Black, D. S. Messerle, B. A.; Clegg, J. K.; Turner, P. *Organometallics* **2006**, *25*, 5800.
- (103) Yi, S. C.; Gao, R. *Organometallics* **2009**, *28*, 6585.
- (104) (a) Rybtchinski, B.; Milstein, D. *J. Am. Chem. Soc.* **1999**, *121*, 4528. (b) Feller, M.; Iron, M. A.; Shimon, L. J. W.; Diskin-Posner, Y.; Leitun, G.; Milstein, D. *J. Am. Chem. Soc.* **2008**, *130*, 14374.
- (105) Swartz, B. D.; Reinartz, N. M.; Brennessel, W. W.; Garca, J. J.; Jones, W. D. *J. Am. Chem. Soc.* **2008**, *130*, 8548.
- (106) (a) Grimster, N. P.; Gauntlett, C.; Godfrey, C. R. A.; Gaunt, M. J. *Angew. Chem., Int. Ed.* **2005**, *44*, 3125. (b) Ranu, B. C.; Chattopadhyay, K.; Adak, L. *Org. Lett.* **2007**, *9*, 4595. (c) Cheng, J.-S.; Wei, G.-F.; Huang, S.W.; Zhao, J.; Jiang, H. F. *J. Mol. Cat.* **2007**, *263*, 169. (d) Zott, A. D.; Prat, F. I.; Baratta, W.; Zangrando, E.; Rigo, P. *Inorg. Chim. Acta* **2009**, *362*, 97.
- (107) (a) Bruce, M. I. *Chem. Rev.* **1991**, *91*, 197. (b) Tani, K.; Kataoka, Y. In *Catalytic Heterofunctionalization*, Togni, A., Grützmacher, H. Eds.; VCH-Wiley: Weinheim, 2001, 199. (c) Bruneau, C.; Dixneuf, P. H. *Angew. Chem., Int. Ed.* **2006**, *45*, 2176.
- (108) (a) Grotjahn, D. B.; Incarvito, C. D.; Rheingold, A. L. *Angew. Chem., Int. Ed.* **2001**, *40*, 3884. (b) Tokunaga, M.; Suzuki, T.; Koga, N.; Fukushima, T.;

-
- Horiuchi, A.; Wakatsuki, Y. *J. Am. Chem. Soc.* **2001**, *123*, 11917. (c) Grotjahn, D. B.; Lev, D. A. *J. Am. Chem. Soc.* **2004**, *126*, 12232. (d) Labonne, A.; Kribber, T.; Hintermann, L. *Org. Lett.* **2006**, *8*, 5853.
- (109) Recent reviews: (a) Trofimov, B. A.; Sobenina, L. N.; Demenev, A. P.; Mikhaleva, A. I. *Chem. Rev.* **2004**, *104*, 2481. (b) Cacchi, S.; Fabrizi, G. *Chem. Rev.* **2005**, *105*, 2873.
- (110) (a) Yi, C. S.; Yun, S. Y.; Guzei, I. A. *Organometallics* **2004**, *23*, 5392.
- (111) Saigo, K.; Osaki, M.; Mukaiyama, T. *Chem. Lett.* **1976**, 163.
- (112) Guo, Y.; Tao, G.; Blumenfeld, A.; Shreeve, J. M. *Organometallics*, **2010**, *29*, 818.
- (113) (a) Bisswanger, H. *Enzyme Kinetics*; Wiley-VCH, Germany, 2002, 28. (b) Cornish-Bowden, A. *Fundamentals of Enzyme Kinetics* 3rd Ed.; Portland Press, London, 2000, 72. (c) Segel, I. H. *Enzyme Kinetics*; Wiley-VCH: New York, NY, 1975.